Gamma-synucleinopathy in mice (and humans?)

Owen Peters

ProQuest LLC
789 East Eisenhower Parkway
P.O. Box 1346
Ann Arbor, MI 48106-1346

Declaration

This work has not previously been accepted in substance for any degree and is not concurrently submitted in candidature for any degree.

Signed ..... Date: 26th April 2011

STATEMENT 1

This thesis is being submitted in partial fulfillment of the requirements for the degree of PhD.

Signed ..... Date: 26th April 2011

STATEMENT 2

This thesis is the result of my own independent work/investigation, except where otherwise stated. Other sources are acknowledged by explicit references.

Signed ..... Date: 26th April 2011

STATEMENT 3

I hereby give consent for my thesis, if accepted, to be available for photocopying and for inter-library loan, and for the title and summary to be made available to outside organisations.

Signed ..... Date: 26th April 2011

Abstract

The alpha-synucleinopathies are a group of neurodegenerative disorders characterised by the accumulation and aggregation of the presynaptic protein alpha-synuclein. Though not currently considered to play a major role in any neurodegenerative condition, gamma-synuclein shares many characteristics with alpha-synuclein. The expression pattern of gamma-synuclein does however differ from alpha-synuclein, predominantly localised in cell bodies, neurites and synapses of motor and sensory neuron populations. In this thesis we have characterised the phenotype developed by a line of mice expressing high levels of gamma-synuclein throughout their nervous system. The pattern of neurodegeneration developed by the animals bore striking resemblance to that seen in the motor neuron disease amyotrophic lateral sclerosis. Accumulation and aggregation of gamma-synuclein was detected throughout the nervous system. Upper and lower motor neuron populations were lost in a selective manner, with neurons of the sensory system spared.

As a result of these findings we assessed the distribution of gamma-synuclein in spinal cord samples of sporadic and familial amyotrophic lateral sclerosis. Though not a component of any typical ALS-associated inclusion bodies, we identified gamma-synuclein positive structures in the corticospinal tracts of several of the cases examined. All these cases shared a common pronounced loss of upper motor neurons and demyelination of the spinal cord portion of their axons. We thus propose that the unidentified gamma-synuclein positive structures represent a novel corticospinal tract inclusion structure or alternatively present a novel marker of a subtype of amyotrophic lateral sclerosis with pronounced upper motor neuron involvement.

Acknowledgements

This project was funded as part of a Wellcome Trust program grant.

I am indebt to Prof. Vladimir Buchman for his guidance, support, and patience during my time spent in his lab and shall always be grateful for having had such a fantastic start to my career. Special thanks are also due to Dr Natalia Ninkina, for her constant help and supervision (and mothering) throughout my project. I would like to thank everyone who has worked in the VLB group during the course of my project, and am particular grateful for the friendship and support given by Steven Millership and Natalie Connor-Robson (technical- and moral- respectively). The assistance of undergraduate student Lora Keeling was also much appreciated, as was the help and hospitality of Dr Alexey Ustyugov and 'honorary' VLB group member Tatyana Shelkovnikova. Every person working on the Fourth and Third floors of Life Sciences Building deserves credit for tolerating me over the past four years.

Many of the experiments in this project relied on the assistance of others. Electron microscopy work could not have been completed without guidance from Dr. Anthony Hann and technical support from Guy Pitt. Assessment of human tissue samples was carried out in the MRC London Brain Bank for Neurodegenerative Diseases, Kings College. I am grateful to Dr Tibor Hortobagyi for selection of sample patients and advice with regards to my findings, and Dr Claire Troakes for assistance with sample collection. DiOlystic staining was carried out in Cardiff Universities School of Optometry in collaboration with Prof. James Morgan and with kind assistance from Peter Williams. I would also like to thank the Brain Repair Group for behavioural testing advice and access to equipment.

I am forever thankful to my parents, family and friends for their support throughout my education. And finally extra special thanks must go to Gaynor Smith – for all her years of devotion, for patiently listening to my endless stupid ideas, for getting me out of bed and into work every morning and for giving me a reason to come home afterwards. It's your turn next...

Contents

Figures

List of abbreviations

ALS	Amyotrophic lateral sclerosis
CNS	Central nervous system
DA	Dopamine
DRG	Dorsal root ganglion
fALS	Familial amyotrophic lateral sclerosis
FTLD	Frontotemporal lobar degeneration
GAD	Gracile axonal dystrophy
GFAP	Glial fibrillary acidic protein
HPLC	High performance liquid chromatography
IP	Immunoprecipitation
KO	Knock-out
MBP	Myelin basic protein
MPTP	1-methyl-4-phenyl-1,2,3,6-tetrahydropyridine
NAC	Non-amyloid component region common to alpha- and gamma-synuclein
NF	Neurofilament – family of three neuron specific intermediate fibres, denoted light (NFL), medium (NFM) and heavy (NFH)
NMJ	Neuromuscular junction
PCR	Polymerase chain reaction
PD	Parkinson's disease
PNS	Peripheral nervous system
RCA	Ricinus Communis Agglutinin
RGC	Retinal ganglion cell
sALS	Sporadic amyotrophic lateral sclerosis
SNARE	Soluble NSF attachment protein receptor
SNpc	Substantia nigra pars compacta
TEM	Transmission electron microscope
TH	Tyrosine hydroxylase
TKO	Triple knock-out mice null for all three synucleins
UPS	Ubiquitin-proteasome system
VTA	Ventral trigeminal area
WT	Wild type

1. Introduction

Through the vast advances in healthcare made over the past century, we currently live in a society with an increasing life expectancy. The benefits of this are clearly numerous, but longer lifespan within the population has also led to a massive increase in the number of people suffering from aging associated disorders. If we are to treat these diseases it is essential we unravel their pathogenesis and ultimately develop effective therapies against them. Included in these aging-associated disorders are degenerative diseases of the nervous system, two of which shall be introduced to provide context for this thesis.

1.1. Amyotrophic lateral sclerosis

Amyotrophic lateral sclerosis (ALS) is the most common form of motor neuron disease, with an incidence of 1:50,000 people in the UK (Worms 2001). ALS exists in both sporadic and familial forms (discussed below), the latter accounting for approximately 5-10% of cases (Byrne et al. 2010). In the late nineteenth century Jean-Martin Charcot systematically described the clinical manifestation of ALS. Average age of onset is 55 years, with a life expectancy of three to five years (Haverkamp et al. 1995). Typically patients develop asymmetrical muscle weakness in one of the limbs often preceded by involuntary twitching, and cramps in the affected limb (Wijesekera and Leigh 2009). The "Babinski sign" is often seen in the feet during early stages of ALS, where stimulation of the lateral portion of the sole results in involuntary flexing and fanning of the toes. Over the course of disease atrophy spreads to all limbs, gradually leaving the patient immobilised. Degeneration of bulbar muscles including the tongue causes loss of speech, difficulty eating and drooling (Kawai et al. 2003). Occulomotor function is generally remarkably well preserved (Gizzi et al. 1992). Eventual atrophy of respiratory muscles results in respiratory and pulmonary difficulties that are generally the cause of death (Wijesekera and Leigh 2009). Symptoms of ALS are predominantly motor, though changes in sensitivity have been reported by patients including burning and numbness in the extremities and loss of sensation (Andersen et al. 1996; Dyck et al. 1975; Kawata et al. 1997). The conservation of sensory and cognitive function unfortunately leave patients in the later stages of disease in a "locked-in" state, where the paralysed body is supported by assisted respiration but mental capacity is intact (Wijesekera and Leigh 2009).

1.1.1. Histopathology of amyotrophic lateral sclerosis

The neuronal degeneration in ALS has been well defined. Neuromuscular deficits are induced by substantial dystrophy of motor neurons populations in the spinal cord, brainstem and neurons within cortical motor regions. The most substantial and consistent loss of motor neurons is seen in the ventral horn of the spinal cord, the population of which has been reported to be reduced by as much as 50% (Wijesekera and Leigh 2009). A distinct pattern of damage has been reported in the efferent axons. Large caliber fibres with the fastest conduction velocities were found to be substantially more vulnerable compared to small caliber fibres, with the slowing of conduction velocities and selective loss of fibres reported (Bradley et al. 1983; Kawamura et al. 1981; Theys et al. 1999). In accordance with the preservation of occulomotor activity, motor neurons of the abducens, trochlear and

occulomotor nuclei appear to be consistently resistant to the dystrophy seen in other brainstem population such as the hypoglossal, facial and motor trigeminal nuclei (DePaul et al. 1988; Kiernan and Hudson 1991; Okamoto et al. 1993a). In addition to disruption of lower motor neurons, damage to upper motor neurons, or Betz cells, is also a feature of ALS. Abnormal morphological changes and degeneration of pyramidal Betz cells, accompanied by substantial levels of gliosis, is seen within the primary motor region of the cerebral cortex. (Hammer et al. 1979; Kiernan and Hudson 1991; Wijesekera and Leigh 2009).

In contrast to the motor system, sensory and cognitive systems are considered more tolerant (Wijesekera and Leigh 2009). In spite of this, limited changes have been reported in 10-20% of ALS patients (Isaacs et al. 2007; Pugdahl et al. 2007). Slowing of conduction velocities and action potential have been recorded in the several sensory nerves (Hammad et al. 2007; Isaacs et al. 2007; Pugdahl et al. 2007; Theys et al. 1999). Loss of fibres and changes in the myelination of axons has been detected in various sensory nerves and ascending sensory columns of the spinal cord (Bradley et al. 1983; Dyck et al. 1975; Hammad et al. 2007; Heads et al. 1991; Kawamura et al. 1981). As with motor axons, the largest caliber of sensory fibre appear most vulnerable to degeneration (Hammad et al. 2007; Heads et al. 1991; Kawamura et al. 1981). There is little evidence of damage to sensory neuron cell bodies, though morphological changes have been noted in mitochondria of the dorsal root ganglia (Sasaki et al. 2007).

The formation of proteinacious intracellular inclusion bodies is seen in ALS. Small, eosinophilic, intracellular structures termed "Bunina bodies" found in motor neurons of the spinal cord and brainstem are considered a hallmark of the disease (Okamoto et al. 2008). Rarely ubiquitinated, the only species of protein currently identified as consistent components of Bunina bodies are cystatin C (Okamoto et al. 1993b) and transferrin (Mizuno et al. 2006). In addition to Bunina bodies, "Lewy body-like" and "skein-like" inclusion bodies are also commonly identified in ALS affected motor neurons. Intracellular skein-like inclusions consist of bundled fibrils staining intensely for ubiquitin (Leigh et al. 1988). The composition of the hyaline Lewy-body-like class of inclusions is better defined, with several proteins having been identified frequently in the structures in addition to ubiquitin (Leigh et al. 1988). Furthermore analysis of the genes encoding several of these component proteins has provided valuable evidence regarding genetic risk factors and cellular mechanisms potentially underlying ALS pathology. The three most common of these shall be discussed.

1.1.2. Cu/Zn superoxide dismutase (SOD1)

SOD1, an antioxidant enzyme that converts superoxide radicals (O_2^-) to oxygen and hydrogen peroxide, was the first gene to be associated with fALS (Rosen et al. 1993) and to have its protein product detected in both sALS and fALS inclusion bodies (Shibata et al. 1996). Currently over 100 unique mutations have been identified in the gene (Valentine et al. 2005), accounting for

approximately 20% of fALS cases (Majoor-Krakauer et al. 2003) and ~5% of sALS (Byrne et al. 2010; Orrell et al. 1999).

Though it was initially hypothesised that loss of normal antioxidant function of SOD1 may be the underlying cause of ALS, subsequent generation of SOD1-mutant or null mice did not recaptiulate motor neuron disease (Reaume et al. 1996). It thus appears that mutations that alter the structure of SOD1 are responsible for toxicity, most likely through a gain of function mechanism leading to the protein's aggregation. Wild type SOD1 is an exceptionally stable molecule: active SOD1 has been isolated from uncontaminated brain tissue of a 3000-year old Egyptian mummy (Weser et al. 1989). When both Cu^{2+} & Zn^{2+} binding sites are filled the enzyme is able to retain functional activity after exposure to temperatures of almost 80°C, chemical denaturing in 10.0M urea and exposure to 4% SDS (Forman and Fridovich 1973). Mutant forms of SOD1 have been found to be only slightly less stable under similar conditions (Rodriguez et al. 2002), suggesting that morphologic changes increasing aggregation occur whilst the protein is in its native state (Shaw and Valentine 2007). The mechanism by which aggregation induces toxicity is the source of much debate (Ross and Poirier 2005). Though large SOD1 containing inclusion bodies are commonly found in motor neurons and some glial cells of ALS patients, these most likely represent a defensive mechanism to sequester smaller toxic species of intermediate protein oligomers. Mutant forms of SOD1 are able to produce a number of these intermediate structures including dimers, pore-like structures and spheroids (Ray et al. 2004; Shaw and Valentine 2007).

1.1.3. TDP-43 & FUS/TLS

For many years SOD1 was considered both the predominant component of inclusion bodies in ALS and major genetic cause of fALS. However the identification of mutations in genes encoding two DNA/RNA binding proteins and the detection of these proteins within inclusion bodies in typical cases of both fALS and sALS has vastly changed this doctrine. Both proteins are believed to normally be involved in several aspect of RNA processing, including the regulation of transcription, splicing and processing of microRNAs (reviewed in Lagier-Tourenne et al. 2010). The first of these to be described was TAR DNA binding protein (TDP-43) (Neumann et al. 2006) a conserved DNA/RNA binding protein expressed in most human and eukaryotic cell types, originally identified through its ability to bind and repress the transcription of TAR DNA sequence motifs in HIV1 (Ou et al. 1995). Hyperphosphorylated TPD-43 was found to translocate from its normal localization in the nucleus to the perikaryal soma of ALS affected motor neurons and glial cells, where it formed spherical and skein-like inclusion (Neumann et al. 2006). This relocalisation is now believed to represent an early aberrant change in ALS pathogenesis (Giordana et al. 2010). Similar TDP-43 positive inclusion bodies were also detected in the hippocampus, frontal and temporal cortex (Arai et al., 2006; Neumann et al. 2006). Following the identification of TPD-43 protein within ALS inclusion bodies, screening of its encoding gene in cases of fALS and sALS identified several autosomal dominant missense mutations, several of which produced truncated products missing their DNA targeting motif (Arai et al. 2006; Gitcho et al. 2008;

Kabashi et al. 2008; Sreedharan et al. 2008). Currently over 38 mutations have been identified in TDP-43, predominantly contained within the glycine rich C-terminus (Lagier-Tourenne et al. 2010). Such mutations account for approximately 3% of fALS and 1.5% of sALS cases (Lagier-Tourenne et al. 2010). The role of TDP-43 in neurodegeneration does not appear to be restricted to ALS, with TDP43 positive inclusion bodies detected in cases of frontotemporal lobar degeneration, a condition that is often accompanied by the development of ALS (Neumann et al. 2006). Furthermore the protein has been detected in inclusion bodies found in conditions including Alzheimer's disease (Lippa et al. 2009), Parkinson's disease (Nakashima-Yasuda et al. 2007), Huntington's disease (Schwab et al. 2008) and Down's syndrome (Lippa et al. 2009) amongst others (Lagier-Tourenne et al. 2010).

Following the identification of TDP-43, two groups independently investigating a region of chromosome 16 with linkage to fALS detected autosomal dominant and recessive missense mutations in the gene encoding a second widely expressed DNA/RNA binding protein, fused in sarcoma/translated in liposarcoma (FUS/TLS) (Kwiatkowski et al. 2009; Vance et al. 2009), an RNA binding protein originally identified as a chromosomal translocating fusion protein in liposarcoma (Rabbitts et al. 1993). As with TPD-43 the normal nuclear localization of FUS/TLS was lost, with perikaryal inclusion bodies present in ALS affected motor neurons but not glial cells (Kwiatkowski et al. 2009; Vance et al. 2009). Currently 30 mutations have been identified in FUS/TLS, mostly within the C-terminus, accounting for approximately 4% fALS (Lagier-Tourenne et al. 2010). FUS/TLS positive inclusion bodies have also been detected in rare cases of FLTD (Neumann et al. 2009). Notably TDP-43 is absent from these structures, as FUS/TLS is absent from inclusion bodies in cases of FTLD with TDP-43 inclusions (Lagier-Tourenne et al. 2010; Neumann et al. 2009). Intra-nuclear inclusion bodies containing FUS/TLS have also been detected in several polyglutamine disorders, including Huntington's disease (Doi et al. 2008) and spinocerrebellar ataxia (Doi et al. 2010).

1.1.4. Neurofilaments

Intermediate cytoskeletal neurofilament proteins are frequently found to accumulate in ALS. Neurofilament proteins have been identified in Lewy-body-like inclusions and atypical, multifocal hyaline conglomerate inclusion bodies within the perikaryal cytoplasm and swollen regions of proximal axon (Hirano et al. 1984; Rouleau et al. 1996). Rare mutations have also been identified in neurofilament heavy subunit (NF-H) (Figlewicz et al. 1994; Tomkins et al. 1998; Al-Chalabi et al. 1999). Such mutations have been predicted to account for approximately 1% of cases of fALS (Menzies et al. 2002). Currently all reported mutations in NF-H are located within a C-terminal domain containing 43 repeats of the three-residue motif Lys-Ser-Pro (KSP), a target site for Ser/Thr protein kinases, suggesting that the changes in the state of neurofilament phosphorylation might contributed to pathogenesis.

1.1.5. Other fALS associated genes

In addition to those of SOD1, TDP-43, FUS/TLS and NF-H, a number other mutantions have been associated with very rare cases of familial ALS. Several autosomal dominant mutations have been detected in ANG, encoding the angiogenesis promoting protein angiogenin (Cronin et al. 2006). Rare autosomal recessive mutations to alsin, a protein carrying several guanine-exchange factors for GTPases, result in a juvenile onset form of ALS (Yang et al. 2001). Linkage analysis has detected association between autosomal dominant fALS and several regions, for example 9p21.2 and 19p13.3 (Pearson et al. 2010; van Es et al. 2009).

Several of these rare mutations implicate the disruption of internal trafficking of vesicles and cellular components in the pathogenesis of ALS. Autosomal dominant mutation has been detected in the dynactin component $p150^{Glued}$, an essential component of the retrograde transport system facilitating the movement of cargo along microtubules (Puls et al. 2003). Mutations have also been found in vesicle-associated membrane protein/synaptobrevin-associated membrane protein B (VAPB), a protein that binds both intracellular vesicles and microtubules (Nishimura et al. 2004). Both autosomal dominant and recessive mutations have been identified in *OPTN*, the gene encoding optineurin (Maruyama et al. 2010). The precise function of optineurin is unclear, though roles in golgi function and exocytosis have been suggested (Sahlender et al. 2005). The autosomal dominant E478G mutation induced the accumulation of optineurin ALS associated Lewy-body-like, intracellular spheroid inclusion bodies (Maruyama et al. 2010). The protein was also identified as a component of skein-like and Lewy-body-like inclusions in cases of sALS and fALS. Interestingly optineurin has also been identified as a causative mutation in glaucoma, a progressive form of blindness characterised by the degeneration of retinal ganglion cells. Mutations in *OPTN*, the gene encoding optineurin, were found in 16.7% of families affected by a dominant-negative form of primary open angle glaucoma (Rezaie et al. 2002).

1.1.6. Rodent models of amyotrophic lateral sclerosis

Though the symptoms and histopathological patterns of neuronal loss and protein aggregation seen in ALS are well defined, the mechanisms underlying this damage are poorly understood. This is due in part to modern medicine allowing patients to be supported until late into disease progression. Consequentially most post-mortem neuronal tissue is in a highly degenerate condition when examined. This gap in knowledge can be overcome through the study of animal models of ALS, in particular models developed in the mouse, with its central nervous system (CNS) relatively homologous to that of humans. The identification of heritable mutations has allowed the development of numerous lines of mice expressing increased levels or null for ALS linked genes. In such model systems ALS pathology can be observed from its earliest, pre-clinical stages, and followed through to complete penetrance of disease.

SOD1

Several lines have been generated expressing high levels of wild type and mutant forms of SOD1. Though overexpression of wild type SOD1 does not consistently induce a ALS-like phenotype (Ceballos-Picot et al. 1991; Epstein et al. 1987; Gurney et al. 1994; Jaarsma et al. 2000), transgenic mice overexpressing gain-of-function mutations $SOD1^{G93A}$ (Gurney et al. 1994) and $SOD1^{G85R}$ (Bruijn et al. 1998) under the control of its endogenous human promoter develop substantial neurodegeneration and are currently the most commonly studied and best-characterised models (reviewed in Kanning et al. 2010). Both lines of mice developed classic murine motor neuron disease, characterised by weakness in the limbs, first visible in the hind limbs from 3-4 months of age, followed by the involuntary clasping of limbs towards the abdomen (Gurney et al. 1994). At approximately 5-months the limbs of the affected animal become paralysed, resulting in significantly reduced movements. Consequentially normal activity such as feeding and grooming become limited, and the mouse is euthanised, normally during the fifth to sixth month.

Motor symptoms were caused by the progressive loss of motor neuron populations in the spinal cord (Gurney et al. 1994), accompanied by increasing levels of both micro- and astrogliosis (Fischer et al. 2004; Saxena et al. 2009). Substantial slowing of axonal transport (Williamson and Cleveland 1999) was found to lead to accumulation of synaptic vesicles and accumulation of cytoskeletal neurofilament components within the perikaryal cytoplasm (Pun et al. 2006). Fragmentation of the golgi apparatus is also detected early in disease (Mourelatos et al. 1996). In a pattern matching that seen in human cases of ALS, brainstem motor neurons of the occulomotor nuclei were found to be selectively resistant to SOD1 induced dystrophy, whereas other brainstem motor neuron populations were depleted (Ferrucci et al. 2010). Further parallels with human ALS were detected in the selective pattern of motor axon loss, the largest caliber of fibre being considerably more vulnerable to damage than smaller fibres, with significant loss of fibres detectable from as early as P20, suggesting a "dying back" mechanism of motor neuron loss (Bruijn et al. 1998; Fischer et al. 2005; Fischer et al. 2004; Kong and Xu 1998). Furthermore degeneration and disconnection of the largest, fastest-firing fibres from their neuromuscular junctions is one of the earliest detectable events in modeled SOD1 pathology (Frey et al. 2000; Pun et al. 2006). Again the smaller, slower firing fibres do not degenerate until considerably later in disease (Frey et al. 2000; Pun et al. 2006). Sensory phenotype in $SOD1^{G93A}$ mice is limited, though morphological changes have been reported (Guo et al. 2009). In addition to the selective loss of motor neurons, SOD1 mutant mice develop widespread neuronal deposition of SOD1 immunoreactive inclusion bodies, matching in structure to those seen in human ALS (Bruijn et al. 1998). Small inclusions initially develop in the synapses and axonal cytoplasm of affected neurons, spreading over the course of disease to the perikaryal cytoplasm where large inclusion bodies form (Kanning et al. 2010).

Surprisingly however, when restricted to neuronal cell types increased SOD1 expression is insufficient to induce motor neuron loss. When overexpressed in all cell types, $SOD1^{G37R}$ induces an ALS-like

phenotype similar to that seen in $SOD1^{G93A}$ mice (Wong et al. 1995b). Neuron specific overexpression of $SOD1^{G37R}$ under transcriptional control of the neurofilament light chain (NF-L) promoter did not however induce any behavioural abnormalities (Pramatarova et al. 2001). Assessment of spinal cord motor neuron populations found neither loss nor signs of dystrophy. A full complement of motor axons was found in lumbar ventral nerve roots. No protein aggregation was reported. A similar pattern was detected when the overexpression $SOD1^{G93A}$ and $SOD1^{G85R}$ was restricted to neuronal cell types by transcription control under a Thy1 promoter (Lino et al. 2002). Though both proteins were found to accumulate in the soma and axons of motor neurons, no behaviour deficits were recorded and thorough histopathological analysis of the cell bodies, axons and neuromuscular junctions reveal not evidence of pathology. In addition to complimentary evidence obtained from primary cultures of mutant SOD1 expressing motor neurons (Nagai et al. 2007), these data suggest that mutant forms of SOD1 are alone insufficient to induce motor neuron degeneration, and that either the involvement of additional mechanisms beyond protein aggregation or further cell types is critical for motor neuron degeneration. Astrocytes have been suggested as a candidate cell type (Di Giorgio et al. 2007; Nagai et al. 2007), however selective overexpression of $SOD1^{G86R}$ in astrocytes does not lead to motor neuron loss in mice (Gong et al. 2000).

TDP-43

Mouse models aberrantly expressing TDP-43 have recently been developed. The first of these expressed mutant human $TDP\text{-}43^{A315T}$ driven by a prion promoter (Wegorzewska et al. 2009). High levels of $TDP\text{-}43^{A315T}$ were expressed in the CNS and lower levels in other tissues. Mice developed motor neurodegeneration identical to that seen in mutant SOD1 transgenic mice, with premature death occurring at five months. Spinal pools of motor neuron cell bodies and axons were depleted by approximately 20%. Despite high levels of expression, $TDP\text{-}43^{A315T}$ was not detected in inclusion bodies, though large ubiquitin positive structures were observed. Accumulation of ubiquitin followed a pattern similar to that seen in human ALS, with high levels found in spinal motor neurons and selectively in layer 5 of cortical motor regions.

Two further lines of TDP-43 transgenic mice have been developed, expressing high pan-neuronal levels of wild type human TDP-43 driven by a Thy1 promoter (Shan et al. 2010; Wils et al. 2010). As with $TDP\text{-}43^{A315T}$ these mice developed an ALS-like behavioural phenotype associated with the loss of spinal motor neurons and a shift toward smaller caliber axons in the ventral root axons. Immature development of neuromuscular junction and a reduction in muscle fibre size indicated neuromuscular atrophy. In contrast to overexpression of the mutant $TDP\text{-}43^{A315T}$, small intranuclear TDP-43-positive inclusion bodies were detect in spinal motor neurons, as were larger cytoplasmic structure containing both TDP-43 and ubiquitin. Surprisingly a portion of the intranuclear structures also contained FUS/TLS (Shan et al. 2010).

1.2. Parkinson's disease

Parkinson's disease (PD) is the most common neurological motor condition, with a prevalence of 1-2% in people aged over 65 (de Rijk et al. 1997), with an estimated 120,000 people affected in the UK (Parkinson's Disease society). Both idiopathic and familial forms of the disease exist, the latter currently accounting for 5-10% of cases (Lesage and Brice 2009). James Parkinson first described the clinical symptoms of PD in his 1817 publication "An essay on the shaking palsy". Symptoms of both the familial and idiopathic forms of PD include four cardinal clinical signs; resting tremor, bradykinesia, rigidity and postural instability (Stewart 2002). One of the first symptoms of resting tremor to be recognised by patients is generally an involuntary, low frequency, pill-rolling motion occurring between the index finger and thumb of one hand. Over the course of disease progression this resting tremor spreads first to either the other upper limb or the ipsilateral leg and eventually encompasses the entire body, head and torso included. Bradykinesia, the slowing of voluntary movement, manifests in many forms in PD patients. Normal movements become progressively slower with disease, eventually resulting in akinesia, where initiation of voluntary movement is lost. In the final stages of disease progression patients may ultimately become entirely paralysed. Notable features of bradykinesia include the slurring of speech, micrographia (reduction in handwriting size) and the loss of arm movement when walking. Characteristic features of the rigidity seen in PD included difficulty initiating large movement, such as walking, and "cog-wheel" movement of the limbs, where by smooth movements become disjointed. The effects of slowing of movement and tremor lead to further deficits in postural stability, gait and balance. PD patients typically develop a hunched posture and reduced stride length, resulting in a characteristic shuffling gait. Motor symptoms are often accompanied by non-motor symptoms including sleep disturbance, depression and in some cases cognitive impairment and dementia (Stewart 2002).

1.2.1. Histopathology of Parkinson's disease

The clinical symptoms of both idiopathic and familial PD are associated with a common pattern of pathophysiological changes seen in most, but not all cases. The discovery by Fredrick Heinrich Lewy in 1912 of "Lewy bodies" within the brainstem of PD patients demonstrated a defining feature of the disease. Lewy bodies are large, eosinophilic structures composed of densely packed, filamentous protein found in the perikaryal cytoplasm. Similar structures termed "Lewy neurites" have also been identified in degenerating neurites. The main component of Lewy bodies was found to be the protein alpha-synuclein (Spillantini et al. 1997), the significance of which shall be discussed in much detail below. Lewy bodies have been identified in various regions of the PD brain, including the locus coeruleus (Greenfield and Bosanquet 1953), dorsal vagus nuclei (Wakabayashi et al. 1999) and cerebral cortex (Ikeda et al. 1978) amongst others. Their presence in the substantia nigra pars compacta (SNpc) of PD patients has been most scrutinised due to a second histopathological hallmark of the disease, the loss of catacholaminergic neurons. Substantial numbers of dopaminergic neurons are lost from the SNpc, with post-mortem examination of the brains of PD patients revealing losses of up to 85% (Stewart 2002, the earliest research in the field is discussed by Greenfield and Bosanquet

1953). Many of the remaining dopaminergic neurons appear dystrophic or to contain Lewy bodies. Further neuronal loss has also been reported in regions including the locus coeruleus (van Dongen 1981), raphe nucleus (Halliday et al. 1990) and dorsal vagal nuclei (Gai et al. 1992).

The formation of Lewy bodies and subsequent loss of SNpc dopaminergic neurons provided early evidence of the major functional disruption underlying PD pathology. Research carried out by Ehringer and Horneykiewicz in 1960 identified this dysfunction. Levels of the catecholemines noradrenaline and dopamine were measured in post-mortem brains of control patients and those with postencephalitic or idiopathic PD. Levels of dopamine in the caudate nucleus and putamen of the Parkinsonian groups were found to be reduced by 70-95% (Ehringer and Hornykiewicz 1960). Both the SNpc and caudate-putamen (the latter collectively termed the "dorsal striatum") are nuclei of the basal ganglia, and compose the nigra-striatal pathway, an essential neuronal circuit controlling voluntary movement (Kandel 2000). The striatum is predominantly comprised of GABA-ergic medium spiny neurons. These modulate the activation of movement through two pathways. The direct pathway promotes movement through the inhibition of the internal globus pallidus (GPi), reducing GPi inhibition of the movement promoting activity of the thalamocortical pathway. The indirect pathway inhibits subthalamic nucleus via the enternal globus pallidus (GPe), promoting GPi inhibition of the thalamocortical movement promotion (Kandel 2000). Release of dopamine by axons projecting from the SNpc to the dorsal striatum modulates the activation of the direct and indirect striatal pathways. Dopamine activates the direct pathway through binding to D1-receptors promoting movement, whereas its binding to D2-receptors inhibits the indirect pathway responsible for the inhibition of movement (Kandel 2000). PD is caused by the diminished SNpc stimulation of the striatum, resulting in disinhibition of the indirect pathway. Consequentially the normal reduced inhibition of thalamocortical pathway is lost, leading to unrestricted inhibition of the corticospinal circuitry (Kandel 2000).

The precise mechanism of PD pathology development and progression has yet to be fully elucidated, with both environmental and genetic factors being implicated. The identification of many of these factors has allowed us to develop animal models of PD, as shall be discuss below.

1.2.2. MPTP, pesticides and mitochondrial dysfunction

Several compounds and gene mutations have been linked to development of PD through their ability to disrupt the normal function of the mitochondria, through either the inhibition of the ATP generating electron transfer chain or by making the organelles more susceptible to oxidative stress. The strongest evidence in support of the importance of mitochondria dysfunction in the development of PD was obtained in the early 1980s, when the neurologist J W Langston described six remarkable cases of young people developing devastating advanced stage PD within a matter of weeks (Langston et al. 1983, eloquently documented in his book "The Case of the Frozen Addicts", J W Langston 1995). Langston was presented with six Californian drug users who had self-administered a compound purported to be a new "synthetic heroin", the meperidine analogue 1-methyl-4-phenyl-propionoxy-

piperidine (MPPP). The users reported unexpectedly strong heroin-like sensations upon intravenous administration of the compound. Over the following six weeks the users rapidly developed resting tremors, loss of intelligible speech and developed a gait, followed by paralysis throughout their bodies. Analysis of the compound administered revealed that though it contained a high concentration of MPPP, it was contaminated with approximately 3% 1-methyl-4-phenyl-1,2,3,6-tetrahydropyridine (MPTP). Due to the Parkinsonian nature of their symptoms all patients were treated with L-dopa and dopamine agonists, to which they responded well. In addition to these patients, re-evaluation of available literature identified a similar case where a 23-year old man had injected a meperidine congener, also suspected to have been contaminated with MPTP (Davis et al. 1979).

Investigation of MPTP action in animals has revealed the drug induces toxicity through the highly selective disruption of mitochondrial complex 1 function in the dopaminergic neurons of the SNpc. This analysis was not without early problems. Rats treated with a sample of the compound self-administered by the individual reported in Davis et al. 1979 did not develop any detectable phenotype. Subsequent assessment following the cases reported by Langston et al has shown that rodents are sensitive to MPTP, but have a considerably higher tolerance than primates. Though mice do not develop any Parkinsonian motor symptoms or Lewy body pathology, they have shown significant loss of dopaminergic neurons in the SNpc (Heikkila et al. 1984). Further testing of MPTP has shown this loss of SNpc dopaminergic neurons to be consistent in primates, dogs, guinea pigs, frogs and several other species as well as in the brains of individuals who have self-administered the substance (reviewed in Kopin and Markey 1988).

Thorough assessment of MPTP in these model systems has elucidated the mechanism by which toxicity is induced. The specific cell loss induced by MPTP administration is not caused directly by the molecule, but though its metabolite 1-methyl-4-phenylpyridinium ion MPP^+. The highly lipophillic/hydrophobic nature of MPTP allows it to easily cross the blood brain barrier where it is converted to MPP^+ by monoamine oxidase type B (MAO-B) within glial cells (Chiba et al. 1984; Di Monte et al. 1996). MPP^+ is then selectively taken up into the dopaminergic neurons of the SNpc by the dopamine transporter (DAT) as efficiently as dopamine (Javitch et al. 1985). Once within dopaminergic neurons, MPP^+ accumulates in mitochondria and inhibits NADH dehydrogenase/complex I of the electron transfer chain, resulting in a loss of energy production and increased production reactive oxygen species (Vyas et al. 1986).

Further evidence linking mitochondrial function disrupting compounds with PD was presented by epidemiological studies that linked exposure to pesticides or herbicides with a significant increased risk of developing PD (Gorell et al. 1998; Menegon et al. 1998). Mice systematically infused with rotenone, a commonly used insecticide acting through the inhibition of mitochondrial NADH dehydrogenase/complex 1, developed behaviour deficits accompanied by selective loss of dopaminergic synapses and neuronal cell bodies from the nigra-striatal system (Betarbet et al. 2000).

Inclusion bodies were also observed within dopaminergic neurons of the SNpc (Betarbet et al. 2000), with subsequent analysis detecting alpha-synuclein as a component (Sherer et al. 2003). Concentration of rotenone in the brain was relatively low, resulting in only partial inhibition of NADH dehydrogenase/complex 1. The authors thus speculated that oxidative stress was the likely factor inducing cell death, a hypothesis support by the attenuation of rotenone induced apoptosis by treating cultured dopaminergic neurons with antioxidants (Seaton et al. 1997). Systematic exposure of mice to the naturally occurring herbicide paraquat has also been demonstrated to induce selective loss of nigra-striatal dopaminergic neurons and induce a Parkinsonian phenotype (Brooks et al. 1999). Though the mechanism of toxicity is less clear than that of rotenone, it has been speculated that paraquat also induces oxidative stress through disruption of mitochondrial complex 1 activity (Dinis-Oliveira et al. 2006).

Finally, rare autosomal recessive mutations have been identified in the genes encoding DJ-1 and PINK1 (Bonifati et al. 2003a; Bonifati et al. 2003b; Valente et al. 2004). The precise function of these proteins is ill defined, though both have been found to associate with mitochondria and appear to play a role in protection of the organelles against damage induced by oxidative stress (Bonifati et al. 2003b; Valente et al. 2004). DJ-1 has recently been demonstrated to attenuate the effects of oxidative stress induced by dopaminergic neurons (Guzman et al. 2010). Both DJ-1 and PINK1 have been demonstrated to protect mitochondria against rotenone induced fragmentation, leading to speculation that both might be involved in the same process protecting against oxidative damage (Thomas et al. 2010). It thus seems feasible their loss of their function through mutation might contribute to the development of PD.

1.2.3. Disruption of the ubiquitin proteasome system

The aberrant deposition of protein into Lewy bodies has led to speculation that disruption of the neuronal protein degradation pathways might be responsible for the underlying toxicity (McNaught et al. 2001). This hypothesis was given support by the identification of several autosomal recessive mutations identified in two genes encoding components of the ubiquitin proteasome system (UPS).

The UPS is responsible for the degradation of damaged, misfolded and sort-lived proteins. At the centre of the UPS is the ATP-dependent 20S proteolytic core particle of the proteasome, which degrades large proteins into small fragments. A highly specialised structure, the 20S core is composed of a cylindrical structure of two core heptameric rings of proteolytic β-subunits, the access to which is gated by two heptameric outer rings of α-subunits (Groll et al. 2000). Two mechanisms of protein degradation are mediated by the proteasome. Ubiquitin independent degradation utilises just the 20S proteolytic core particle. The second more complex process of ubiquitin depended degradation allows for the tightly regulated targeting of proteins for proteosomal degradation. For ubiquitin-dependent degradation, the cylindrical 20S core particle co-assembles with two additional 19S regulatory particle "lids", forming a structure termed the "26S proteasome" (Voges et al. 1999). The 19S regulatory

particles carry out a number of functions, including facilitating the unfolding of proteins for access to the proteosome, but more importantly restrict the access of proteins to the catalytic core to those labelled with ubiquitin (Voges et al. 1999). Proteins are targeted for 26S-mediated degradation by the activity of three of enzymes. Briefly, monomeric ubiquitin is activated by E1 enzymes and transferred to an ubiquitin-conjugating E2 enzyme. An E3 ubiquitin-ligase then facilitates the covalent binding of the C-terminal of the activated ubiquitin molecule to a lysine residue of the target protein. Successive rounds of ubiquitination produce a branched poly-ubiquitin chain on the target protein, allowing the 19S regulatory particle to recognise the labelled protein as a substrate for degradation. Following targeting the substrate protein is deubiquitinated and degraded by the 20S core. The separated poly-ubiquitin chain is hydrolysed into subunits that are subsequently reused (McNaught et al. 2001; Pickart 2000).

The ability of a small number of toxins to inhibit normal mitochondrial function was described above. The disruption UPS function by toxic substances has also been proposed as a pathway to development of PD, in part due the natural occurrence of some proteasome inhibitors (Kisselev and Goldberg 2001). In 2004, McNaught et al published data demonstrating that systematic exposure of rats to the synthetic proteasome inhibitor Z-Ile-Glu(OtBu)-Ala-Leu-CHO (PSI) induced a phenotype with remarkable similarity to that seen in human PD (McNaught et al. 2004). Behavioural abnormalities synonymous with nigra-striatal system were visible two weeks after treatment induced. Populations of neurons within the SNpc, locus coeruleus and dorsal vagal nucleus were depleted, as was striatal dopamine release. Lewy-body like inclusion structures were observed throughout the SNpc and locus coeruleus, and were found to contain alpha-synuclein and ubiquitin amongst several other proteins. The remarkable nature of these finding has since become viewed with some caution, due to inconsistent finding by groups replicating the work. Two independent laboratories produced results confirming the work of McNaught et al (Schapira et al. 2006; Zeng et al. 2006). Other groups however found no evidence of pathology, despite every effort to replicate the original study being taken (to the extent of the original authors visiting one group to demonstrate preparation and administration of the PSI) (Bove et al. 2006; Kordower et al. 2006; Manning-Bog et al. 2006). This disparity has been blamed on possible differences in the properties of PSI used, such as potency and solubility, or local environmental factors (McNaught and Olanow 2006).

Genetic modelling has also demonstrated the relevance of the UPS to PD. A phenotype bearing remarkable similarity to PD was described in mice where 26S proteasome formation was selective disrupted through the conditional inactivation of PSMC1, an essential component of the 19S regulatory particle (Bedford et al. 2008). These mice developed substantial loss of SNpc dopaminergic neurons and reductions in striatal dopamine concentration. Lewy-body/pale-body like inclusion bodies containing densely accumulated alpha-synuclein were also present. Though PSMC1 has not been linked to PD pathology, several mutations have been identified in genes coding for components of the UPS. The most common of these mutations are autosomal recessive mutation in *PARK2*, a gene

encoding the E3 ubiquitin-protein ligase parkin (Shimura et al. 1999). Several point mutations and/or deletions result in a loss of normal parkin function (Farrer et al. 2001; Kitada et al. 1998; Mori et al. 1998; Pramstaller et al. 2005; Shimura et al. 2000; Shimura et al. 1999). Mice null for parkin develop deficits in neurotransmitter handling and release in their nigra-striatal system, including increased striatal dopamine content, decreased synaptic vesicle release and increased dopamine metabolism. These changes result in behavioural abnormalities typical of reduced dopamine signalling, such as diminished basal locomotor activity. Loss of SNpc dopaminergic neurons however was not detected (Goldberg et al. 2003; Itier et al. 2003). In addition to these recombinant model animals, mice carrying a spontaneous deletion of parkin were also identified. The "quaking viable" mice develop severe CNS demyelination, increased dopamine metabolism, and reduced locomotor activity (Lockhart et al. 2004).

Genetic analysis has identified a second UPS-associated protein linked to familial cases of PD. Ubiquitin carboxyl-terminal hydrolase L1 (UCH-L1) is one of the most abundant proteins in the brain, accounting for 1-2% of total protein (Wilson et al. 1988). UCH-L1 facilitates neuron specific deubiquitination of proteins and hydrolysis of polyubiquitin chains, though when dimerised the protein has been reported to also carry out the opposing function of ubiquitin ligation (Liu et al. 2002; Wilkinson et al. 1989). Several findings have demonstrated the association of UCH-L1 with PD. Wild type UCH-L1 has been identified as a component of Lewy bodies, though it should be noted these were identified in cases of diffuse Lewy body disease (Lowe et al. 1990). A genetic link was made between UCH-L1 and PD, following the identification of a rare I93M autosomal dominant mutation in a German family with typical PD (Leroy et al. 1998). UCH-L1^{I93M} was associated with a 50% reduction in the proteins deubiquitination activity (Leroy et al. 1998). The authors suggested that the reduced catalytic activity of UCH-L1^{I93M} might result in the accumulation of unidentified ubiquitinated substrates. The association between UCH-L1^{I93M} and PD was corroborated by the development of a line of mice expressing high levels of UCH-L1^{I93M} under the control of the platelet-derived growth factor (PDGF) promoter (Setsuie et al. 2002). These were found to develop a reduction of the SNpc dopaminergic neuron population with age, in addition to a lower concentration of striatal dopamine. Such changes were not detected in a line of UCH-L1^{WT} developed in parallel to the UCH-L1^{I93M} line. In contrast to the increased risk of PD associated with UCH-L1^{I93M}, an apparently protective S18Y polymorphic variant of UCH-L1 has also been identified, associated with a reduced susceptibility to PD (Carmine Belin et al. 2007; Facheris et al. 2005; Maraganore et al. 2004; Wintermeyer et al. 2000). *In vitro* analysis of mutant UCH-L1^{S18Y} found an association with a reduced ability to dimerise, resulting in limited ligase activity, though hydrolysis activity was normal (Liu et al. 2002). These data suggest that the protective action of UCH-L1^{S18Y} might be facilitated through the limiting of the proteins ability to ubiquitinate particular unknown substrates. Interference of UCH-L1 dimerisation may thus be a viable therapy for PD (Liu et al. 2002).

Further evidence of a role for UCH-L1 dysfunction in PD was presented by a line of mice that were found to develop spontaneous gracile axonal dystrophy, termed "GAD mice" (Yamazaki et al. 1988).

Genetic analysis found that these mice carried a sporadic deletion of UCH-L1 coding exons 7 and 8, truncating the catalytic site of the protein (Saigoh et al. 1999). GAD mice develop a sensory ataxia and motor deficits associated with the degeneration of gracile tract of the spinal cord and medulla oblongata and of spinal motor neurons (Saigoh et al. 1999; Wang et al. 2004; Yamazaki et al. 1988). Neurodegeneration of the gracile tract was associated with the formation of ubiquitinated axonal spheroid inclusion bodies (Osaka et al. 2003; Wu et al. 1995), composed of several aggregation prone proteins including amyloid-beta (Saigoh et al. 1999) and synuclein proteins (Wang et al. 2004).

1.2.4. LRRK2 and increased kinase activity

PD associated familial mutations have also been detected in non-mitochodria/UPS associtated proteins. Of these the most prominent are autosomal dominant mutations in leucine rich repeat kinase-2 (LRRK2) (Kachergus et al. 2005; Paisan-Ruiz et al. 2004; Zimprich et al. 2004). Though these mutations represent a particularly common form of familial PD with typical features (Zimprich et al. 2004), the function of LRRK2 in degeneration is poorly defined. LRRK2 is believed to be a GTP-dependent protein kinase, due to the fact it carries several well-defined domains that facilitate protein-protein interaction, including leucine rich repeat, GTPase and a MAPK region (Anand et al. 2009). It has been proposed that changes in this kinase function might be responsible for neurodegeneration in PD.

In vitro studies have demonstrated that several heritable mutations within the domains highlighted above increase the kinase activity of LRRK2 (Gloeckner et al. 2006; Smith et al. 2006; Smith et al. 2005; West et al. 2007). More so, LRRK2 kinase activity promoting mutations, including G2019S and R1441C, have been found to induce degeneration of neurons *in vitro* (Greggio et al. 2006; Smith et al. 2006). A role for LRRK2 kinase activity in promoting dopamine release was reported following the investigation of a line of mice expressing high levels of wild type LRRK2 under transcriptional control of a bacterial artificial chromosome (BAC) (Li et al. 2010). Evoked dopamine release experiments found $LRRK2^{WT}$ overexpressing mice had increased release of striatal dopamine. This change in dopamine handling was associated with both hyperactivity and enhanced performance in behavioural tests. These changes in motor function were found to be ameliorated in mice expressing knocked-in mutant $LRRK2^{R1441C}$ (Tong et al. 2009) or overexpressing high levels of $LRRK2^{R1441G}$ (Li et al. 2010) and $LRRK2^{G2019S}$ (Li et al. 2009), though deficits in dopamine handling were detected. These included reduced striatal dopamine content, decrease dopamine uptake, reduced vesicle release and an absence of locomotor activity increase following treatment with amphetamine (Li et al. 2010; Tong et al. 2009). Changes in striatal dopamine were not detected in mice null for LRRK2 (Andres-Mateos et al. 2009; Tong et al. 2010), though interestingly alpha-synuclein was found to accumulate in the kidneys of affected animals (Tong et al. 2010).

1.3. Alpha-synuclein

Of all genes, mutations and proteins associated with the development of PD, alpha-synuclein has become the most intensely studied. Several mutations have robustly linked the gene encoding alpha-synuclein to PD, as well as several other neurodegenerative disorders. Furthermore alpha-synuclein is a major component of the Lewy bodies seen in PD. To provide context for this thesis the characteristics of alpha-synuclein, and the small family of synuclein proteins of which it is a member, shall be described in more detail. Both the normal function of the synucleins and their known roles is disease shall be discussed.

Alpha-synuclein is the most studied member of a small family of conserved presynaptic proteins consisting of three members; alpha-, beta- and gamma-synuclein. Alpha-synuclein was first identified in the cholinergic presynaptic nerve terminals of the Pacific electric ray *Torpedo californica* (Maroteaux et al. 1988) and found to consist of a 143-residue, 17.5kDa protein, containing six imperfect repeats of an 11-residue unit with a hydrophilic core motif of Lys-Thr-Lys-Glu-Gly-Val (KTKEGV), and a hydrophobic C-terminus (Maroteaux et al. 1988). The homologous human alpha-synuclein protein is coded for by the six-exon *SNCA* gene, located on chromosome 4q21.3-q22 (Spillantini et al. 1995; Touchman et al. 2001). The protein has been found to be highly conserved in vertebrate evolution, with the rodent and zebrafinch proteins showing 95 and 86% homology to human respectively, with the most frequent variation found in the hydrophobic C-terminus (George et al. 1995; Goedert 1997; Maroteaux et al. 1988; Ueda et al. 1993). Alpha-synuclein has been predominantly associated with CNS presynaptic terminals and their vesicles, including those of the cerebral cortex, hippocampus, amygdala and olfactory tubercle (George et al. 1995; Iwai et al. 1995; Jakes et al. 1994).

1.3.1. Alpha-synuclein structure

Alpha-synuclein carries several distinct morphological features. Though less well conserved between species than the N-terminus, the acid and hydrophobic nature of alpha-synucleins C-terminus remains consistent (Maroteaux et al. 1988). N-terminal residues 1-102 are able to interact and bind lipid membranes, an ability that can be disrupted by the introduction of charged residues (Perrin et al. 2000). This ability correlates with the localization of alpha-synuclein to presynaptic terminal vesicles, suggesting that the protein may act in synaptic processes such as vesicle release (George et al. 1995; Iwai et al. 1995; Jakes et al. 1994). Alpha-synuclein resides in a "natively unfolded" conformation when in solution, lacking typical secondary structural features such as a hydrophobic core (Weinreb et al. 1996), though the N-terminus has been found to have a slight helical tendency (Eliezer et al. 2001). When bound to lipid membranes the N-terminus takes on a more helical conformation, though the C-terminus retains its disordered morphology (Eliezer et al. 2001; Sung and Eliezer 2007). The intrinsically disordered nature of alpha-synuclein leaves many hydrophobic residues exposed, and thus it has been attributed to the protein's high propensity to aggregate (Weinreb et al. 1996, see below). One region in particular, the 35-residue non-amyloid-β component (NAC), contains a high concentration of hydrophobic residues and is found to interact with the acidic C-terminus (Sung and

Eliezer 2007). A fragment of the NAC has been identified in 10% of the amyloid-plaques typical of Alzheimer's disease (Han et al. 1995; Ueda et al. 1993).

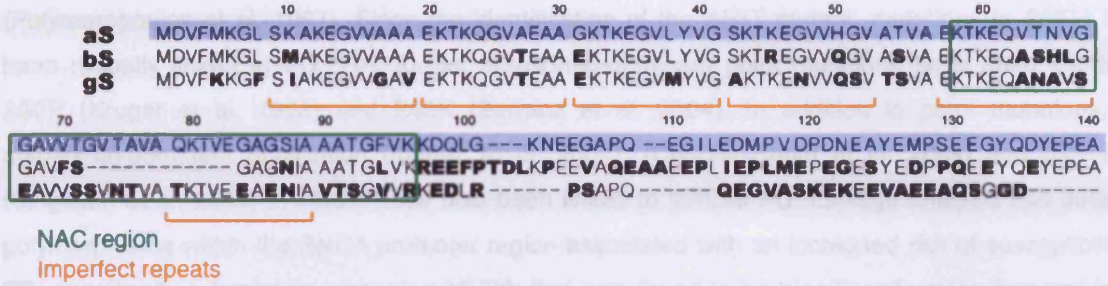

The amino acid sequences of alpha- beta- and gamma-synuclein. Blue highlighting = alpha-synuclein; Green = non-amyloid component region; Red = imperfect KTKEGV repeat motifs (adapted from Sung and Eliezer 2007).

1.3.2. Alpha-synuclein function

The normal physiological role of alpha-synuclein is yet to be fully elucidated. A vast number of proteins have been claimed to interact with alpha-synuclein, though the evidence supporting many of these is limited (reviewed in Dev et al. 2003). Research focused on the dopaminergic system has suggested the protein might play a role in regulation of dopamine production. Alpha-synuclein was found to co-immunoprecipitate with tyrosine hydroxylase (TH) in rat brain homogenate and stable dopaminergic MN9D cells (Perez et al. 2002). Concentration of dopamine in the MN9D cells moderately overexpressing alpha-synuclein was found to be reduced, due not to increased dopamine degradation, but to an increased proportion of a less active non-phosphorylated form of TH. A yeast two-hybrid study also demonstrated the ability of alpha-synuclein to interact with the dopamine transporter (Lee et al. 2001). Overexpression was also found to increase the concentration and activity of the dopamine transporter (DAT) on the membrane of cultured HEK293 cells (Lee et al. 2001). Due to the predicted lipid binding morphology of the N-terminus of alpha-synuclein, association between the protein and presynaptic vesicles was made soon after its discovery (George et al. 1995; Jakes et al. 1994). The most compelling evidence supporting a normal function of alpha-synuclein has come from investigation of its role in synaptic function, particularly the release of synaptic vesicles. Much of this has been carried out in synuclein-null mouse models and shall be discussed below.

1.3.3. SNCA, mutations and Parkinson's disease

Interest in alpha-synuclein exploded in 1997 following the publication of two seminal works of PD research, demonstrated that changes in alpha-synuclein were associated with both idiopathic and familial forms of the disease. In the first of these studies, an autosomal dominant mutation in the *SNCA* gene was identified in a large Italian family and three smaller Greek families with a relatively

early onset form of familial PD (Polymeropoulos et al. 1997). A single base pair substitution of guanine 209 to adenine resulted in the coding of threonine as position 53 instead of the wild type alanine (*SNCA*^{A53T}). This variation was predicted to disrupt the regions normal alpha-helical structure and extend an adjacent beta-sheet region, resulting in a protein with a more aggregation prone structure (Polymeropoulos et al. 1997). Since the identification of the A53T mutant, mutations in *SNCA* have been robustly linked to PD. Two further autosomal-dominant point mutations have been identified, A30P (Kruger et al. 1998) and E46K (Zarranz et al. 2004). In addition to point mutations, the autosomal-dominant duplication (Ibanez et al. 2004); (Chartier-Harlin et al. 2004) and triplication (Singleton et al. 2004) of SNCA have also been linked to familial PD. Linkage analysis has detected polymorphisms within the SNCA promoter region associated with an increased risk of susceptibility to PD, specifically a haplotype spanning 15.3kb that was found to be significantly more frequent in PD patients (Pals et al. 2004). The most robust genetic evidence of alpha-synucleins role in PD has come from four recently completed genome wide association studies. (Edwards et al. 2010; Pankratz et al. 2009; Satake et al. 2009; Simon-Sanchez et al. 2009). Sample groups made up of individuals of European (Edwards et al. 2010; Pankratz et al. 2009; Simon-Sanchez et al. 2009) or Asian ancestry (Satake et al. 2009), with familial forms of PD of unidentified genetic origin, were assessed for genetic association with the disease. Prior to investigations, individuals carrying known PD associated mutations were removed from the sample groups. In addition to SNPs previously identified in known PD risk loci, including genes encoding microtubule associated tau (Edwards et al. 2010; Pankratz et al. 2009; Simon-Sanchez et al. 2009) and LRRK2 (Satake et al. 2009), each of the four studies independently identified several SNPs reaching genome wide significance within the SNCA locus. The significance of several of the SNPs identified was further confirmed by replication of the GWAS in additional sample groups (Satake et al. 2009; Simon-Sanchez et al. 2009).

1.3.4. Alpha-synuclein aggregation and synucleinopathy diseases

A second major development in PD research was the identification of alpha-synuclein amyloid fibrils as a key component of Lewy bodies (Spillantini et al. 1997). Analysis of SNpc post mortem tissue collected from six cases of idiopathic PD revealed dense staining of alpha-synuclein within cytoplasmic and extracellular Lewy bodies. The localization of alpha-synuclein within Lewy bodies in PD has been robustly demonstrated by countless groups and is now considered a hallmark histopathological feature of the disease. In addition to PD, alpha-synuclein positive inclusion bodies have been identified in several other neurodegenerative disorders, all of which are characterised by neuronal and/or glia protein aggregation. Collectively termed "synucleinopathies" these disorders include dementia with Lewy bodies (Galvin et al. 1999; Spillantini et al. 1998b; Spillantini et al. 1997), multiple system atrophy (Gai et al. 1998; Spillantini et al. 1998a; Tu et al. 1998), Lewy body variant of Alzheimer's disease (Lippa et al. 1998) and Hallervorden-Spatz syndrome (Galvin et al. 2000; Tu et al. 1998).

In vitro research of alpha-synuclein protein has further confirmed the link between alpha-synuclein and Lewy body formation, and also offered some insight into the mechanism underlying synucleinopathy pathogenesis. Both wild type and mutant proteins readily aggregate in solution and form fibrils similar to those seen in human disease (Conway et al. 1998). The rate of this aggregation is depended on several factors, including temperature, agitation, buffer composition, concentration and protein species (Conway et al. 1998; Uversky et al. 2001; Uversky et al. 2002). Alpha-synuclein aggregation followed a classical nucleation or "seeding" mechanism of fibrilisation in solution, where by a lag period occurs prior to fibril formation, during which small oligomeric seeds form onto which fibrils develop (Uversky et al. 2002). The A53T and A30P mutant variants have been demonstrated to have greater propensity to form fibrous structures than the wild type protein, with the A53T mutant form aggregating most efficiently (Conway et al. 1998; Narhi et al. 1999). It is thus feasible that familial mutations that alter the morphology of alpha-synuclein (Kruger et al. 1998; Polymeropoulos et al. 1997; Zarranz et al. 2004) or increase the intracellular concentration of the protein (Ibanez et al. 2004; Chartier-Harlin et al. 2004; Singleton et al. 2004), result in the promotion of alpha-synuclein protein aggregation leading to the generation of toxic protein species.

The mechanism by which aggregation induces toxicity, if at all, is the source of debate. In particular the question of whether Lewy bodies are toxic or the result of an intrinsic mechanism to protect the neuron from hazardous intermediate species remains to be answered (Tompkins and Hill 1997). The latter hypothesis is supported by both lack of Lewy body pathology in some cases of familial PD and in transgenic alpha-synuclein mice with clear evidence of degenerative changes in their nervous system (see below, (Hardy 2010; Masliah et al. 2000) and conversely by the detection of Lewy bodies in the brains of individuals with no evidence of neurodegenerative disease of any sort (Goldberg and Lansbury 2000). There are several possible route by which alpha-synuclein may produce large structures such as Lewy bodies, some of which require the formation of intermediate structures which may include small oligomers, pore-like structures and protofibrils. The concentration of such oligomeric forms of alpha-synuclein is significantly elevated in post-mortem cerebrospinal fluid of PD patients (El-Agnaf et al. 2006). Wild type, A53T and A30P forms of alpha-synuclein have been shown to produce both pores and protofibrils, with the mutant forms forming such structures with greater efficiency than the wild type (Conway et al. 2000; Lashuel et al. 2002; Li et al. 2001). The pore-like annular protofibrils structures were demonstrated to be able to bind synthetic phospholipid membranes resulting in the formation of aberrant channels (Lashuel et al. 2002). Protofibrils have similarly been found to bind to and permeabilise membranes (Volles et al. 2001). Such disruption of membranes may have serious consequences on the health of the neuron, for example it might cause changes in calcium homeostasis through leakage of extracellular calcium (Kawahara and Kuroda 2000). Alternatively, permeabilisation of synaptic vesicles in dopaminergic presynaptic terminals would lead to increased concentration of free cytoplasmic dopamine, which is toxic and causes oxidative damage of synapses (Chen et al. 2008).

Finally much research regarding the ability of alpha-synuclein aggregation to induce neuronal toxicity has been carried out in transgenic mice expressing high levels of wild type or mutant SNCA. This data shall be discussed below.

1.4. Beta synuclein

Following the discovery of alpha-synuclein, a second synuclein protein was identified in humans (Jakes et al. 1994). A 134-residue protein sharing 61% homology (Goedert 1997) and similar anatomical distribution to human alpha-synuclein was identified in the tissue of healthy and Alzheimer's disease afflicted human brains (Jakes et al. 1994). This protein shared homology with a previously identified, KTKEGV motif containing protein termed PNP14, identified in bovine brain, rodents, chickens, frogs and fish (Nakajo et al. 1993). Due to the high level of homology between PNP14 and alpha-synuclein, the protein was renamed beta-synuclein (Jakes et al. 1994). The beta-synuclein gene *SNCB*, mapped to chromosome 5q35, is relatively homologous to *SNCA* being composed of 6 exons, five of which are coding (Lavedan et al. 1998c; Spillantini et al. 1995). The most notable difference between SNCA and SNCB is the truncation of exon 4 in the latter. This results in an eleven-residue deletion in the transcribed protein that encompasses a large portion of the NAC region and a KTKEGV motif that would be present in alpha synuclein (Sung and Eliezer 2007; Ueda et al. 1993). The free-state secondary structure of beta-synuclein is thus less organised than that of alpha-synuclein, being less helical and more random-coil like (Sung and Eliezer 2007). Due to the disruption of the negatively charged NAC region, interaction between the acidic C-terminus and N-terminus of beta-synuclein is negligible (Sung and Eliezer 2007).

1.4.1. Beta-synuclein aggregation

As a result of structural differences, beta-synuclein possesses a propensity to aggregate far limited compared to that of alpha-synuclein (Park and Lansbury 2003; Uversky et al. 2002). At a neutral, physiological pH, beta-synuclein was incapable of producing stable oligomers, even after several weeks of incubation, in contrast to alpha-synuclein that forms aggregate structures within a matter of hours (Uversky et al. 2002). Furthermore beta-synuclein was not found to produce the oligomeric pore-like structures formed by alpha-synuclein (Park and Lansbury 2003). The contrasting *in vitro* behaviour of alpha- and beta-synuclein was most notably demonstrated following investigation of their ability to interact with one another in solution. Beta-synuclein was found to inhibit the aggregation of alpha-synuclein in solution. A 1:1 ratio of alpha- to beta-synuclein led to significant retardation of alpha-synuclein fibrilisation, with fewer aggregates being produced though significantly slower aggregation kinetics. Increasing the proportion of beta-synuclein to 4:1 was found to almost entirely block alpha-synuclein fibrilisation (Uversky et al. 2002). Both the inability of beta-synuclein to aggregate and its ability to disrupt alpha-synuclein aggregation *in vitro* appear to be paralleled *in vivo.* Animal models of wild type beta-synuclein overexpression have failed to induce a phenotype comparable to that seen in alpha-synuclein overexpression models. Remarkably, modeling in rodents has also revealed that the disruption of alpha-synuclein aggregation by beta-synuclein occurs *in vivo*,

and results in a significantly attenuated phenotype (Fan et al. 2006; Hashimoto et al. 2001). Findings from these models of beta-synuclein overexpression shall be discussed in further detail below.

1.4.2. Beta-synuclein and disease

Beta-synuclein is not considered a normal component of any common inclusion bodies such as Lewy bodies, and has only very rarely been detected in atypical structures. Rare examples of such structures have been identified in cases of PD, Lewy body dementia and Hallervorden-Spatz syndrome, where axonal spheroids containing beta synuclein were reported (Galvin et al. 2000; Galvin et al. 1999). Genetic analysis has determined that mutations in *SNCB* are unlikely to be a common contributing factor in human disease. No mutations in *SNCB* have been associated with PD (Lavedan et al. 1998a). Two rare mutations have however been associated with another synucleinopathy, dementia with Lewy bodies, though their role in the disease is highly unclear (Ohtake et al. 2004). The mutations, V70M and P123H, are both contained within a highly conserved region of beta-synuclein and were predicted to cause significant alteration of structure. Surprisingly however, though alpha-synuclein positive Lewy bodies were present in the brain of the $SNCB^{P123H}$ patient, the mutation did not result in accumulation of beta-synuclein. It was thus predicted that these mutations represented an increased risk factor for dementia with Lewy bodies, most likely acting through loss of a protective mechanism mediated by beta-synuclein, for example the disruption of alpha-synuclein aggregation. Animal modeling of P123H mutant beta-synuclein overexpression have however suggested that this hypothesis may be untrue and shall be discussed below.

1.5. Gamma-synuclein

The last identified and least studied member of the synuclein family is gamma-synuclein (Buchman et al. 1998b; Ji et al. 1997; Lavedan et al. 1998b). The human gamma-synuclein gene SNCG consists of ~5kbp, composing 5-coding exons (Lavedan et al. 1998b; Ninkina et al. 1998). In contrast to alpha- and beta-synucleins, the 10q23 gamma-synuclein locus does not contain non-coding exons, though regions of exon-intron junction remain homologous (Lavedan 1998). The expressed protein is highly conserved in vertebrate evolution, with the human protein sharing approximately 68% homology with that of the chordata lamprey (Petromyzon marinus). Comprising of 127 amino acids, gamma-synuclein shares 55.9% homology with alpha-synuclein and 54.3% with beta-synuclein (Lavedan et al. 1998b). The acidic C-terminus of gamma-synuclein is the most diverse region, the N-terminus carrying both the six copies of the KTKEGV repeat motif and full NAC region found in alpha-synuclein (Lavedan et al. 1998b). The free-state residual secondary structure of gamma-synuclein has a tendency to form helical structures and thus is more similar to alpha-synuclein than the more random-coil structure of beta-synuclein (Sung and Eliezer 2007). The transient lipid-bound structure however is more comparable to beta-synuclein (Sung and Eliezer 2007).

1.5.1. Gamma-synuclein cellular distribution

As well as being structurally distinct from alpha- and beta-synuclein, both the anatomical expression profile and intracellular compartmentalisation of gamma-synuclein are also markedly different. The development and postnatal expression of both alpha and beta-synuclein is predominantly restricted to the brain, whereas gamma-synuclein is found in select populations of CNS neurons (Buchman et al. 1998b). These include lower motor neurons in the spinal cord and brain, sensory neurons of the dorsal root and various cranial ganglia, upper motor neurons in the cerebral cortex and dopaminergic neurons of the SNpc (Buchman et al. 1998b; Ninkina et al. 2003). Moreover, the intracellular compartmentalisation of alpha- and beta-synuclein is restricted to the presynaptic terminals of neurons, where as gamma-synuclein is found diffusely throughout the cytoplasm of the synapses, neurites and cell bodies. During the development of mice (E13), gamma-synuclein protein initially localised to the perikaryal cytoplasm, however by E18 compartmentalisation shift to both the perikaryal and axonal cytoplasm of motor and sensory neurons (Ninkina et al. 2003). Post-natal localization remains consistent in sensory populations, however differs slightly in motor neuron populations, with little protein remaining in the perikaryal cytoplasm (Ninkina et al. 2003). Post-natal cortical expression of gamma-synuclein increases with age, in contrast to the decreasing expression of alpha-synuclein (Buchman et al. 1998b).

Gamma-synuclein has also been identified in non-neuronal cell populations, though its function within these cells is unclear. Both *SNCG* mRNA and gamma-synuclein protein have been identified within the stratum granulosum of the skin of embryonic and post-natal mice (Ninkina et al. 1999). Gamma-synuclein is present in the white adipose tissue of mammals and in humans its expression is increased in obese individuals (Oort et al. 2008). The relationship between gamma-synuclein and diet induced obesity is currently being investigated by our laboratory (manuscript in preparation). Much interest in gamma-synuclein has also come from the proteins identification as a marker of malignant breast carcinomas, leading to it initially being named breast cancer specific gene 1 (*BCSG1*) (Ji et al. 1997). Though this nomenclature is no longer in use, gamma-synuclein up regulation has become associated with numerous further forms of cancer, including ovarian, cervical, colon, gastric, prostate and lung (Bruening et al. 2000; Ji et al. 1997; Liu et al. 2010; Liu et al. 2005). Unfortunately current opinion regarding the function of gamma-synuclein in oncological diseases is mostly conjecture. Discussion of these data is beyond the scope of this thesis, though interested readers may refer to a review published by Ahmad et al. 2007.

* * *

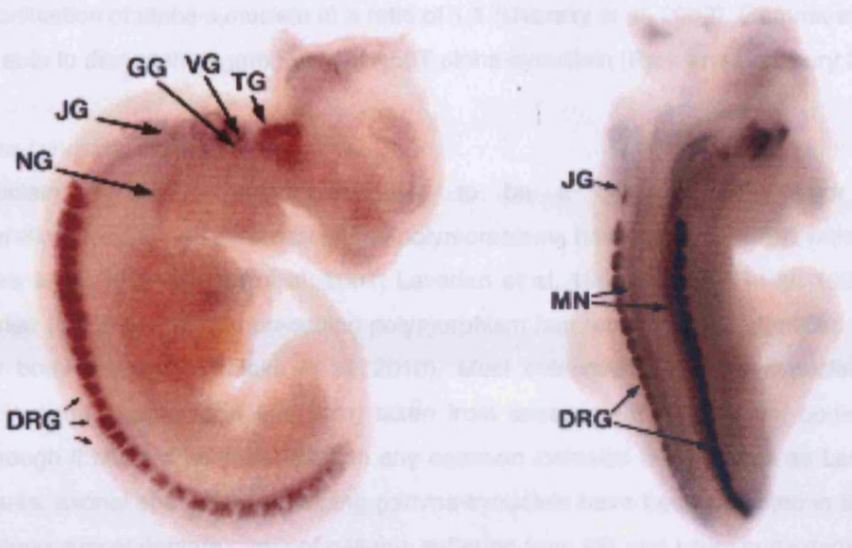

Gamma-synuclein expression in the developing mouse CNS. *In situ* hybridization with DiG labeled probes against *SNCG* mRNA show expression of gamma-synuclein in whole mounted E11 mouse embryos. DRG = dorsal root ganglion; GG = geniculate ganglion, JG = jugular ganglion, MN = spinal cord motor neurons, NG = nodose ganglion, TG = trigeminal ganglion, VG = vestibular ganglion (Image taken from Buchman et al. 1998b).

* * *

1.5.2. Gamma-synuclein function and aggregation

Though the anatomical and intracellular localization of gamma-synuclein is well defined in the CNS, very little is known with regard to the normal physiological function of the protein. Acute overexpression of *SNCG* was not found to induce death in cultured sensory neurons (Buchman et al. 1998a). Interestingly however, overexpression was found to cause disruption to the cytoskeleton of approximately 80% of these neurons. Immunohistochemical staining of these cultured detected decreased staining of neurofilaments-H, -L and –M. Such changes were not detected in the levels of microtubules, actin or peripherin. Western blot analysis revealed a smear of small polypeptides of NF-H, though not –L or –M. Addition of calpeptin, an inhibitor of the calcium-dependent calpain class of protease, blocked the degradation of the neuronal cytoskeleton. It was proposed that gamma-synuclein may play a currently unidentified role in human neurodegeneration, influencing the health of neurons by disrupting the stability of their neuronal cytoskeleton.

Cell-free investigation of the aggregation kinetics of gamma-synuclein also suggests the protein might have a role in human disease. Though less efficient than alpha-synuclein, gamma-synuclein is able to form stable oligomers and protofibrils in solution (Park and Lansbury 2003; Uversky et al. 2002). Analysis of the fibrils formed by gamma-synuclein by electron microscope found them to be identical in appearance to those formed by alpha-synuclein (Uversky et al. 2002). Surprisingly however gamma-synuclein appeared to also share a defining characteristic of beta-synuclein, being able to efficiently

disrupt the fibrilisation of alpha-synuclein at a ratio of 1:1 (Uversky et al. 2002). Gamma-synuclein was not however able to disrupt the aggregation of A53T alpha-synuclein (Park and Lansbury 2003).

1.5.3. Gamma-synuclein in disease

Gamma-synuclein is not currently considered to be a common risk factor in human neurodegeneration. No PD and ALS associated polymorphisms have been detected within the SNCG locus (Flowers et al. 1999; Kruger et al. 2001; Lavedan et al. 1998a; Lincoln et al. 1999), though it should be noted that a significant non-coding polymorphism has recently been identified in a study of diffuse Lewy body disease (Nishioka et al. 2010). Most evidence of gamma-synuclein's possible involvement in neurodegeneration has been taken from assessment of inclusion bodies in human disorders. Though it has not been detected in any common inclusion bodies such as Lewy bodies or amyloid plaques, axonal spheroids containing gamma-synuclein have been detected in the molecular layer of the hippocampal dentate gyrus of patients suffering from PD and Lewy body dementia (Galvin et al. 1999), and also in the mid-frontal and cingulated gyrus of Hallervorden-Spatz syndrome patients (Galvin et al. 2000). Axonal spheroids positive for gamma-synuclein have also been detected in the mouse models of neurodegeneration, in particular GAD mice (see above), where eosinophilic spheroids positive for gamma-synuclein were detected in the degenerating spinal gracile tract and nucleus (Wang et al. 2004).

The most robust evidence of the involvement of gamma-synuclein in human neurodegeneration has come from studies of glaucoma, the second most frequent cause of permanent blindness, characterised by an increased intraocular pressure and the substantial loss of retinal ganglion cells (RGCs) and the portion of their axon within the optic nerve (Quigley and Broman 2006). Gamma-synuclein is specifically expressed in both adult and developing RGCs, compartmentalising in the perikaryal and axonal cytoplasm (Farkas et al. 2004; Mu et al. 2004; Surgucheva et al. 2002; Trimarchi et al. 2007). *SNCG* expression in RGCs is promoted by Brn3B, a transcription factor essential for their normal differentiation and development (Mu et al. 2004). A distinct change has been reported in gamma-synuclein expression in patients with glaucoma, the normal localisation seen in RGC axons becoming diminished (Surgucheva et al. 2002). More so, a subset of astroglia within the *lamina cribrosa* portion of the optic nerve were found to be aberrantly expressing gamma-synuclein and contained atypical inclusion bodies positive for the protein (Surgucheva et al. 2002). Similar changes have been reported in animal models of glaucoma. Astrocytes containing atypical cytoplasmic inclusion bodies positive for gamma-synuclein were reported in rats with mechanically increased IOP (Surgucheva et al. 2002). In DBA/2J mice, a strain that spontaneously develop glaucoma, a progressive down regulation of *SNCG* expression has been reported, correlating with the progressive loss of RGCs (Buckingham et al. 2008). Spheroid inclusion bodies containing gamma-synuclein have however been identified in these animals (Nguyen et al. 2011), suggesting the down regulation might occur in response to the proteins accumulation. Decreased expression correlated with the loss of retrograde labelling in individual cells, suggesting the disconnection of the RGCs with their

targets within the cortex (Soto et al. 2008). Decreased mRNA expression in the RGCs of DBA/2J mice was not however restricted to *SNCG*, appearing to be a general early process of pathology. Furthermore many RGCs were found to continue expressing gamma-synuclein after becoming disconnected from their neurites, suggesting its loss was not an essential event in degeneration.

1.6. Synuclein knock out mouse models

Attempts to characterise the function of the synuclein proteins in both normal physiology and pathophysiology have led to the generation of several lines of knock out and transgenic mice.

1.6.1. Alpha-synuclein null mice

Knock out mouse models of all three synuclein proteins individually and in all possible combination have been developed by various laboratories. Due to its identification in PD pathogenesis, alpha-synuclein knock out models were the first to be generated, the earliest described by Abeliovich et al 2000. The mice showed an 18% reduced in striatal dopamine concentration and a reduced locomotion response to amphetamine treatment, suggesting impaired dopamine production and release (Abeliovich et al. 2000). Other groups however have not detected decreased dopamine concentration in the striatum of mice of this line on a pure C57Bl6J genetic background, however modest reduction of SNpc dopaminergic cells has been reported (Robertson et al. 2004). Changes in striatal dopamine concentration were also not detected in other lines of alpha-synuclein null mice (Chandra et al. 2004; Schluter et al. 2003). Further discrepancy to the data reported by Abeliovich et al was detected in alpha-synuclein null mice produced by Cabin et al (2002), which had a normal response to amphetamine treatment. Synaptic function deficits were detected in primary cultured hippocampal neurons derived from alpha-synuclein null animals. These neurons had a reduced reserve pool of synaptic vesicles and showed deficits in synaptic response following repetitive electrical stimulation (Cabin et al. 2002). No changes in the normal behaviour of alpha-synuclein null mice have been reported by any of the above research groups. In summary ablation of alpha-synuclein appears to have only limited to negligible effects on the murine CNS, a point supported by the identification of a commercial line of "wild type" C57Bl6J mice with no behavioural or physiological abnormalities supplied by Harlan UK that we found to carry a spontaneous deletion encompassing the entire SNCA locus (Specht and Schoepfer 2001).

An unexpected characteristic of alpha-synuclein null mice is their reduced sensitivity to the mitochondria inhibitor MPTP (see above). Dauer et al. 2002 showed that alpha-synuclein null mice were almost entirely resistant to both acute and chronic exposure to MPTP. The SNpc population was insignificantly affected in knock out mice, as were striatal dopamine concentrations (Dauer et al. 2002; Robertson et al. 2004). The finding should be treated with some caution, as tolerance to MPTP appears to be dependent on strain differences. Mice carrying a spontaneous deletion of alpha-synuclein were found to be equally vulnerable to MPTP toxicity as wild type control mice (Schluter et

al. 2003). If correct however the above data indicates that the normal physiological function of nigra-striatal alpha-synuclein might lie within the dopamine handling system.

1.6.2. Beta-synuclein null mice

Due to evidence suggesting a possible neuroprotective function possessed by beta-synuclein, SNCB null mice were generated (Chandra et al. 2004). Similar to alpha-synuclein null mice however the beta-synuclein null mice developed no discernable phenotype. The lack of overt phenotype in both alpha- and beta-synuclein null mice was suggested to be due in part to their close structural homology and matching pattern of localization leading to functional redundancy. Chandra et al thus produced mice doubly null for alpha- and beta-synuclein by breeding the individual knock out lines. Though no changes were observed in synaptic morphology, synaptic plasticity, vesicle handling or release in alpha-/beta-synuclein null mice, a modest reduction in striatal dopamine concentration was detected. It was concluded that there might be some degree of functional redundancy between alpha- and beta-synuclein, though the possibility of subtle deficits might occur (Chandra et al. 2004).

1.6.3. Gamma-synuclein null mice

Similar to alpha- and beta-synuclein null mouse lines, endogenous gamma-synuclein null mice develop no overt phenotype (Ninkina et al. 2003). Ablation of gamma-synuclein had no impact upon the size of the neuron populations in which it is normally expressed (Ninkina et al. 2003; Papachroni et al. 2005; Robertson et al. 2004). Behavioural analysis detected neither motor nor sensory deficits. The SNpc dopaminergic neuron population was slightly depleted, though striatal dopamine concentration was found to be normal (Robertson et al. 2004). Similar to alpha-synuclein ablation, gamma-synuclein knock out mice were found to be resistant to MPTP, suggesting some functional homology between the proteins (Robertson et al. 2004). This latter point is supported by the identification of altered expression of a number of overlapping genes in both alpha- and gamma-synuclein knock out mice (Kuhn et al. 2007). The products of several of these genes have been implicated in the modulation of tyrosine hydroxylase activity, including 14-3-3 and MAPK1, and thus changes in alpha- and gamma-synuclein function might have a direct impact upon dopamine production.

1.6.4.Triple-synuclein null mice

Evidence of synuclein family functional redundancy has necessitated the development of mice triply null for all three family members (TKO). Recent collaborative efforts by several groups have led to the generation and study of these animals (Burre et al. 2010; Greten-Harrison et al. 2010, our unpublished findings – in press). During the first year of life TKO appeared indistinguishable from control animals. At the age of ten months however significant deficits in balance, coordination and strength were detected by behavioural analysis (Burre et al. 2010, our unpublished findings – in press). A significant number of mice went on to develop a clasping reflex during the second year (Burre et al. 2010). Subsequently a significant number of TKO mice died a premature death. Significant

neurodegeneration was not reported (Burre et al. 2010; Greten-Harrison et al. 2010; our unpublished findings – in press).

In spite of apparently normal morphology several lines of evidence suggested that subtle changes did occur within the CNS of TKO mice, particularly affecting the function of various synapses. TKO mice carried a full complement of SNpc dopaminergic neurons, however striatal dopamine concentrations were depleted by approximately 40% (our unpublished findings – in press). In contrast to mice individually null for alpha- or gamma-synuclein, TKO mice were found to be as sensitive to exposure to MPTP as control animals (our unpublished finding – in press). Synaptic density, neuronal density and inducible synaptic function in the hippocampus were found to be unchanged in ten-month old TKO mice (Burre et al. 2010). Subtle changes were however detected in the size of the presynaptic terminal in both the CA1 and CA3 regions of three-month old TKO hippocampus, both presenting a significant decrease in area (Greten-Harrison et al. 2010). Deficits in retina function and vision were also noted in aged TKO mice (Greten-Harrison et al. 2010).

The most striking changes in TKO synaptic function were detected in the assembly of the SNARE complexes essential for facilitating vesicle fusion at the presynaptic terminal. From whole brain homogenate of one-month old TKO mice, Burre et al detected a significant 25% reduction in the co-immunoprecipitated levels of the three core SNARE complex components; SNAP25, syntaxin1 and synaptobrevin 2/VAMP. This reduction increased to over 50% in ten-month old mice. The level of synaptobrevin 2/VAMP was significantly reduced in the both age groups of TKO mice (Burre et al. 2010). Contrasting changes in SNARE complex component levels were reported by Greten-Harris et al, who detected a significant 20% increase in levels of synaptobrevin 2/VAMP, but additionally detected a 20% decrease in levels of SNAP25 (Greten-Harrison et al. 2010). Assessment of SNARE complex components in the striatum of four-month old TKO mice however failed to detect any changes in their levels (our unpublished findings – in press). In summary, data from TKO mice suggests the synuclein proteins might play a role in normal presynaptic function in a subset of CNS neurons.

1.7. Synuclein transgenic mice

Several factors have linked aberrant forms of alpha-synuclein with PD; autosomal dominant mutations in SNCA, the increased propensity of mutant protein forms to aggregate and the presence of alpha-synuclein protein in inclusion bodies found in both idiopathic and familial forms of PD. These findings have led to the generation of numerous lines of mice that express high levels of human wild type or mutant forms of SNCA in an effort to unravel the pathophysiology of alpha-synuclein. Several lines of mice were generated expressing varying increased levels of human wild type *SNCA* (h*SNCA*^{WT}) under the transcriptional regulation of the non-specific platelet derived growth factor promoter PDGFβ (Masliah et al. 2000). Alpha-synuclein positive inclusion bodies were detected in all lines produced, most frequently within the cortex, but also observed in the CA3 region of the hippocampus, olfactory bulb and SNpc. Overexpression of PDGFβ-h*SNCA*^{WT} induced a dose-dependent neurodegeneration. Alpha-synuclein positive inclusion bodies were most abundant in the highest expressing line "D". Striatal TH levels, TH activity and striatal dopaminergic terminals were all significantly diminished in the most affected animals, though it should be noted SNpc population size was not investigated. Furthermore behavioural deficits, assessed by rotarod, were only detected in line D.

1.7.1. Alpha-synuclein overexpression: PrP-promoter

Utilising the mouse/hamster prion promoter (PrP), several lines of mice have been generated overexpressing h*SNCA*^{WT} (Giasson et al. 2002; Gispert et al. 2003; Gomez-Isla et al. 2003; Lee et al. 2002) and the human mutants A53T (h*SNCA*^{A53T}) (Giasson et al. 2002; Gispert et al. 2003; Gomez-Isla et al. 2003; Lee et al. 2002) or A30P (h*SNCA*^{A30P}) (Gomez-Isla et al. 2003; Lee et al. 2002) specifically in neurons. In spite of high-level expression, PrP-h*SNCA*^{WT} transgenic mice were consistently found not to develop any perceptible neurodegenerative phenotype (Giasson et al. 2002; Gispert et al. 2003; Gomez-Isla et al. 2003; Lee et al. 2002). PrP-h*SNCA*^{A53T} overexpression induced dose dependent neurodegeneration with signs of defective motor function (Gispert et al. 2003). Accumulation and ionic-detergent insoluble aggregation of mutant alpha-synuclein was detected in the various regions including cerebellum, cortex, pons and spinal cord (Giasson et al. 2002; Lee et al. 2002), though it should be noted one line expressing high levels of PrP-h*SNCA*^{A53T} developed no inclusion bodies (Gispert et al. 2003). Dystrophic axons were detected in the spinal cord and ventral nerve roots of one line of mice (Giasson et al. 2002). High-level expression of h*SNCA*^{A30P} also induced motor dysfunction accompanied with increased CNS astrogliosis, though mutant alpha-synuclein aggregation was not reported (Gomez-Isla et al. 2003).

1.7.2. Alpha-synuclein overexpression: Thy1-promoter

Neuron specific alpha-synuclein overexpression mouse models have also been generated using the Thy1 promoter, a useful promoter since it is activated from P4-10 (Aigner et al. 1995), allowing any changes observed to be attributed to the transgene product. Overexpression of Thy1-h*SNCA*^{WT}, Thy1-h*SNCA*^{A53T} and Thy1-h*SNCA*^{A30P} has been shown to induce neurodegeneration (Chandra et al. 2005; Rockenstein et al. 2002; van der Putten et al. 2000). Thy1 expression was found to produce more

widespread neuronal expression of higher levels of alpha-synuclein than previously seen in the PDGFβ-h*SNCA*^{WT} overexpression model, though it was conceded that the latter model produced a more physiologically relevant pattern of expression (Rockenstein et al. 2002). Overexpression of Thy1-m*SNCA*^{WT} was not found to induce any signs of pathology (Chandra et al. 2005). Thy1-h*SNCA*^{WT} mice however were found to develop somatomotor abnormalities, including deficits in footplacing, co-ordination and strength (Fleming et al. 2004). Inclusion bodies containing alpha-synuclein were widespread in the cortex and striatum (Rockenstein et al. 2002; van der Putten et al. 2000). Investigation of Thy1-h*SNCA*^{WT} transgenic mice did reveal some contrasting data. High levels of wild type alpha-synuclein accumulation have been reported in spinal motor neurons (van der Putten et al. 2000), as has the depletion of spinal motor neuron cell bodies and their neurites (Chandra et al. 2005). No accumulation of alpha-synuclein was detected in neurons of the SNpc (van der Putten et al. 2000). In contrast Rockenstein et al detected substantial accumulation of wild type alpha-synuclein in the SNpc, but found no evidence of protein accumulation in spinal cord motor neurons (Rockenstein et al. 2002). Similar results were detected in the pathology presented in mice overexpressing Thy1-h*SNCA*^{A53T} (Chandra et al. 2005; van der Putten et al. 2000) and Thy1-h*SNCA*^{A30P} (Chandra et al. 2005; Rockenstein et al. 2002). The reason for the discrepancy was unclear, though strain differences were proposed as a potential cause.

1.7.3. Alpha-synuclein overexpression: TH-promoter

Though many of the above alpha-synucleinopathy mouse models result in a movement disorder associated with the accumulation of alpha-synuclein, their use as clinically relevant model of human PD is debatable. The motor deficits developed by these animals were often attributed to spinal cord dystrophy, not considered a normal feature of PD pathology. Clinically relevant levels of nigra-striatal dysfunction or SNpc dopaminergic neuron loss were not reported. Furthermore, though alpha-synuclein inclusion bodies were detected, none of these were reported to possess the hallmark Lewy body structures. Attempts were made to produce more accurate recapitulation of the dopaminergic system dysfunction typical of PD through the generation of mice expressing alpha-synuclein under the control of the dopaminergic neuron specific tyrosine hydroxylase (TH) promoter. The results of these studies have unfortunately been underwhelming. Mice expressing high levels of the wild type, A30P or A53T forms of human alpha-synuclein were not found to develop any signs of overt neurodegeneration or deficits in motor function (Matsuoka et al. 2001). Quantification of SNpc dopaminergic neuron population and striatal dopamine concentration also failed to detect any changes (Matsuoka et al. 2001; Rathke-Hartlieb et al. 2001). An independently produced line of mice expressing wild type human alpha-synuclein under TH-promoter control also failed to develop any detectable phenotype (Richfield et al. 2002). Though specific to dopaminergic neurons, the TH promoter results in relatively weak transgene expression. It appears that such selective and low levels of transgene are insufficient to induce the damage seen in other alpha-synuclein transgenic lines. The most severe synucleinopathy phenotype produced by utilising the TH promoter was observed in a line of mice expressing a doubly mutant form of alpha-synuclein carrying both the A30P and A53T

mutations. In contrast to the wild type and single mutant mice, the TH-h*SNCA*$^{A30P/A53T}$ line developed an age-related decrease in locomotor activity, associated with a reduced concentration of striatal dopamine and loss of SNpc dopaminergic neurons (Richfield et al. 2002; Thiruchelvam et al. 2004). Though a neurodegenerative phenotype was observed, the models can be criticized due to the non-physiologically relevant nature of the mutations. Furthermore these findings were not however seen in a second independently produced line of TH-h*SNCA*$^{A30P/A53T}$ mice, though mitochondria dysfunction was reported (Maskri et al. 2004; Stichel et al. 2007).

In summary, though numerous lines of mice overexpressing alpha-synuclein have been generated, these models all have various faults. To date none of these models result in a phenotype that fully recapitulates all the typical clinical features of PD. The non-specific expression of many of the promoters used often leads to the strongest transgene expression being localised to populations not normally associated with the disease, for example spinal motor neurons. When more selective promoters such as TH are used, alpha-synuclein expression induces little discernable phenotype, suggesting that alpha-synuclein overexpression alone is unlikely to be the sole underlying pathology of PD.

1.7.4. Alpha-synuclein overexpression on an endogenous SNCA null background

The endogenous SNCA alleles have been suggested to confer a degree of protection in transgenic mice expressing high levels of human alpha-synuclein (Cabin et al. 2005). Cabin et al. demonstrated that in comparison to transgenic mice carrying the wild type *SNCA* allele, those null for endogenous SNCA developed a more pronounced pathology when overexpressing PrP-h*SNCA*^{A53T}. Though histopathological signs were similar in both groups of animals, the exacerbated pathology was characterised by an earlier death and accelerated progression of disease. Cabin et al. suggested that the protective effect might be due to disruption of transgenic human alpha-synuclein aggregate seeding by the less aggregate prone endogenous murine protein. The possibility of strain differences was also raised, due to the endogenous alpha-synuclein null animals being derived from a mixed 129/FVB background, where as the *SNCA*^{A53T} transgenic mice were on a more pure FVB/N background.

1.7.5. Alpha-synuclein overexpression on a CSPα null background

SNCA overexpression has been used to elucidate the normal function of alpha-synuclein and have yielded remarkable data. Mice null for CSPα, a presynaptic terminal, vesicle-associated protein with chaperone-like activity (Tobaben et al. 2001), developed an aggressive form of neurodegeneration, associated with stunted development and death by p80 (Fernandez-Chacon et al. 2004). Substantial motor deficits were observed, caused by the progressive degeneration of synapses including neuromuscular junctions (Fernandez-Chacon et al. 2004), associtated with reduced levels of the SNARE complex component SNAP25 (Chandra et al. 2005). In 2005, Chandra et al demonstrated the

surprising finding that both human and mouse *SNCA*^{WT} overexpression were able to rescue CSPα-null mice from neurodegeneration (Chandra et al. 2005). Conversely ablation of alpha- and beta-synuclein exacerbated the CSPα-null phenotype. Interestingly h*SNCA*^{A53T} was also able to ameliorate symptoms, however h*SNCA*^{A30P} was not. Spinal gliosis and neuromuscular junction degeneration were reduced in h*SNCA*^{WT} but not by h*SNCA*^{A30P} groups. Thy1-h*SNCA*^{WT} overexpression partially rescued the defective SNARE complex assembly seen in CSPα-null mice, however this was not achieved through rescue of SNAP25 levels. Complementary to its inability to ameliorate the CSP null phenotype, h*SNCA*^{A30P} was also ineffective in rescuing SNARE complex assembly. The authors speculated that though alpha-synuclein possesses no chaperone activity and is neither structurally nor functionally homologous to CSPα, the two proteins may act within a similar protective pathway in the presynaptic terminal (Chandra et al. 2005). Recent investigation has fuelled this speculation, following the identification of a highly significant doubling of CSPα protein levels in whole brain homogenate of triply synuclein null mice (Burre et al. 2010). This change is not however universal across the brain, as CSPα levels were unchanged in the striatum of TKO mice (our unpublished findings – in press).

1.7.6. Beta-synuclein transgenic mice

Though it has been identified in rare inclusion bodies (see above), there is scant data implementing the direct involvement of beta-synuclein in the pathogenesis of the synucleinopathies (Ohtake et al. 2004). Accordingly overexpression of *SNCB*^{WT} was found to induce neither a behavioural phenotype nor changes in neuronal function, and that the proteins limited capacity to aggregate *in vitro* is mirrored *in vivo*. (Hashimoto 2001; Fan 2006). Hashimoto et al developed a line of beta-synuclein transgenic mice expressing high levels of h*SNCB*^{WT} under the transcriptional control of a Thy1 promoter (Thy1-h*SNCB*^{WT}) (Hashimoto et al. 2001). Despite producing near double the level of protein to a comparable Thy1-h*SNCA*^{WT} line, no signs of behavioural or histological pathology were detected. In an independently produced line of Thy1-h*SNCB*^{WT} mice that again developed no pathology, Fan et al detected a modest decrease in endogenous alpha-synuclein protein level, suggesting functional redundancy between the two synucleins, though it should be noted beta-synuclein levels are unchanged in alpha-synuclein transgenic mice (Fan et al. 2006). These findings raise the possibility that beta-synuclein might be able to actively reduce alpha-synuclein levels as part of a protective mechanism.

Remarkably, the co-overexpression of Thy1-h*SNCB*^{WT} drastically ameliorated the neurodegeneration seen in PDGFβ-h*SNCA*^{WT} mice (Hashimoto et al. 2001). The loss of striatal dopaminergic synapses normally seen in PDGFβ-h*SNCA*^{WT} mice was significantly reduced in the bigenic mice. The apparent neuroprotection provided by beta-synuclein overexpression was also observed in a line of mice co-overexpressing PrP-hSNCA^{A53T} and PrP-h*SNCB*^{WT}, where motor performance and lifespan were improved significantly in comparison to control alpha-synuclein overexpression mice (Fan et al. 2006). Interestingly in all lines of bigenic mice developed, alpha-synuclein positive inclusion bodies were

significantly less abundant than in control alpha-synuclein transgenic mice. Both groups suggested differing explanations for this reduction. Fan et al proposed that beta-synuclein overexpression resulted in a down-regulation of alpha-synuclein expression, limiting the amount of protein available to produce inclusion bodies. Hashimoto et al proposed an alternative hypothesis, suggesting that beta-synuclein inhibited the aggregation of alpha-synuclein through direct interaction with the protein. This hypothesis was supported by co-immunoprecipitation experiments in transfected cell lines, where beta-synuclein was found to directly interact with soluble alpha-synuclein. These *in vivo* findings appear to parallel *in vitro* data demonstrating alpha-synuclein fibrillation and pore formation being disrupted by co-incubation with beta-synuclein (Park and Lansbury 2003; Tsigelny et al. 2007; Uversky et al. 2002). Furthermore the findings raise the question of whether beta-synuclein may function as an endogenous regulator of alpha-synuclein aggregation, a scenario that has been proposed as having potential therapeutic use (Hashimoto et al. 2004; Masliah and Hashimoto 2002).

Recently however the widely accepted view that beta-synuclein was limited to a benign or protective role in human disease has been called into question, following the identification of mutant forms of *SNCB* in familial cases of dementia with Lewy bodies (Ohtake et al. 2004). Though the role of these mutant forms of beta-synuclein in the disease were suggested to be a possible loss of normal neuroprotective studies, the recent development of a line of transgenic mice expressing the human form of $SNCB^{P123H}$ under Thy1 transcriptional control (Thy1-h$SCNB^{P123H}$) have suggested an alternative hypothesis (Fujita et al. 2010). The Thy1-h$SCNB^{P123H}$ mice were found to develop mild abnormalities in cognitive and motor function. In contrast to the absence of beta-synuclein positive inclusion bodies found in the brains of dementia with Lewy body patients carrying $SNCB^{P123H}$ (Ohtake et al. 2004), such structures were widespread in the brains of Thy1-h$SCNB^{P123H}$ mice. Accumulated mutant beta-synuclein was detected in dendrites within the hippocampus and cortex, with dense "globules" of the mutant protein identified in the striatum. These data are further supported by an earlier finding that both P123H and V70M have a slight propensity to aggregate, substantially greater than the negligible kinetics of the wild type protein (Park and Lansbury 2003; Uversky et al. 2002; Wei et al. 2007). To further investigate the role of mutant beta-synuclein in disease, a line of bigenic mice co-overexpressing Thy1-h$SNCB^{P123H}$ and Thy1-h$SNCA^{WT}$ were generated (Fujita et al. 2010). The resulting mice were found to develop an augmented neurodegenerative phenotype compared to that seen in the control singly transgenic mice. Significantly higher levels of neuropathology were detected, most prominently in the hippocampus where high levels of apoptosis and neuron loss were described. This latter finding suggested that the association of $SNCB^{P123H}$ with dementia with Lewy bodies might not be through loss-of-function in the transcribed protein, but that mutated beta-synuclein may be actively promoting alpha-synuclein pathology.

1.7.7. Gamma-synuclein transgenic mice

Though gamma-synuclein null mice have been produced, prior to this thesis no model of gamma-synuclein overexpression has been reported. Such a model merits research for several reasons. Gamma-synuclein shares several structural and functional characteristics with alpha- and beta-synuclein. Of these the most fascinating is the propensity of the gamma-synuclein to aggregate. Though not as efficient as alpha-synuclein, it is able to form stable oligomers *in vitro* (Park and Lansbury 2003; Uversky et al. 2002). However similar to beta-synuclein it is also able to disrupt alpha-synuclein fibrillation (Uversky et al. 2002). It is thus unclear whether gamma-synuclein is likely to follow the trend of wild type and mutant forms of alpha-synuclein to induce neurodegeneration of the mouse CNS, or whether the protein is more benign, as in the case of beta-synuclein. Secondly both the anatomical distribution and cellular compartmentalisation of gamma-synuclein differ from the other synuclein proteins. Where alpha- and beta-synuclein predominantly localised to presynaptic terminals in the brain, gamma-synuclein is found diffusely throughout perikaryal, axonal and synaptic cytoplasm of select groups of CNS and PNS neurons, in particular those of the SNpc, motor nuclei and sensory ganglia (Buchman et al. 1998b). A flaw of the above alpha- and beta-synuclein overexpression models is the non-physiological cellular and anatomical distribution of their overexpressed protein. The consequence of this is most manifest in the loss of spinal motor neurons in alpha-synuclein transgenic mice, as the population does not express the protein in normal physiological conditions. Use of the same pan-neuron promoters would however give a more physiologically relevant pattern of expression if gamma-synuclein were expressed in the place of the other synucleins. Finally gamma-synuclein have emerged as a possible contributing factor in several neurodegenerative conditions. Several studies have reported the accumulation of gamma-synuclein in atypical inclusion bodies (Galvin et al. 2000; Galvin et al. 1999; Wang et al. 2004). Changes in the expression of SNCG have recently been identified as a risk factor in diffuse Lewy body disease (Nishioka et al. 2010). Furthermore inclusion bodies containing gamma-synuclein and changes in the expression of SNCG have been detected in both human and animal models of glaucoma (Mu et al. 2004; Nguyen et al. 2011; Soto et al. 2008; Surgucheva et al. 2002).

A Thy1 promoter was chosen to drive gamma-synuclein overexpression for several reasons. Firstly, the promoter has been used by several other groups to generate alpha- (Chandra et al. 2005; Rockenstein et al. 2002; van der Putten et al. 2000) and beta-synuclein (Hashimoto et al. 2001) transgenic mouse lines on C57Bl/6J backgrounds. This allows any phenotype we see in the gamma-synuclein transgenic mice to be comparable with these models. Due to the promoter having been used in these animals, and also in several other murine models of protein overexpression (for example Aigner et al. 1995, Caroni et al. 1997, Belle et al . 2007, Allen et al. 2002), we also have a relatively clear idea of the spatial and temporal expression profile of the promoter. In most neurons the Thy1 promoter is not active until post-natal days 4-10 (Aigner et al. 1995, Caroni et al. 1997), though a subset of neurons in the cerebellum have been shown to express the promoter slightly earleir, though still postnatally (Carnoni et al. 1997). Such late expression of the promoter in development will allow

us to attribute any pathological changes that may occur in the gamma-synuclein transgenic mice to post-natal transgene overexpression, and not to a disruptive influence by the transgene product during embryonic development. With regard to the spartial profile of Thy1 expression, *in situ* hybridisation experiments carried out by Carnoi et al. 1997 in several lines of mice with Thy1-driven overexpression of neuron growth-assocaited proteins demonstrated high levels expression in the cerebral cortex, thalamus, amygdala, brain stem motor nuclei, all regions of the hippocampus and cerebellum (Caroni et al. 1997). The expression of Thy1 in the CNS is not however universal, with the nigrastriatal system, hypothalamus and globus pallidum expressing only limited levels of Thy1 in comparison to other regions of the CNS (Caroni et al. 1997, Van der Putten et al. 2000). The highest levels of expression were consistently found to be within spinal cord motor neurons (Caroni et al. 1997, Allen et al. 2002, van der Putten et al. 2007). Thy1-driven overexpression of green fluorescent protein (GFP) has also demonstrated the intense activation in sensory neurons of the dorsal root and trigeminal ganglia (Belle et al. 2007). The strong expression of Thy1 in the sensory, cortical and motor neuron populations makes the promoter a particularly valid choice for gamma-synuclein overexpression, as the protein is most strongly expressed in these populations under normal physiological conditions.

It is important to note however that although Thy1 is able to drive the expression of a transgene, all mRNA produced is not necessarily translated into the final protein, and furthermore this protein may be rapidly degraded. Thus the expression pattern described above might not precisely match that seen in the gamma-synuclein transgenic mice generated, and thus the anatomical distribution of the protein shall be assessed as part of this project.

1.8. Generation and early characterisation of gamma-synuclein transgenic mice

1.8.1. Generation of gamma-synuclein transgenic mice

Work detailing the generation of the gamma-synuclein transgenic mice used in this project has been published in Ninkina 2009, in which the author of this thesis is a co-author. A line of gamma-synuclein overexpressing mice was generated by our laboratory in collaboration with Dr Herman van der Putten of the Novartis Institute for Biomedical Research. The *Thy1*mγSN line was produced by a standard protocol for generating transgenic overexpression models. Expression was driven by a neuron specific Thy1 cassette, which has previously been used to generate various transgenic mouse lines, including alpha-synuclein (Chandra et al. 2005; Rockenstein et al. 2002; van der Putten et al. 2000) and beta-synuclein (Hashimoto et al. 2001) overexpressing mice. A gamma-synuclein clone was previously isolated from cDNA library, derived by a subtractive cloning protocol designed to isolate mRNA highly expressed in E13 mouse trigeminal ganglion but not in E13 forebrain (Buchman et al. 1998b). This clone, termed "pD53", contains the 5' untranslated region (UTR), full gamma-synuclein cDNA and 3' UTR with its polyadenylation signal. Primers were designed to target the 5' and 3' UTRs of the pD53 gamma-synuclein fragment. These primers additionally contained *XhoI* linkers to facilitate cloning into an *XhoI* site contained the *Thy1* promoter plasmid (see below). Using pD53 as a PCR template, the primers amplified murine gamma-synuclein cDNA along with 34bp and 64bp of the 5' and 3' untranslated regions, flanked by *XhoI* linkers.

Primers:
mgSN XhoI-F: 5'-CTACTGTCCGCTCGAGCTTGCAGCAGCCAGGTTC-3'
mgSN XhoI-R: 5'-CTACTGTCCGCTCGAGGCCTTCTAGTCTTCTCCAC-3'

The amplified fragments were ligated into the Thy-1 promoter plasmid 323-pTSC21k (Luthi et al 1997), facilitated by an XhoI restriction site between exons II and IV of the Thy1 gene (Fig. 1). *Not1* restriction enzymes were used to cut the final eukaryotic insert from the plasmid. The resulting fragment was then purified using a commercial kit (QIAgen) and injected into the pronucleus of mouse oocytes derived from a pure C57Bl6 line, where the linear construct randomly integrated into the genome. Transformed oocytes were then transferred to foster mothers. Founder animals were selected for presence in the genome of the transgene cassette using PCR analysis of genomic DNA extracted from ear biopsies. Detection of 1kb product in a PCR reaction with the primers below indicated transgene presence.

Primers:
Gamma-synuclein: Forward 5'-ACACCCCTAAAGCATACAGTCAGACC-3'
Gamma-synuclein: Reverse 5'-GGCCTTCTAGTCTTCTCCACTCTTG-3'

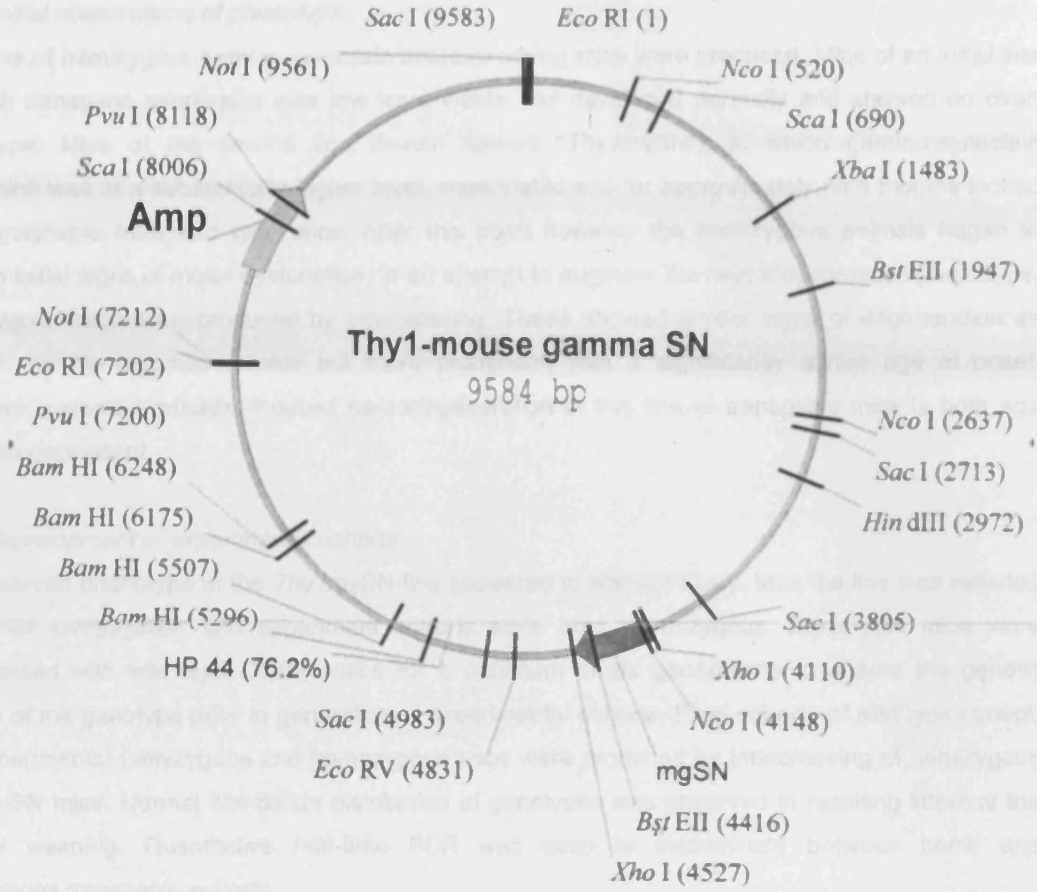

Fig. 1. The Thy1mγSN plasmid. Map showing the final Thy1mγSN expression plasmid and restriction sites. The insert fragment was cut from the construct by digestion with NotI, purified and injected in C57Bl6 oocytes.

1.8.2. Initial observations of phenotype

Two lines of hemizygous gamma-synuclein overexpressing mice were produced. Mice of an initial line in which transgene expression was low were viable and developed normally and showed no overt phenotype. Mice of the second line (herein termed "*Thy1*mγSN"), in which gamma-synuclein expression was at a substantially higher level, were viable and for approximately nine months looked indistinguishable from wild type mice. After this point however the hemizygous animals began to develop initial signs of motor dysfunction. In an attempt to augment the neurodegenerative phenotype, homozygous mice were produced by intercrossing. These showed similar signs of degeneration as seen in the hemizygous animals but more prominent, with a significantly earlier age of onset. Therefore, gamma-synuclein–induced neurodegeneration in this line of transgenic mice is both age and dose-dependent.

1.8.3. Development of experimental cohorts

The observed phenotype of the *Thy1*mγSN line appeared to warrant study, thus the line was selected for further investigation and experiment cohorts were bred. Hemizygous *Thy1*mγSN mice were backcrossed with wild type C57Bl6 mice for a minimum of six generations to ensure the genetic stability of the genotype prior to generation of experimental cohorts. Final cohorts of wild type control, and experimental hemizygous and homozygous mice were produced by intercrossing of hemizygous *Thy1*mγSN mice. Normal Mendelian distribution of genotypes was observed in resulting litters at the time of weaning. Quantitative real-time PCR was used to discriminate between hemi- and homozygous transgenic animals.

1.8.4. Confirmation of Thy1 *mγSN transgene expression*

Expression of gamma-synuclein was assessed in various regions of the nervous system of *Thy1*mγSN mice. As the trigeminal ganglion of newborn mice consists of a relatively homologous population of sensory neurons expressing high endogenous levels of gamma-synuclein, it was used as a reference tissue to compare levels of gamma-synuclein expression from endogenous promoter in the wild type mice and Thy1 promoter in *Thy1*mγSN mice. Transgene expression within the spinal cord of eight week hemizygous *Thy1*mγSN mice was found to be 10-fold that of the baseline trigeminal ganglion level (Fig. 2b.). The level of expression in the spinal cord of eight-week old homozygous mice was found to be approximately double the level in matching hemizygous animals (17 times higher than the baseline trigeminal ganglion level Fig. 2b.). The level of expression in dorsal root ganglia of twelve-month old *Thy1*mγSN mice was found to be approximately 7 times higher than the level in the same tissue of wild type animals, with spinal cord expression level approximately 11 times above this baseline (Fig. 2c.). It should be noted that endogenous spinal cord gamma-synuclein mRNA expression is normally difficult to detect, being restricted to motor neurons that account for only a fraction of cells within this portion of the CNS. Accurate quantification of spinal cord transgene expression (as folds of the endogenous expression) is therefore complicated by the nature of Thy1 cassette, which drives transgene expression in the majority of neurons of the nervous system,

including all neuronal populations of the spinal cord. Thus all measurements of spinal cord expression need to be interpreted with a degree of caution.

Western blot analysis confirmed that high levels of gamma-synuclein transgene expression resulting in significantly increased levels of the corresponding protein throughout the brain and spinal cord of both hemi- and homozygous *Thy1*mγSN mice (Fig. 2d, e). Homozygous *Thy1*mγSN tissue contained substantially higher levels of gamma-synuclein protein than that detected in hemizygous mice. The increased expression of gamma-synuclein had no impact on the levels of alpha- or beta-synuclein expression in the nervous system (Fig. 2e.). Thus any phenotype observed could be attributed to the increased neuronal gamma-synuclein content and not changes in beta- or alpha-synuclein.

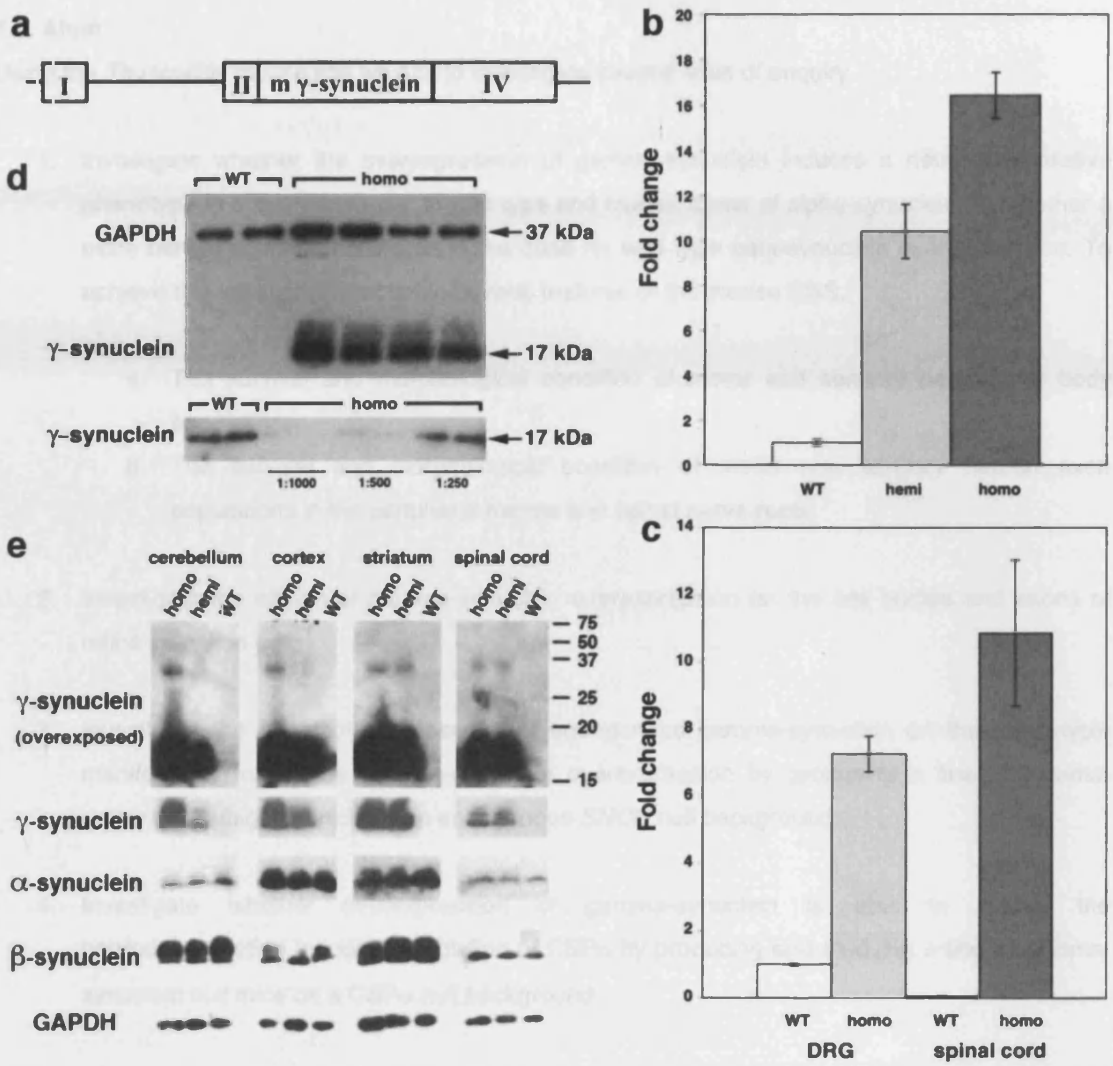

*Fig. 2. Gamma-synuclein expression in Thy1*mγSN *mice.* The *Thy1*mγSN expression cassette, containing a fragment of murine gamma-synuclein cDNA inserted between exons II and IV of murine Thy-1 (a). Bar charts (mean±SEM) showing gamma-synuclein expression in the murine nervous system (b, c). Gamma-synuclein mRNA expression in the spinal cord of 8-week old hemi- and homozygous *Thy1*mγSN mice, compared against a reference level in the trigeminal ganglia of newborn wild type mice (b). Expression in the dorsal root ganglia and spinal cord of 12-month old *Thy1*mγSN mice was compared to the reference level of age-matched wild type tissues (c). Gamma-synuclein protein levels in the spinal cord of wild type and *Thy1*mγSN mice assessed using Western blot analysis (d, e). Normalised Western blots probed with antibodies against gamma-synuclein, with GAPDH control (d). The lower panel shows undiluted wild type samples compared with 1:1000, 1:500 and 1:250 diluted samples from homozygous *Thy1*mγSN spinal cord (d). Representative Western blots showing levels of alpha-, beta- and gamma-synuclein in the brain and spinal cord (e). Gamma-synuclein overexpression does not affect the expression of alpha- or beta-synuclein. Adapted from Ninkina et al 2009.

1.9. Aims

Using the *Thy1*mγSN mouse line we aim to investigate several lines of enquiry.

1. Investigate whether the overexpression of gamma-synuclein induces a neurodegenerative phenotype in a manner similar to wild type and mutant forms of alpha-synuclein, or whether a more benign scenario occurs as is the case for wild type beta-synuclein overexpression. To achieve this we shall characterise several features of the mouse CNS.

    a. The survival and morphological condition of motor and sensory neuron cell body populations
    b. The survival and morphological condition of motor and sensory neuron axon populations in the peripheral nerves and spinal nerve roots

2. Investigate the effects of gamma-synuclein overexpression on the cell bodies and axons of retinal ganglion cells.

3. Investigate the effect of the absence of endogenous gamma-synuclein on the phenotypic manifestation of murine gamma-synuclein overexpression by producing a line of gamma-synuclein transgenic mice on an endogenous *SNCG* null background.

4. Investigate whether overexpression of gamma-synuclein is able to rescue the neurodegeneration induced by ablation of CSPα by producing and studying a line of gamma-synuclein null mice on a CSPα null background.

Finally we aim to investigate the presence of gamma-synuclein in the human CNS in healthy and disease samples. We have been given access histological samples of spinal cord and frontal lobe tissue donated by healthy individuals and patients with sporadic and familial forms of ALS and FTLD.

2. Methods

2.1. Generation of transgenic mice

2.1.1. Thy1mγSN mice

A line of C57Bl6/J mice expressing high levels of gamma-synuclein under the transcriptional control of a neuron specific thy1 promoter was developed prior to the onset of this project (Ninkina *et al.* 2009). The generation of these *Thy1*mγSN mice is described in the introduction.

2.1.2. Gamma-synuclein null mice

The generation of gamma-synuclein null has been described previously (Ninkina *et al.* 2003).

2.1.3. Thy1mγSN/CSPαKO

$CSP^{+/-}$ mice on an Ola129/C57Bl6 background were kindly gifted by Professor T C Südhof (University of Texas). The $CSP\alpha^{+/-}$ genotype was transferred to a pure C57Bl/6J background through six round of backcrossing. $CSP\alpha^{+/-}$ mice were then mated to produce $CSP^{-/-}$ mice. Further $CSP\alpha^{+/-}$ mice on the C57Bl/6J background were intercrossed with homozygous mGammaThy1 (*Thy1*$mγSN^{TG/TG}$) to produce $CSP\alpha^{-/+}$ *Thy1*$mγSN^{tg/TG}$ mice. These were then mated to produce both $CSP\alpha^{-/-}$Thy1$mγSN^{tg/TG}$ and $CSP\alpha^{-/-}$Thy1$mγSN^{TG/TG}$ genotypes. Gamma-synuclein transgene expression was detected as described above.

2.1.4. Husbandry information

Mice were held in two animal units, caged either individually or in small groups (<5 per cage), with a light cycle of 12 hours light/12 hours dark and *ad libitum* access to food and water. All work on animals was carried out in accordance with the United Kingdom Animals (Scientific Procedures) Act (1986) and European Directive EC 86/609.

2.2. Genotyping

2.2.1. Thy1mγSN

Though standard PCR could be used for detection of the *Thy1*mγSN transgene in the mouse genome, the technique is unable to differentiate between hemi- and homozygous transgenic mice. To overcome this issue we utilised quantitative real-time PCR to measure levels of genomic *Thy1*mγSN transgene. Forward and reverse primers were designed based on the sequence of the *Thy1*mγSN transgene and the housekeeping gene GAPDH as an internal control.

Gamma-synuclein: Forwards	5'-CCATGGACGTCTTCAAGAAAGG-3'
Gamma-synuclein: Reverse	5'-CGTTCTCCTTGGTTTTGGTG-3'

GAPDH: Forwards	5'-CACTGAGCATCTCCCTCACA-3'
GAPDH: Reverse	5'-GTGGGTGCAGCGAACTTTAT-3'

Genomic DNA was purified from ear biopsy tissue using a commercial kit (Promega Wizard SV Genomic DNA purification kit). Quantitative real-time PCR was then performed using a DyNAmo HS SYBR Green qPCR kit (Finnzymes) in a thin-walled 48-well PCR plate (Bioplastics) on an Applied Biosystems StepOne thermal cycler. A stock solution of reaction buffer was prepared according to the manufacturers instructions. The DyNAmo HS SYBR Green supermix contains all reagent required, including hot-start DNA polymerase. ROX, a passive reference dye used for equipment calibration was also added.

Master mix solution (sufficient for two 48 well plates)

Water	200µl
DyNAmo qPCR kit (2x)	250µl
ROX	5.0µl
Forward primers	2.5µl
Reverse primers	2.5µl

To ensure accuracy samples were loaded in triplicate. 2µl of purified genomic DNA was added to a well with 18µl of master mix solution. Samples underwent the following protocol in the qPCR thermal cycler.

Initial denaturation:	95°C	10 min
40 cycles of...		
Denaturation:	95°C	15 sec
Annealing/Extension:	60°C	60 seconds

Step-wise melt curve determination was additionally carried out in increments of 0.3°C. Fold change was calculated using the $2^{-\Delta\Delta Ct}$ comparative method using StepOne v2.0 software.

2.2.2. SNCG$^{-/-}$ Thy1mγSN$^{TG/TG}$ & CSPα$^{-/-}$ Thy1mγSN$^{TG/TG}$

Standard PCR protocols described in previous publications (Fernandez-Chacon et al. 2004; Ninkina et al. 2003) were used to discriminate between wild type and null alleles of SNCG or CSPα genes. Genomic DNA was purified from digested ear biopsy tissue using a commercial kit (Promega Wizard SV Genomic DNA purification kit). In both cases the knockout allele was detected using an upstream primer common to both alleles, with downstream primers specific to the wild type and knockout alleles. Stock solutions of primers were made up at a concentration of 100μM.

For endogenous gamma-synuclein genotyping:

Common upstream	5'-AGTCCTGGCACCTCTAAGCA-3'
Wild type downstream	5'-GGGCTGATGTGTGGCTATCT-3'
Knock-out downstream	5'-GAAGAACGAGATCAGCAGCC-3'

A wild-type band of 480bp and a knock out band of 397bp were detected.

For endogenous CSPα genotyping:

Common upstream	5'-AAAGTCCTATCGGTAAGCAGC-3'
Wild type downstream	5'-CTGCTGGCATACTAATTGCAG-3'
Knock-out downstream	5'-GAGCGCGCGCGGCGGAGTTGTTGAC-3'

A wild-type band of 607bp and a knock out band of approximately 400bp were detected.

Reaction buffer containing dNTPs, primers and taq polymerase was produced in a sufficient volume for the number of reactions required.

	For 10 reactions
dH_2O	440μl
PCR buffer (x10)	50μl
dNTPs (25mM)	4μl
Common primers	2.5μl
Wild type primers	2.5μl
Knock-out primers	2.5μl
Taq Pol	2.5μl

5μl of purified genomic DNA (Promega Wizard SV Genomic DNA purification kit) was loaded into PCR reaction tubes. To this 45μl of reaction buffer was added. Mixtures underwent the following reaction in the PCR thermal cycling apparatus (see over).

Initial denaturation	94°C	2 minutes
45 cycles of...		
Denaturation	94°C	30 seconds
Annealing	60°	30 seconds
Extension	72°	40 seconds

After reaction cycling was completed, samples were run on a 2% agarose gel until resolved sufficiently for viewing.

TAE	100ml
Ethidium bromide	4μl
Agarose	2g

2.3. Behavioural testing

2.3.1. Rotarod

The rotarod is a horizontal rotating beam used to test balance of mice. Beneath the beam is a trip switch operated timer. Mice are placed on the beam and the latency to fall recorded when the animal is no longer able to remain on the beam. The apparatus (Ugo Basil 7650 Rotarod) has two test settings.

- *Constant mode:* Four-minute trial period with the rotarod rotating at 24rpm
- *Accelerating mode:* Five-minute test period where the rotarod accelerated from 4 to 40rpm in 30-second intervals

Mice were moved into the test procedure room in their home cages 60-minutes before testing and allowed to acclimatize. Prior to testing mice underwent a practice session upon the constant speed mode rotarod, followed by a 60-minute rest period. Mice were tested on each mode three times, with a minimum rest period of 40-minutes between tests. The mean latency to fall on each mode was recorded for each mouse (Robertson *et al.* 2004).

2.3.2. Inverted grid test

To assess coordination and strength, a mouse was placed onto a 30cm by 30cm square mesh consisting of 5mm squares of 0.05mm diameter wire. The grid was slowly rotated to inverted position and held 30cm above the surface of a thick layer of bedding material. If a mouse fell from the inverted grid earlier than the maximum test time of one minute the latency to fall was noted and after an appropriate rest in the home cage the test was repeated. The best time from three attempts was used for statistical analysis.

2.3.3. Horizontal beam walking

Co-ordination and balance of the was tested on a raised wooden rod, of 500mm length and 20mm diameter, with a baited escape box at one end. Mice were place at the free hanging end, facing away for the escape box. The length of time taken by the mice to turn a full 180°, with all four paws on the beam, and the subsequent time taken to traverse the beam to the escape box were measured. The mean times for each stage were recorded.

2.3.4. Auditory startle test

Mice were physically restrained in clear Perspex tubes. These were placed upon a base mounted with piezoelectric sensors contained within a darkened startle test chambers (SR Lab software San Diego Instruments Startle Response Testing System). After a five-minute acclimatization period under 70dB white noise, mice were exposed to pseudo-randomized 30ms startle stimuli at 120 or 105dB. Peak

startle responses were measured by the piezoelectric sensors beneath the animal. In addition to the basic startle test, prepulses of 0, 2, 4, 8 and 16dB over background noise were also sounded 20ms prior to startle stimuli. Tests were separated by variable intervals of 20 to 30 seconds. Each stimulus was tested 10 times during the test period.

2.3.5. Analysis of hind paw withdrawal threshold following tactile stimulation

Mice were placed in a plastic cage with a mesh base composed of 5mm squares of 0.5mm diameter wire and allowed 30 minutes to habituate. Tests were only carried out when the animal was still, with all four paws on the cage surface. Von Frey hairs (SOMEDIC, Sweden) of varying force (0.12g – 6.20g) were applied from beneath the animal to the plantar surface, taking care to avoid the footpads, for approximately 2 seconds. Each hair was applied ten times, alternating between the left and right foot. Increasing force of von Frey hair was used until either the highest force hair or the 100% withdrawal threshold was met. Responses considered valid were the lifting of paws from surface of the grid or the spanning of digits upon stimulation. The latter response was frequently observed when the lowest force hairs were used.

2.4. Protein and neurotransmitter quantification

2.4.1. Western blotting

One of the standard procedures in molecular biology, Western blotting can be used to assess the proportion of total protein content made up by single protein. Total tissue proteins were extracted from fresh/snap frozen tissue by homogenization in the SDS gel-loading buffer (Laemmli 1970) followed by a ten-minute incubation at 100°C. The mass of sample and volume of buffer used for homogenization were recorded for future reference. Prior to running proteins on SDS-PAGE, protein levels were normalised to ensure comparable levels of total protein were being assessed. Total proteins concentration was measured using a commercial protein assay kit (BioRad), based on the Bradford procedure (Bradford 1976). Homogenized protein samples were passed through a two layer polyacrylamide gel, consisting of a 6% upper "stacking gel" layer, followed by a higher concentration "resolving gel", typically 10-20% acrylamide. The percentage of polyacrylamide contained in the resolving gel was altered according to the weight of proteins being assessed. Generally for smaller weight proteins a high percentage gel was used, slowing the movement of the proteins through the gel and allowing a greater degree of protein separation. Normalised levels of protein were loaded into the stacking gel wells. Prestained protein weight marker ladder (Fermentas PageRuler Plus) was added to an additional well. Voltage and length of run time varied depending on the molecular weight of the protein being assessed.

Stacking gel

	6% gel
dH_2O	1.65ml
Acrylamide (30%)	0.50ml
Tris (pH 6.8)	310µl
SDS (10%)	25µl
APS (10%)	3µl
TEMED	2µl

Resolving gel

	10% gel	*16% gel*
dH_2O	3.97ml	2.00ml
Acrylamide (30%)	3.33ml	5.30ml
Tris (pH 8.8)	2.5ml	2.50ml
SDS (10%)	100µl	100µl
APS (10%)	100µl	100µl
TEMED	10µl	10µl

Following electrophoresis, proteins were transferred from the polyacrylamide resolving gel to a PVDF membrane, using the high efficiency iBlot dry transfer system following the manufacturer instructions (Invitrogen). Membranes were blocked in a solution of 3% non-fat milk (Marvel) in TBS-T for one hour. Blocking solution was removed and the membrane incubated in primary antibodies in 3% non-fat milk (Marvel) in TBS-T for overnight at +4°C. Primary antibody solution was removed and the membrane washed thoroughly in TBS-T. Samples were then incubated with anti-rabbit or anti-mouse secondary HRP conjugated antibodies (Amersham) for 1-2 hours. Protein bands were then imaged using the ECL or ECL+ chemiluminescent detection systems in accordance with the manufacturers instructions (Amersham). Band intensities were analysed using AlphaImager 2200 analysis software. Following analysis, membranes were washed with TBS-T to remove ECL/ECL+. Membranes were reblocked and probed with antibody against GAPDH. Relative concentrations of test protein in samples were calculated by normalising band intensities against intensities of GAPDH.

2.4.2. Sequential protein extraction from neural tissue samples

Protocol was carried out as described in Giasson et al. 2002. Fresh tissue was collected from twelve-month old wild type and symptomatic *Thy1*mγSN mice. Samples were homogenized in a high salt buffer at a sample to buffer ratio of 1:5. Post-mitochondrial (PM) fractions were isolated by centrifugation at 12000g for 15 minutes. The supernatant was transferred to a fresh tube from which a sample aliquot was collected and mixed with the gel loading buffer. The rest of supernatant was centrifuged at 100,000g at 4°C for 20 minutes. Resulting supernatant was removed, a sample aliquot collected and mixed with the gel loading buffer (HS fraction). The pellet was washed with high salt buffer and resuspended in high salt buffer containing 1% Triton-X_{100}. Samples were again spun at 100,000g at 20 minutes. The process of supernatant sample collection and pellet resuspension was repeated with RIPA buffer. The final pellet was resuspended in 50µl of gel loading buffer and boiled for 5 minutes.

2.4.3. Immunoprecipitation

Fresh spinal cords were collected from twelve-month old wild type and symptomatic *Thy1*mγSN mice and ~100µg homogenized in 0.5ml of immuno-precipitation buffer. Triton X_{100} soluble fractions were isolated by centrifugation homogenates at 10,000g for 10 minutes at 4°C. A small quantity of cytosolic fraction was collected as an input reference for immunoprecipitation. To each sample was added antibodies raised against either NF-L (5µl) or gamma-synuclein (20µl) and 50µl of Protein G Sepharose beads. The suspension was rotated for two hours at 4°C. Sepharose beads were collected by centrifugation at 1000g for one minute. IP buffer was added to wash the beads, which were again centrifuged at 1000g for one minute. This process was repeated four times. Bound proteins were then eluted from the beads by adding 50µl of the SDS gel loading buffer followed by boiling for 10 minutes. Immunoprecipitated and co-immunoprecipitated proteins were detected by Western blot analysis using corresponding primary and secondary antibodies. Protocol has been described in Ninkina et al. 2009.

2.4.4. Neurotransmitter measurement

Levels of striatal neurotransmitters were measured by high-performance liquid chromatography (HPLC). Approximately 5mg of freshly dissected dorsal striatum was homogenized in 0.5ml of 0.06M $HClO_4$ and the homogenate centrifuged at 16000g for 15 minutes (4°C). Striatal neurotransmitters were measured by HPLC with a 4.6 x 150mm electrochemical detection microsorb C18 reverse-phase column (Varian) and Decade II ECD with a Glassy carbon-working electrode set to +0.7V, with a Ag/AgCl reference electrode (Antec Leyden). Mobile phase consisted of 12% methanol, 0.1M monosodium phosphate, 0.68mM EDTA and 2.4mM 1-octane sulphonic acid (pH 3.1).

2.5. Histology

2.5.1. Tissue fixation and paraffin embedding

For general histology and immunohistochemistry mice were sacrificed by a Schedule 1 method and the tissues rapidly collected. Sample were placed in labeled plastic cassettes and immersion fixed overnight at +4°C in one of the following fixative solutions:

- Carnoy's fixative: 60% ethanol, 30% chloroform, 10% glacial acetic acid (Bancroft and Gamble 2002).
- 4% paraformaldehyde in phosphate buffered saline (pH 7.4)
- 10% neutral buffered formalin (Pre-prepared Sigma-Aldrich)

Tissues were then dehydrated through one of the following series.

For 4% PFA or 10% NBF:

PBS	15 mins (x4)
70% ethanol	Overnight
95% ethanol	5 mins (x3)
100% ethanol	10 mins
100% ethanol	30 mins
1:1 ethanol:chloroform	30 mins
Chloroform	60 mins
Chloroform (+4°C)	Overnight

For Carnoy's fixative

95% ethanol	5 mins (x3)
100% ethanol	10 mins
100% ethanol	30 mins
1:1 ethanol:chloroform	30 mins
Chloroform	60 mins
Chloroform (+4°C)	Overnight

Following final dehydration in chloroform, tissues were infiltrated in paraffin wax (RA Lamb) at 60°C for three hours. Tissues were then placed in stainless steel moulds that were subsequently filled with paraffin wax, a labeled plastic base mounted and left to set on a chilled ice plate.

2.5.2. Sectioning and mounting of samples

To prepare slides for use in histological staining techniques, 8µm sections were cut from samples contained in paraffin blocks using a microtome fitted with a razor-cutting blade. Sections were floated

upon the surface of dH_2O heated in a 40°C water bath. Sections were collected onto poly-L-lysine coated slides (Thermo-Fischer) and allowed to dry overnight at room temperature.

2.5.3. Haemotoxalin and eosin staining

Samples were processed by an automated system. Sections were dewaxed in xylene and brought to water. Sections were then incubated in Gill's haemotoxylin (Leica) for 5 mins. Excess staining was washed under running H_2O, followed by a 30 second differentiation in acidified ethanol (1% glacial acetic acid). Following further washing in H_2O samples were incubated in 1% eosin for 5 minutes. Samples were again washed, brought to xylene and glass coverslips mounted with DPX.

2.5.4. Fluorescent Congo red staining

Sections were dewaxed and brought to water, followed by incubation in 0.5% Congo red in 50% ethanol for 7 minutes. Slides were washed with 50% ethanol followed by differentiation of staining with 0.2% potassium hydroxide in 80% ethanol for 5 minutes. Sections were then thoroughly washed with dH_2O and glass coverslips mounted with aqueous media (Thermo Scientific). Slides were allowed to dry and stored in the dark at +4°C. For quantification of amyloid positive structures, sections were randomly selected from all regions of the spinal cord. A $0.1mm^2$ field of the ventral horn was photographed under fluorescent microscope, the number of structures strongly stained with Congo red were counted. Final means were calculated for the cervical, thoracic and lumbar spinal cord separately. Protocol adapted from Bancroft and Gamble 2002.

2.5.6. Thioflavin-S staining

For qualitative aggregate detection, sensory ganglion sections were incubated in 1% thioflavin S (Sigma-Aldrich, MO) in dH_2O for 5 minutes, followed by differentiated in 70% alcohol for 5 minutes. Sections were then washed in dH_2O and mounted with aqueous mounting media (Thermo-Fisher Scientific, MA). Protocol adapted from Bancroft and Gamble 2002.

2.5.7. Nissl staining

Sections were dewaxed and brought to water. Samples were stained in 0.5% cresyl violet acetate in dH_2O followed by thorough washing. Staining was then dissociated in 0.25% acetic acid in 100% ethanol. Sections were again washed with dH_2O, taken to xylene and glass coverslips mounted with DPX. Following Nissl staining cranial and spinal motor neuron cell bodies and also the sensory cell bodies located within the dorsal root ganglia are easily identifiable. All have particularly large cell body densely stained with Nissl granules. The nuclear envelope remains clear but the nucleolus remains intensely stained, the presence of which is used to determine which cells are counted. Protocol adapted from Bancroft and Gamble 2002.

2.5.8. Spinal motor neuron cell body quantification

Sections were randomly selected from all levels of the spinal cord. The number of motor neuron cell bodies within each ventral horn was quantified separately. Final means were calculated for the cervical, thoracic and lumbar spinal cord separately.

2.5.9. Cranial motor neuron cell body quantification

Serial sections of the abducens, facial and trigeminal motor nucleus were collected with every 10^{th} section sampled. The fractionator technique of correction used to estimate total neuron populations.

2.5.10. Dorsal root ganglion sensory cell body quantification

Serial sections of L4/5 dorsal root ganglion were collected with every 6^{th} section sampled. The fractionator technique of correction was used to give estimate the total population.

2.5.11. The fractionator correction technique

The fractionator correction technique (Howard and Reed, 1998) allows a total population to be estimated from quantification of a smaller sample fraction, using the following formula.

$$Nt = 1/f \times Nf,$$

Where Nt = total population, Nf = number counted in the fraction,
f = sampling fraction (i.e. for DRG population "6").

2.6. Immunostaining

2.6.1. Standard immunohistochemistry

Sections were cleared in xylene and brought down to water. Antigen retrieval was carried out by microwaving at 750W for ten minutes in 10mM sodium citrate (pH 6.0). Endogenous peroxidase activity was quenched by incubation with 3% hydrogen peroxide in methanol. Tissues were then washed with PBS and a blocking solution of 10% appropriate serum (i.e. horse, goat) in PBS containing 0.4% triton-X_{100} was applied for 30 minutes. Sections were incubated in primary antibodies in blocking solution either overnight (+4°C) or for 2 hours at room temperature. Tissues were then washed with PBS, followed by incubation in a corresponding biotinylated secondary antibodies (Vector) in 0.4% T-PBS, for an hour. The tissues were washed, followed by incubation in ABC solution (Vector) containing avidin-biotin HRP complex, applied for 30 minutes at room temperature. After washing with dH_2O tissues were incubated with the HRP substrate 3,3'-diaminobenzidine (DAB) (Sigma) until brown colouring was sufficient. If necessary colouring reaction speed could be slowed down through use of diluted DAB. Tissues were then washed in dH_2O and, if required, counterstained by immersion in haematoxylin solution for 30 seconds. Samples were then taken to xylene and a glass coverslip mounted with DPX (RA Lamb).

2.6.2. Fluorescent immunostaining

Tissues were dewaxed and brought to water. Antigen retrieval was carried out, by microwaving at 750W for ten minutes in 10mM sodium citrate (pH 6.0). The sections were then washed with PBS and a blocking solution of 3% bovine serum albumin and 5% goat serum in PBS applied for one hour. Tissues were incubated in primary antibodies in blocking solution for two hours. The sections were then washed in PBS followed by a one-hour incubation in secondary Alexafluor conjugated antibodies (Molecular Probes). The sections were then washed and a glass cover slip mounted with aqueous mounting media (Thermo Scientific). Slides were stored in the dark at +4°C. Fluorescent images were captured using a Leica TCS SP2 laser scanning confocal microscope (Leica Microsystems, Germany) or Olympus BX61 fluorescent microscope (Olympus, PA).

2.7.3. Quantification of dopaminergic neurons in the substantia nigra pars compacta and ventral tegmental area.

The number of dopaminergic neurons within the substantia nigra pars compacta (SNpc) and (ventral tegmental area) VTA were counted using a previously described protocol (Robertson *et al.* 2004). Prior to staining, whole SNpc and VTA were serial sectioned and mounted onto polysine coated slides (Thermo-Fisher) in a pattern producing two duplicate sets of slides as shown below.

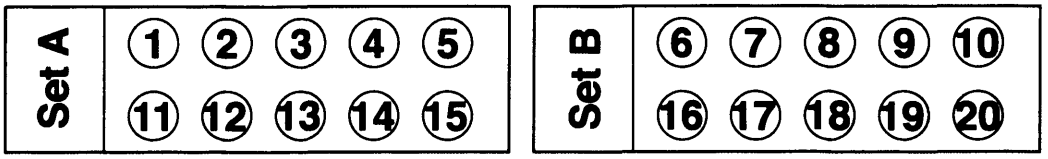

One set of slides was stained, with the second kept for any further analysis or repetition required. Staining was carried out using the standard immunostaining method described above, using mouse primary antibodies raised against tyrosine hydroxylase at a 1:1000 dilution. All counts were carried out blindly. From the first slide of the series containing SNpc/VTA, a section was randomly selected i.e. section "2". The total number of nuclei of tyrosine hydroxylase-positive cell bodies was counted for both the left and right regions of the SNpc and VTA at 40x magnification and recorded seperately. This was then repeated on every tenth section of the series throughout the entire SNpc/VTA region i.e. "2", "12", "22" etc. The mean nuclear diameter of 30 TH-positive was recorded for each set of tissue analysed (AnalySIS imaging software). Total cell populations were estimated using the Abercrombie correction technique (Abercrombie 1946):

$$P = (1/f) \times A(M/D+M)$$

Where P=corrected cell count; f=frequency of cell count (i.e. 1/10=0.1); M=section thinness (μm); D=average nuclear diameter.

2.7.4. DiOlistic labelling of retinal ganglion cells

DiOlistic staining is a recently developed technique that allows the fluorescent imaging of both living and fixed cells (Gan et al. 2000). Staining is achieved by firing tungsten beads coated with the lipophilic fluorescent dyes 3,3′-dioctadecyloxacarbocyanine perchlorate (DiO) and 1,1′-dioctadecyl-3,3,3′,3′-tetramethylindocarbocyanine perchlorate (DiI). DiOlistic staining was carried out in collaboration with the laboratory Prof. James Morgan in the Cardiff University School of Optometry, with kind assistance from Peter Williams.

Firstly tungsten particle were coated with the fluorescent dyes. This process may be carried out in advance as the dye-loaded "bullets" produced can be stored for several months. 2mg of DiI (Sigma) or 4mg of DiO (Sigma) were suspended in 200μl of methylene chloride by vortexing. The dissolved dye was then added to 200mg of 1.3-1.7μm tungsten particles placed upon a glass slide. The dye and tungsten particle mixture was spread out into a thin film and allowed several minutes to dry. The dried powder was then transferred to a 15ml falcon tube to which 5mls of MilliQ dH_2O was added, followed by 3-5 minutes further vortexing. Using a syringe the slurry was drawn into silicon tubing coated with polyvinyl pyrrolidone (Sigma) to facilitate particle sticking to the tubing walls and allowed several minute to settle. A syringe was then used to draw remaining water from the tubing. The coated tubing was then dried with a flow of nitrogen (0.2-0.4lpm) and cut to the required "bullet" length (approx. 2cm).

For labelling of RGCs, intact retina were rapidly dissected from the eyes of twelve month old wild type and *Thy1*mγSN$^{TG/TG}$ mice, whole-mounted on a glass coverslip and allowed 5 minutes adhere. The coverslips were then placed beneath a membrane filter with 3μm pores (Falcon tissue culture inserts), dye coated bullets were loaded into a gene gun and the tungsten beads contained fired into the tissue at a pressure of 60-120psi. Labeled tissue was then incubated at 37.5°C for 20 minutes to allow diffusion of lipophilic dye across the RGC phospholipid membranes. Tissues were then fixed with 4% PFA for 10 minutes, washed with PBS and mounted to a glass slide with aqueous mounting media. The fluorescent staining by DiO/DiI has a relatively short lifespan and so it is essentially to image the samples within 48-hours of staining. 20x magnification Z-stack images encompassing all visible neurites emerging from one RGC were produced by fluorescent confocal microscopy, taking care not to image any amacrine cells that may have also been labeled. Scholl analysis, the measurement of dendritic branching at various distances from the soma, was carried out using ImageJ.

2.7. Transmission Electron Microscopy:

2.7.1. Tissue preparation

Nerves were dissected from twelve-month-old animals as required and immediately immersion fixed in a glass bijou containing cold 2% PFA 2% gluteraldehyde in 0.1M Sorensons PB overnight at 4°C. Samples were then washed thoroughly in 0.1M Sorensons PB and post-fixed in 1% osmium tetraoxide for two hours at room temperature. Samples were again washed followed by block stained in 0.5% uranyl acetate overnight at +4°C. After samples were washed in dH_2O they were passed through a graded dehydration series. It is critical that this stage is carried out slowly and carefully. Both sudden osmotic changes and the consequence incomplete dehydration on subsequent steps in the protocol can cause substantial damage to the myelin sheaths surrounding axons resulting in useless samples. The concentration of alcohol bathing the sample was increased every 5 minutes in increments of 5%. The samples were then bathed in a final solution of 100% ethanol for 90 minutes, with the solution replaced four times. 100% ethanol was then replaced with by propylene oxide, which was again replaced by fresh solution after 10 minutes and allowed a further 20-minute incubation. Pure propylene oxide was then replaced by a solution of 1:1 propylene oxide and araldite solution for overnight infiltration. The samples were removed from this final solution and embedded in pure araldite for 48 hours at 60°C. Protocol adapted from Hayat 1989.

2.7.2. Sectioning

Plastic-embed section cannot be cut using the apparatus used for standard histological section, due to both the relative bluntness of a standard razor blade and the inability of the equipment to accurately section below 1µm. For ultra-thin sectioning we used a diamond knife (Diatome) attached to a small bath of dH_2O. The cutting equipment is mounted in an ultra-tome (Reichert-Jung Ultracut E microtome), apparatus specifically designed for cutting sections on a nanometer scale. Two types of section, each with differing applications, can be cut:

1. Semi-thin sections

Varying in colour, these >0.1µm section were used for tolouidine staining, a quick means of assessing the quality and morphology of prepared tissue. To mount semi-thin sections, a bubble of dH_2O was formed on the surface of a poly-L-lysine coated slide (Thermo-Fischer). Samples were collected on the tip of a nylon filament and transferred to the bubble. The slide was then placed on a hot plate (80-100°C) and the bubble allowed to dry. For tolouidine staining, a drop of 1% tolouidine blue, 1% borax in dH_2O was place upon the dried sections. The slide was again returned to the hotplate and dried. Residual staining solution was then removed by washing the slide under a running tap. The slide was then dried upon the hot plate, allowed to cool and a coverslip mounted with DPX.

2. Ultra-thin sections

Silver-gold in colour, these sections were used for high quality transmission electron microscopy. Mounting and preparation of ultra-thin sections is more complex than semi-thin. A glass slide was briefly soaked in a solution of 0.8% pioloform in chloroform. The slide was removed and allowed to dry. The edges of the slide were then scoured with a razor blade and the slide slowly dipped vertically into a bath of dH_2O to remove the pioloform film from the slides surface. 3mm diameter copper and nickel grids with a 2x1mm slot cut into their centre (Agar) were placed upon the floating layer of film and given several minutes to adhere. A clean layer of parafilm was then placed upon the floating film/grids and slowly pulled from the water surface, bringing with it the film coated grids. After being allowed to dry at room temperature the grids were ready for use.

Following cutting, ultra-thin sections were collected from the surface of the water bath onto a film coated copper or nickel slot grid and allowed to dry. For counterstaining, sections carrying grids were floated upon a drop of 0.5% uranyl acetate for 10 minutes, followed with two 5-minute washes upon a drop of dH_2O. Sections were further counter-stained with Reynold's lead citrate solution (Reynolds 1963) for 5 minutes, followed by a further two dH_2O washes and drying to room temperature. Stained tissues were then visualized under a Philips TEM 208 transmission electron microscope.

2.7.3. Morphometric analysis: Sciatic nerve and spinal nerve roots

Myelinated A-fibres and unmyelinated C-fibre were counted at 2.0kx magnification. All A-fibres were counted recording their morphological condition, with fibres classed as either normal or damaged. Healthy fibres were defined as those with both axons and myelin sheath intact. Unhealthy fibres had dense, vacuous or absent axons, substantial abnormalities in the myelin sheath, or a combination of both. Damaged axons fully enveloped by phagocytes were not counted as the digestive process of these cells made accurate quantification impossible. C-fibres were classified as either normal, with a turgid cluster of fibres engulfed by a Schwann cell, or atypical, where turgidity is lost and the bundle morphology was consequently abnormal. All counts were normalized to a $100\mu m^2$.

2.7.4. Morphometric analysis: Optic nerve

Myelinated A-fibres were quantified at 6.3kx magnification. As few damaged fibres were detected, only total number of fibres was recorded. All counts were normalized to a $100\mu m^2$.

2.8. Statistics

All statistics was carried out on Minitab 15th Edition except the χ^2 test, for which Microsoft Excel was used. Guidance for testing was taken from Minitab Workbook for Biosciences: Minitab 14 edition. DW Bowker & PF Randerson. Cardiff School of Biosciences. 2004/5.

Statistical analysis was performed to reveal whether differences seen were mathematically significant, or if not then negligible. A p-value is generally calculated, representing the probability that the hypothesis being tested is true, and did not occur by chance, with a low value denoting higher probability, and accordingly increased confidence. Generally, it is the likelihood of H_0 occurring by chance that is being tested. A p-value ≤0.05 confers a 5% chance of this occurrence, and is widely accepted as the level at which H_0 is rejected. Three levels of confidence were used in the analysis of the data collected below and are annotated with asterisks as shown:

p-value ≤0.05	*	"Significant"
p-value ≤0.001	**	"Highly significant"
p-value ≤0.0001	***	"Very highly significant"

Where there were more than two groups in an experiment, One Way Analysis of Equal Variance tests (ANOVA) were used to test for differences. Prior to testing with ANOVA, it is essential to test whether the observations conform to a number of assumptions test makes. These are that the data is distributed normally (i.e Gaussian distribution) and the variance is equal between curves. Anderson-Darling test was employed to test for normality of distribution of data and Bartlett's test used to test the homogeneity of variance between datasets. Data that conformed to the assumption made by ANOVA was deemed parametric and tested using a one-way ANOVA test. Data violating either/both assumptions was deemed non-parametric and tested using a Kruskal-Wallis test; a less powerful means of analysis that does not assume equal variance. Untransformed data was used throughout. If significance was detected, pairwise post-hoc testing was then carried out with Fisher's a priori test to detect differences between specific pairs.

Where differences between only two datasets were being investigated, a two-sample t-test or its non-parametric equivalent, the Mann-Whitney U-test, were utilised. These test investigate the hypothesis that all data has come from an equivalent dataset. Again, prior to analysis, the conformity of the data to two assumptions must be tested. Anderson-Darling testing was again used to test normality of distribution. An F-test was used to investigate the equality of variance between the datasets. Specifically, this test measures the ratio of variance between the groups differs significantly from 1.0. Again, data violating either/both assumptions was deemed non-parametric and tested accordingly.

Significant differences in the observed percentage of groups able to complete a test (i.e. the percentage of mice able to complete the beam test) were investigated using a Chi-squared goodness of fit test (χ^2 test). The χ^2 test analyses the H_0 that the observed data does not differ from the expected data, using the equation...

$$\chi^2 = \Sigma((O-E)^2/E)$$

Where O=observed data, E=expected data.

The χ^2 number is then tested against a critical value at p=0.05. If the χ^2 value calculated is greater than the critical value, H_0 is rejected. The critical figure is derived from a statistics table and is selected dependant of the number of degrees of freedom (DF) in the test. The DF is value calculated from the number of independent datasets minus one. As all tests which used χ^2 analysis contained two datasets, control and experimental, there was only ever one degree of freedom.

The expected result for the experimental group was calculated from the proportion of control mice able to complete the test from the total number tested. This was then compared against the observed number of experimental mice able to complete the test. Thus in the below hypothetical experiment...

	Control Group	Experimental Group
	(n=50)	(n=70)
Expected	50	34/50 x 70 = 47.6
Observed	34	23

2.9. Solutions

Congo Red

Congo red	0.5%
50% ethanol	

Diaminobenzidine solution

Supplied by Sigma:	
3,3'-Diaminobenzidine	3.3mM
Urea Hydrogen Peroxide	7.0mM
Tris buffer	60 mM

High Salt Buffer with 1% Triton-X_{100}

Tris-HCL (pH 7.5)	50mM
NaCl	750mM
Triton-X_{100}	1%

Protease inhibitors, according to manufactures instructions (Complete Mini from Roche)

Immunoprecipitation buffer

Tris-HCL (pH 7.5)	50mM
NaCl	150mM
$MgCl_2$	1.5mM
Triton X_{100}	1%

Protease inhibitors, according to manufactures instructions (Complete Mini from Roche)

SDS gel loading buffer

Tris pH 6.8	0.1M
Glycerol	20%
SDS	4%
Bromo phenol Blue	0.02%
Beta mercaptoethanol	0.2M

Nissl stain

Cresyl violet acetate (Fluka)	0.5% in dH_2O

Solution was passed through filter paper prior to use to remove any precipitate.

PCR Buffer (10x)

KCl	0.5M
Tris pH 9.0	0.1M
$MgCl_2$	15mM
Triton-X_{100}	1%

Phosphate buffered saline: Dulbecco A (pH 7.3±0.2)

Supplied by Oxoid:

NaCl	0.1M
KCl	2.6mM
Sodium Phosphate dibasic	6.5mM
Potassium phosphate monobasic	1.2mM

Potassium hydroxide

Potassium hydroxide	0.2%
80% Ethanol	

Quench solution

Hydrogen peroxide	3%
Methanol	

RIPA Buffer

NaCl	150 mM
Tris HCl pH 8.0	50 mM
EDTA	5 mM
NP40	1%
Sodium deoxycholate	0.5%
SDS	0.1%

Sodium citrate buffer (pH 6.0)

Sodium citrate tribasic salt dihydrate	10mM
dH_2O	
pH adjusted to 6.0 using HCl	

Sorenson's phosphate buffer (0.1M)

Solution A	
Sodium Phosphate dibasic	0.2M
Solution B	
Potassium phosphate monobasic	0.2M

For 100ml 0.1M Sorensons phosphate buffer (0.1M, pH 7.4)

Solution A	81.8ml
Solution B	18.2ml

TAE

For one litre of 50x stock solution.

Tris	2.0M
EDTA 0.5M (pH 8.0)	100ml
Glacial acetic acid	57.1ml
dH_2O	

For working concentration dilute TAE stock 1:50 dH_2O.

Toluidine blue

Toluidine blue	1%
Borax	1%
dH_2O	

Tris buffered saline (pH 8.0)

Supplied by Sigma-Aldrich:	
Tris	0.5M
NaCl	138mM
KCl	2.7mM

TBS-T

Tris buffered saline (pH 8.0) containing 0.1% $Tween_{20}$

2.9. Antibodies

2.9.1. Primary antibodies

Alpha-synuclein: Mouse monoclonal, clone 42, BD Transduction Laboratories

Alpha-tubulin: Mouse monoclonal, clone DM 1A, Sigma

Beta-synuclein: Mouse monoclonal, clone 8, BD Transduction Laboratories

GAPDH: Mouse monoclonal, clone 6C5, Santa Cruz Biotechnology

Gamma-synuclein (anti-mouse): Rabbit polyclonal SK23, affinity purified

Gamma-synuclein (anti-human): Rabbit polyclonal SK109, affinity purified

Gamma-synuclein (anti-human): Goat polyclonal E20, Santa Cruz Biotechnology

GFAP: Rabbit polyclonal, Sigma-Aldrich

Myelin basic protein: Mouse monoclonal, clone MAB387, Chemicon

Neurofilament-L: Mouse monoclonal, clone DA2, Cell Signaling

Neurofilament-M: Mouse monoclonal, clone NN18, Sigma

Neurofilament-H: Rabbit polyclonal, Sigma

NeuN: Mouse monoclonal, clone A60, Chemicon

Peripherin: Rabbit polyclonal, clone Ubi-1, Chemicon

Ubiquitin: Mouse monoclonal, clone Ubi-1, Zymed Laboratories Inc.

RCA biotinylated lectins: Vector

2.9.2. Secondary antibodies

Biotinylated secondary antibodies 1:1000 (Vector)

Alexa Fluor-conjugated secondary antibodies 1:1000 (Invitrogen)

HRP conjugated secondary antibodies 1:3000 (Amersham)

3. Gamma-synuclein overexpression in the murine nervous system: Behaviour, cell bodies and aggregation

3.1. Overview

For over a decade the accumulation and aggregation of alpha-synuclein has been associated with the synucleinopathy family of neurodegenerative disorders (Spillantini et al. 1997), substantiated by the identification of several autosomal recessive point mutations (Kruger et al. 1998; Polymeropoulos et al. 1997; Zarranz et al. 2004), duplication (Chartier-Harlin et al. 2004; Ibanez et al. 2004), triplication (Singleton et al. 2004) of the *SNCA* gene in Parkinsonian syndromes and its identification as a risk factor in several genome wide association studies (Edwards et al. 2010; Pankratz et al. 2009; Satake et al. 2009; Simon-Sanchez et al. 2009). The link between alpha-synuclein aggregation and neurodegeneration has been further demonstrated in numerous transgenic animal models with aberrant alpha-synuclein expression and inclusion formation (see section 1.7.). In contrast beta-synuclein has an extremely low propensity to aggregate in vitro (Fan et al. 2006; Park and Lansbury 2003) and is able to ameliorate the degeneration induced by alpha-synuclein overexpression in mice (Hashimoto et al. 2001).

Though the primary structure of gamma-synuclein is diverse compared that of the other synucleins (Sung and Eliezer 2007) it has nevertheless been demonstrated to share characteristics with both other family members. For example gamma-synuclein is able to form stable oligomeric structures in solution (as alpha-synuclein) (Park and Lansbury 2003) but also capable of disrupting alpha-synuclein aggregation (as beta-synuclein) (Uversky et al. 2002). The expression profile and intracellular localisation of gamma-synuclein are unique in the family; whereas alpha- and beta-synuclein predominantly compartmentalise to the presynaptic terminals of CNS neurons, gamma-synuclein is found diffusely throughout select pools of neurons in CNS and PNS (Abeliovich et al. 2000; Buchman et al. 1998b; Li et al. 2002; Surgucheva et al. 2002).

To investigate whether gamma-synuclein shares the ability of alpha-synuclein to induce substantial degeneration when overexpressed, or follows the benign scenario of beta-synuclein overexpression, we have produced a line of mice expressing high levels of murine gamma-synuclein throughout their nervous system. This chapter concerns the assessment of motor performance, sensory perception and characterisation of various populations of neuronal cell bodies within the CNS of these mice.

3.2. Results: Phenotype and behaviour

3.2.1. Phenotype

*Thy1*mγSN mice are viable and during the first 3-5 months of life are indistinguishable from wild type controls. From 5 months onwards however, homozygous *Thy1*mγSN mice begin to develop characteristics typical of motor neurodegeneration. Clinical signs were found to progressively worsen with age. Many homozygous *Thy1*mγSN mice had to be culled at approximately 12-months due to substantial motor dysfunction and physical weakness, due in part to reduced ability to feed. Typical signs of ill health including a hunched posture and piloerection were frequently observed (Fig. 3b). Hemizygous mice also developed substantial motor dysfunction, however at an older age than homozygous mice, generally becoming manifest from 12-months onwards, suggesting a correlation between transgene dose and disease severity. The most pronounced of sign of early motor deterioration was the dystonic clasping of limbs against the abdomen (Fig. 3a.). This symptom began with clenching of the hind paw digits, with the whole leg rapidly becoming affected. Through hind limbs symptoms became detectable earliest in disease progression, the phenotype eventually encompassed all limbs. This loss of motor function had much consequence on the general behaviour of the *Thy1*mγSN mice. Assessment of gait, achieved by painting the paws of the mice and allowing them to run over paper, revealed a marked deficit in foot placing (Fig. 3c). In contrast to the orderly foot placing of wild type control mice, nine-month old homozygous *Thy1*mγSN mice were found to misplace or drag their paws, with the phenotype worsening with disease progression (see Fig. 3c). Righting reflex was found to be decreased in *Thy1*mγSN mice, in particular the homozygous cohort (Fig. 3d.). When placed on their back a healthy mouse will instantaneously right itself onto its feet. At later stages of disease many homozygous *Thy1*mγSN mice performed very poorly at this test. Subsequently failure to right after one minute was deemed an experimental end point and the animal sacrificed.

3.2.2. Survival

Gamma-synuclein overexpression, and the subsequent motor deficits induced, had a pronounced effect upon the survival of mice (Fig. 3e). Wild type mice normally live for approximately 2.5 years. The survival of our control cohort was assessed during the first 2 years, with modest loss of 20% recorded. Both hemi- and homozygous *Thy1*mγSN mice had a significantly reduced life span. At the age of 2-years just over 40% of the hemizygous cohort had perished. The survival of homozygous *Thy1*mγSN mice was substantially diminished. Half of the colony had perished by 11-months, with no animals surviving past 14-months.

To assess the onset and progression of the motor deficits observed in the *Thy1*mγSN cohort, a battery of motor tests were carried out upon the animals.

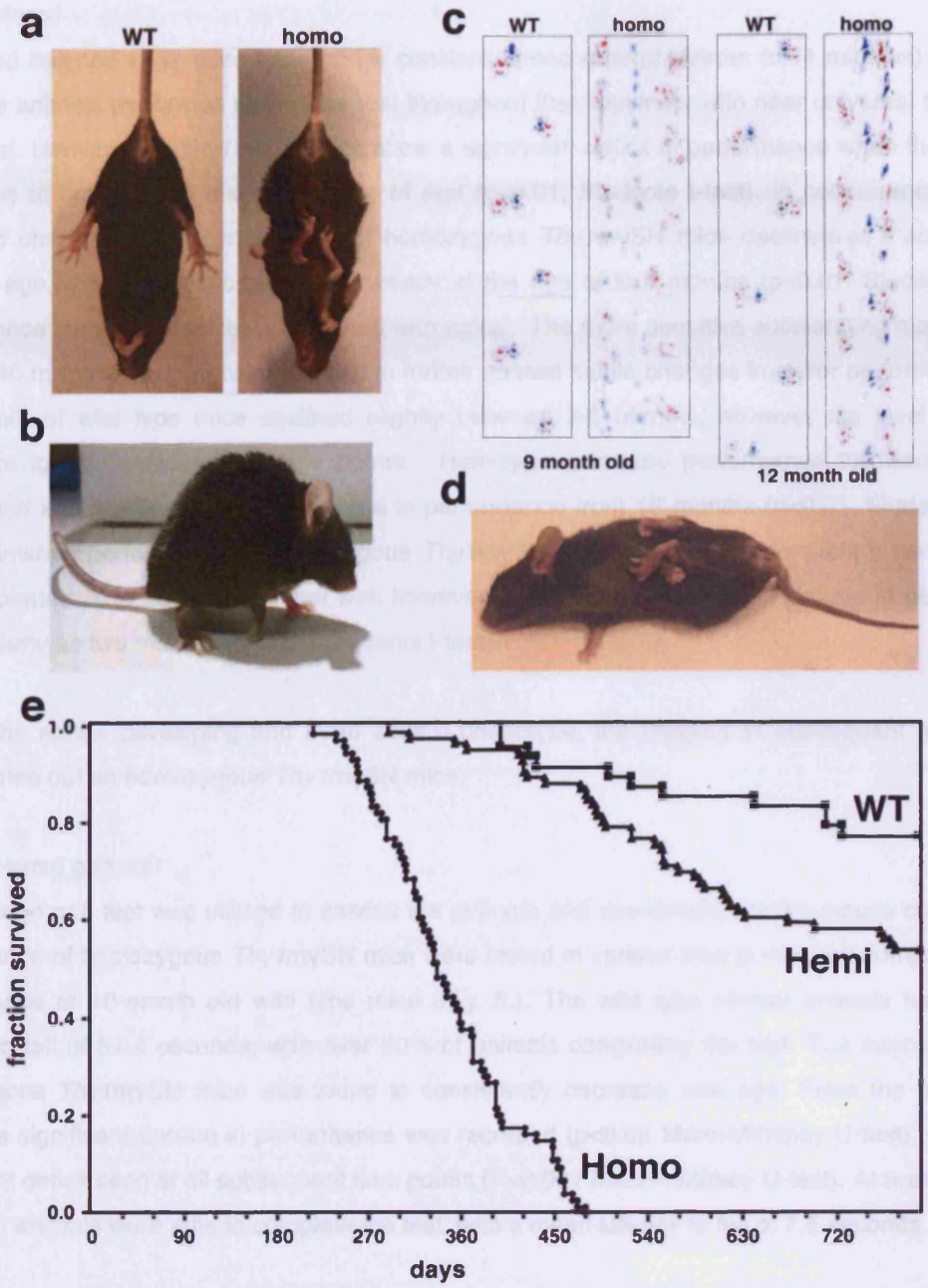

*Fig. 3. Physical manifestation of Thy1*mγSN *phenotype and effect on survival. Twelve-month old h*omozygous *Thy1*mγSN mice at the advanced stage of disease progression show dystonic clasping of all limbs against their abdomen (a). Neuromuscular dysfunction subsequently leads to a decreased righting reflex in mice with highly advance phenotype (d). Typical signs of ill health, including hunched posture and piloerection are frequently seen in symptomatic animals (b). The footprint pattern of *Thy1*mγSN mice shows clear abnormalities in foot placing (c), shown at 9 and 12 months. Kaplan–Meier plot of wild type (squares, n=49), hemizygous *Thy1*mγSN (triangles, n=87) and homozygous *Thy1*mγSN (circles, n=74) mice survival over the 26 months period (e). Adapted from Ninkina et al. 2009.

3.2.3. Rotarod

Motor and balance skills were tested on a constant speed rotarod (24rpm for 4 minutes) (Fig. 4a.). Wild-type animals performed well at the test throughout their lifetimes, with near universal completion of the test. Hemizygous *Thy1*mγSN mice show a significant deficit in performance when the test was performed at both the 18 and 24 months of age ($p<0.01$, Students t-test). In concurrence with the observed phenotype, the performance of homozygous *Thy1*mγSN mice declined at a substantially younger age, with significance reached already at the age of four months ($p<0.01$, Students t-test). Performance then progressively diminished with aging. The more sensitive accelerating mode rotarod test (4 - 40 rpm over 5 minutes) was used to further assess subtle changes in motor performance (Fig. 4b.). That of wild type mice declined slightly between 2-6 months, however the level remained consistent for the remainder of age points. Hemizygous mouse performance followed a similar pattern, but again with a significant decline in performance from 18 months ($p<0.01$, Students t-test). The diminished performance of homozygous *Thy1*mγSN mice seen in the constant speed test was again repeated. The accelerating test was however able to detect significant deficits in performance from as early as two months ($p<0.01$, Students t-test).

Due to the earlier developing and more severe phenotype, the majority of subsequent motor tests were carried out on homozygous *Thy1*mγSN mice.

3.2.4. Inverted grid test

The inverted grid test was utilised to assess the strength and coordination of the mouse cohorts. The performance of homozygous *Thy1*mγSN mice were tested at various time points and compared to the performance of 18-month old wild type mice (Fig. 5.). The wild type control animals had a mean latency to fall of 57.4 seconds, with over 80% of animals completing the test. The latency to fall of homozygous *Thy1*mγSN mice was found to consistently decrease with age. From the age of four months a significant decline in performance was recorded ($p<0.05$ Mann-Whitney U-test), with highly significant deficit seen at all subsequent time points ($P<0.001$ Mann-Whitney U-test). At twelve-months of age no animals were able to complete the test, with a mean latency to fall of 7.5 seconds.

3.2.5. Acoustic startle test

The acoustic startle test was initially used as an assessment of prepulse inhibition (PPI), a complex motor phenomenon whereby startle response is muted by exposure to an auditory prepulse, played fractions of a second prior to the startle stimuli. Surprisingly PPI could not be accurately recorded in 24-week old *Thy1*mγSN mice due to a substantially reduced startle response, found to be less than 20% that of age matched wild type controls (Fig. 6b.). An obvious possibility was that the *Thy1*mγSN mice were deaf, however homozygous mice of various age were observed to be responsive to noise made in the vicinity of their home cage. Dysfunction was initially attributed to the significant motor deficits recorded in the older *Thy1*mγSN mice, and thus further attempts to record PPI were carried out in younger animals. Strikingly startle response was found to be reduced by over 80% in 6-week

(data not shown) and 3-week old *Thy1*mγSN mice (Fig. 6a.), the latter being the youngest age feasible for testing. Hemizygous mice also showed a 68% decrease in response to the loudest startle stimuli (Fig. 6a).

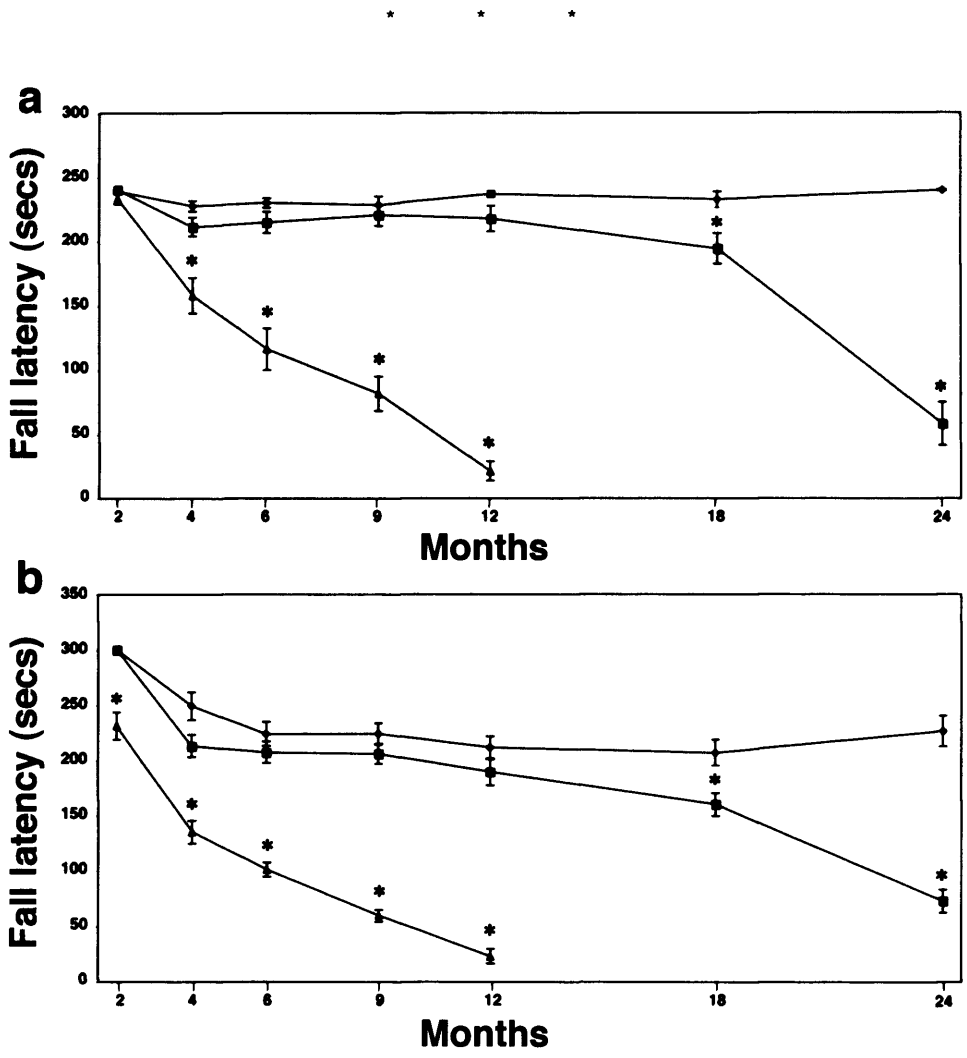

Fig. 4. Age related decline in performance of homozygous Thy1mγSN mice on rotarod. Performance of wild type (diamonds), hemizygous (squares) and homozygous (triangles) *Thy1*mγSN mice on constant speed (a) and accelerating speed (b) rotarod tests (mean±SEM, * = $p<0.01$ Students t-test). Constant speed rotarod n-values for 2m, 4m, 6m, 9m, 12m, 18m and 24m respectively: Wild type – 11, 28, 35, 34, 23, 17, 16; Hemizygous *Thy1*mγSN – 12, 27, 40, 36, 26, 21, 19; Homozygous *Thy1*mγSN – 13, 21, 23, 23, 14, 0, 0. Accelerating speed rotarod n-values for 2m, 4m, 6m, 9m, 12m, 18m and 24m respectively: Wild type – 11, 14, 34, 32, 24, 17, 16; Hemizygous *Thy1*mγSN – 12, 19, 40, 36, 26, 22, 15; Homozygous *Thy1*mγSN – 13, 18, 22, 23, 15, 0, 0. Adapted from Ninkina et al. 2009.

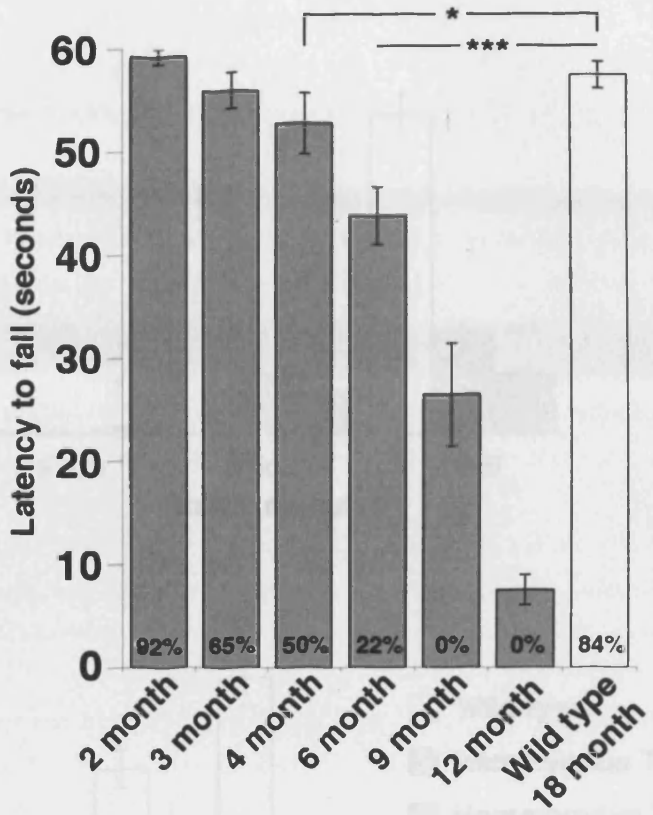

Fig. 5. Age related deficit in performance of homozygous Thy1mγSN on the inverted grid. Inverted grid test of 18-month wild type and various age *Thy1*mγSN$^{TG/TG}$ mice (grey columns, mean±SEM * $p<0.05$, *** $p<0.001$ Mann-Whitney U-test). The ability of *Thy1*mγSN mice to hang from an inverted grid diminishes substantial with age. Inset number denotes percentage of animals able to remain on test for the full 60 seconds test period. *Thy1*mγSN$^{TG/TG}$ n; 2m = 25; 3m = 17; 4m = 10; 6m = 22; 9m = 9; 12m = 22. WT n; 18m = 32.

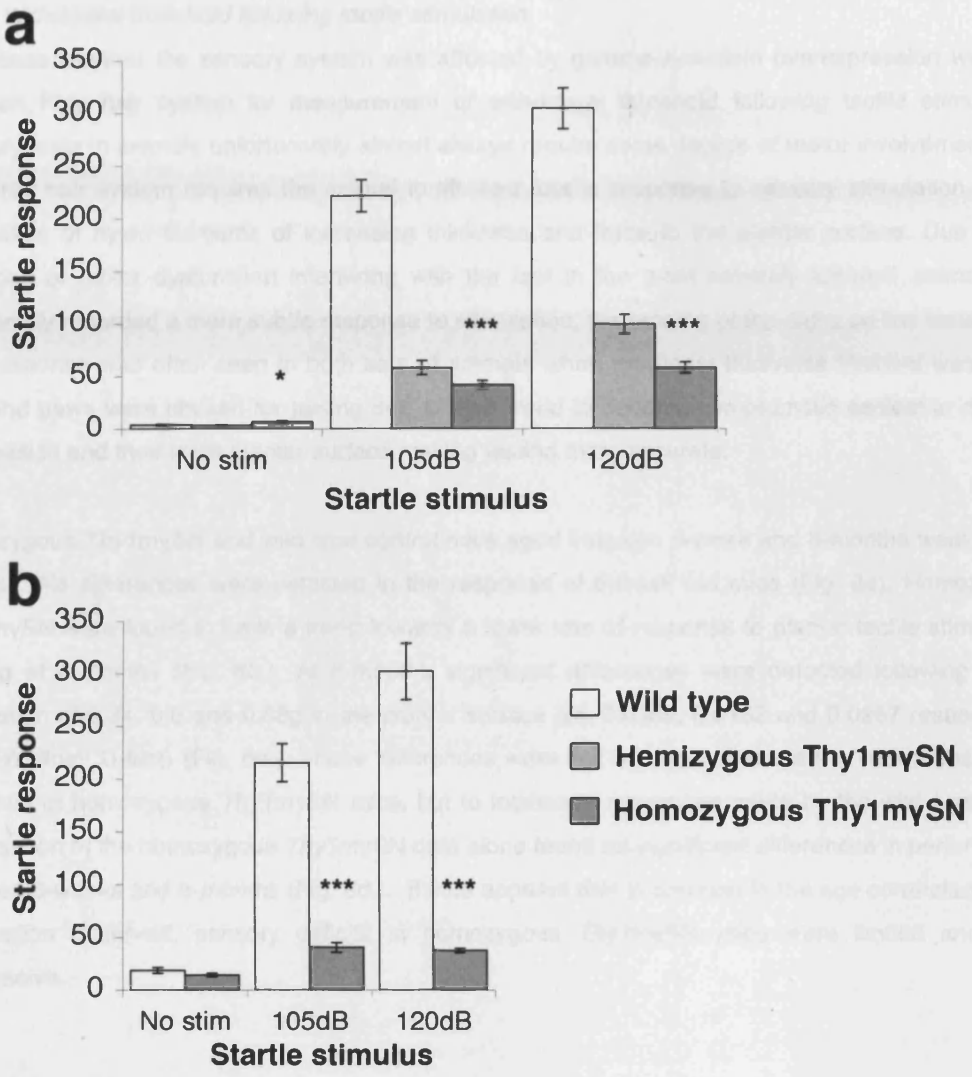

Fig. 6. Diminished response of Thy1mγSN mice to acoustic startle stimulation. Response of wild type, hemizygous and homozygous Thy1mγSN mice to 105 and 120dB acoustic startle stimuli at 3 weeks (a) and wild type and homozygous Thy1mγSN mice at 24 weeks (b) (mean±SEM, * $p<0.05$, *** $p<0.001$ Mann-Whitney U-test). 3 week n; wild type = 6; hemizygous Thy1mγSN = 6; homozygous Thy1mγSN = 8. 24 weeks n; wild type = 6; homozygous Thy1mγSN = 10.

3.2.6. Withdrawal threshold following tactile stimulation

To assess whether the sensory system was affected by gamma-synuclein overexpression we used the Von Frey hair system for measurement of withdrawal threshold following tactile stimulation. Sensory tests in animals unfortunately almost always require some degree of motor involvement. The Von Frey hair system requires the animal to lift their foot in response to sensory stimulation by the application of nylon filaments of increasing thickness and force to the plantar surface. Due to the likelihood of motor dysfunction interfering with the test in the most severely affected animals, we additionally recorded a more subtle response to stimulation, the fanning of the digits on the tested foot. This response was often seen in both sets of animals when the finest thickness filament was used. The hind paws were chosen for testing due to their trend to become symptomatic earliest in disease progression and their large plantar surface making testing more accurate.

Homozygous *Thy1*mγSN and wild type control mice aged between 6-week and 8-months were tested (Fig. 6.). No differences were detected in the response of 6-week old mice (Fig. 6a). Homozygous *Thy1*mγSN were found to have a trend towards a lower rate of response to plantar tactile stimulation of 0.6g at 4-months (Fig. 6b.). At 8-months significant differences were detected following tactile stimulation of 0.34, 0.6 and 0.88g to the plantar surface ($p= 0.0369$, 0.0182 and 0.0267 respectively, Mann-Whitney U-test) (Fig. 6c.). These differences were not however attributed to reductions in the response of homozygous *Thy1*mγSN mice, but to increased responses made by the wild type mice. Comparison of the homozygous *Thy1*mγSN data alone found no significant differences in performance between 6-weeks and 8-months (Fig. 6d.). It thus appears that in contrast to the age correlated motor dysfunction observed, sensory deficits in homozygous *Thy1*mγSN mice were limited and non-progressive.

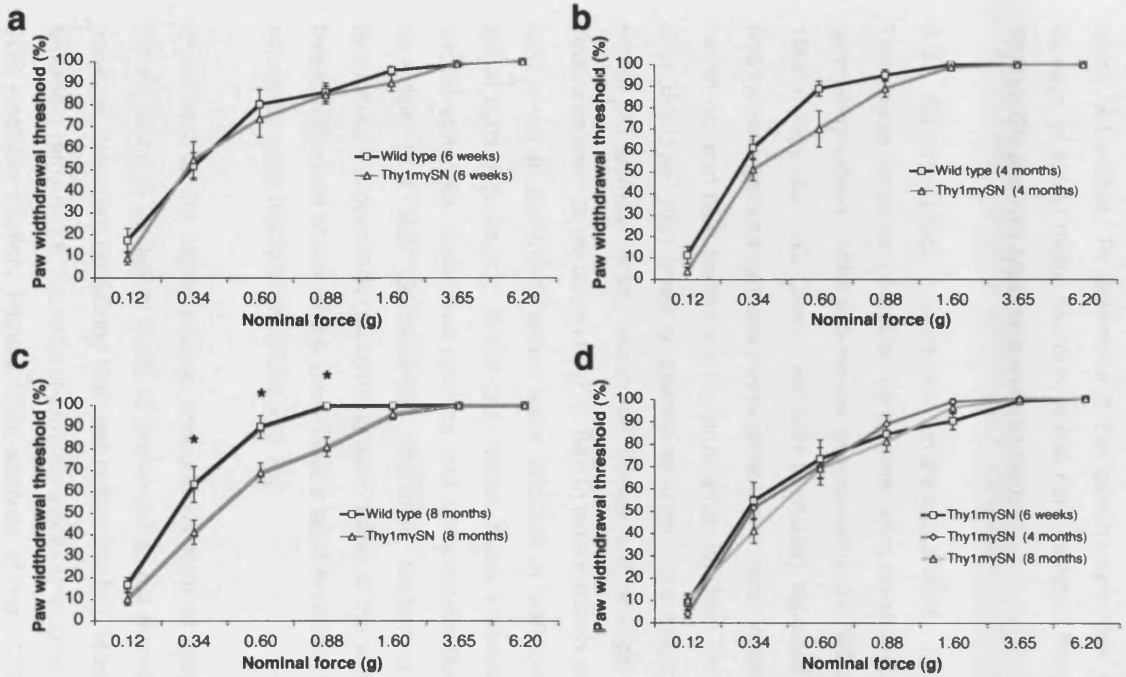

Fig. 7. Paw withdrawal threshold following sensory stimuli. Paw withdrawal response following sensory stimuli of wild type and *Thy1*mγSN mice at 6 weeks (a), 4 months (b) and 8 months (c) (mean±SEM, Mann-Whitney U-test, * $p<0.05$). No progressive deficit in performance was detected in the response of *Thy1*mγSN mice to sensory stimulation (d). The response of wild type mice however appears to improve with age, resulting in significant differences to the *Thy1*mγSN response at 8-months. WT n; 6w = 6; 4m = 6; 8m = 6. Homozygous *Thy1*mγSN n; 6w = 9; 4m = 8; 8m = 10.

3.3. Results: Spinal cord pathology

The phenotype induced by gamma-synuclein overexpression has characteristics typical to those seen in many animal models with compromised motor systems (Allen et al. 2002; Bruijn et al. 1998; van der Putten et al. 2000; Wegorzewska et al. 2009). Damage in these animals is often found to be most substantial in the spinal cord, with the ventral horn population of motor neurons often found to be highly vulnerable. To determine if the gamma-synuclein overexpression phenotype led to similar damage of spinal motor neurons, spinal cord samples from two- and twelve-month old homozygous *Thy1*mγSN and wild type mice were studied.

3.3.1. Gamma-synuclein aggregation in the spinal cord

Transverse sections of spinal cord were immuno-stained with antibodies raised against murine gamma-synuclein (rabbit anti-mouse gamma-synuclein SK23 affinity purified antibody (Buchman *et al.* 1998)) (Figs. 8a, 9a). Concurrent with previously reported data (Ninkina et al. 2003) low levels of endogenous gamma-synuclein were detected in motor neurons and neuropil of both two- and twelve-month old wild type control spinal cords (Figs. 8a, 9a). The spinal cords of homozygous *Thy1*mγSN mice displayed high levels of gamma-synuclein throughout both the grey and white matter. In two-month old animals motor neuron cell bodies and neuropil were intensely stained, though inclusion structures were rarely observed (Fig. 8a). In twelve-month old symptomatic *Thy1*mγSN mice however, high levels of gamma-synuclein were detected in widespread aggregate structures throughout the spinal cord (Fig. 9a, b). In the grey matter, these inclusion bodies took the form of perikaryal and axonal spheroids, ballooned neurites and Lewy-neurite-like structures densely stained for gamma-synuclein (Fig. 9a). Spheroid-like structures containing gamma-synuclein were also detected throughout the descending/ascending axon tracts of the white matter (Fig. 9b). H&E staining showed that in a manner typical of the Lewy bodies seen in human PD, a small proportion of the intracellular spheroids were highly eosinophilic (Fig. 9a).

In contrast to the highly soluble endogenous form of gamma-synuclein, a large proportion of the protein found in the spinal cords of twelve-month old homozygous *Thy1*mγSN mice was insoluble in non-ionic detergent containing high salt buffer (Fig 9c). Moreover, a substantial proportion of gamma-synuclein remained in fractions of proteins insoluble in ionic detergent containing buffers, including an SDS insoluble fraction. Immuno-TEM analysis of the SDS insoluble fraction revealed long straight gamma-synuclein positive fibrils typical for amyloid depositions found in various neurodegenerative conditions (data not show).

Typically the proteins contained within inclusion bodies in both human disease and animal models are ubiquitinated. To assess whether the gamma-synuclein containing structures seen in aged homozygous *Thy1*mγSN mice were similarly ubiquitinated, we fluorescently immunostained transverse sections of spinal cord with antibodies against both gamma-synuclein and ubiquitin (Fig. 9d). Though structures containing both proteins were observed, many were found to exclusively contain either

gamma-synuclein or ubiquitin. It thus appears that ubiquitination of gamma-synuclein is not an essential event in the development of *Thy1*mγSN pathology.

3.3.2. Amyloid containing inclusion quantification

Congo red staining revealed that amyloid containing structures were present in the spinal cords of twelve-month old homozygous *Thy1*mγSN mice (Fig. 10). The simplicity and relatively low cost of Congo red staining made it a practical high throughput method for the quantification of amyoid inclusion presence in the experimental cohorts. Four groups of twelve-month old animals were analysed; wild-type controls, hemizygous *Thy1*mγSN mice, homozygous *Thy1*mγSN with mild symptoms and homozygous *Thy1*mγSN mice with advanced penetrance of the neurological phenotype. The number of amyloid positive structures was counted within a $0.1mm^2$ field of the ventral horn in randomly selected transverse sections from the cervical, thoracic and lumbar regions of the spinal cord. Quantification revealed amyloid positive structures were occurred at a negligible frequency in control spinal cords (Fig. 10e). In contrast a significant number of such structures were observed in all three transgenic groups ($p<0.0001$, Kruskal Wallis, Fischer's *a priori*). The presence of amyoid bodies was most pronounced in homozygous mice with advanced pathology, with an average of 27.8 observed per $0.1mm^2$ field. Though significant, the number of amyloid structures in the hemizygous and mildly symptomatic homozygous *Thy1*mγSN mice was lower than in the advanced stage animals with an average of 14.5 and 8.8 per $0.1mm^2$ field respectively. Results following a similar pattern to the mean values were obtained from cervical, thoracic and lumbar levels of spinal cord (see appendix 1).

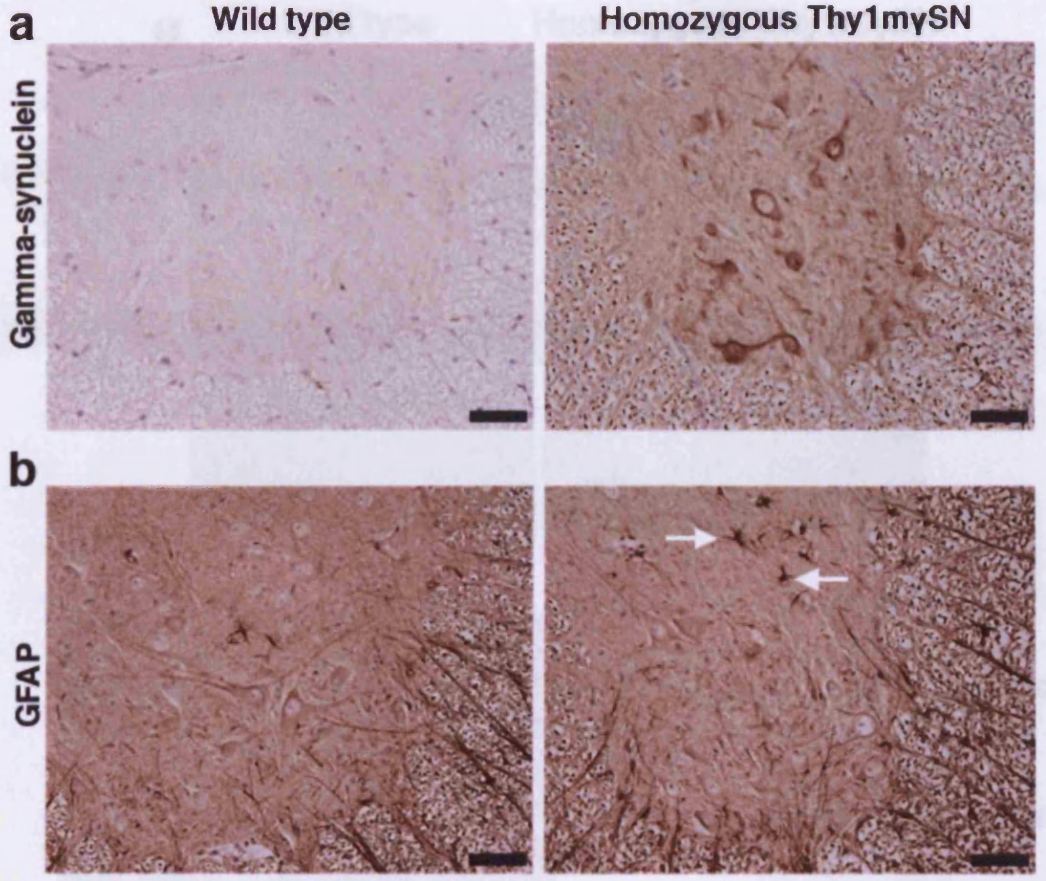

Fig. 8. Gamma-synuclein in the spinal cord of 2-month old homozygous Thy1mySN mice. Representative transverse sections of thoracic spinal cord collected from two-month old wild type (left panels) and homozygous *Thy1*mγSN mice (right panels) immunostained with antibodies raised against gamma-synuclein (SK23, 1:100) (a) and GFAP (1:400) (b). Arrows = activated astrocytes. Scale bars = 50μm

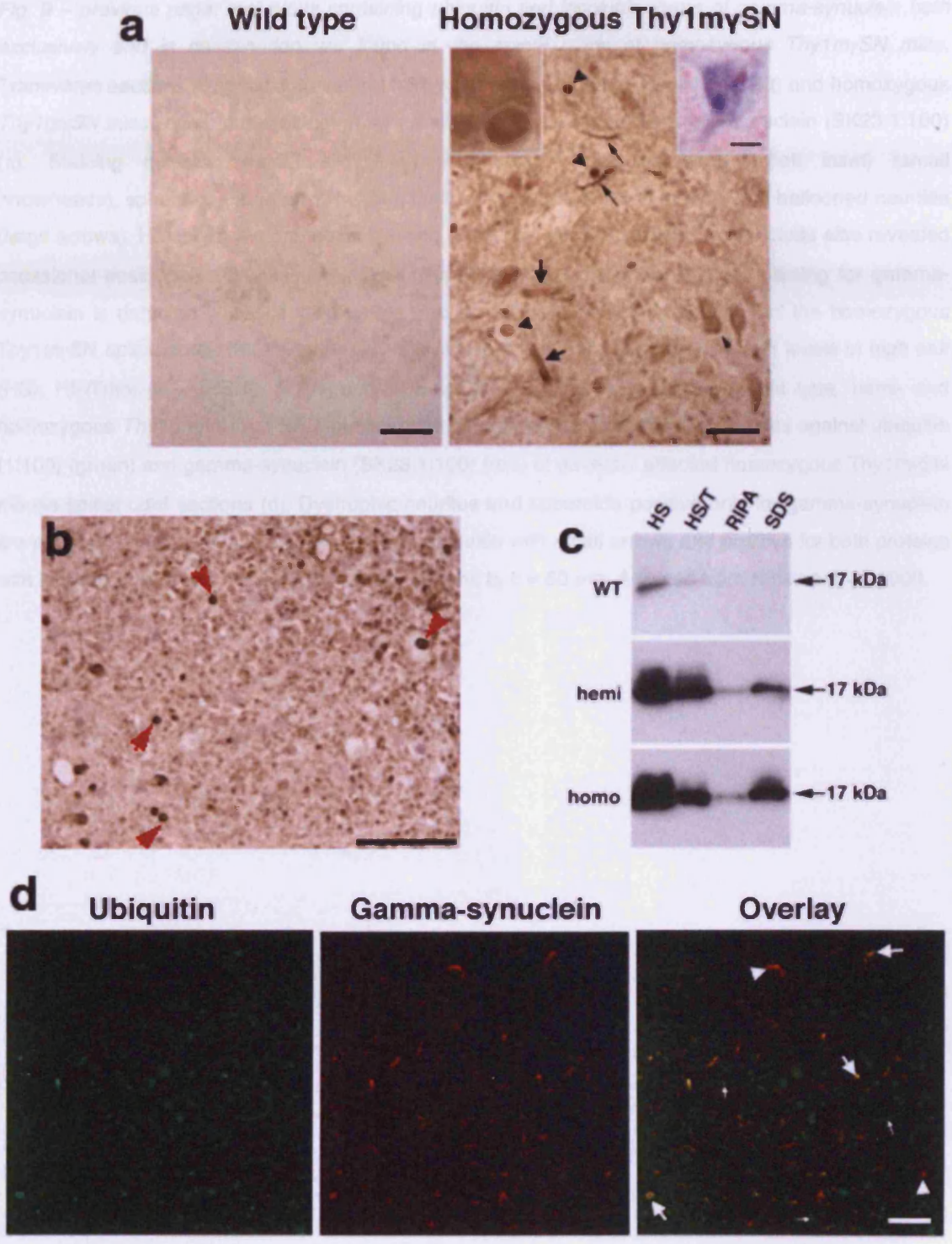

Fig. 9. Inclusions containing gamma-synuclein and ubiquitin both exclusively and in combination are found in the spinal cords of homozygous Thy1mγSN mice.

Fig. 9 – previous page. Inclusions containing ubiquitin and insoluble forms of gamma-synuclein both exclusively and in combination are found in the spinal cords of homozygous Thy1mγSN mice. Transverse sections of spinal cord ventral horn from twelve-month old wild type (left) and homozygous *Thy1mγSN* mice (right) immunostained with antibodies raised against gamma-synuclein (SK23 1:100) (a). Staining detected gamma-synuclein-positive cytoplasmic inclusions (left inset) (small arrowheads), spheroids (large arrowheads), dystrophic neurites (small arrows) and ballooned neurites (large arrows). Haematoxylin and eosin staining of homozygous Thy1mγSN spinal cords also revealed occasional eosinophilic cytoplasmic inclusion (right insert). Abnormally intense staining for gamma-synuclein is detected in descending axons (red arrowheads) in lateral columns of the homozygous Thy1mγSN spinal cords (b). Western blot analysis of spinal cord gamma-synuclein levels in high salt (HS), HS/Triton-X_{100} (HS/T), RIPA- and SDS-soluble fractions collected from wild type, hemi- and homozygous *Thy1mγSN* mice (c). Double immunofluorescent staining with antibodies against ubiquitin (1:100) (green) and gamma-synuclein (SK23 1:100) (red) of severely affected homozygous Thy1mγSN mouse spinal cord sections (d). Dystrophic neurites and spheroids positive only for gamma-synuclein are marked with arrowheads, positive only for ubiquitin with small arrows and positive for both proteins with large arrows. Scale bars a=50μm, insert=20μm; b, c = 50 μm. Adapted from Ninkina et al. 2009.

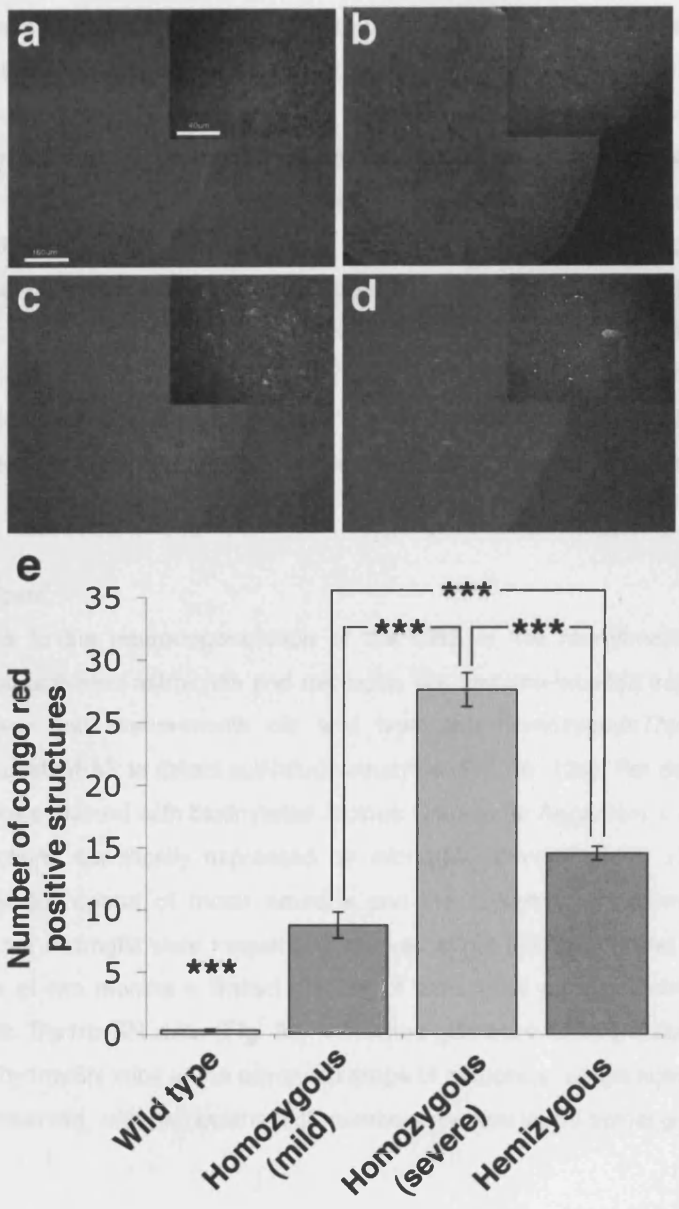

Fig. 10. *Amyloid positive aggregates are present in the spinal cords of symptomatic homozygous Thy1mγSN mice.* Representative Congo red staining of the spinal cords of wild type (a), hemizygous (b), mildly (c) and severely (d) affected homozygous *Thy1*mγSN mice. Amyloid positive aggregates appear as bright red dots. Mean numbers of aggregates counted per 0.1mm^2 region of 12-month old spinal cord analyzed (e) (Mean ± SEM, Kruscal-Wallis, Fisher's a priori test *** $p<0.001$). Scale bars a-d Insert = 160μm, main panel = 40μm. Number of animals: wild type, homozygous (severe) and hemizygous = 5, homozygous (mild) = 4. Number of sections sampled: wild type = 104, mildly affected homozygous *Thy1*mγSN 72, severely affected homozygous *Thy1*mγSN 93, hemizygous *Thy1*mγSN 121. Adapted from Ninkina et al. 2009.

3.3.3. *Spinal motor neuron population quantification*

The presence of gamma-synuclein positive inclusion bodies and widespread gliosis within the spinal cord of homozygous *Thy1*mγSN mice, combined with the profound motor deficits they develop suggested the likelihood of damage to spinal motor neurons. Nissl staining allowed us to quantify this population of cells in the same twelve-month old sample groups used for the assessment of amyloid deposition (Fig. 11a-d). Quantification revealed significant numbers of spinal motor neurons were lost throughout the spinal cord in all transgenic groups (One-way ANOVA, Fisher's a priori test, $p<0.001$) (Fig. 11e). The loss of spinal motor neurons correlated with the presence of amyloid positive structures. Accordingly the greatest cell loss occurred in the advanced stage homozygous *Thy1*mγSN mice, with a mean loss of 62.7%. Both the mildly affect homozygous *Thy1*mγSN and hemizygous *Thy1*mγSN mice also had highly significant motor neurons losses of 52.5 and 35.6% respectively. Similar results to mean values were obtained from cervical, thoracic and lumbar levels of spinal cord (see appendix 2).

3.3.4. Spinal cord gliosis

A common response to the neurodegeneration of the CNS is the recruitment and activation of neuroglia, in particular activated astrocytes and microglia. We immuno-labelled transverse sections of spinal cord from two- and twelve-month old wild type and homozygous *Thy1*mγSN mice with antibodies raised against GFAP to detect activated astrocytes (Fig. 8b, 12a). For detection of activated microglia, samples were stained with biotinylated Ricinus Communis Agglutinin 1 (RCA), a lectin that bind to the glycoproteins specifically expressed by microglia (Mannoji et al. 1986) (Fig. 12b). In concurrence with the full cohort of motor neurons and the absence of inclusion bodies, neither activated astrocytes nor microglia were frequently observed within wild type spinal cords at either age sampled. At the age of two months a limited number of astrocytes were detected within the spinal cords of homozygous *Thy1*mγSN mice (Fig. 8b). Activated glia were substantially more abundant in the spinal cords of *Thy1*mγSN mice at the advanced stage of pathology. Large numbers of both micro- and astroglia were observed, with particularly high numbers present in the spinal grey matter (Fig 12a, b).

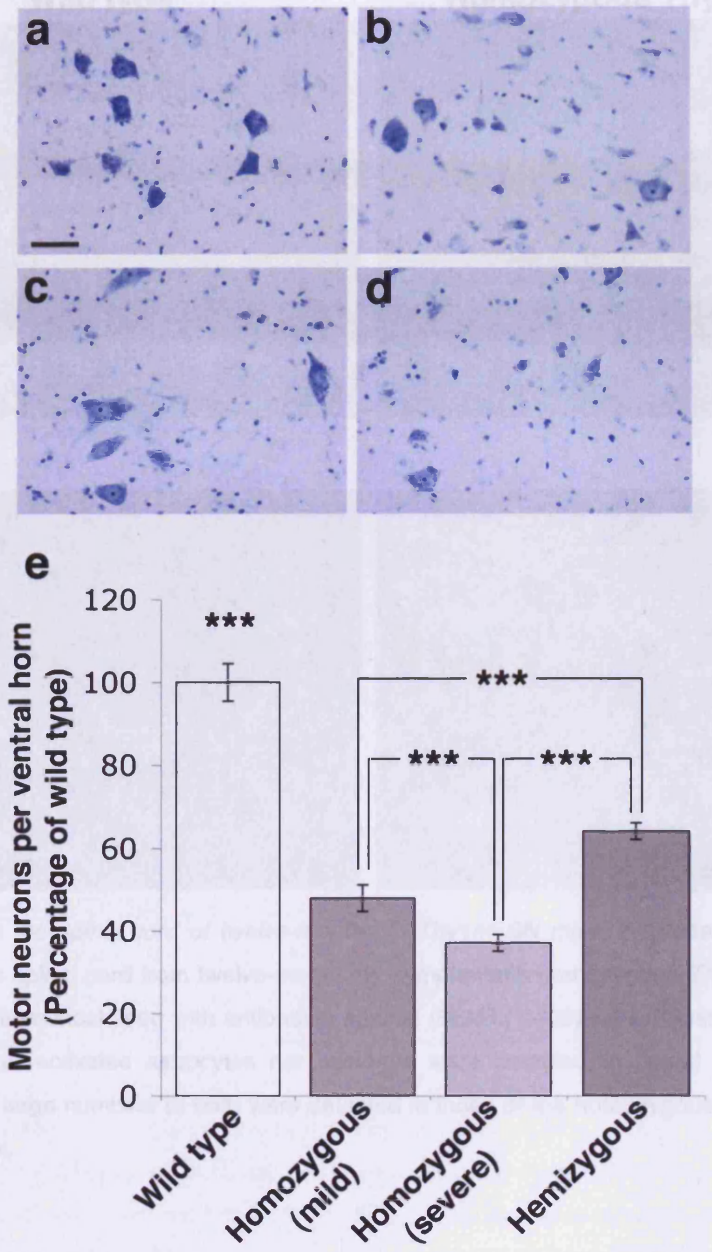

Fig. 11. Spinal motor neurons are lost in Thy1mγSN mice. Representative Nissl staining of the ventral horn region of spinal cords from twelve-month old wild type (a), hemizygous (b), mildly affected (c) and severely affected homozygous *Thy1mγSN mice* (d). Number of motor neurons counted within the ventral horn region of the twelve-month old spinal cord sections analyzed (e) (Mean±SEM expressed as percentage of mean number from wild type, One-way ANOVA, Fisher's a priori test *** $p<0.001$). Scale bar a-d = 50µm. Number of animals: wild type, homozygous (severe) and hemizygous = 5, homozygous (mild) = 4. Number of sections sampled wild type = 160, mildly affected homozygous *Thy1*mγSN 149, severely affected homozygous *Thy1*mγSN 195, hemizygous *Thy1*mγSN 285. Adapted from Ninkina et al. 2009.

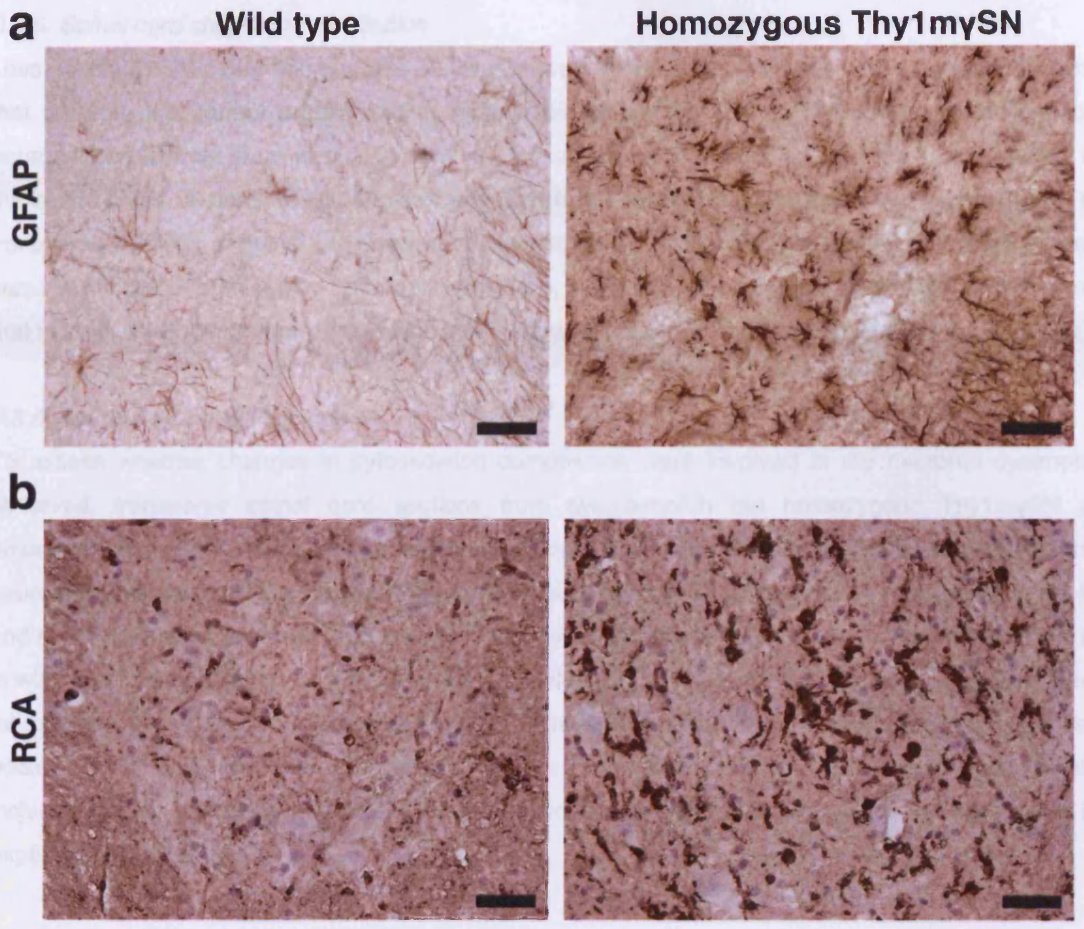

Fig. 12. Gliosis in the spinal cord of twelve-month old Thy1mγSN mice. Representative transverse section of thoracic spinal cord from twelve-month old symptomatic homozygous *Thy1*mγSN and wild type control mice immunostained with antibodies against GFAP (1:400) (a) or biotinylated lectin RCA (1:100) (b). Neither activated astrocytes nor microglia were detected in spinal cord of wild type animals, however large numbers of both were detected in those of the homozygous *Thy1*mγSN mice. Scale bars = 50μm.

3.3.5. Spinal cord chaperone distribution

Loss of spinal cord motor neurons has previously been attributed to dysfunction of chaperone proteins that facilitate the correct protein folding. The levels of HSP70 and HSP27/HSPB1, both common neuronal chaperones, were assessed by Western blotting, with increase levels of the latter detected in the spinal cords of symptomatic homozygous Thy1mγSN mice (data not shown). Immunostaining of transverse sections of spinal cord with antibodies against HSP27/HSPB1 revealed that this increase was not attributed to increased neuronal expression, which unexpectedly was considerably lower than that seen in wild type controls, but to high levels within the surrounding activated astrocytes (Fig. 13a).

3.3.6. Spinal cord neurofilaments

To assess whether changes in cytoskeleton composition were involved in the neuronal dystrophy observed, transverse spinal cord sections from twelve-month old homozygous Thy1mγSN at advanced stages of disease and age-matching wild type mice were labeled with antibodies against the neuron specific intermediate filaments NF-L, NF-M and NF-H (Fig. 13b). Though differences in NF-M and NF-H distribution between both groups were limited, pronounced changes were detected in NF-L. In wild type animals intense staining was seen in cell bodies and neurites, the latter being well defined morphologically. In aged homozygous Thy1mγSN mice NF-L staining was notably reduced in the cell bodies and virtually absent from emerging neurites. Though the presence of neurofilaments within inclusion bodies has been previously reported in synucleinopathies no such structures were found in experimental animals.

3.3.7. Interaction between gamma-synuclein and neurofilament-L

Gamma-synuclein overexpression has previously been reported to increase the susceptibility of neurofilament networks in cultured neurons to degradation by calcium dependent proteases through an unclear mechanism. To investigate whether the damage presented in *Thy1*mγSN mice was associated with direct interaction between the two proteins we immunoprecipitated soluble NF-L from the spinal cords of twelve-month old wild type and *Thy1*mγSN mice (Fig. 13c). Immunoprecipitation of NF-L was followed by analysis of levels of co-immunoprecipitated gamma-synuclein. We found high levels of gamma-synuclein co-precipitated with NF-L in all *Thy1*mγSN groups and was not detected in wild type tissues. Interestingly the highest levels were detected in *Thy1*mγSN mice with only mildly affected by pathology at the age of twelve-months, suggesting that the association between gamma-synuclein and soluble NF-L may be a contributing factor in pathogenesis. Furthermore the association between gamma-synuclein and NF-L most likely occurs in intact or partially intact neurons, where at the later stages of disease neurons are either highly degenerate or lost entirely.

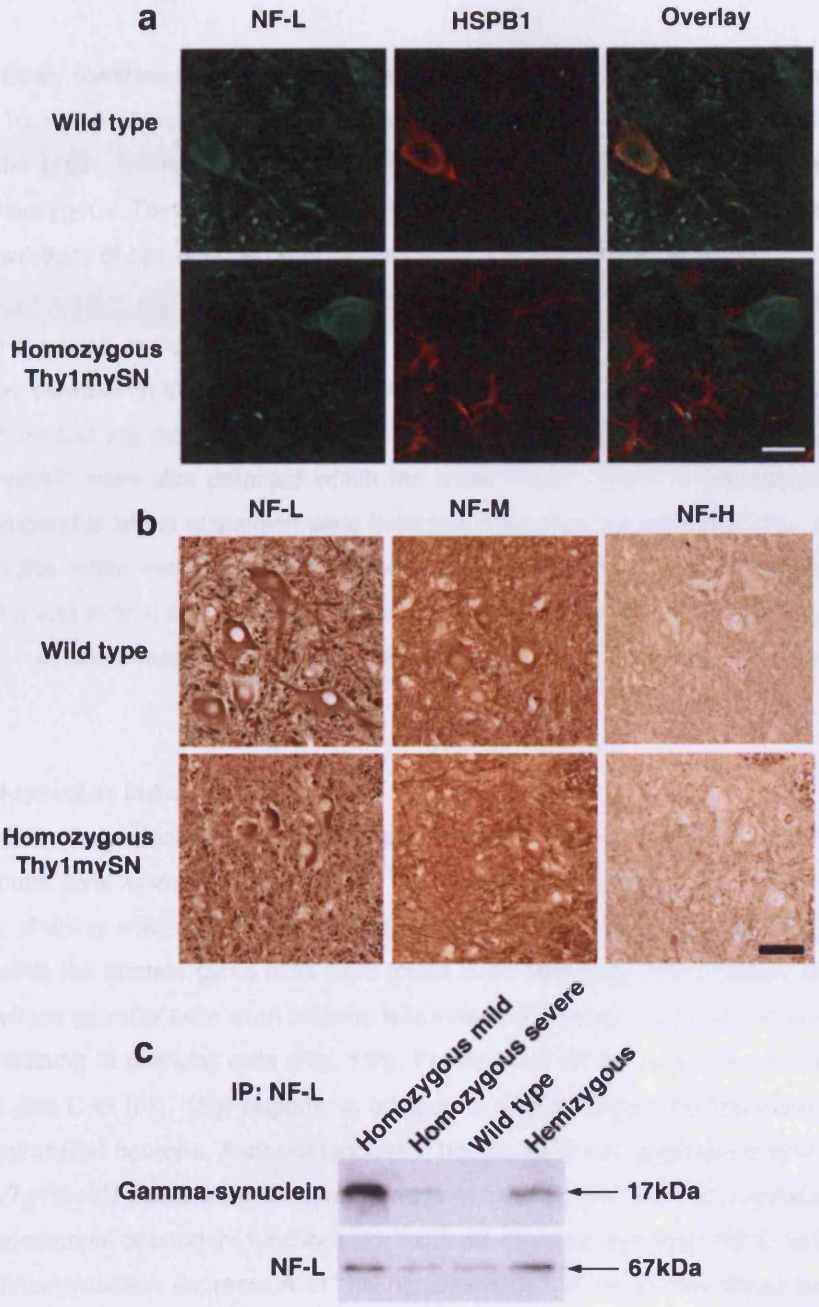

Fig. 13. Changes in levels of spinal neurofilaments are linked to the binding of gamma-synuclein with soluble neurofilament-L. Representative double immunofluorescent staining of spinal cord sections from matching mice with antibodies against neurofilament-L (1:200, green) and HSPB1 (1:20, red) (a). Immunostaining against NF-L (1:250), NF-M (1:250) and NF-H (1:250) in transverse section of the ventral horn region of spinal cords from twelve-month old wild type and severely affected homozygous *Thy1*mγSN mice (b). Co-immunoprecipitation of gamma-synuclein and NF-L from cytosolic fractions of twelve month old spinal cord from wild type and *Thy1*mγSN mice (c). Scale bars a, b = 20μm. Adapted from Ninkina et al. 2009.

3.4. Results: Brain pathology

We have previously confirmed levels of gamma-synuclein protein to be high in the brain of *Thy1*mγSN mice (Fig. 2). To further characterise the anatomical distribution of Thy1-driven expression of gamma-synuclein in the brain, we immunostained sagittal brain sections of severely symptomatic twelve-month old homozygous *Thy1*mγSN mice with affinity purified SK23 antibodies raised against the protein. Brain sections of age matched wild type mice were stained for control.

3.4.1. Gamma-synuclein in the cerebellum

In the wild type cerebellum low levels of gamma-synuclein were restricted to the Purkinje cell layer (Fig. 14c), with no staining detected in either the molecular or granular layers (Fig. 14b, c). Low levels of gamma-synuclein were also detected within the white matter tracts. In homozygous *Thy1*mγSN cerebellum comparable levels of staining were detected in the Purkinje cell layer (Fig. 14f), but axonal staining within the white matter region (Fig. 14e) and granular layers (Fig. 14f) was substantial. Beaded neurites and axonal spheroid were frequent throughout both structures. Without quantification of neuron survival, the consequence of such high levels of gamma-synuclein in the cerebellum is unclear.

3.4.2. Gamma-synuclein in the hippocampus

Gamma-synuclein was restricted to the dentate gyrus of the wild type hippocampus (Fig. 15a). Axons within the granular layer were gamma-synuclein positive, as were infrequent neurons within the hilus (Fig. 15d). No staining was observed within either the CA1 (Fig. 15b) or CA3 (Fig. 15c) regions. Similar cells within the dentate gyrus hilus were found to be stained in homozygous *Thy1*mγSN mice (Fig. 15h). However granular cells axon staining was substantially more pronounced and accompanied by perikaryal staining in granular cells (Fig. 15h). Furthermore diffuse neuropil staining was seen in CA1 (Fig. 15f) and CA3 (Fig. 15g) regions, in addition to high levels of staining within the perikaryal cytoplasm of pyramidal neurons. Abnormal inclusion bodies were not observed in any neurons of the homozygous *Thy1*mγSN hippocampus. Quantification of hippocampal neuron population survival and analysis of hippocampal dependent functions, for example memory, are required to further assess the effects of gamma-synuclein expression in the hippocampus. Unfortunately these experiments are beyond the scope of this project.

3.4.3. Gamma-synuclein in the olfactory tubercle

In wild type mice low-level endogenous gamma-synuclein was detected in the perikaryal cytoplasm of olfactory tubercle mitral cells (Fig. 16b). No further staining was detected. In homozygous *Thy1*mγSN mice, diffuse neuropil staining was observed throughout the olfactory tubercle (Fig. 16c). Furthermore both the cell bodies and processes of mitral neurons were densely stained for gamma-synuclein (Fig. 16d), though intracellular inclusion bodies were not detected. Punctate staining was detected throughout the granular layer (Fig. 16d).

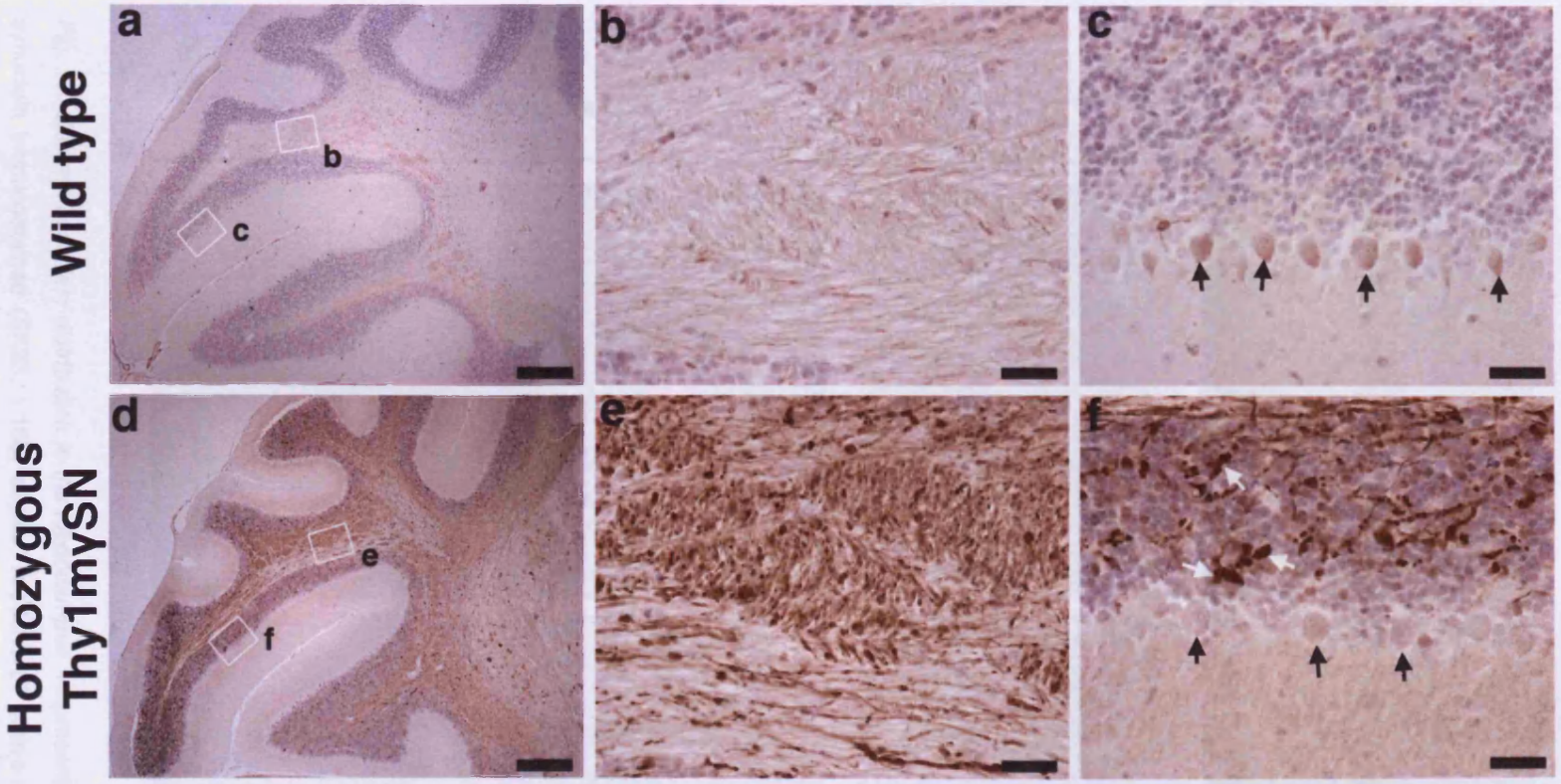

Fig. 14. Gamma-synuclein distribution in the cerebellum. Representative images showing gamma-synuclein immunostained (SK23, 1:100) sagittal sections (lateral 1.44mm) of cerebellum from twelve-month old wild type (a-c) and homozygous *Thy1*mγSN (d-f) mice. High magnification images of the 6th cerebellar lobule white matter (b, e), Purkinje and granular layers (c, f). Arrows = Purkinje cell layer. Scale bars a, d = 250μm, b, c, e, f = 25μm.

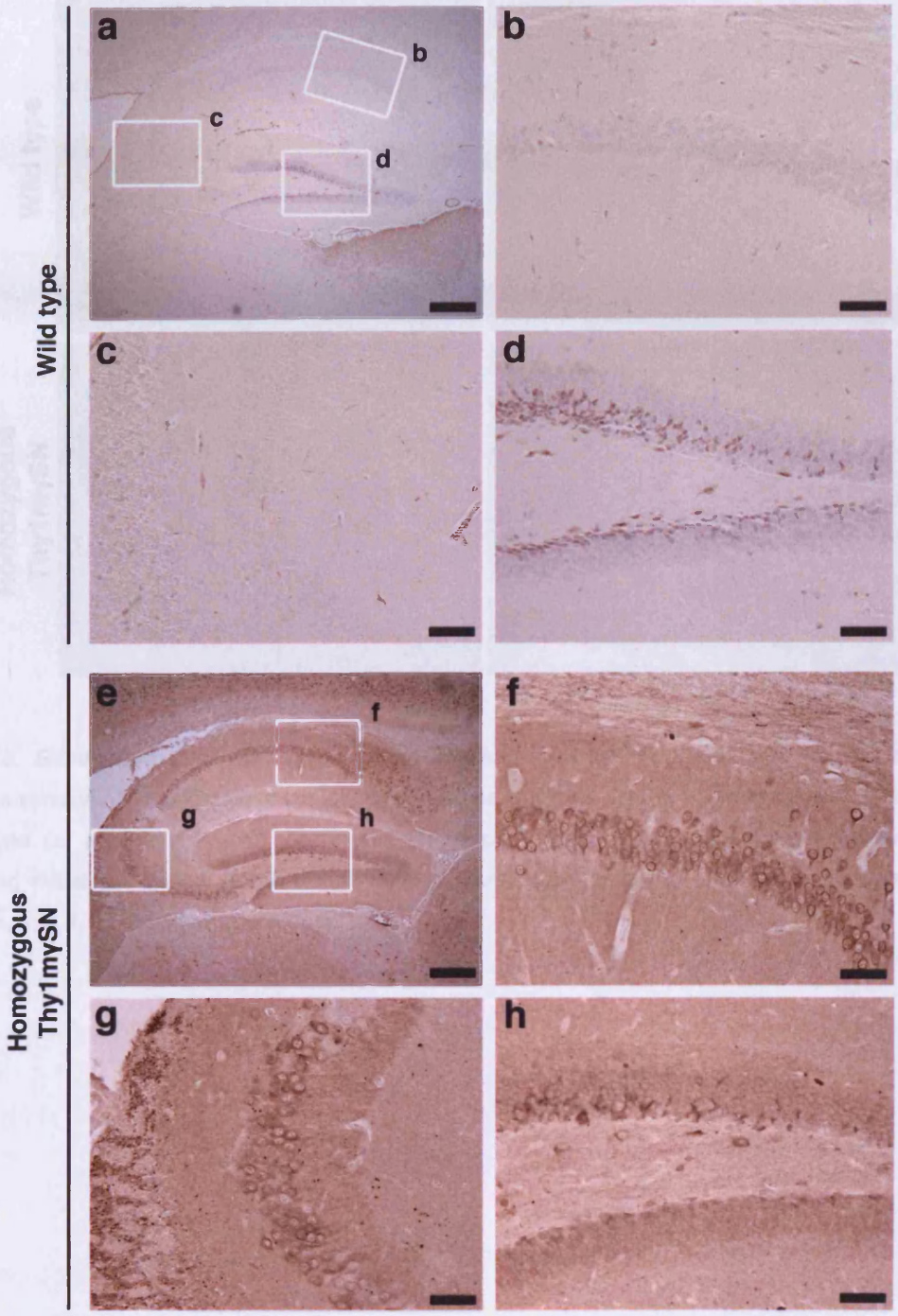

Fig. 15. Gamma-synuclein distribution in the hippocampus. Representative images showing gamma-synuclein immunostained (SK23, 1:100) sagittal sections of twelve-month old wild type (a-d) and homozygous *Thy1*mγSN (e-h) hippocampal regions CA1 (b, f), CA3 (c, g) and the dentate gyrus (d, h). Scale bars a, e = 250μm, b-d, f-h = 50μm.

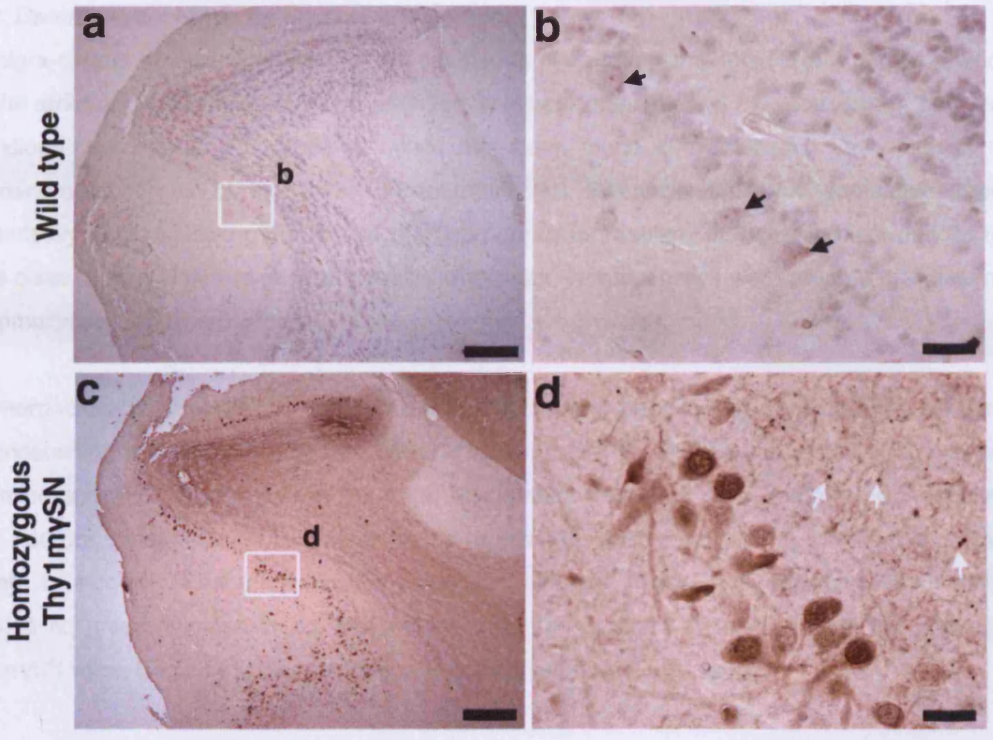

Fig. 16. Gamma-synuclein distribution in the olfactory tubercle. Representative images showing gamma-synuclein immunostained (SK23, 1:100) sagittal sections (lateral 1.44mm) of twelve-month old wild type (a) and homozygous *Thy1*mγSN (c) olfactory bulbs. High magnification images (c, d) showing mitral cell bodies (black arrows) and punctate staining (white arrows). Scale bars a, c = 100μm, b, d, f, h = 25μm, e, g = 250μm.

3.4.4. Gamma-synuclein in the nigrà-striatal system

The nigra-striatal system, composed of the substantia nigra pars compacta (SNpc) and its projections into the striatum, is the focus of much attention in synucleinopathy and PD research. In both familial and idiopathic forms of PD alpha-synuclein has been found in cytoplasmic Lewy bodies within dopaminergic neurons of the SNpc. Furthermore the SNpc dopaminergic population becomes substantially depleted during the course of PD progression, resulting in the movement deficits typical of the disease. We aimed to assess if similar dystrophic characteristics were present in twelve-month old homozygous *Thy1*mγSN mice.

For morphological analysis, the striatum and SNpc were identified in sagittal brain sections by immunostaining with antibodies against tyrosine hydroxylase, an enzyme essential for the synthesis of dopamine specific to dopaminergic neurons. The striatum consists of a "matrix" region of medium spiny neurons striated by "white matter tracts" containing bundles of axons. The SNpc contains a discrete cluster of DA neurons located within the midbrain. Tyrosine hydroxylase immunostaining revealed no gross changes in the morphology of either structure in twelve-month old homozygous *Thy1*mγSN mice (Fig. 17d, j) in comparison to control animals (Fig. 17a, g).

Assessment of inclusion body formation was carried out through immuno-staining with affinity-purified antibodies against gamma-synuclein. In control wild type brains staining was found to be absent from matrix regions and white matter tracts of the striatum (Fig. 17b, c), with only very low levels detected in the dopaminergic cells of the SNpc (Fig. 17h, i). In age matched homozygous *Thy1*mγSN tissue, diffuse neuropil staining accompanied by widespread punctate staining was seen throughout both structures, including the striatal matrix. The striatal white matter tracts contained axons densely stained for gamma-synuclein, many with an abnormal, disordered morphology (Fig. 17f). Though some densely stained cells were observed, gamma-synuclein staining was largely absent from the dopaminergic cells of the SNpc (Fig. 17k), most likely due to the weak expression of the Thy1 promotor within this cell type (van der Putten et al. 2000). Abnormal axonal inclusion structures were observed throughout the SNpc, with beaded neurites and spheroids widespread (Fig. 17l).

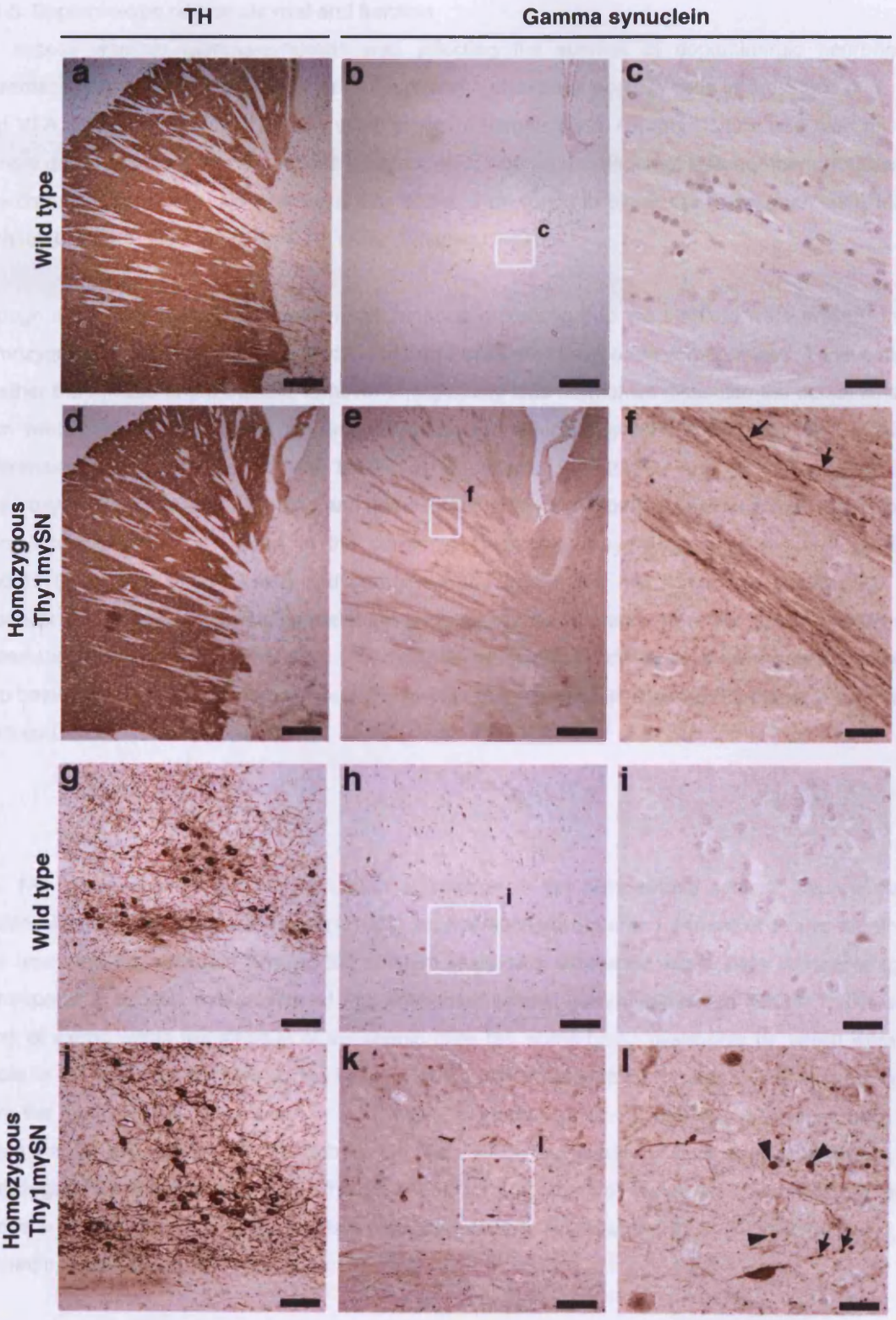

Fig. 17. Gamma-synuclein expression in the nigra-striatal system.

3.4.5. Dopaminergic neuron survival and function

To assess whether gamma-synuclein was affecting the survival of dopaminergic neurons we stereotactically quantified the population of tyrosine hydroxylase positive cells in the SNpc (Fig. 18c) and VTA (Fig. 18d, appendix 3) of a small group of homozygous *Thy1*mγSN and wild type mice. A sample group of coronal serial sections were counted, with an estimation of total number calculated by Aberchrombie correction. No significant differences were found in either the SNpc ($p=0.2491$, Mann-Whitney U-test) or the VTA ($p=0.4712$, Mann-Whitney U-test).

Though a full complement of dopaminergic neurons projecting into the striatum were present in the homozygous *Thy1*mγSN mice, the function of these cells may have been compromised. To investigate whether the release and metabolic turnover of dopamine was normal we dissected the dorsal striatum from twelve-month old animals for analysis of neurochemicals by HPLC (Fig. 19). No significant differences were detected in the levels of dopamine ($p=0.2556$, and its metabolites 3,4-dihydroxyphenylacetic acid (DOPAC) and homovanillic acid (HVA) ($p=0.4168$ & $p=0.2556$ respectively, Mann-Whitney U-test), or those of the serotonin metabolite 5-hydroxyindoleacetic acid (5-HIAA) ($p=0.8710$, Mann-Whitney U-test) and norepinephrine ($p=0.6162$, Mann-Whitney U-test) (Fig. 19a, appendix 4). The level of dopamine metabolic turnover can be estimated from the ratio of dopamine to its metabolites HVA and DOPAC (Fig. 19b, c). Again no significant differences were detected in either ratio between wild type and homozygous *Thy1*mγSN mice ($p=0.4168$ & $p=0.6261$ respectively, Mann-Whitney U-test).

* * *

Fig. 17 - previous page. Gamma-synuclein expression in the nigra-striatal system. Representative tyrosine hydroxylase immunostained (1:1000) sagittal sections (lateral 1.44mm) of twelve-month old wild type and homozygous *Thy1*mγSN striatum (a,d) and substantia nigra *pars compacta* (g, j). Corresponding section immunostained with antibodies against gamma-synuclein (SK23, 1:100) show tracts of axons within the striatum of transgenic mice (e), some being dystrophic (f), which were not visible in the wild type animals (b, c). Staining of the *Thy1*mγSN striatal matrix is low, though higher than the endogenous level seen in wild types. Gamma-synuclein labelling is absent from the dopaminergic cell bodies of the substantia nigra *pars compacta* of both wild type (h, i) and homozygous *Thy1*mγSN (k, l) mice, though spheroids and tracts of axons are present in the latter. Arrows = dystrophic axons, arrowheads = axonal spheroids, scale bars a, b, d, e = 250μm; g, h, j, k = 100μm; c, f, i, l = 25μm.

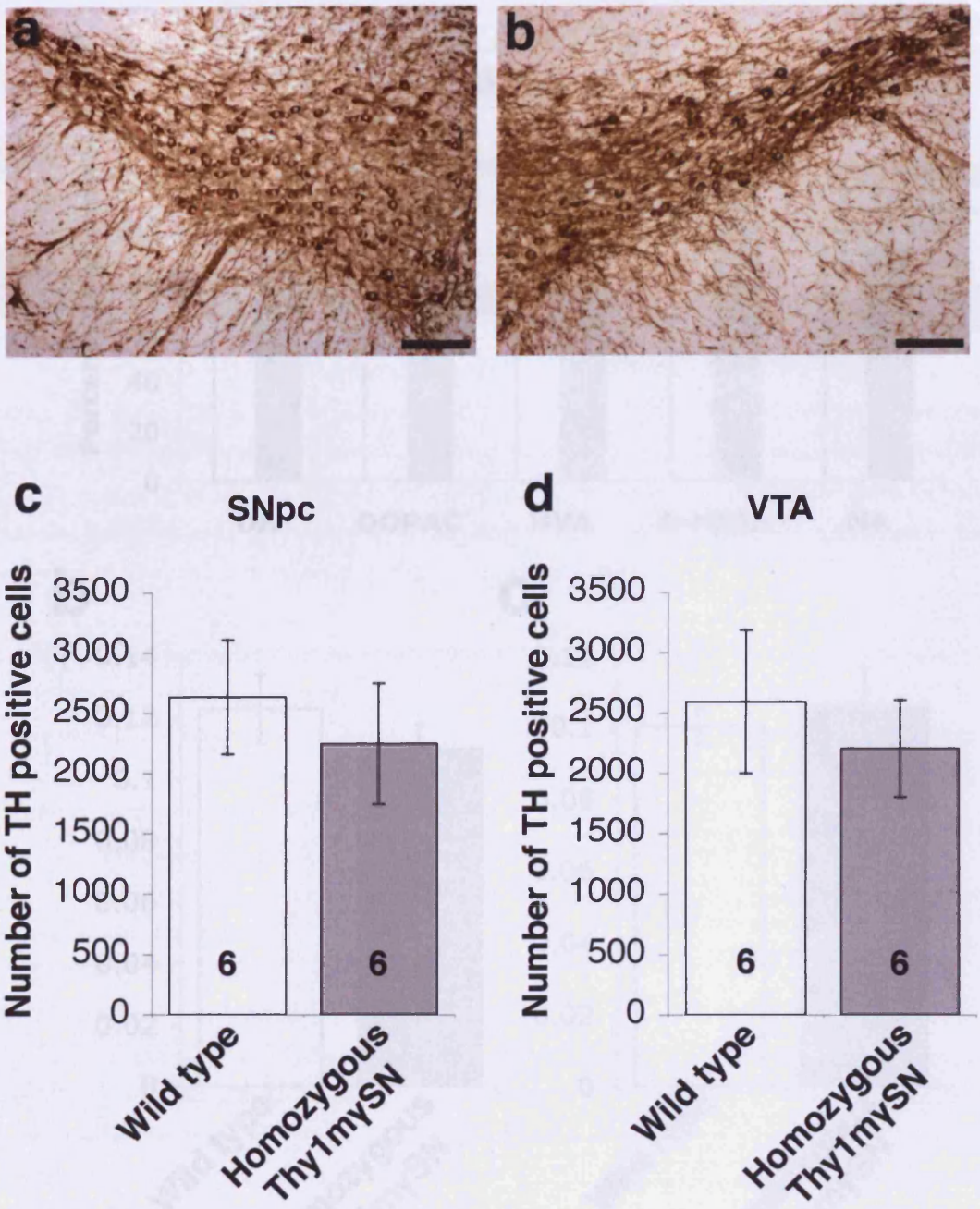

Fig. 18. No loss of dopaminergic neurons from the SNpc or VTA of homozygous Thy1mySN mice. Representative images of transverse sections of brain from twelve-month old wild type (a) and homozygous Thy1mySN mice (b) immunostained with antibodies against tyrosine hydroxylase (1:100). Quantification of dopaminergic neuron populations from the SNpc (c) or VTA (d) of the above mice (mean±SEM). Insert number denotes number of respective regions quantified, derived from three animals in each group.

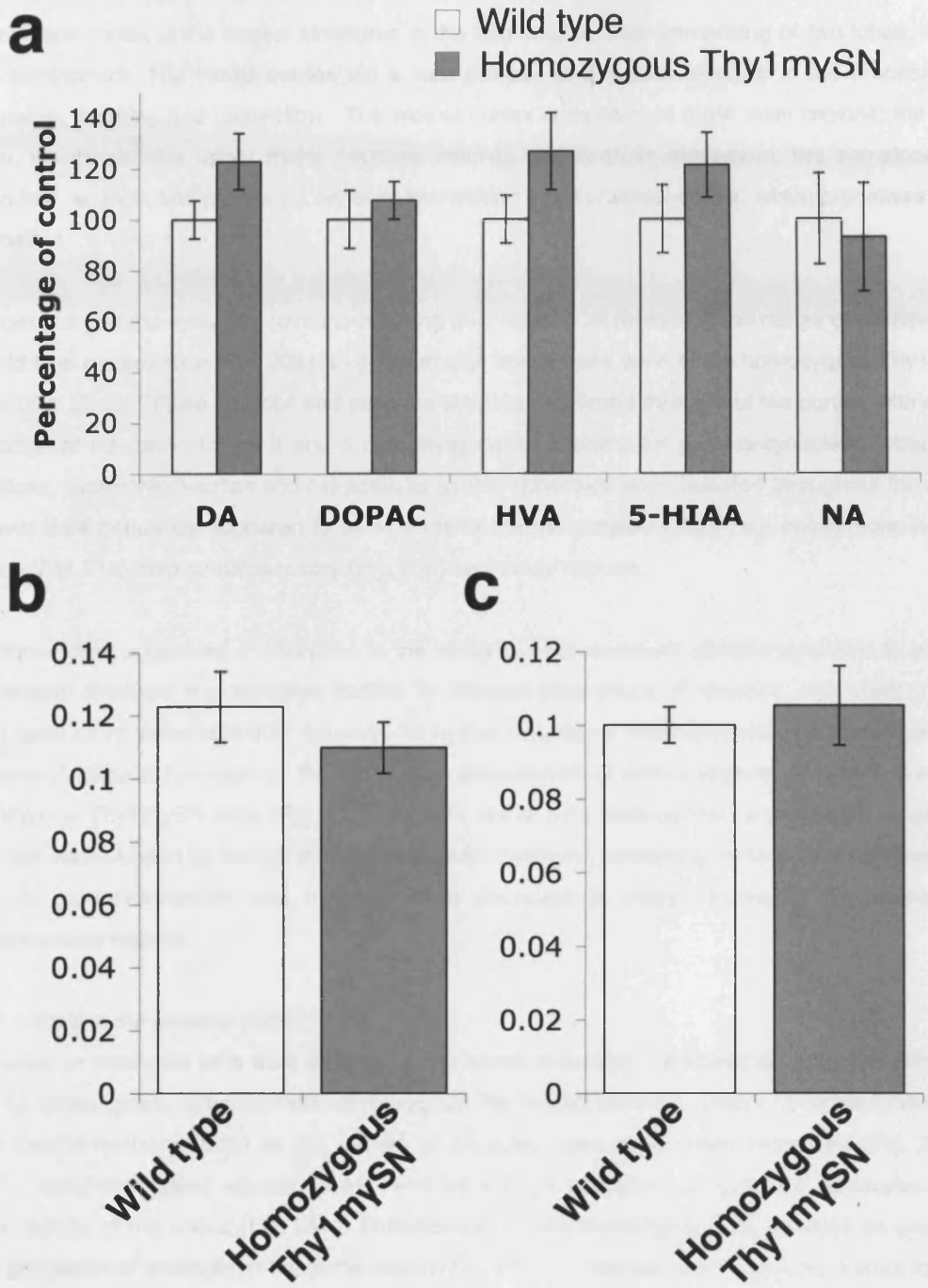

Fig. 19. Striatal neurotransmitter levels and dopamine turnover are unaffected in homozygous Thy1mγSN mice. (a) Striatal levels of dopamine, DOPAC, HVA, 5-HIAA and norepinephrine in twelve-month old wild type and homozygous Thy1mγSN mice. Ratio of striatal dopamine to metabolites (b) DOPAC and (c) HVA. All bars show mean±SEM. WT n = 5, homozygous Thy1mγSN n = 7.

3.4.6. Gamma-synuclein in the cerebral cortex

The cerebral cortex is the largest structures in the mammalian brain comprising of two lobes, one on each hemisphere. The cortex carries out a vast number of functions involved in the processing of information, learning and perception. The mouse cortex comprises of three main regions; the motor region, which contains upper motor neurons, initiates and controls movement, the somatosensory region that receives and processes sensory information and the visual cortex, which processes visual information.

Endogenous gamma-synuclein immuno-labelling was weak in all regions of the cortex of twelve-month old wild type control mice (Fig. 20a_i). In contrast high levels were seen in the homozygous Thy1mγSN cortex (Fig. 20a_{ii}). Diffuse neuropil and punctate staining was found throughout the cortex, with a large proportion of neuron in layers 3 and 5 containing dense staining for gamma-synuclein. Intracellular inclusions, dystrophic neurites and extracellular axonal spheroids were detected throughout the cortex, however their frequency appeared to be in a rostral-caudal gradient (Fig 21a_{ii}), being more in motor regions (Fig. 21a) than somatosensory (Fig. 21b) and visual regions.

The above data suggested a difference in the ability of overexpressed gamma-synuclein to produce pathological changes, e.g. inclusion bodies, in different populations of neurons, with cortical motor areas been more vulnerable than sensory. To further investigate this hypothesis we investigated the solubility of gamma-synuclein in the motor and somatosensory cortex regions of twelve-month old homozygous Thy1mγSN mice (Fig. 21d). As with spinal cord (see above), a proportion of gamma-synuclein was found to be insoluble in high salt, ionic detergent containing buffer in both cortices. This insoluble gamma-synuclein was however more abundant in motor regions of the cortex than somatosensory regions.

3.4.7. Gliosis in the cerebral cortex

Few astro- or microglial cells were detected in the cortex of healthy, 12-month old wild type mice (Fig. 21b_i, c_i). In the cortex of symptomatic homozygous *Thy1*mγSN mice the pattern of gliosis followed the same caudal-rostral gradient as the pattern of insoluble gamma-synuclein inclusions (Fig. 20b_{ii}-c_{ii}, 21b-c). Antibodies raised against GFAP detected a large population of activated astrocytes within motor regions of the cortex (Fig. 21b_i). Immunostaining with biotinylated RCA detected an additional large population of microglia in the same region (Fig. 21c_i). In contrast both populations were found to be fewer in number in somatosensory and visual regions of the cortex (Fig. 21b_{ii}, Fig c_{ii}).

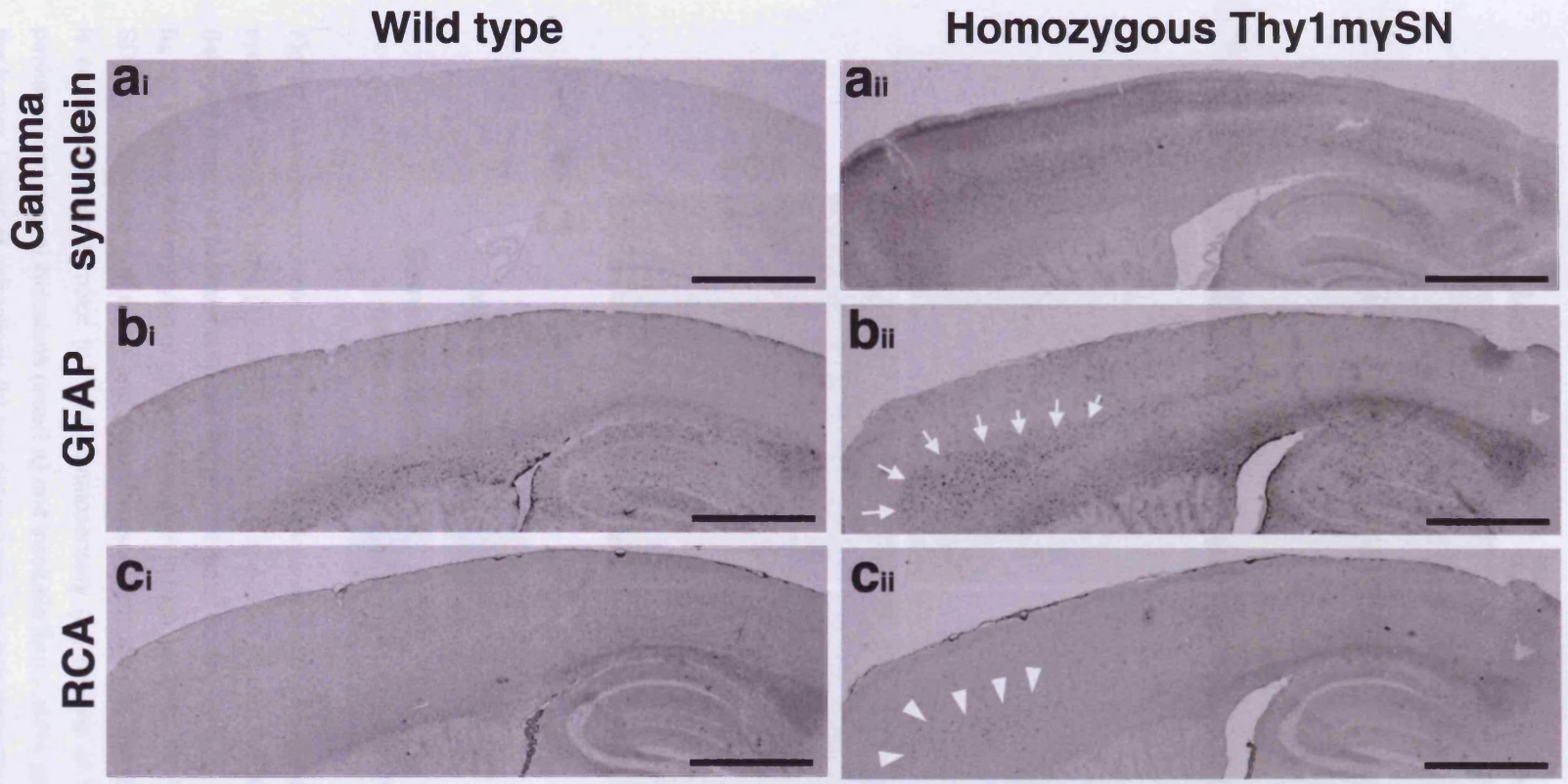

Fig. 20. Gamma-synuclein expression and gliosis in the cortex. Representative sagittal sections of cortex from twelve-month old wild type (a_i, b_i, c_i) and homozygous *Thy1mySN mice* (a_{ii}, b_{ii}, c_{ii}) immuno-stained with antibodies raised against gamma-synuclein (SK23, 1:100) (a), GFAP (1:400) (b) and biotinylated lectin RCA (1:100) (c). Arrows = astroglia, arrowheads = microglia. Scale bars = 1mm.

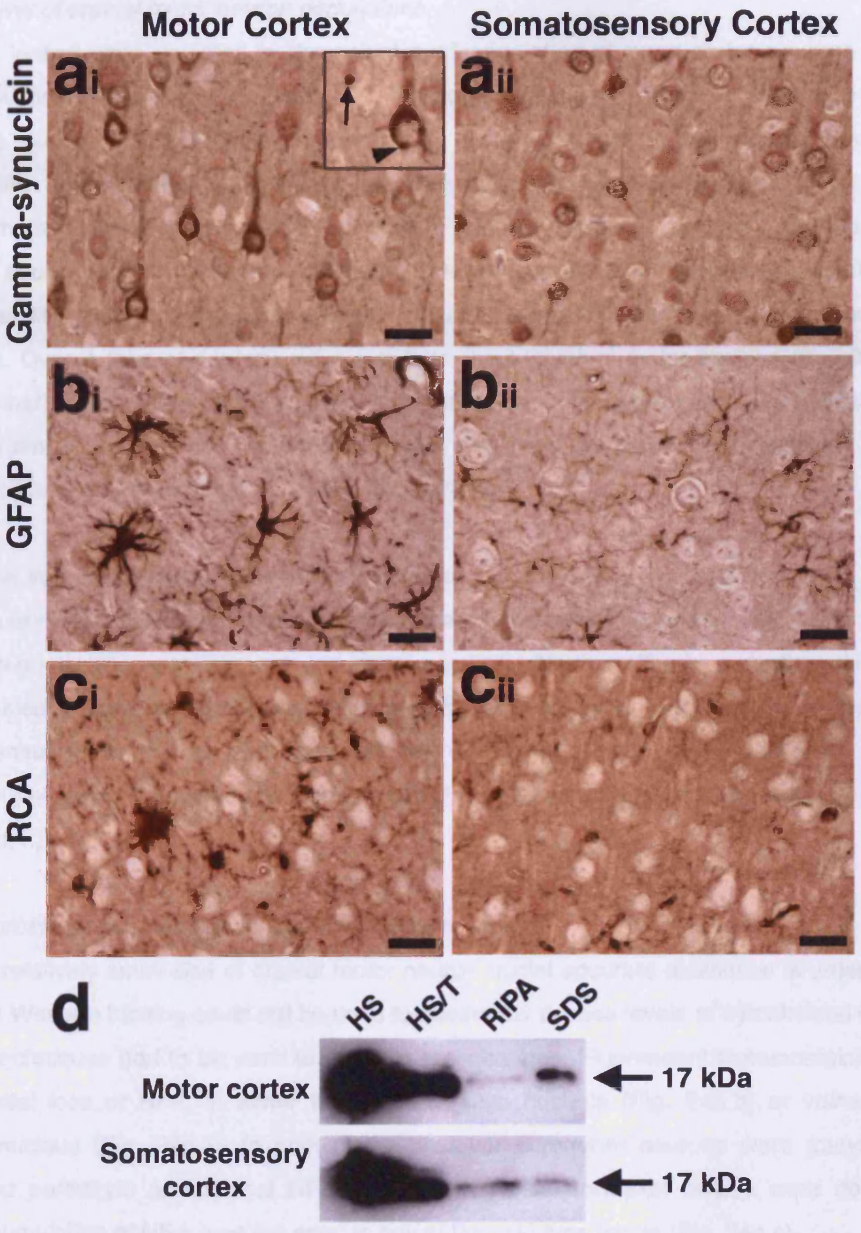

*Fig. 21. Gamma-synuclein accumulation and gliosis in the Thy1*mγSN *cortex.* Representative gamma-synuclein (SK23, 1:100) (a), GFAP (1:400) (b) and RCA (1:100) (c) immunostained sagittal sections (lateral 1.44mm) of twelve-month old *Thy1*mγSN motor cortex (a_i, b_i, c_i) and somatosensory cortex (a_{ii}, b_{ii}, c_{ii}). Western blot analysis of gamma-synuclein in high salt (HS), HS/Triton X-100 (HS/T), RIPA- and SDS-soluble fractions of motor and somatosensory cortices (d). The distribution of gamma-synuclein is consistent in both motor (a_i) and somatosensory (a_{ii}) regions of the cortex, however abnormal perikaryal and axonal inclusions (insert a_i) and insoluble forms of the protein (d) are most prominent in the former. Levels of astrogliosis (b) and microgliosis (c) were distinctly higher in the *Thy1*mγSN motor cortex (b_i and c_i respectively) than the somatosensory cortex (b_{ii} and c_{ii} respectively). Arrow = axonal spheroid, arrowhead = perikaryal accumulation. Scale bars = 50μm.

3.4.8. Survival of cranial motor neuron populations

Substantial losses were detected in the spinal cord population of lower motor neurons in severely symptomatic twelve-month old homozygous *Thy1*mγSN mice (see above). We aimed to further assess the survival of lower motor neurons in discrete nuclei of the mouse hindbrain. We stereologically counted the motor neurons in the abducens (Fig. 22a,b), facial (Fig. 22c,d) and trigeminal motor nuclei (Fig. 22e,f) on Nissl stained sections (also see appendix 5). Total number of neurons in each population was estimated using the fractionator technique. Unexpectedly we found that vulnerability of neurons to gamma-synuclein overexpression was not universal across these populations. Over a third of neurons were lost from the trigeminal motor nucleus ($p=0.0013$, Mann-Whitney U-test), comparable to the depletion seen in spinal cord populations (Fig. 22i). In contrast a full complement of neurons were found in both the abducens ($p=0.9645$, Mann-Whitney U-test) and facial nuclei ($p=0.824$, Mann-Whitney U-test) (Fig. 22g,h).

3.4.9. Gliosis in the proximity of cranial motor neurons

The pattern of differential lower motor neuron vulnerability observed was paralleled by the activation of the glia. Co-immunofluorescence with the neuron specific NeuN antibody and other raised against GFAP revealed a more numerous population of activated astrocytes in the vicinity of the vulnerable motor trigeminal nucleus (Fig. 23d) compared to the tolerant facial nucleus (Fig. 23b). Biotinylated RCA staining revealed a matching pattern of microglia activation, the cells being more frequent within the (Fig. 23f, h).

3.4.10. Neurofilament-L distribution in cranial motor neurons

Due to the relatively small size of cranial motor neuron nuclei accurate dissection is unfeasible. Thus quantitative Western blotting could not be used to accurately assess levels of cytoskeletal components and other techniques had to be used to observe any changes. Fluorescent immunostaining revealed no substantial loss of NF-L in either the tolerant facial nucleus (Fig. 24a,b) or vulnerable motor trigeminal nucleus (Fig. 24c,d). In both nuclei however infrequent neurons were found to contain accumulated perikaryal and axonal NF-L, though no typical inclusion bodies were detected (Fig. 24b,d). Accumulation of NF-L was not seen in any of the wild type tissue (Fig. 24a,c).

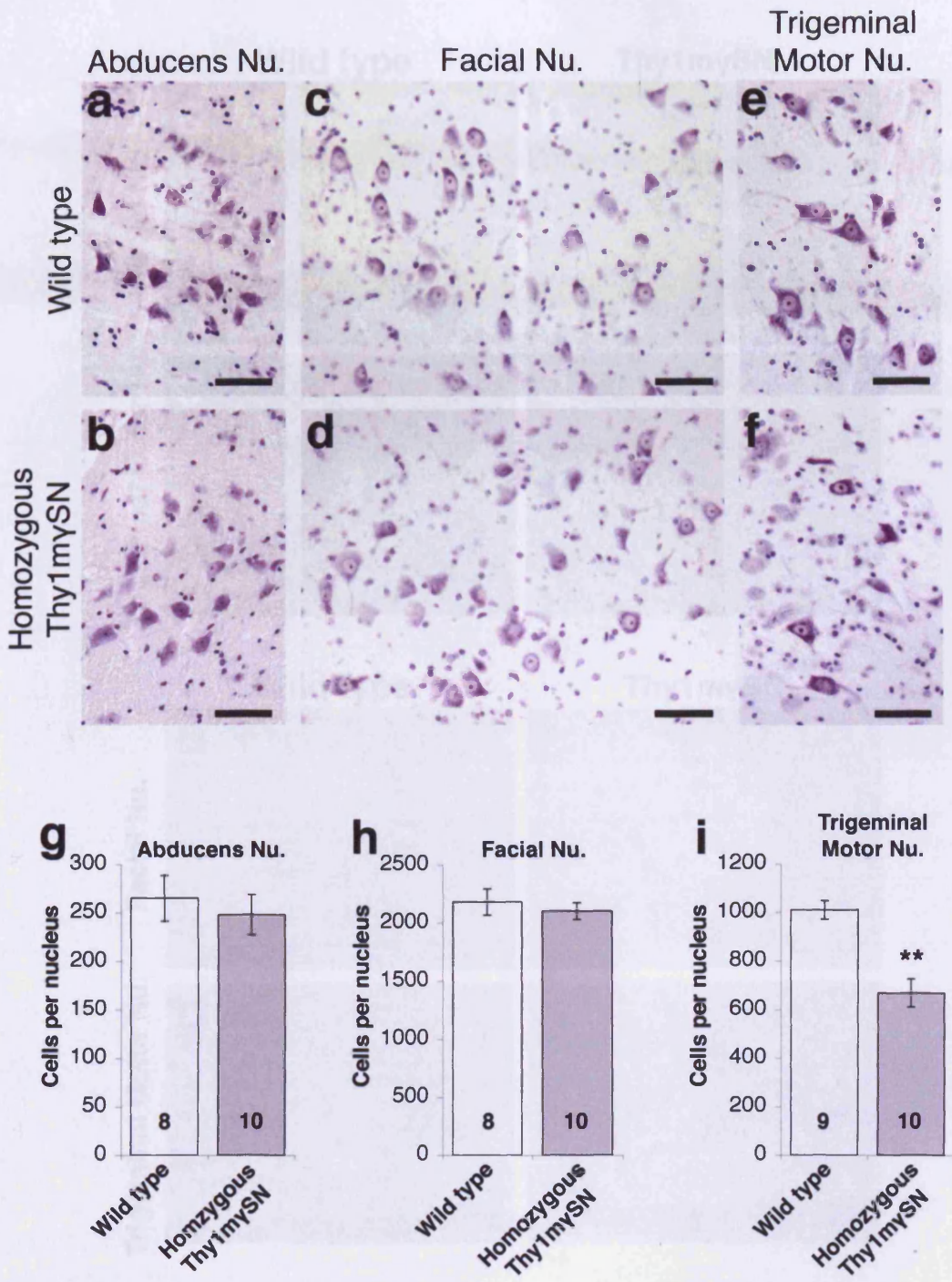

Fig. 22. *Differential vulnerability of cranial motor neuron pools was seen in homozygous Thy1mγSN mice.* Representative images of Nissl stained abducens (a, b), facial (c, d) and trigeminal motor (e, f) nuclei of wild type (a, c, e) and homozygous *Thy1*mγSN mice (b, d, f). Quantification of motor neuron population in the abducens (g), facial (h) and trigeminal motor nucleus (i). (mean±SEM, Mann-Whitney U-test ** $p<0.001$). Scale bar a-f = 25μm. Each group contained five animals, the insert number denoting the total number of nuclei counted.

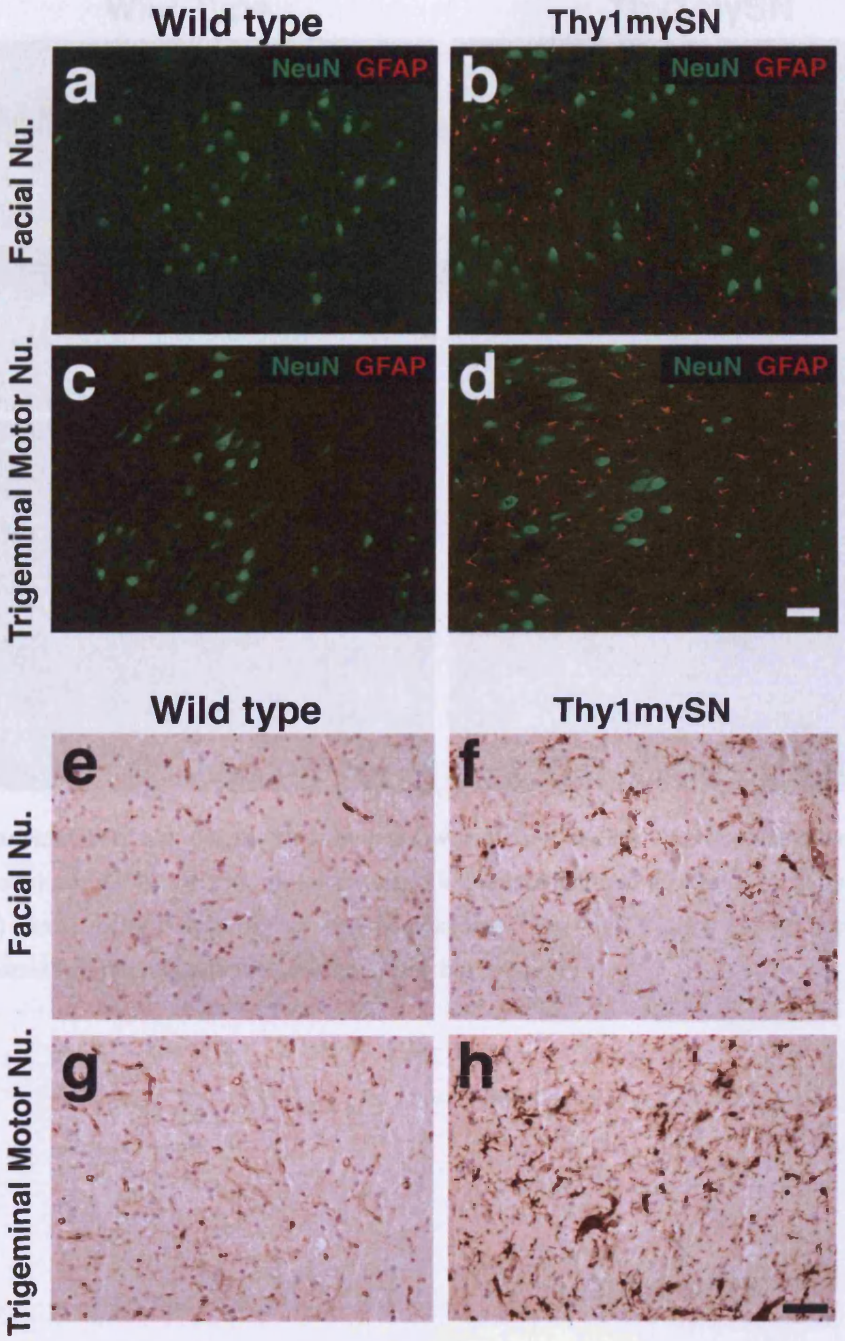

Fig. 23. Differential activation of gliosis in cranial motor neuron populations. Representative transverse sections of facial (a, b, e, f) and trigeminal motor nuclei (c, d, g, h) from twelve-month old wild type and homozygous Thy1mγSN mice stained with antibodies raised against NeuN (1:100) (green) and GFAP (1:400) (red) (a-d) or biotinylated lectin RCA (1:100) (e-h). Scale bars = 50μm.

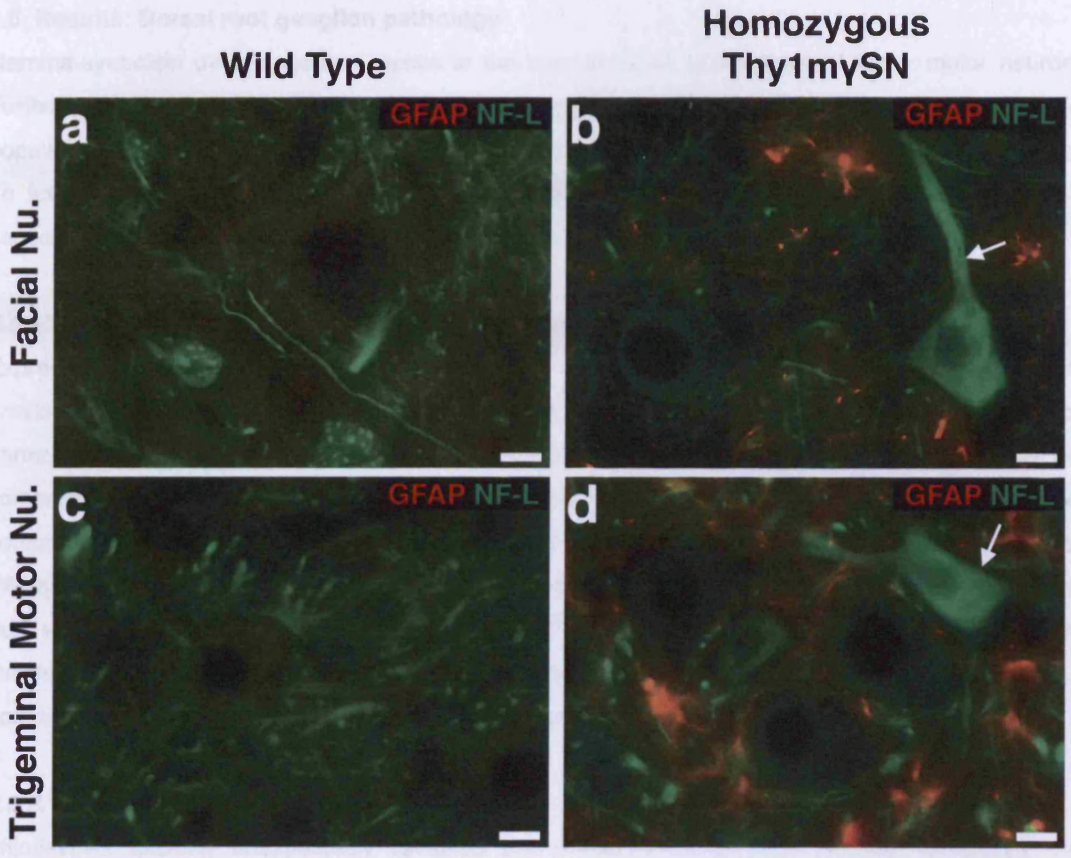

Fig. 24. Accumulation of neurofilaments in cranial lower motor neurons. Representative images of NF-L (1:250, green) and GFAP (1:400, red) fluorescent immunostaining in the facial (a, b) and trigeminal motor (c, d) nuclei of wild type (a, c) and homozygous *Thy1*mγSN mice (b, d). Arrows = cells containing excessive neurofilament-L staining. Scale bar = 20μm

3.5. Results: Dorsal root ganglion pathology

Gamma-synuclein overexpression results in the loss of select populations of lower motor neurons. Furthermore morphological analysis of the cortex suggests that effect upon motor and sensory neuron populations in this brain region is also selective, with sensory neurons appearing resistant to damage. To further test this hypothesis, we assessed the survival and morphology of the discrete pool of sensory neurons contained within dorsal root ganglia.

3.5.1. Gamma-synuclein expression in dorsal root ganglia

Expression of gamma-synuclein in wild type adult dorsal root ganglia (DRGs) has been reported previously (Buchman et al. 1998b). Furthermore we have found that in *Thy1*mγSN transgenic mice, gamma-synuclein mRNA expression in the DRG was seven-fold that of the wild type levels and comparable to the level of in expression their spinal cord (Fig. 2c). Through immuno-staining we confirmed the presence of gamma-synuclein protein in L4/5 DRGs collected from twelve-month old wild type mice (Fig. 25a), with diffuse cytoplasmic staining in all neuron cell bodies. DRGs collected from age matched, severely affected, homozygous *Thy1*mγSN contained a higher level of cytoplasmic staining (Fig. 25b). In contrast to motor neurons however all sensory neurons examined were free of both intra- and extracellular gamma-synuclein positive inclusion structures.

3.5.2. Amyloid staining in dorsal root ganglia

Thioflavin-S staining unexpectedly revealed the presence of granular amyloid structures, that appeared to be extracellular or possibly intra-axonal, and also fibrous amyloid material within the cytoplasm of a small fraction of cells (Fig. 26b, d). Such structures were not found in wild type tissue (Fig. 26a, c). Though gamma-synuclein positive inclusion bodies were not detected in sensory neurons, it was feasible that other protein may form such structures, for example such as the ubiquitin positive gamma-synuclein negative structure that were found in the spinal cord (see above). Immunostaining against neurofilaments (Fig. 25d) and ubiquitin (Fig. 25f) however did not reveal any structures. Thus the composition of the sensory amyloid structures remains unclear.

3.5.3. Assessment of gliosis in dorsal root ganglia

Neuroinflamation was investigated by immunostaining of DRGs from twelve-month old wild type and severely symptomatic homozygous *Thy1*mγSN mice with antibodies raised against GFAP for astrogliosis (Fig. 27a,b) and biotinylated RCA for assessment of microgliosis (Fig. 27c,d). Neither cell type was found activated in the DRGs of homozygous *Thy1*mγSN mice (Fig. 27b, d).

3.5.4. Dorsal root ganglion sensory neuron population quantification

Though gliosis was not detected, the presence of amyloid structures suggested possible damage to sensory neurons. Thus we carried out Nissl staining to quantify the population of sensory neurons contained within the L4/5 DRGs of 12-month old wild type and homozygous *Thy1*mγSN mice (Fig. 28, appendix 5). For each mouse all four ganglia were serial sectioned, a sample portion stereologically

counted and total population estimated using the fractionator technique. Significant difference was not detected between the mean total population of wild type and homozygous *Thy1*mγSN mice (p=0.441, Mann-Whitney U-test).

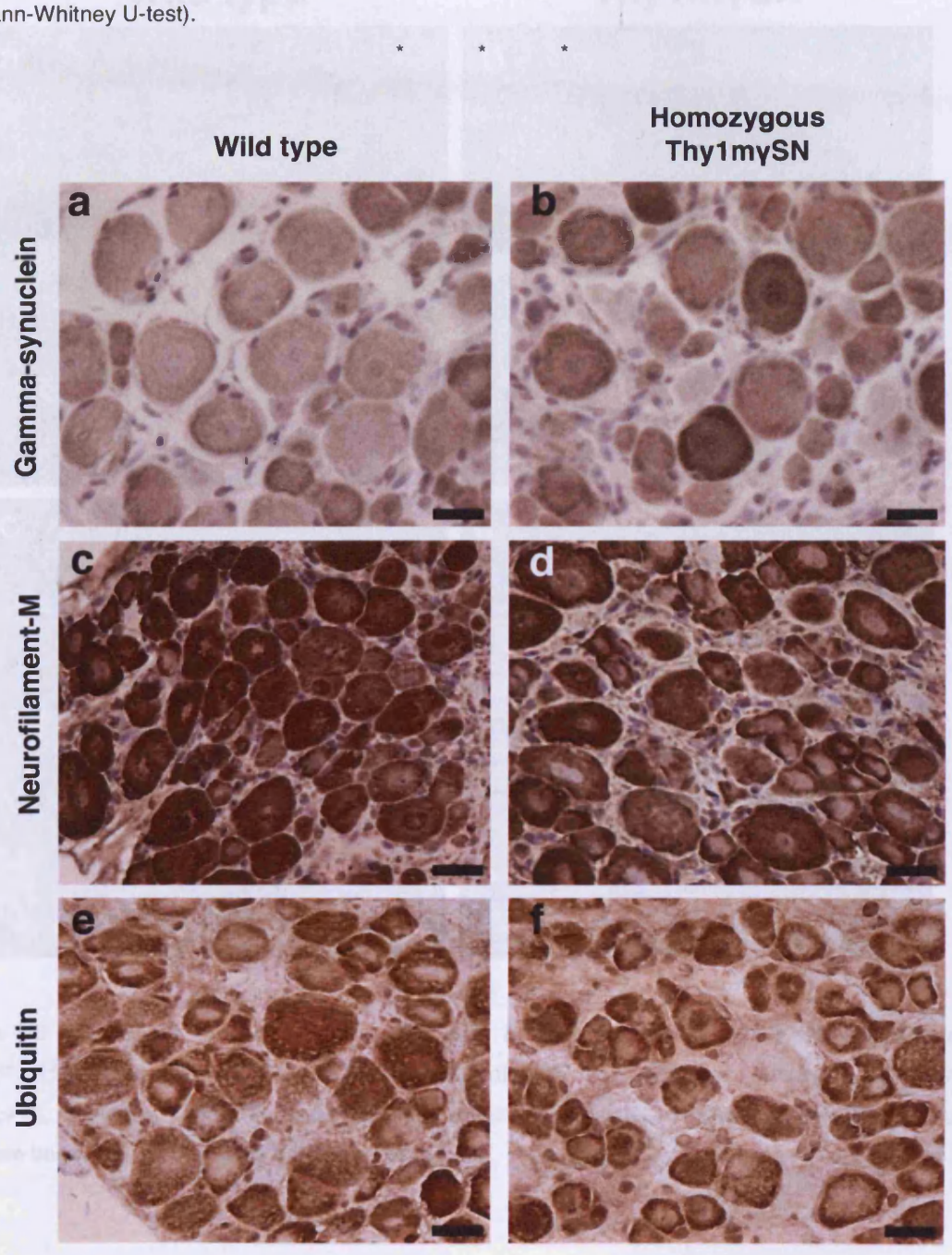

Fig. 25. D*orsal root ganglia of homozygous Thy1mγSN mice do not contain inclusions positive for gamma-synuclein, NF-M or ubiquitin.* Representative images of lumbar DRGs immuno-stained for gamma-synuclein (1:100) (a,b), NF-M (1:250) (c, d) and ubiquitin (1:250) (e, f) from wild type (a, c, e) and homozygous *Thy1*mγSN (b, d, f) mice. Scale bars a-f = 25μm.

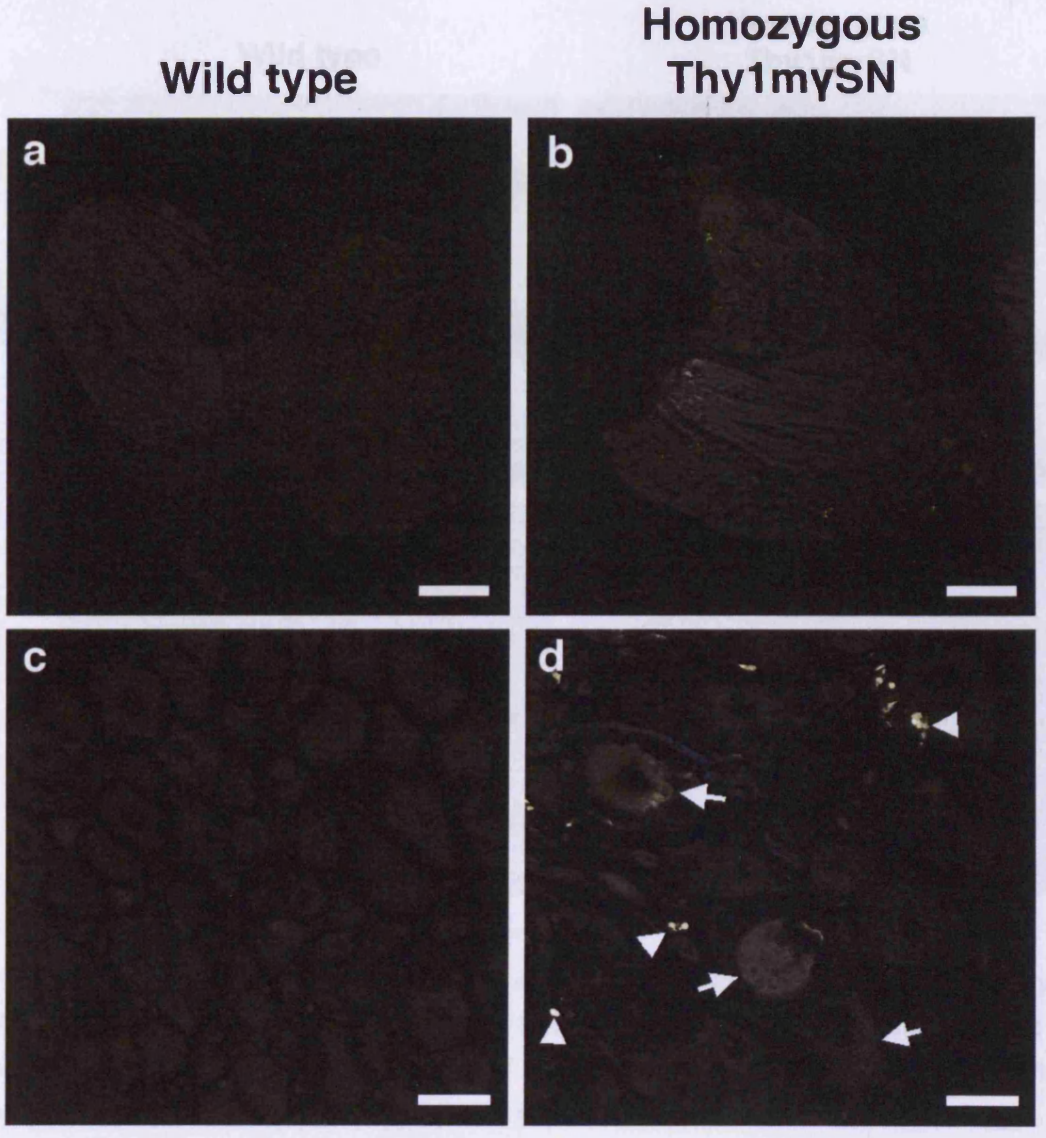

Fig. 26. Dorsal root ganglia of Thy1mγSN mice contain amyloid-like structures. Representative thioflavin-S staining of L4/5 DRG of twelve-month old wild type (a, c) and homozygous *Thy1*mγSN mice (b, d). Arrows = intracellular fibrous amyloid positive material. Arrowheads = granular structures. Scale bar a, b = 200um, scale bar c, d = 25μm.

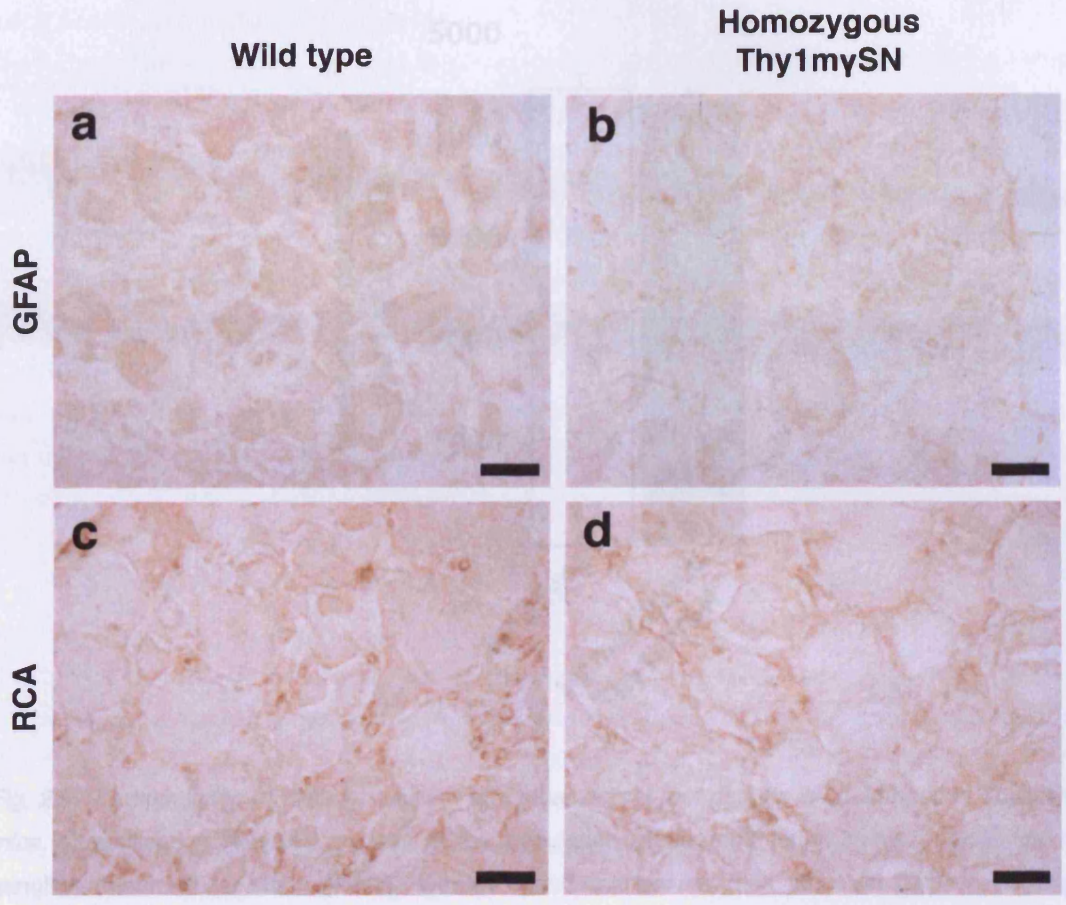

Fig. 27. Neither astrocytes nor microglia are activated in the dorsal root ganglia of homozygous Thy1mγSN mice. Representative section of L4/5 DRG from twelve-month old wild type and homozygous Thy1mγSN mice immunostained with antibodies against GFAP (1:400) (a, b) and biotinylated lectin RCA (1:100) (c, d). Scale bars = 25μm.

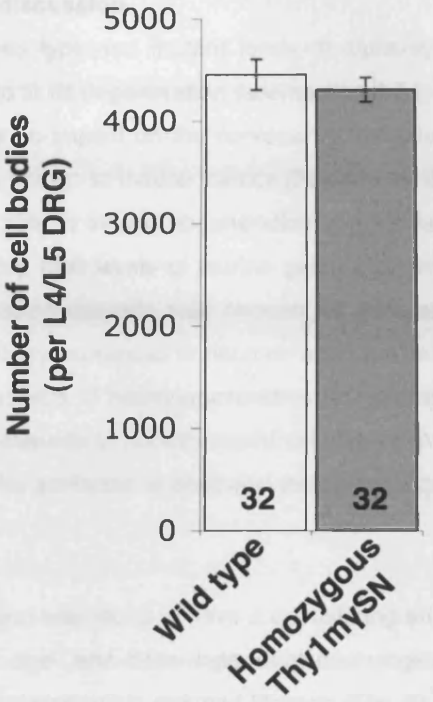

Fig. 28. The population of sensory neurons in lumbar dorsal root ganglia is unchanged in Thy1mγSN mice. Quantification revealed no loss in the population of neurons found within L4/5 dorsal root ganglion (mean±SEM, Mann-Whitney U-test). Insert number denotes the total number of ganglia quantified, with each group containing eight animals.

3.6. Summary of results and discussion

The overexpression of both wild type and mutant forms of alpha-synuclein in the murine nervous system has been robustly linked to its degeneration (see section 1.3.). In contrast, the overexpression of wild type beta-synuclein has no impact on the nervous system (Hashimoto et al. 2001), though a mutant form has recently been shown to induce toxicity (Fujita et al. 2010). To test whether gamma-synuclein overexpression was able to induce degeneration in a similar manner to alpha-synuclein, a line of C57Bl/6J mice expressing high levels of murine gamma-synuclein within the nervous system was generated. A *Thy1* expression cassette was chosen for generation of transgenic mice, as the promoter is strongly and selectively expressed in neurons and thus has previously been utilized in the production of several model systems of neurodegeneration (for example van der Putten et al. 2000). Secondly the *Thy1* expression cassette in not expressed until P4-10 (Aigner et al. 1995), and therefore any neurological effects could be attributed to postnatal transgene expression and not developmental defects.

Gamma-synuclein overexpression was found to have a devastating effect upon the nervous system of *Thy1*mγSN mice, inducing an age- and dose-dependent neurological phenotype characterised by deficits in motor function and a significantly reduced lifespan (Fig. 3). This motor function deficiency clearly not caused by damage or dysfunction of the nigra-striatal system, with neither dopaminergic cell number or striatal neurotransmitter concentration diminished (Fig. 18, 19). Similar to mice with *Thy1* controlled alpha-synuclein overexpression (van der Putten et al. 2000), motor dysfunction in *Thy1*mγSN mice was attributed to the gradually developing damage of spinal cord motor neurons and their axons. Widespread depletion of spinal motor neurons was accompanied by deposition of gamma-synuclein in perikaryal and axonal inclusion bodies, in addition to substantial gliosis (Fig. 8, 9, 12). Similar inclusion formation and gliosis was observed in the brain of homozygous *Thy1*mγSN mice, though the extent varied between regions (Fig. 14-17, 20). Surprisingly both inclusion bodies and gliosis were absent from the DRGs of affected animals (Fig. 25-27).

3.6.1. Effects of gamma-synuclein overexpression are dose dependent

Gamma-synuclein overexpression in the *Thy1*mγSN line induced toxicity in a dose dependent manner. A preliminary line of mice generated alongside the *Thy1*mγSN line carried a low gamma-synuclein transgene copy number and did not develop a detectable phenotype (see section 1.8.). Homozygous *Thy1*mγSN mice, in which transgene copy number was substantially greater than that of the low copy number line, developed visible signs of neurodegeneration such as hind-limb clasping from five-months of age, with symptoms leading to death from approximately eight months (Fig. 3). The onset of visible clinical signs in hemizygous *Thy1*mγSN mice (where copy number was half that of homozygous *Thy1*mγSN mice) occurred much later in life, from twelve-months of age onwards, with death generally occurring between 18- and 24-months. This dose-dependent development of symptoms was confirmed by analysis of motor function by rotarod. In both constant and accelerating test modes homozygous *Thy1*mγSN mice were found to develop significant differences at least fourteen-months

prior to the onset of deficits in hemizygous *Thy1*mγSN mice (Fig. 4). This positive correlation between transgene copy number and onset of clinical signs was expected. What is less clear is why such a high level of *Thy1*mγSN transgene expression is necessary to induce neurodegeneration. A similar situation is presented by alpha-synuclein. In familial cases of human PD both duplication and triplication of *SNCA* are sufficient to induce the symptoms of disease (Chartier-Harlin et al. 2004; Ibanez et al. 2004; Singleton et al. 2004) Mouse models of alpha-synucleinopathy however require substantially higher levels of transgene overexpression to induce neuronal dystrophy (for examples see section 1.7.). Why high levels of expression are required is unclear, but is most likely due to an increased load of protein toxicity being required to induce neurodegeneration during the relatively short lifespan of the mouse.

A striking feature of the gamma-synuclein overexpression induced pathology observed in the *Thy1*mγSN line was its selective nature. This selectivity was found to occur not only between motor and sensory neurons, but also between different populations of motor neurons.

3.6.2. Tolerance of sensory neurons to gamma-synuclein overexpression

Peripheral and central sensory neurons were found to be either resistant, or substantially less vulnerable to *Thy1*mγSN transgene induced toxicity than motor neuron populations. This bias towards motor dysfunction was detected in both the behaviour of the transgenic mice and following histological analysis of neuron populations. Where motor performance analysis robustly demonstrated deficits that progressed with age (Figs. 4-6), studies of withdrawal response to tactile stimulation indicated that changes in sensory function were not progressive, though older homozygous *Thy1*mγSN mice did have a lower response than age-matched control animals (Fig. 7). This deficit in the oldest animal is likely to be due to significant motor deficits impeding their response to tactile stimulation. Analysis of homozygous *Thy1*mγSN data alone showed no significant change in performance (Fig. 7d), contrasting wild type mice in which an improvement in tactile sensitivity was observed (Fig 7a-c). Thus any effects of gamma-synuclein overexpression upon tactile sensitivity are limited. In spite of comparable levels of *Thy1*mγSN mRNA expression (Fig. 2), sensory neuron cells bodies of the dorsal root ganglia and sensory regions of the cortex appeared significantly less vulnerable to the pathology that compromised the motor system. The DRG sensory neuron population was undiminished, and neither gamma-synuclein positive inclusion bodies nor activated glia were detected (Figs. 26-28). With regard to sensory regions of the cortex, gamma-synuclein positive inclusions, concentration of insoluble forms of gamma-synuclein and numbers of activated glia were all lower than in adjacent motor regions (Fig. 20-21).

The potential involvement of gamma-synuclein in sensory neuropathies is not without precedent, having been identified in mouse models of two neurodegenerative disorders affecting sensory neurons. In DBA/2J mice, a line that spontaneously develop glaucoma, spheroids containing gamma-synuclein have been identified in the axons of retinal ganglion cells, a population of sensory fibres that

form the optic nerve (Nguyen et al. 2011). Furthermore, accumulation of gamma-synuclein within astrocytes has been identified in mouse models of glaucoma and in the optic nerves of humans suffering from the disease (Nguyen et al. 2011; Surgucheva et al. 2002). The development of gracile axonal dystrophy in UCH-L1 null mice is accompanied by the formation of spheroid inclusion structures containing gamma-synuclein (Wang et al. 2004). In both these examples however, gamma-synuclein predominantly is found in axonal inclusion bodies, and not found to accumulate in perikaryal cytoplasm of sensory neurons. It thus is necessary to access the condition of sensory axons in *Thy1*mγSN mice prior to making conclusions with regard to the resistance of sensory neurons to gamma-synuclein overexpression. This analysis shall be detailed in the following chapter.

3.6.3. Differential vulnerability of motor neuron populations

In contrast to sensory neurons, motor neurons were vulnerable to gamma-synuclein overexpression induced degeneration, however the loss of the cells appeared to be highly selective. Those of the spinal cord were universally sensitive, with significant deficits found at all spinal cord levels (Fig. 11). Cranial lower motor neuron populations however showed a profile of differential vulnerability/resistance (Fig. 22). Comparable with the spinal pool, depletion of over 30% was recorded within the motor trigeminal nucleus that innervates masticatory muscle. In contrast both the orofacial-innervating facial nucleus and the occulomotor-innervating abducens nucleus contained a full complement of motor neurons. Further evidence of selective neuronal dystrophy was suggested by uneven distribution of the population of activated glia in the brains of homozygous *Thy1*mγSN mice. Numbers of activated micro- and astroglial cells within the facial and abducens nuclei were comparable to those in the surrounding tissue. In the degenerating motor trigeminal nuclei however, numbers of both activated mico- and astroglial cells were notably higher than surrounding tissues, suggesting their increased infiltration in response to neurodegeneration (Fig. 23). Increased numbers of activated glial cells was also a prominent feature of motor regions of the cortex of *Thy1*mγSN mice (Fig. 20).

Degeneration of spinal cord neuron populations has been previously observed in models of alpha-synucleinopathies. Loss of spinal motor neurons has been reported in numerous lines of transgenic mice overexpressing alpha-synuclein (Giasson et al. 2002; Lee et al. 2002; van der Putten et al. 2000). There is however no published evidence of either the selective loss/survival of cranial motor neurons or the discrete dystrophy of cortical motor regions in these mice. A similar pattern of motor loss does however occur in amyotrophic lateral sclerosis (ALS), a common form of motor neuron disease. More so, this pattern has been well recapitulated in transgenic mouse models of the disease. The familial and sporadic ALS are characterised by substantial loss of motor function through the selective loss of both upper motor neuron pools in the motor regions of the cortex, and lower motor neuron pools in the brainstem and spinal cord (Wijesekera and Leigh 2009), though it should be noted that mild changes in sensory function have been also been reported (Hammad et al. 2007; Isaacs et al. 2007; Pugdahl et al. 2007). The selective loss of motor neurons in cranial nuclei described in

*Thy1*mγSN mice is also a frequently observed characteristic of ALS. Moreover, observed mouse pathology shares the selectivity pattern with the human disease. Generally motor neurons innervating orofacial muscles degenerate during the course of ALS progression, contributing in symptoms including dysphagia and dysarthria. These vulnerable populations include the facial muscle-innervating facial nucleus, the motor trigeminal nucleus that stimulates muscles involved in mastication and the tongue-innervating hypoglossal nucleus (Kiernan and Hudson 1991). In contrast motor neurons located in nuclei that innervate targets in the occulomotor system appear to resist degeneration. Both the abducens and occulomotor nuclei have been found to remain intact late into disease, allowing some ALS patients to retain some degree of eye movement (Wijesekera and Leigh 2009).

The pattern of motor neuron loss observed in human cases of ALS is recapitulated in transgenic mouse models of the disease. Spinal motor neurons are lost from all levels of the spinal cords during the progression of ALS pathology. The spinal cord motor neuron population of end-stage $SOD1^{G93A}$ mice is reduced by 50-60% (Chiu et al. 1995; Kanning et al. 2010; Kong and Xu 1998). The largest volume motor neurons appear most vulnerable to degeneration, being diminished by over 90% in end-stage mice (Kong and Xu 1998). A significant increase in the populations of activated astrocytes (Gould et al. 2006) and microglia (Saxena et al. 2009) has also been found to correlate with the progression of motor neuron loss in the spinal cords of $SOD1^{G93A}$ mice. In the more recently developed TDP-43 transgenic mouse lines, spinal motor neurons have been found more modestly depleted by 20-25% (Shan et al. 2010; Wegorzewska et al. 2009; Wils et al. 2010). In addition to loss of spinal cord motor neurons, brainstem populations are also selectively diminished in mutant SOD1 transgenic mice. Several groups have carried out detailed quantification of brainstem motor neuron populations in mutant SOD1 transgenic mouse lines, where a relatively consistent pattern is observed (Ferrucci et al. 2010; Haenggeli and Kato 2002; Nimchinsky et al. 2000; Zang et al. 2004). Motor neurons pools innervating oromotor targets, including the hypoglossal nucleus, dorsal vagus nucleus, motor trigeminal nucleus and facial nucleus are found to be significantly susceptible to $SOD1^{G93A}$ and $SOD1^{G86R}$ induced degeneration. In 120 day old, end-stage SOD1 mutant mice, losses of up to 70% have been reported in the tongue innervating hypoglossal nucleus (Ferrucci et al. 2010) and up to 50% in the facial muscle-innervating facial nucleus (Nimchinsky et al. 2000; Zang et al. 2004) and mastication controlling motor trigeminal nucleus (Ferrucci et al. 2010). Furthermore, progressive motor neuropathy (pmn) and "wobbler" mice, that develop a spontaneous ALS-like motor neuron disease, both recapitulate these losses (Haenggeli and Kato 2002). In contrast to the consistent loss of oromotor motor neuron populations, those innervating occulomotor targets appear to be spared from degeneration. Pools of motor neurons within the eye muscle innervating occulomotor nucleus and abducens nucleus are found to be unaffected in both end-stage $SOD1^{G93A}$ and $SOD1^{G86R}$ transgenic mice (Ferrucci et al. 2010; Haenggeli and Kato 2002; Nimchinsky et al. 2000; Zang et al. 2004) and also spared in end stage wobbler mice (Haenggeli and Kato 2002). Inconsistency has however been noted in pmn mice, which were found to develop a highly significant loss of approximately 36% in the

occulomotor nuclei (Haenggeli and Kato 2002). Currently there are no reports of quantification of brainstem motor neuron populations in TDP-43 transgenic mice.

Symptomatic homozygous *Thy1*mγSN mice partially recapitulated this typical ALS associated pattern of selective brainstem motor neuron degeneration. The 30% loss of motor trigeminal nucleus motor neurons and survival of those within the abducens nucleus was comparable to the reported findings in mutant SOD1 lines. The survival of facial nucleus does however present an inconsistency, as this population degenerates in both models of ALS and human cases of the disease. This discrepancy may be due to several factors. The level of *Thy1*mγSN transgene expression has been demonstrated in the above data, with hemizygous transgenic mice developing a delayed phenotype compared to that of homozygous mice. The lack of degeneration in the facial nucleus and abducens nucleus might be the result of transgene expression being below the level necessary to induce degeneration. The expression pattern of gamma-synuclein within cranial motor neurons of wild type mice might also suggest a factor in the survival of the facial nucleus. In contrast to all other cranial motor neuron populations where perikaryal gamma-synuclein translocates to the axon, the facial nucleus partially retains gamma-synuclein in the cytoplasm of the cell body (Ninkina et al. 2003). Thus as gamma-synuclein is normally present within the cell bodies of this populations, they might carry some degree of tolerance to the high levels expressed in homozygous mice. Finally, ALS is a diverse disorder, with familial cases associated with numerous genetic risk factors and sporadic disease with little evidence of causative factors. It therefore seems feasible that the pattern of neuronal degeneration seen in mutant SOD1 associated ALS might vary from that induced by gamma-synuclein overexpression. A more detailed assessment of motor neuron loss in spinal cord and cranial populations could be achieved by immunostaining against apoptotic markers, for example cleaved caspase-3, or the TUNEL staining technique. Both processes could be carried out at different time points during the development of pathology in transgenic mice, and might give us a more clear idea of the dynamics and time course of motor neuron loss in these populations.

In summary, the above data shows that the pan-neuronal overexpression of gamma-synuclein triggers an age- and dose-dependent neuronal dystrophy in mice with substantial loss of motor function. Affected animals develop dramatic motor deficits, whilst only subtle changes occur in tactile sensitivity. The phenotype is characterised by widespread loss of spinal motor neurons, selective loss of cranial motor neurons and dystrophy in motor regions of the cortex. In contrast sensory neurons of the dorsal root ganglion are not lost and dystrophy within sensory regions of the cortex is less pronounced than that seen in motor regions. The phenotype suggests that gamma-synuclein overexpression induces a process of selective degeneration comparable to that seen in ALS.

4. Gamma-synuclein overexpression in the murine nervous system: The effect of gamma-synuclein upon motor and sensory neurites

4.1. Overview

The previous chapter described the ability of gamma-synuclein to induce a selective neuronal dystrophy when overexpressed. Discrete populations of motor neuron cell bodies were lost from the spinal cord and brains of twelve-month old homozygous *Thy1*mγSN with severe clinical signs of neurodegeneration. In contrast the sensory neuron pool contained within dorsal root ganglia of these mice was complete, with only limited evidence of dystrophy. Furthermore behavioural analysis revealed a progressive loss of motor function in the homozygous *Thy1*mγSN mice that was not seen in sensory perception.

These data suggest it is feasible that gamma-synuclein might play a role in human disease that has yet to be fully elucidated. There is a small body of evidence in favour of this possibility. Gamma-synuclein has been detected in rare, atypical inclusion bodies, all of which are found in axonal lesions. Axonal spheroids have been reported in the hippocampal dentate molecular region in cases PD and dementia with Lewy bodies (Galvin et al. 2000) and also in the cingulate and midfrontal cortices in Hallervorden-Spatz sufferers (Galvin et al. 2000). Gamma-synuclein positive inclusions have also been reported in the sensory gracile and dorsal spinocerebellar tracts of gracile axonal dystrophy (gad) mice, a strain which develop a sensory ataxia (Wang et al. 2004). Furthermore atypical gamma-synuclein positive structures have been isolated in both human cases and animals of glaucoma (Buckingham et al. 2008; Nguyen et al. 2011; Soto et al. 2008; Surgucheva et al. 2002). The intra-neuronal localization of gamma-synuclein, which differs substantially from the other members of the synuclein family, appears to be a factor in the formation of these structures. Whereas alpha- and beta-synuclein are restricted to presynaptic terminal within the brain, gamma-synuclein is found diffusely throughout the soma, neurites and synapses of select populations of CNS and PNS neurons (Buchman et al. 1998b).

In this chapter we shall assess the effect of gamma-synuclein overexpression upon discrete pools of motor and sensory axons in the sciatic nerve and its spinal nerve roots. In particular we shall focus on whether any degeneration seen is selective in nature, or affects all fibre types equally. Furthermore we shall assess the morphology of sensory fibres in optic nerve and the retinal ganglion cells from which they originate to determine whether gamma-synuclein overexpression can induce glaucoma-like symptoms.

4.2. Results: Sciatic nerve

To investigate the effects of gamma-synuclein overexpression on neurites we investigated the morphology of the sciatic nerve. Composed of motor and sensory fibres emerging from dorsal and ventral lumbar spinal nerve roots, the sciatic nerve is the primary sensory-motor nerve in the hind limbs of mammals. The sciatic nerve was chosen over the equivalent forelimb medial nerve due to the earlier onset of motor deficits in the hind limbs.

Fluorescent gamma-synuclein immunostaining of longitudinal sections of sciatic nerve collected from twelve-month old wild type confirmed the expression and localization of the protein in the axonal cytoplasm (Fig. 29a_i). Diffuse staining was found throughout the sciatic nerve, with some regions of punctate staining. Similar staining of age matched tissue from severely affected homozygous *Thy1*mγSN mice revealed dense staining throughout the sciatic nerve (Fig. 29a_{ii}). Many neurites were found to containing dense strands of gamma-synuclein positive material along the length of the axon, with others found to contain dense clusters of aggregated protein.

4.2.1. Neurofilament-L distribution in the sciatic nerve

Immunostaining revealed that gamma-synuclein overexpression results in a visible depletion of neurofilaments from axons and cell bodies within the spinal cord. To investigate if similar damage occurred in the sciatic nerve we immunostained longitudinal sections from twelve-month old symptomatic homozygous *Thy1*mγSN and wild type mice with antibodies raised against NF-L. In control sciatic nerves, NF-L was found uniformly localised throughout the length of the axons (Fig. 29b_i). In concurrence with the spinal cord, the level of NF-L was substantially diminished in the sciatic nerves of transgenic mice (Fig. 29b_{ii}). Though a portion of axons were normal in appearance, many axons were found to be totally absent of NF-L, whereas other contained regions of sparse staining.

4.2.2. Cytoskeletal proteins in the sciatic nerve

The reduction of sciatic nerve NF-L content observed in the above immunostaining experiment was confirmed through semi-quantitative western blotting (Fig 29c, Appendix. 6). In addition to NF-L, we measured the levels of several major axonal cytoskeletal proteins in the sciatic nerves of severely affected twelve-month old Thy1mγSN mice with severe motor phenotype, and also those with milder developing symptoms. In mildly affected homozygous Thy1mγSN mice significant reductions were not seen in neurofilaments-L, -M or –H, peripherin, alpha-tubulin or actin. Reductions of approximately 39% and 66% were however respectively detected in the 21kDa and 18kDa isoforms of myelin basic protein, a major component of the axonal myelin sheath. In the severely affected group of homozygous Thy1mγSN mice reductions of over 50% were recorded for all neurofilaments, alpha-tubulin and both the 18kDa and 21kDa isoforms of myelin basic protein. Levels of peripherin and beta-actin were unaffected.

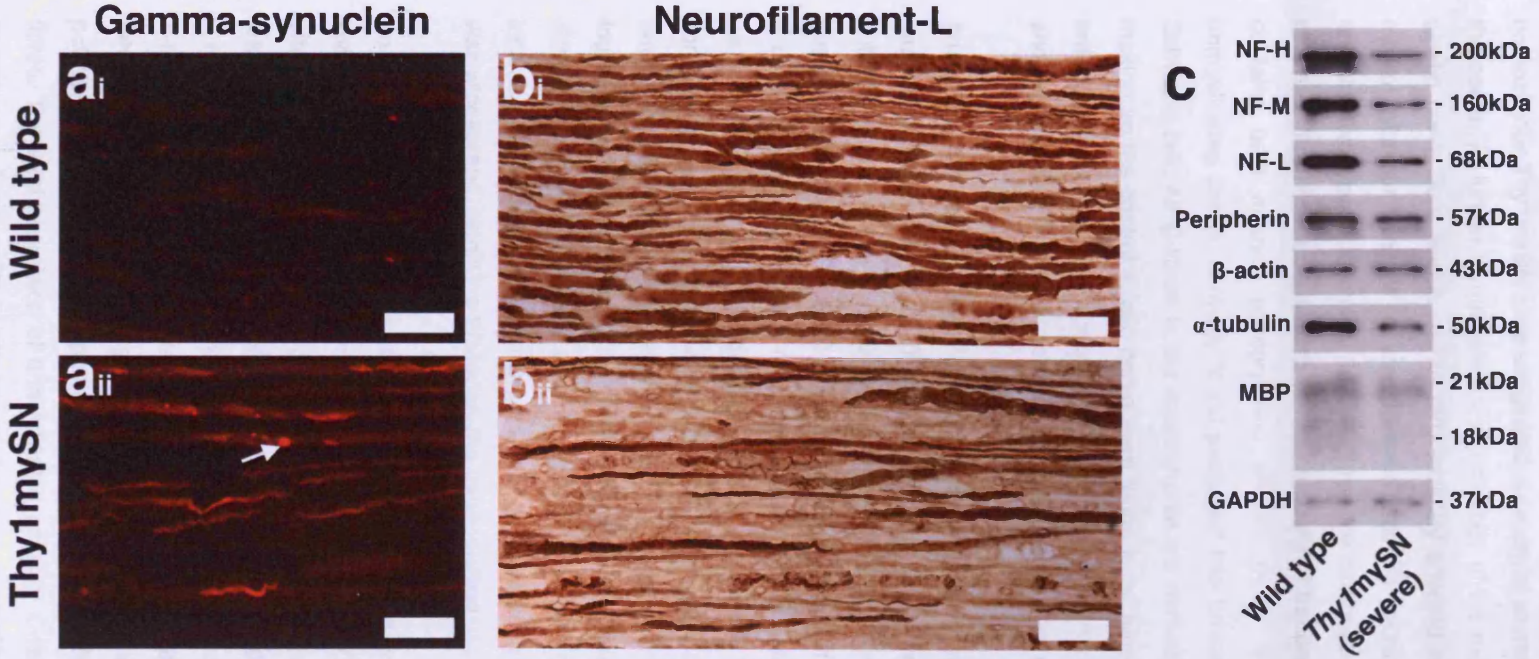

Fig. 29. Gamma-synuclein disrupts neurofilament distribution in the sciatic nerve. Representative transverse sections of sciatic nerve from twelve-month old wild type (a_i, b_i) and homozygous *Thy1*mγSN (a_{ii}, b_{ii}) immunostained with antibodies against gamma synuclein (SK23, 1:100) (a) and neurofilament-L (1:250) (b). Increased levels of gamma-synuclein were present in the axons of homozygous *Thy1*mγSN mice, including spheroid inclusion bodies (white arrows) accompanied by substantial reductions of NF-L. Representative Western blot showing levels of several neuronal structural proteins in the sciatic nerves of twelve-month old, severely symptomatic homozygous *Thy1*mγSN and healthy control mice (c). Adapted from Ninkina et al. 2009.

4.2.3. Ultrastructure analysis of the sciatic nerve

The substantial losses of axonal and myelin cytoskeletal component in the nerves of severely affected homozygous Thy1mγSN mice suggested substantial alteration to the structure of the fibres composing the nerve. To further investigate the morphology of the axonal ultrastructure we prepared samples of sciatic nerve from twelve month old, severely affected homozygous Thy1mγSN and age-matched control mice for analysis by transmission electron microscopy (TEM). The wild type sciatic nerve contains two type of fibre (Fig. 30a). A-fibres are composed of a single axon enveloped by a Schwann cell, and vary in size depending on their velocity of transmission and neuron type. The sciatic nerve contains both afferent sensory and efferent motor A-fibres. C-fibres are a smaller class of unmyelinated axons, normally found packaged into bundles that were tightly enveloped by a single Schwann cell. All C-fibres in the sciatic nerve are derived from sensory neurons. Both fibre classes making up the control sciatic nerve were found to be turgid and densely packed into the nerve in an orderly fashion, with little space remaining between fibres. Nuclei of Schwann cell nuclei were visible and sparsely distributed across the transverse section. No other cell types were detected.

Analysis of the sciatic nerves of severely affected homozygous Thy1mγSN mice revealed a notably sparser distribution of fibres (Fig. 30b, 31, 32b, d). Deterioration of A-fibres was clear with a large number found to have a highly abnormal morphology. The myelin sheaths of many cells contained abnormal structures (Fig. 32b_i) or debris between layers of myelin (Fig. 32b_{ii}). The origin of this debris is unclear, with both the axon and Schwann cell possible sources. Many axons were found to contain vacuole or swollen mitochondria (Fig. 32b_{iii}), or be in a highly degenerate state (Fig. 32b_{iv}). Many fibres were found to be totally absent of axon, with only a multilamellar, Schwann cell derived structure remaining (Fig. 32$b_{v, vi}$). Further abnormally was detected in the bundling of C-fibres, with many cluster found to be loosely bundled or totally absent of the enveloping Schwann cell (Fig. 32d). Unbound Schwann cell processes were also occasionally observed (Fig. 30b). In addition to fibre degeneration, infiltration by microglia (Fig. 31a), and large phagocytic cells, believed to be macrophages (Fig. 31b) was widespread, signifying Wallerian-like degeneration of the nerve was likely.

To further assess the extent of pathology, we quantified both the number of healthy and unhealthy A-fibres and the number of normal and atypically bundled C-fibres (Fig. 32a, c, appendix 7). In mildly affected homozygous Thy1mγSN mice a full complement of both A- and C-fibres was present, though a small but statistically significant portion of A-fibres was damaged (Mann-Whitney U-test, $p=0.0493$). A more prominent significant reduction of 24.9% was detected in the total population of sciatic nerves A-fibres in severely symptomatic homozygous Thy1mγSN mice ($p=0.0005$, Mann-Whitney U-test). When these were grouped by condition a loss of 38.6% of healthy fibres (Mann-Whitney U-test, $p<0.0001$) was found, accompanied by an approximate 8 times increase in population of damaged fibres. The total population of unmyelinated sensory C-fibres was undiminished in the symptomatic homozygous Thy1mγSN sciatic nerve, however a significant proportion, over 40%, of these fibres were found within atypical bundles (Mann-Whitney U-test, $p<0.0001$).

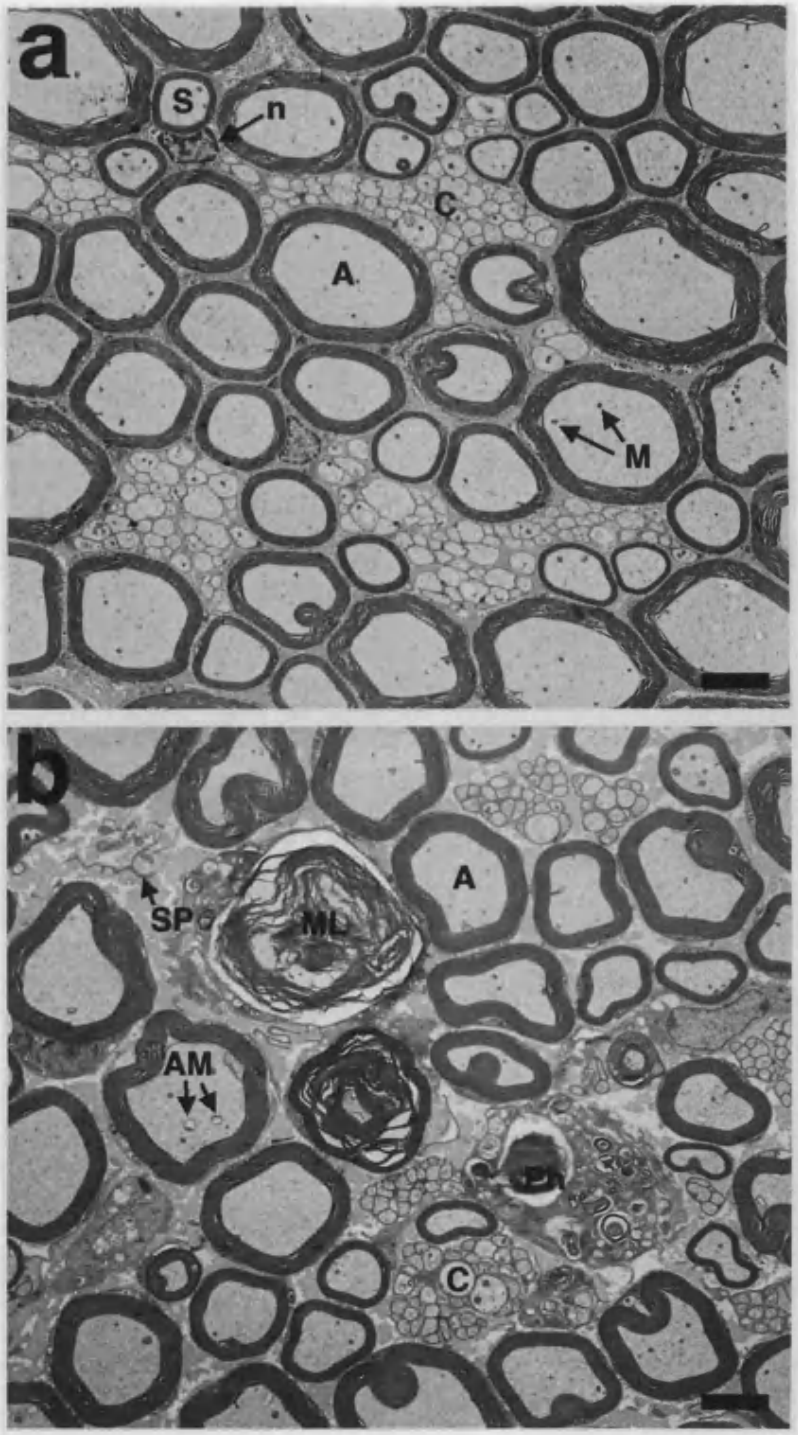

Fig. 30. Severe damage of nerve fibres in the sciatic nerves of mice overexpressing gamma-synuclein. Representative electron micrographs of transverse sections of the sciatic nerve from twelve-month old healthy wild type (a) and severely affected homozygous *Thy1*mγSN (b). A – healthy myelinated A-fibre, C – healthy bundle of C-fibres, M – healthy mitochondria, S – A-fibre with visible Schwann cell nucleus, n – Schwann cell nucleus, ML – abnormal multilamellar A-fibre remnant, SP – unbound Schwann cell processes, Ph – phagocyte, AM – abnormal mitochondria. Scale bar a-b=3μm.

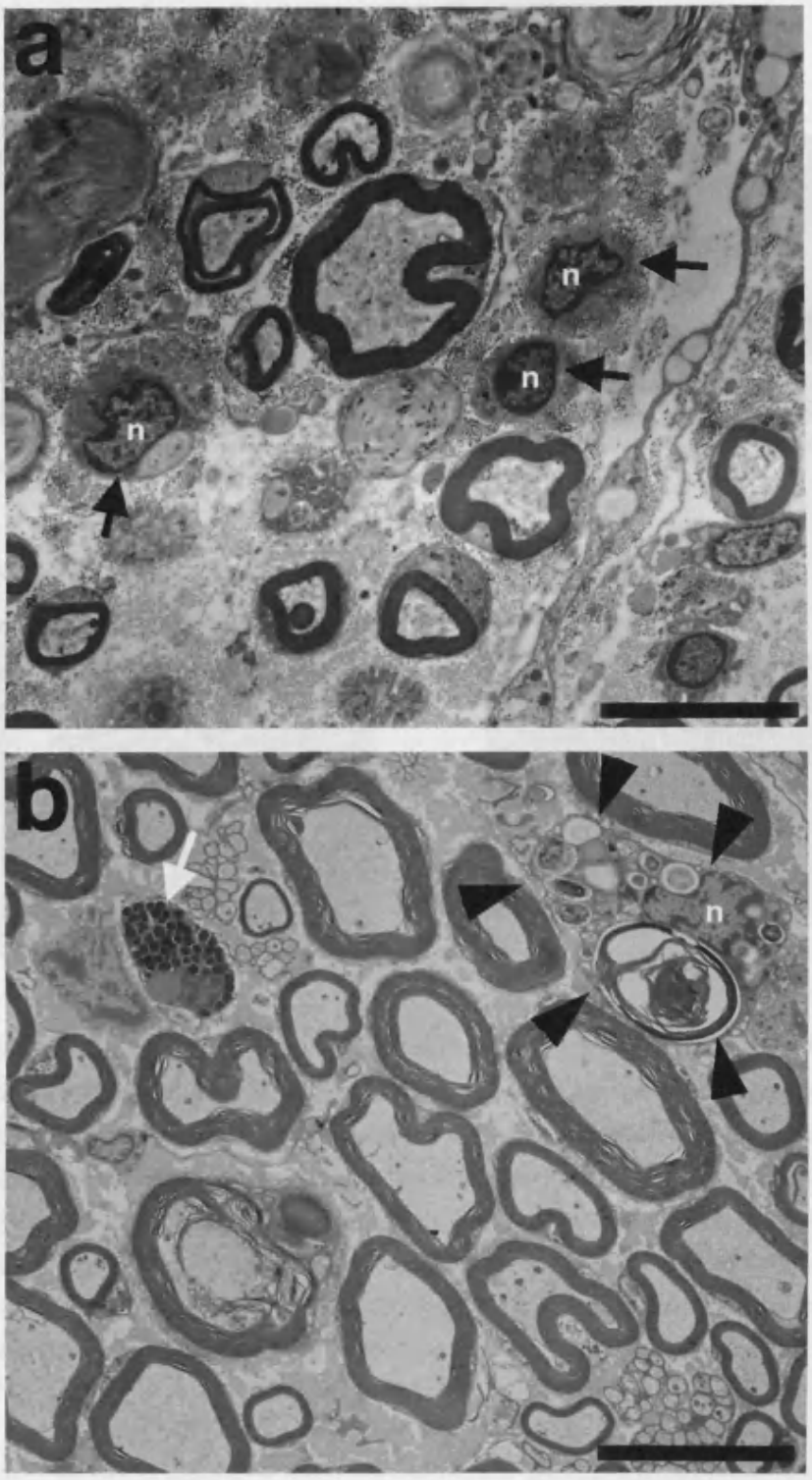

Fig. 31. Non-neuronal cell types in the sciatic nerve of homozygous Thy1mγSN mice. Representative transverse sections of sciatic nerve from twelve-month old severely affected homozygous *Thy1*mγSN mice (a, b). n – nucleus of microglial cell (a) or phagocyte (b), black arrowheads – phagocytes, black arrows – microglia, white arrows – mast cell. Scale bar = 10μm.

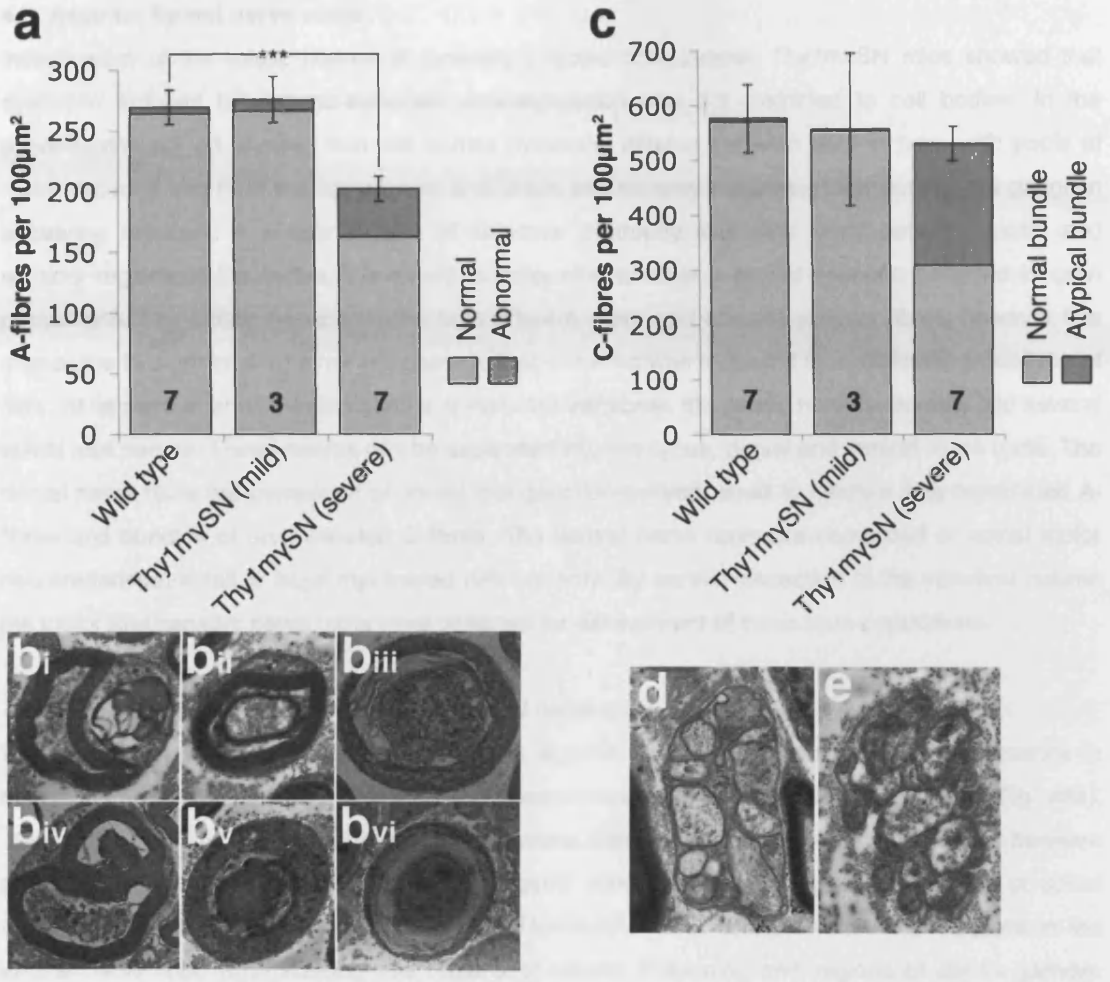

Fig. 32. Loss of normal fibre morphology and population in the Thy1mγSN sciatic nerve. Quantification of total, healthy and damaged A-fibres (a) and total, normally and atypical encapsulated C-fibres (c) in the sciatic nerve of twelve month old wild type, mildly and severely affected homozygous *Thy1*mγSN mice (Mean±SEM, *** $p<0.001$, Mann-Whitney U-test). High magnification electron-micrographs of various degenerating A-fibres (b_i-b_{vi}). A healthy bundle of C-fibres from wild type sciatic nerves, enveloped by a single Schwann cell sheath (d). An atypically enveloped bundle of C-fibres from severely affected homozygous *Thy1*mγSN sciatic nerve (e). Insert number denotes the number of nerves assessed, each collected from a separate animal.

4.3. Results: Spinal nerve roots

Investigation of the sciatic nerves of severely affected homozygous *Thy1*mγSN mice showed that dystrophy induced by gamma-synuclein overexpression was not restricted to cell bodies. In the previous chapter we showed that cell bodies dystrophy differed between neuron type, with pools of motor neurons lost from the spinal cord and brain, but sensory neurons of the dorsal root ganglion appearing resistant. A similar pattern of selective dystrophy was also found between motor and sensory regions of the cortex. We aimed to determine whether a similar scenario occurred in axon populations. The sciatic nerve contains both efferent motor and afferent sensory fibres, however it is impossible to determine whether the damage that occurred was restricted to a particular group/type of fibre. At its point of entry into the lumbar spinal cord vertebrae, the sciatic nerve separates into several spinal root nerves. These nerves can be separated into two types, dorsal and ventral nerve roots. The dorsal nerve roots are composed of dorsal root ganglion-derived, small to medium size myelinated A-fibres and bundles of unmyelinated C-fibres. The ventral nerve roots are composed of spinal motor neuron-derived, small to large myelinated A-fibres only. By careful dissection of the vertebral column the motor and sensory nerve roots were collected for assessment of these pure populations.

4.3.1. Gamma-synuclein distribution in the spinal nerve roots

Immunostaining with affinity purified antibodies against gamma-synuclein revealed its presence in both dorsal and ventral nerve root axons of twelve-month old wild type control animals (Fig. 33a). Staining was diffuse and even throughout the axons, though the intensity of staining varied between axons. High levels of gamma-synuclein expression were detected throughout both class of spinal nerve root in severely affected homozygous *Thy1*mγSN mice, though were more frequent in the ventral nerve root. Both staining-free regions of neurite ballooning and regions of dense gamma-synuclein accumulation within collapsed, strand-like neurites were detected. Immuno-staining against NF-M displayed similar ballooned structures in the nerve roots of *Thy1*mγSN mice (Fig. 33b$_{iii,iv}$).

4.3.2. Semi-thin ultrastructure analysis of the spinal nerve roots

To gain deeper insight into the pathological process within the spinal nerve roots, which accompany phenotypical changes in *Thy1*mγSN mice, we stained with toluidine blue semi-thin transverse sections of roots dissected from twelve-month old mice. In dorsal nerve roots various size of healthy myelinated A-fibres were present, with C-fibres bundles interspersed between (Fig. 34 – top left). Non-neuronal cell types were rarely observed. Age matched tissue from symptomatic homozygous *Thy1*mγSN mice displayed tightly packed fibres, however a portion of fibres were appeared to have an abnormal morphology, including both dense and severely bloated fibres (Fig. 34 – top right). Infiltration by non-neuronal cell types was also apparent. The ventral nerve roots of wild type mice contained tightly packed large and small myelinated A-fibres of normal appearance (Fig. 34 – bottom left). As with the wild type dorsal nerve root, non-neuronal cell types were infrequent in number. The ventral nerve roots of severely affected homozygous *Thy1*mγSN mice presented striking pathology (Fig. 34 – bottom

right). Significant loss of myelinated A-fibres was clear, with non-neuronal cell types occupying space between fibres. A-fibres of abnormal morphology were widespread.

4.3.3. Ultra-thin ultrastructure analysis of the spinal nerve roots

TEM was utilised to carry out detailed assessment of spinal nerve root morphology. Dystrophic axons containing vacuoles and swollen mitochondria (Fig. 35d) and multilamellar structures void of axons (Fig. 35e) similar to those described in the sciatic nerve (see above) were found in both dorsal and ventral nerve roots, however were substantially more frequent in the latter. Quantification revealed that myelinated A-fibres were significantly fewer in number and more likely to be dystrophic in the motor ventral nerve root than the sensory dorsal nerve root (Fig. 35a,b, appendix 8). Though a small fraction of myelinated A-fibres were found to be damaged in the dorsal nerve roots of twelve-month old, symptomatic, homozygous *Thy1*mγSN mice (6.1%, $p<0.001$ Mann-Whitney U-test), no total loss of fibres was detected. In contrast we found an 18% decrease in total A-fibre population in the ventral nerve roots of twelve-month old symptomatic homozygous *Thy1*mγSN mice (Mann-Whitney U-test, $p=0.0005$). Within the remaining population we found a 33.9% decrease in the number of healthy fibres (Mann-Whitney U-test, $p<0.0001$). The number of damaged fibres was 10.8 times higher than the level seen in control ventral nerve roots (Mann-Whitney U-test, $p<0.001$ for all). Statistically significant numbers of phagocytes containing swirls of digested myelin (Fig. 36) were seen in both dorsal (Mann-Whitney U-test, $p=0.0002$) and ventral nerve roots (Mann-Whitney U-test, $p=0.0001$), though the number per $100\mu m^2$ was higher in ventral nerve roots.

The above data suggested that, in a pattern similar to neuronal cell bodies, the motor axons were more susceptible to gamma-synuclein overexpression induced dystrophy than sensory axons. We found that within the cranial motor neuron population, vulnerability was selective. As the caliber of an axon denotes its class of neuron, we measured the area of myelinated A-fibres within the nerve roots to assess whether a similar selectivity occurred within the populations of motor and sensory axons. The combined area of the axon and myelin sheath was measured using Image-J software, and calculated the mean area and size distribution of A-fibres (Fig. 37). Striking differences were detected in the ventral nerve roots of twelve-month old homozygous *Thy1*mγSN mice (Fig. 37a), with a 49.5% decrease in mean fibre area. Plotting of A-fibre size distribution revealed a substantial loss of the largest caliber axons. In contrast no difference in either the mean size or distribution of A-fibres was detected between the wild type or homozygous *Thy1*mγSN dorsal nerve roots (Fig. 37b).

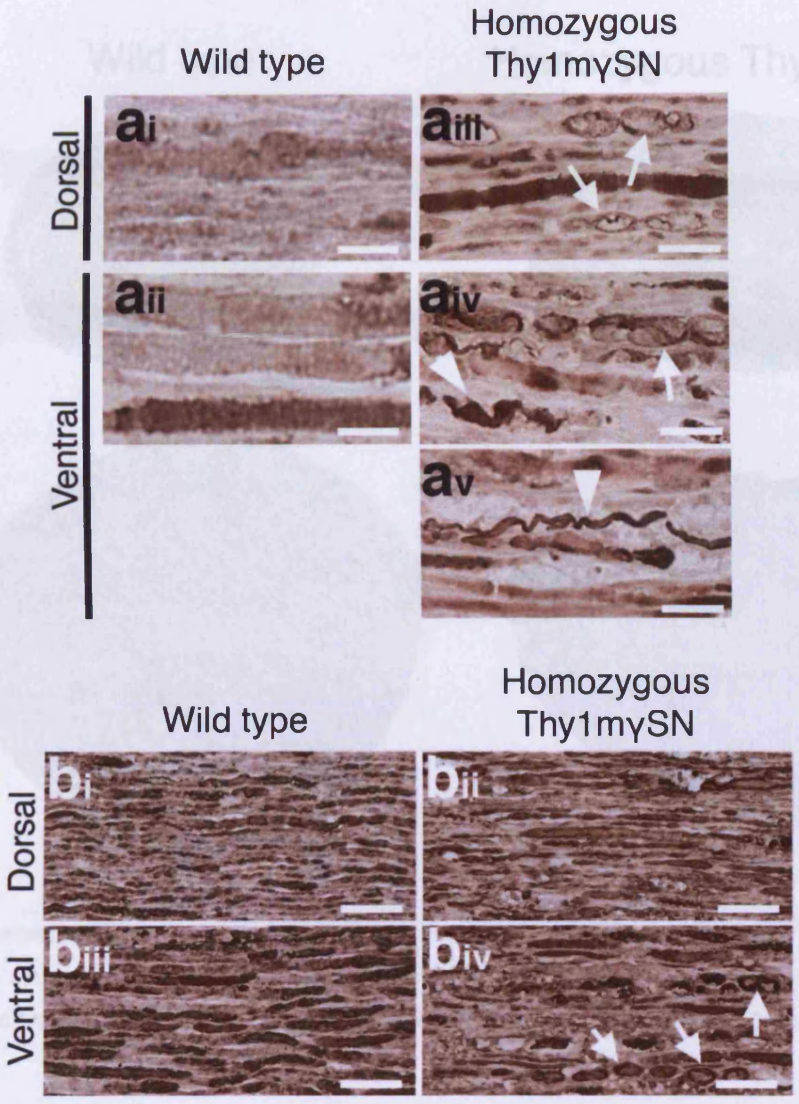

Fig. 33. Gamma-synuclein accumulates in spinal nerve root axons of aged Thy1mγSN mice and disrupts neurofilament-H distribution. Representative longitudinal sections of dorsal (a_i) and ventral (a_{ii}, a_{iii}) nerve roots from twelve-month old *Thy1*mγSN mice immunostained with antibodies raised against gamma-synuclein (SK23, 1:100). Dorsal and ventral nerve roots from twelve-month old wild type (b_i and b_{iii} respectively) and *Thy1*mγSN mice (b_{ii} and b_{iv} respectively) immunostained with antibodies raised against neurofilament-H (1:250). Two signs of damage were generally found, ballooning (arrows) and dense intra-neuronal accumulation (arrowheads). Scale bars: a = 25μm; b, c = 50μm.

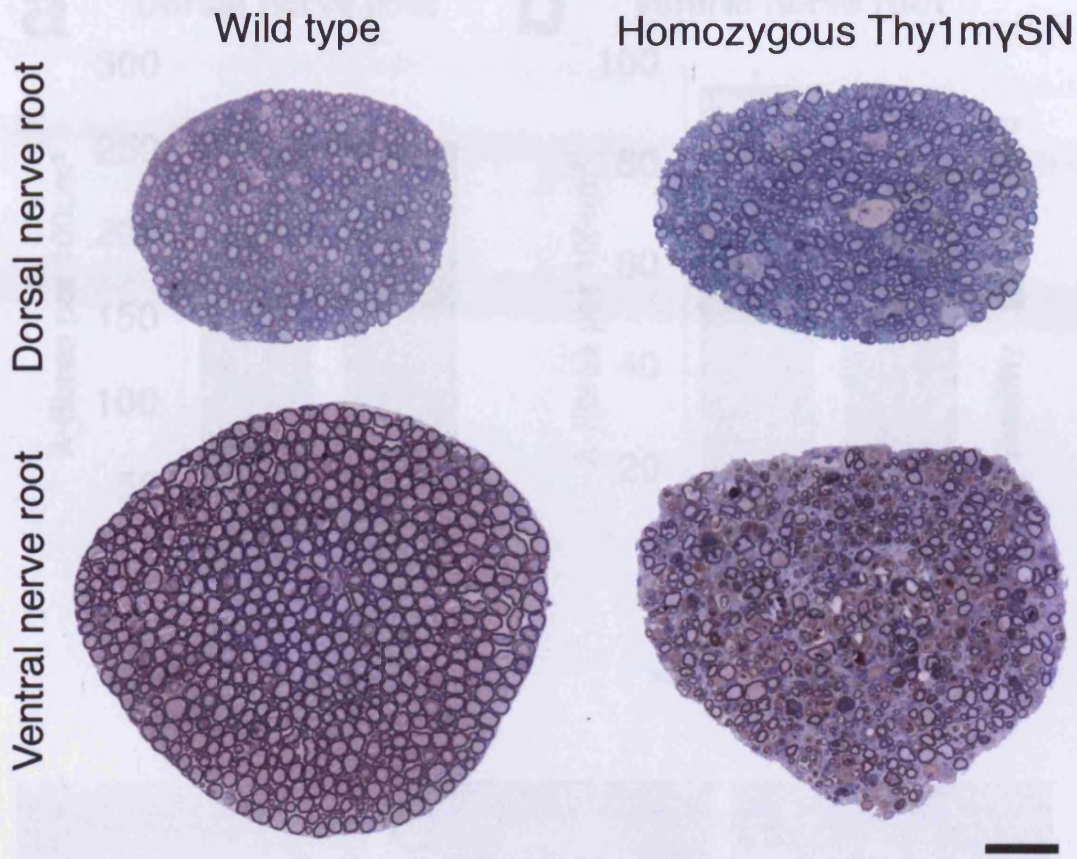

Fig. 34. Substantial degeneration in the ventral nerve roots of Thy1mγSN mice. Representative toluidine blue stained transverse semi-thin sections through ventral and dorsal nerve roots of twelve-month old wild type and symptomatic homozygous *Thy1*mγSN mice. Scale bar = 50µm.

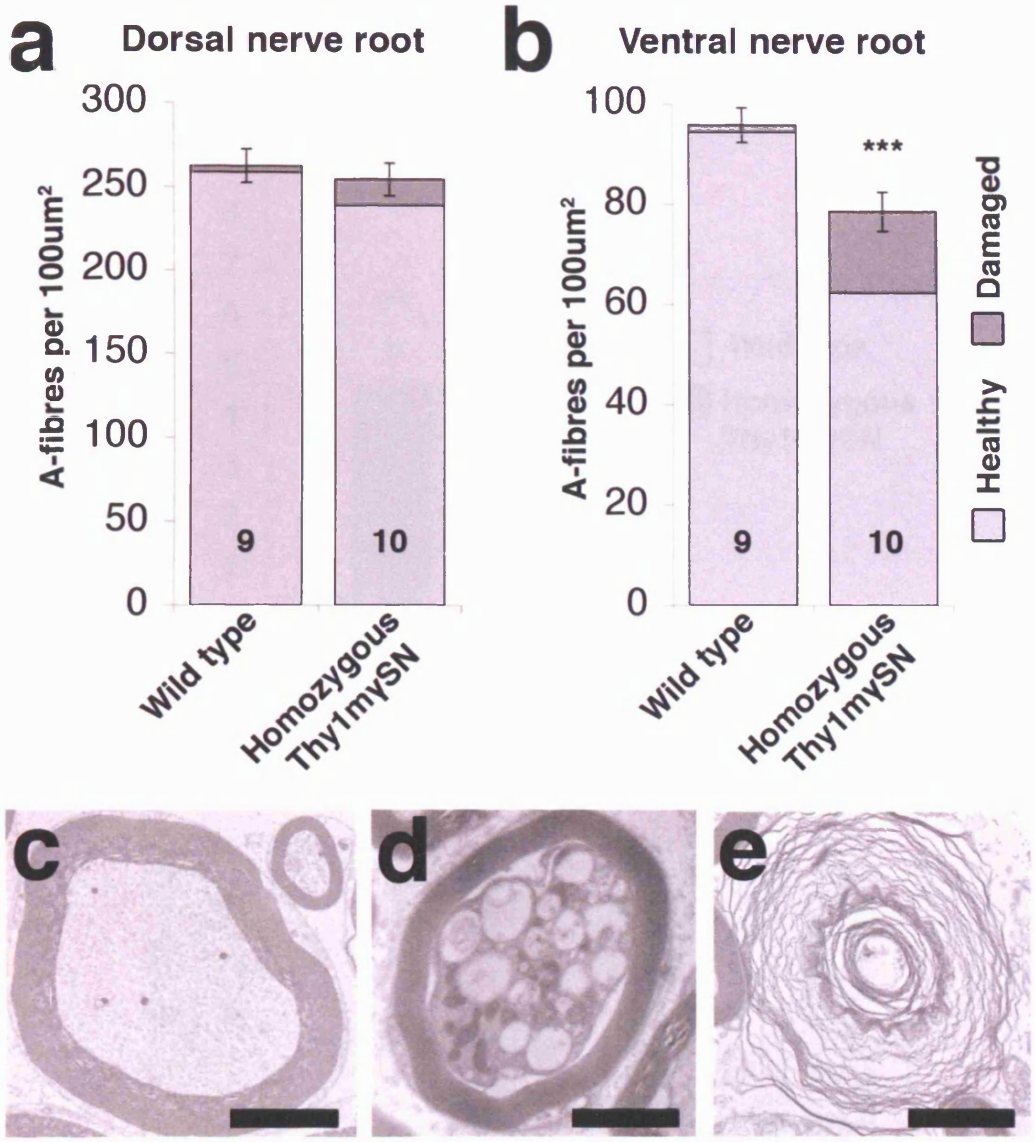

Fig. 35. The population of motor fibres entering the sciatic nerve are both damaged and diminished in Thy1mγSN mice. Quantification of total, healthy and damaged myelinated fibres in L4-L5 ventral (a) and dorsal (b) nerve roots of twelve-month old wild type and symptomatic homozygous *Thy1*mγSN mice (mean±SEM, *** $p<0.001$ Mann-Whitney U-test). High magnification electron-micrographs showing the normal myelinated A-fibres of wild type ventral nerve roots (c), in contrast to those of homozygous *Thy1*mγSN mice, where abnormal axons containing vacuoles and enlarged mitochondria (d), and multi-lamellar structure without axons (e) are found throughout. Scale bars c-e = 3μm. The insert number denotes the number of nerves assessed, each collected from a separate animal.

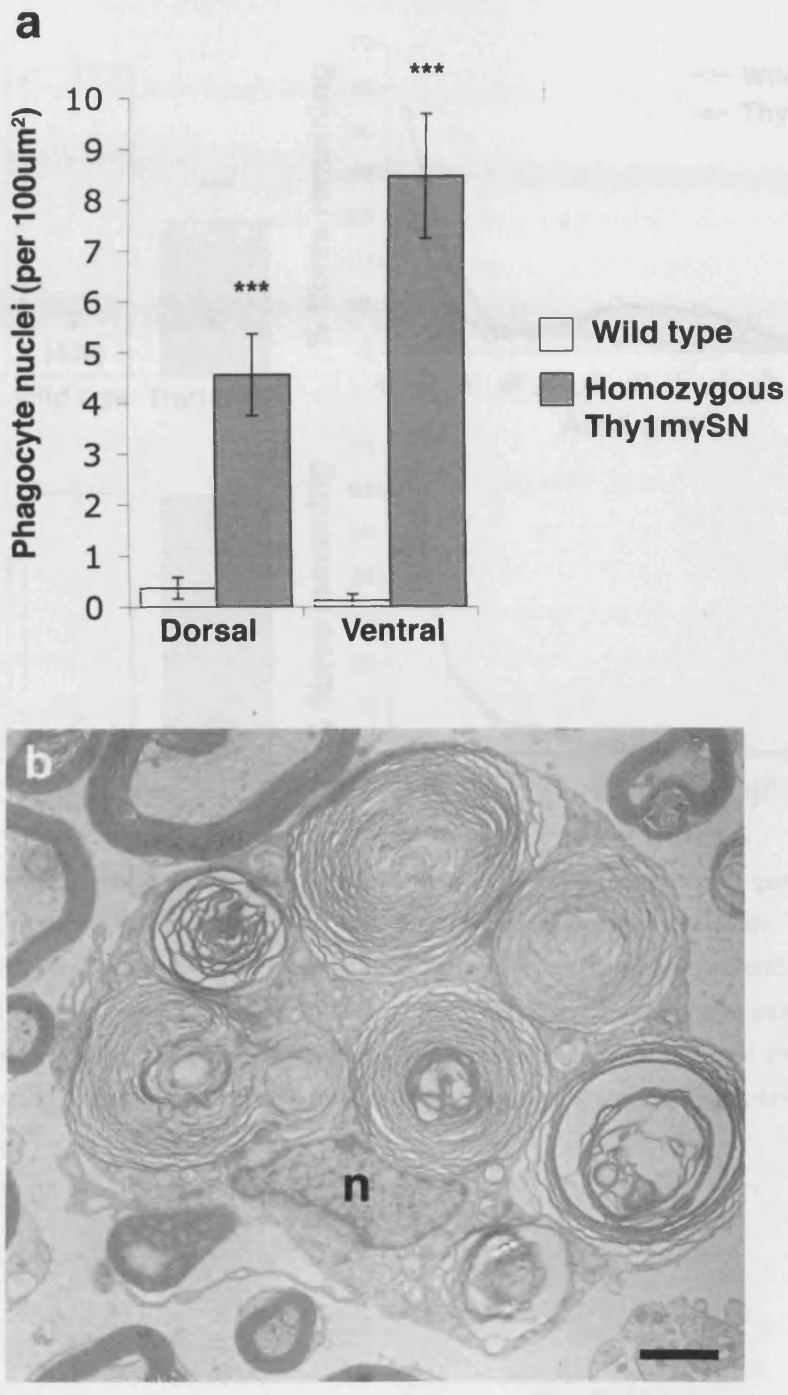

Fig. 36. Pronounced phagocyte infiltration occurs in the nerve roots of Thy1mγSN mice. The number of phagocytes (n=7, mean±SEM, ***p<0.001, Mann-Whitney U-test) found to have infiltrated the sensory and motor nerve roots of *Thy1*mγSN mice (a) and the EM image of infiltrating phagocyte in the motor nerve root (b). Arrows indicate phagocytosed myelin, 'n' indicates the nucleus. Scale bar = 3μm. WT n = 9, homozygous Thy1mγSN n = 10.

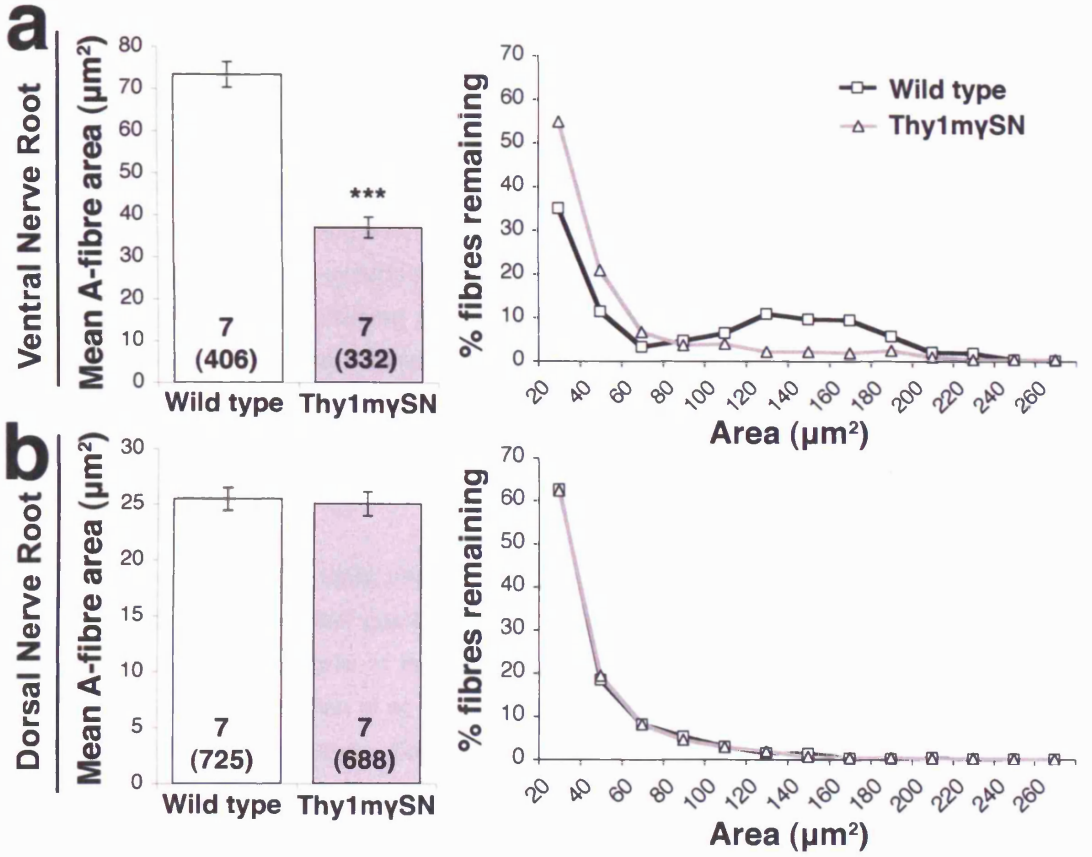

Fig. 37. The largest motor fibres of Thy1mγSN mice are most sensitive to gamma-synuclein overexpression induced degeneration. The size distribution of motor nerve fibres is significantly smaller in the ventral nerve root of twelve-month old *Thy1*mγSN than age-matched wild type mice due to a distinct shift towards smaller classes of fibre surviving (a). The mean area and size distribution of sensory fibres do not differ between genotypes (b). The number of animals analysed and total number of fibres measured (in brackets) are shown (mean±SEM, *** $p<0.001$, Mann-Whitney U-test).

4.4. Results: Retinal ganglion cells and the optic nerve

4.4.1. Confirmation of gamma-synuclein expression

Sections of eye from twelve-month old wild type and homozygous *Thy1*mγSN mouse were immuno-stained with antibodies raised against gamma-synuclein (Fig. 38a, b). In confirmation of previous reports gamma-synuclein staining was restricted to inner layers of the retina (Surgucheva et al. 2002). Perikaryal staining for gamma-synuclein was seen in neurons of the retinal ganglion cell layer of wild type mice, with less defined staining also observed in the inner plexiform layer (Fig. 38a). In the homozygous *Thy1*mγSN retina, staining was again restricted to outer layers of the retina. Denser cytosolic staining was observed in the RGC layer than that seen in wild type animals, with widespread punctate staining in the inner plexiform layer (Fig. 38b). No further differences between control and *Thy1*mγSN groups were detected in the level of staining in other retinal layers.

4.4.2. Assessment of RGC dendritic tree complexity

In an effort to determine whether gamma-synuclein overexpression was affecting the morphology of RGCs, we assessed the integrity of the neurons complex network of dendritic processes using the DiOlistic staining technique (Gan et al. 2000). This analysis was carried out in collaboration with the laboratory of Prof. James Morgan, Cardiff University School of Optometry. Whole mounted retina collected from wild type and homozygous *Thy1*mγSN mice were impregnated with a fluorescent lipophilic dye, staining both the soma and neurites of RGCs (Fig. 38c-f). Due to the limited penetration range of the dye-coated beads, bar infrequent retinal amacrine interneurons non-RGC cell types were not stained.

RGCs with large dendritic trees and defined axons were dispersed throughout the retina of both wild type (Fig. 38c, d) and homozygous *Thy1*mγSN mice (Fig. 38e, f). Signs of overt damage such as total loss of the dendritic tree or disruption of the axon were not observed in homozygous *Thy1*mγSN retina. Observation alone however was insufficient to accurately measure any subtle differences that may have occurred. Thus we measured dendritic complexity using Scholl analysis, an analytical technique that plots the number of dendrite bifurcation/intersections and their distance from the soma. Scholl analysis detected no differences between control and homozygous *Thy1*mγSN mice in either the number of dendritic intersections or in their distance from the soma (Fig. 38g).

4.4.3. Ultra-thin ultrastructure analysis of the optic nerve

Optic nerves were collected from twelve-month old wild type and severely affected homozygous *Thy1*mγSN mice and prepared for analysis by transmission electron microscopy (Fig. 39, appendix 9). The optic nerves of both control and experimental mice were composed of densely packed, small-caliber A-fibres, interspersed with infrequent astrocytes and microglia. Damaged A-fibres were rarely observed in either group, though swollen mitochondria and small vacuoles were common in both groups. Quantification (Fig. 39b) revealed neither significant loss of fibres (Mann-Whitney U-test,

p=0.0750) nor changes in fibre size (Mann-Whitney U-test, p=0.9398). In addition to population and fibre size, we additionally measured the ratio between axon area to fibre area, termed the g-ratio, substantial changes in which indicate axonal dystrophy. No significant difference was detected between mean g-ratio values (Two-sample t-test, p=0.262).

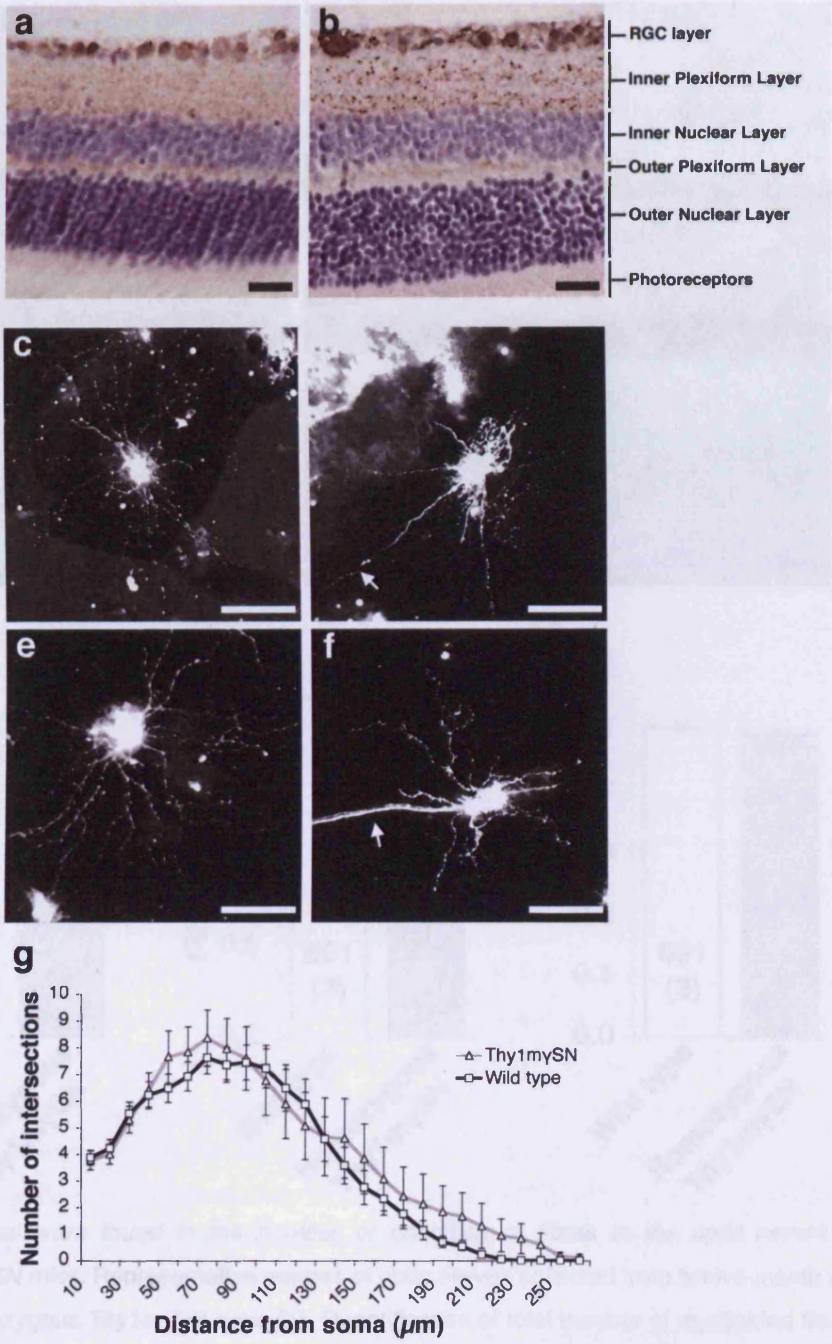

Fig. 38. Overexpression of gamma-synuclein does not affect the dendrites of retinal ganglion cells. Representative images of retina collected from wild type (a) and homozygous *Thy1*mγSN (b) mice immunostaining with antibodies against gamma-synuclein (SK23, 1:100). Representative images of diOlistically labeled retina ganglion cells from wild type (c, d) and homozygous *Thy1*mγSN mice (e, f), axons marked by arrows. Scholl analysis (e) revealed no differences in dendritic complexity between wild type and *Thy1*mγSN mice (mean±SEM). Wild type n=23 cells from 6 retina. *Thy1*mγSN n=17 cells from 5 retina. Scale bars a-b = 25μm, d-f = 100μm.

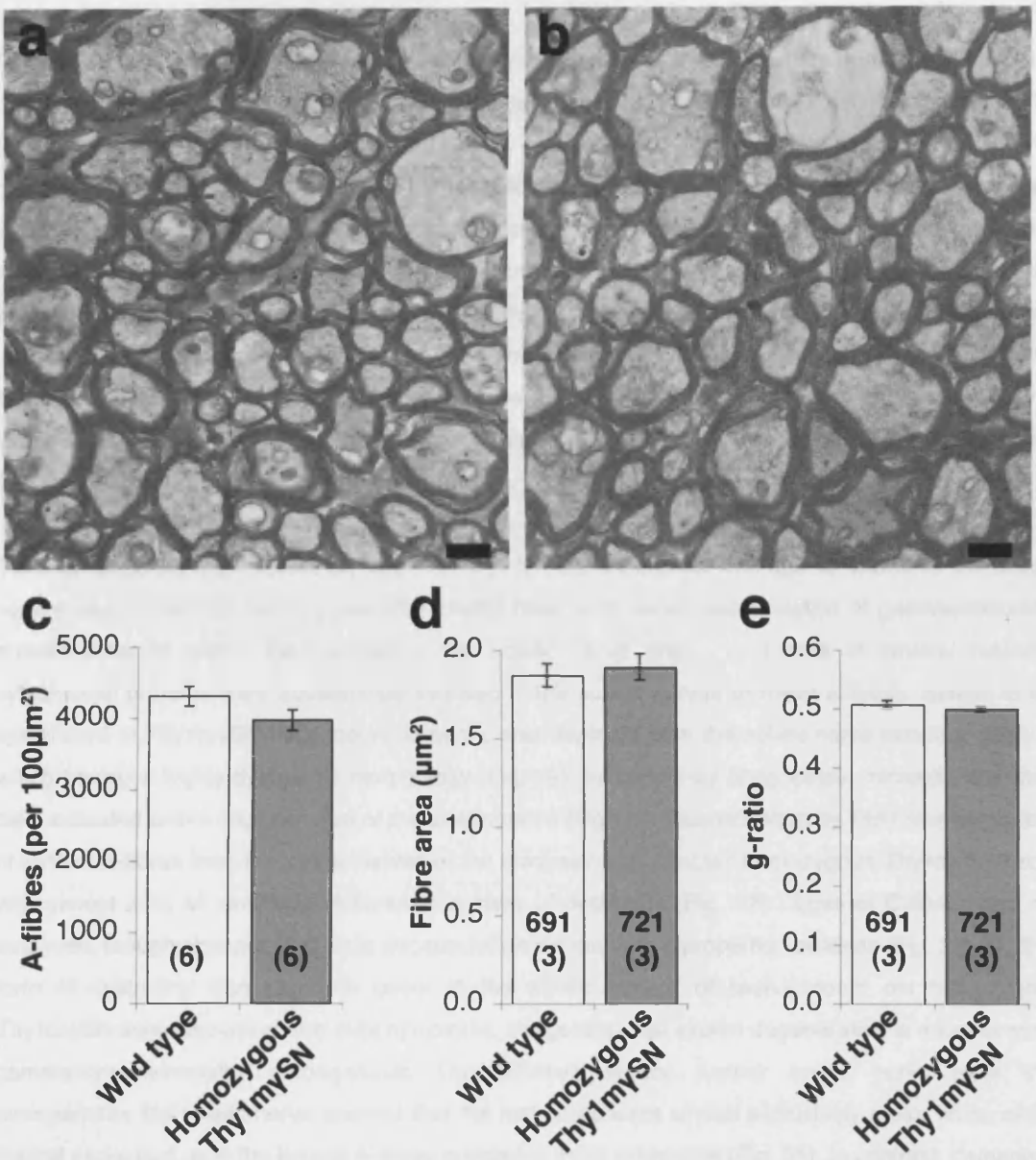

Fig. 39. No differences were found in the number or condition of fibres in the optic nerves of homozygous Thy1mySN mice. Representative images of optic nerves collected from twelve-month old wild type (a) and homozygous *Thy1*mγSN mice (b). Quantification of total number of myelinated fibres (c), mean fibres area (d) or g-ratio (e) of fibres composing the optic nerves of twelve-month old wild type and homozygous *Thy1*mγSN mice (mean±SEM, Mann-Whitney U-test). Within each bar the number = number of fibres assessed, and (number) = number of nerves sampled.

4.5. Summary of results and discussion

Gamma-synuclein has been identified in axonal inclusion bodies in several human diseases including PD, Hallervorden-Spatz syndrome, DLB and glaucoma (Galvin et al. 1999). (Galvin et al. 2000; Surgucheva et al. 2002). Furthermore the protein has been detected in similar structures in UCH-L1 null GAD mice (Wang et al. 2004) and rodent models of glaucoma (Nguyen et al. 2011). It is unclear whether gamma-synuclein plays an active role in the neurodegeneration that occurs in the above examples, or its accumulation is a passive secondary event. In the previous chapter we noted the presence of axonal spheroid inclusion bodies in the brain and spinal cord of aged homozygous *Thy1*mγSN mice, suggesting that gamma-synuclein was impacting upon the normal morphology and function of CNS axons. To test this hypothesis we assessed the morphology and survival of pools of axons within the sciatic nerves, lumbar spinal nerve roots and optic nerves of control and homozygous *Thy1*mγSN mice.

Gamma-synuclein overexpression was found to induce substantial damage to axons of the sciatic nerves of symptomatic homozygous *Thy1*mγSN mice, with dense accumulation of gamma-synuclein protein detected within the neurites of the sciatic nerve (Fig. 29). Levels of several neuronal cytoskeletal proteins were substantially reduced in the sciatic nerves of these animals. Similar to the spinal cord of *Thy1*mγSN mice, neurofilament-L was depleted from the sciatic nerve neurites, many of which having a highly dystrophic morphology (Fig. 29). Infiltration by phagocytes, microglia and mast cells indicated active degeneration of the sciatic nerve (Fig. 31). Quantification by TEM revealed a loss of 25% of A-fibres from the sciatic nerves of the most severely affected homozygous *Thy1*mγSN mice, with almost 20% of remaining A-fibres in a state of dystrophy (Fig. 32). Loss of C-fibres was not observed, though changes in bundle encapsulation did occur in a proportion of fibres (Fig. 32). Neither form of dystrophy was found to occur in the sciatic nerves of twelve-month old homozygous *Thy1*mγSN mice displaying only mild symptoms, suggesting that axonal degeneration is a key event in gamma-synucleinopathy pathogenesis. Quantification of the lumbar spinal nerve roots that emerge/enter the sciatic nerve showed that the lost fibres were almost exclusively motor fibres of the ventral nerve root, with the largest A-fibres appearing most vulnerable (Fig. 35). In contrast, damage to the efferent sensory neurons of the dorsal nerve root was limited, with no fibre loss recorded, though a small proportion of fibres were damaged (Fig. 35). Neither loss of optic nerve efferent sensory axons nor abnormalities in the complexity of the dendritic tree of RGCs were detected in symptomatic homozygous *Thy1*mγSN mice (Figs. 38, 39).

The previous chapter drew comparison between the pattern of neuronal cell body loss detected in *Thy1*mγSN mice and that seen in both human ALS and in mouse models of the disease. The above axonal morphology data is concurrent with this resemblance, describing a pattern of axonal damage typical of both human and modeled ALS.

4.5.1. Differential vulnerability between motor axon types

Analysis of axon number and morphology in the spinal nerve roots of *Thy1*mγSN mice further demonstrates the selective nature of the gamma-synucleinopathy. Over a third of myelinated motor fibres were either lost or damaged in the ventral spinal nerve roots of twelve-month old homozygous *Thy1*mγSN mice, with the largest appearing most vulnerable (Fig. 35, 37). In patients affected by ALS, selectivity is seen in the vulnerability of motor neurons and their axons. Examination of lumbar ventral nerve roots and spinal cord descending motor columns shows that the largest caliber fibres are disproportionately lost (Kawamura et al. 1981). Measurement of deep peroneal nerve conduction velocities has confirmed that the slowing of conduction velocity, concurrent with the selective loss of fast firing motor fibres, occurs with the progression of ALS (Theys et al. 1999). Our ability to assess factors contributing to this selective loss in human tissues in more detail is confounded by that fact that much of the available human ALS tissue is derived from patients at the late stages of disease progression, and is thus insufficient to accurately determine the dynamics of motor neuron degeneration. Fortunately the recapitulation of ALS in animal models of the disease have allowed us to achieve this, with selective motor neuron loss particularly well characterised in mutant SOD1 mouse lines (reviewed in (Kanning et al. 2010).

The earliest detectable changes in $SOD1^{G93A}$ mice are found in the innervation of neuromuscular junctions (NMJs). From approximately P50 partial denervation of NMJs in the medial gastrocnemius, soleus, and tibialis anterior muscles has been observed (Fischer et al. 2004), soon followed by the selective degeneration of fast-firing fatigable neuromuscular junctions (Frey et al. 2000; Gordon et al. 2010; Hegedus et al. 2008; Pun et al. 2006). Denervation of fast-fatigue-resistant and slow neuromuscular junctions occurs significantly later in disease progression (Frey et al. 2000; Pun et al. 2006). This pattern of loss has also been observed in pmn and mnd mice (Frey et al. 2000). The disproportionate loss of fast-firing motor units has led to the suggestion that the increased metabolic load of the fastest firing fibres is a factor in selective degeneration.

The caliber of an axon is proportional to its conduction velocity, with large fibres firing at the greatest velocity. This allows researchers to identify which class of motor neuron degenerate during the progression of ALS. Complementary to the early degeneration of their neuromuscular junctions, the large axons of fast-firing fatigable motor neurons type are consistently found to become dystrophic early in disease progression in mice expressing mutant SOD1 with significant loss of the largest caliber fibres detectable from as early as P20 (Bruijn et al. 1998; Fischer et al. 2005; Fischer et al. 2004; Kong and Xu 1998). As motor deficits develop, a shift towards a higher proportion of small caliber fibres occurs. This shift has been attributed to both the loss of large fibres and to the partial regeneration of dystrophic fibres, generally resulting in a smaller axon caliber (Fischer et al. 2004; Kanning et al. 2010). At the stage of paralysis the largest axons are almost entirely lost (Kong and Xu 1998). Matching findings have been reported in the $SOD1^{G85R}$ line, where 70% of the largest ventral root axons were lost with no loss of the smallest fibres (Bruijn et al. 1998). Thy1-hTDP-43 transgenic

mice also develop a similar phenotype, with significant losses detected in largest caliber of ventral nerve axons from as early as 3 weeks of age (Shan et al. 2010). Thus the selective loss of large caliber motor axons in gamma-synuclein transgenic mice appears to be a common feature of ALS and previously produced mouse models of this disease.

4.5.2. Tolerance of sensory neurites to gamma-synuclein overexpression

In contrast to the motor axon damage seen in the ventral spinal nerve roots of *Thy1*mγSN mice, sensory axons of dorsal nerve roots were found to survive. Only a small fraction of fibres showed signs of damage (Fig. 35), consistent with the condition of sensory neurons in lumbar DRG of these animals where only limited abnormalities were detected (see section 3.5.). Furthermore encapsulation of sensory C-fibre was found to be abnormal in the sciatic nerves of the most severely affected twelve-month old *Thy1*mγSN mice, though no fibres were lost (Fig. 32c). Though not considered a widespread symptom of ALS, sensory neuropathy has been reported in human cases. Patients are often reported to experience feelings of burning (Andersen et al. 1996) or numbness in the extremities (Dyck et al. 1975; Kawata et al. 1997). Moderate slowing of sensory neuron conduction velocity and/or action potentials have been reported in various sensory nerve of ALS patients (Hammad et al. 2007; Isaacs et al. 2007; Pugdahl et al. 2007; Theys et al. 1999). It has been noted that sensory deficits are more common in familial ALS compared to the sporadic form of disease (Li et al. 1988), with sensory neuropathy reported in $SOD1^{G93S}$ (Kawata et al. 1997) and $SOD1^{D90A}$ pedigrees of ALS (Andersen et al. 1996). Such functional abnormalities have been attributed to degeneration and loss of sensory axons. Remyelination, a sign of axonal stress followed by regeneration, has been reported in sural nerve biopsy tissue (Hammad et al. 2007; Heads et al. 1991). More so, substantial loss of myelinated A-fibres has been reported in the sural nerve (Bradley et al. 1983; Hammad et al. 2007; Heads et al. 1991), superifical peroneal nerve (Dyck et al. 1975) and ascending spinal cord sensory columns (Kawamura et al. 1981) of ALS patients. Similar to the pattern seen in motor axons, these losses have been noted to affect the largest caliber of sensory fibre (Hammad et al. 2007; Heads et al. 1991; Kawamura et al. 1981).

In contrast to the detailed examination of motor axon degeneration, remarkably little work has been carried out to assess the extent of sensory damage seen in mouse models of ALS. Quantification of sensory A-fibres in the dorsal nerve roots of the $SOD1^{G93A}$ line of mice found losses varying from modest and non-progressive (Dal Canto and Gurney 1995; Sun et al. 2002) to decreases of over 50% (Fischer et al. 2005; Guo et al. 2009). Assessment of the femoral nerve of end-stage mice expressing prion promoter driven $TDP43^{A315T}$ however failed to detect any loss of sensory fibres (Wegorzewska et al. 2009), demonstrating the variable nature of ALS pathology.

The mechanisms governing the selective vulnerability of motor fibres and relative resistance of sensory fibres are currently under much scrutiny. As the pathologies seen in the motor and sensory cell bodies of *Thy1*mγSN were also found to follow the same pattern, factors that might determine their

vulnerability and how they might relate to gamma-synucleinopathy shall be discussed in the final chapter as a whole (see below).

4.5.3. Gamma-synuclein and glaucoma

Glaucoma appears to be the most likely neurodegenerative disease in which gamma-synuclein might play a role. The pathogenesis of this disease is unclear, with degeneration of RGCs and their processes within the optic nerve head linked to an increase in IOP. Involvement of gamma-synuclein in this degeneration has been suggested by several studies. Changes in the expression of gamma-synuclein have been linked to both normal RGC development (Mu et al. 2004) and to the development of glaucoma (Soto et al. 2008). The role of gamma-synuclein in glaucoma is yet to be elucidated. The protein has been found within atypical inclusion bodies in both the axons of the optic nerve and in a subset of optic nerve astrocytes of both human patients and animal models of the disease (Nguyen et al. 2011; Surgucheva et al. 2002). The issue has been further complicated by the recent findings by Nguyen et al, in which the authors suggest that gamma-synuclein might even play a protective role in glaucoma, activating phagocytic activity in a subgroup of astrocytes within the myelination transition zone of the optic nerve (Nguyen et al. 2011).

We found no evidence that gamma-synuclein overexpression is a causative factor in the degeneration of either the optic nerve or the RGC dendritic tree of symptomatic homozygous *Thy1*mγSN mice (Figs. 38, 39). Additional unpublished results obtained in collaboration with laboratory of Dr. Nicholas Marsh-Armstrong in John Hopkins University School of Medicine, Baltimore support this finding. Automated quantification of retinal ganglion cell bodies in whole mounted retinas found a full complement in the retina of the most symptomatic homozygous *Thy1*mγSN mice despite very high level of transgene expression in these cells (Nicholas Marsh-Armstrong, personal communication). Neuronal gamma-synuclein overexpression alone is thus insufficient to induce RGC degeneration. We speculate that the reported accumulation of gamma-synuclein into atypical inclusion structures in both axons and glia most likely represents a secondary process occurring during RGC degeneration. It is feasible however that the reported appearance of gamma-synuclein within activated optic nerve astrocytes of glaucoma patients play a role in RGC degeneration (Surgucheva et al. 2002), explaining the lack of glaucoma-like degeneration in *Thy1*mγSN mice. This hypothesis may be relatively easily tested, through the development of transgenic mice with astrocyte targeted overexpression gamma-synuclein, for example utilising a GFAP-promoter (Brenner et al. 1994).

5. Influence of endogenous gamma-synuclein upon the phenotype induced by the Thy1mγSN transgene

5.1. Overview

Cabin et al (2005) described the apparent ability of endogenous murine alpha-synuclein to confer a degree of resistance to the toxicity induced by overexpression of prion-promoter driven human alpha-synuclein transgene. Mice null for the endogenous alpha-synuclein gene were found to present a more pronounced transgene-induced phenotype in comparison to those whom have developed with the endogenous gene (Cabin et al. 2005). To test whether a similar scenario is true with regards to gamma-synuclein, we bred a previously generated line of C57Bl6/J mice null for the endogenous SNCG gene (Ninkina 2003) with the Thy1mγSN line. We subsequently generated a cohort of endogenous SNCG null mice homozygously expressing the Thy1mγSN transgene (*SNCG*$^{-/-}$ Thy1mγSN$^{TG/TG}$). A cohort of homozygous Thy1mγSN mice (Thy1mγSN$^{TG/TG}$) were used as control animals.

5.2. Results: Behaviour and survival

5.2.1. Survival

The lifespan of *SNCG*$^{-/-}$ Thy1mγSN$^{TG/TG}$ was compared against that of Thy1mγSN$^{TG/TG}$ mice (Fig. 40). Any animals sacrificed due to unrelated health problems were disqualified from the study. 17 Thy1mγSN$^{TG/TG}$ mice and 28 *SNCG*$^{-/-}$ Thy1mγSN$^{TG/TG}$ deaths were recorded. No significant difference was found between the survival of *SNCG*$^{-/-}$ Thy1mγSN$^{TG/TG}$ and Thy1mγSN$^{TG/TG}$ mice (log rank test for equality of survival p=0.1532, generalized Wilcoxon test for equality of survival, p=0.2285).

Though the survival of *SNCG*$^{-/-}$ Thy1mγSN$^{TG/TG}$ mice was comparable to that of Thy1mγSN$^{TG/TG}$, differences in the onset and severity of disease were feasible. Thus behavioural tests were carried out to analyse the motor performance of these mice;

5.2.2. Rotarod

Mice were tested on both constant and accelerating rotarod modes. At each time point between 21 and 63 mice we tested. No significant differences in performance were detected on the constant speed mode (Kruskal-Wallis, Mann-Whitney U-test, all p>0.05) (Fig. 41a). The more sensitive accelerating mode detected a significant difference in performance at 2-months (Kruskal-Wallis, Mann-Whitney U-test p=0.0045) (Fig. 41b), where the *SNCG*$^{-/-}$ Thy1mγSN$^{TG/TG}$ cohort performed 20.4% worse than the control Thy1mγSN$^{TG/TG}$ group (Mann-Whitney U-test, p=0.0045). No further differences in performance were detected (Kruskal-Wallis, Mann-Whitney U-test, all p>0.05).

5.2.3. Beam test

The ability of *SNCG*$^{-/-}$ Thy1mγSN$^{TG/TG}$ and Thy1mγSN$^{TG/TG}$ cohorts to complete an 180^{o} turn (Fig. 42a) and traverse the length of a 500mm length and 20mm diameter wooden beam was assessed (Fig. 42b). At each time point between 26 and 63 mice were tested. At the 2-, 4- and 6-month test points the completion rate of the turn phase was equal in both groups. An improved turn performance was seen

in 9-month old *SNCG*$^{-/-}$ Thy1mγSN$^{TG/TG}$ mice, completing 21.0% more turns than the Thy1mγSN$^{TG/TG}$ cohort (χ^2 value 4.777, critical value 3.841), however at twelve-months this difference had diminished to an insignificant 12.5%. No differences were detected in the ability of either group to complete the traverse phase.

5.2.4. Inverted grid test

The strength and coordination of both cohorts was assessed at 6-, 9- and 12-months upon an inverted mesh grid for a 60-second test period (Fig. 43). A trend towards an improved performance was observed in the 12-month trial by the *SNCG*$^{-/-}$ Thy1mγSN$^{TG/TG}$ group. In spite of this trend, no significant differences were detected at any time points (p=4398, 0.3038, 0.1857 for 6-, 9- and 12-months respectively, Mann-Whitney U-test).

* * *

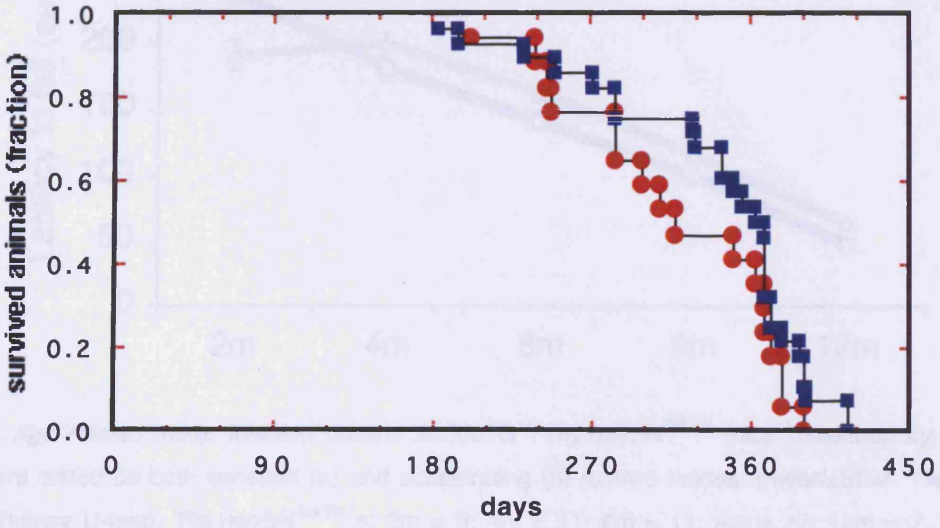

Fig. 40. The survival of SNCG$^{-/-}$ *Thy1mγSN*$^{TG/TG}$ *mice.* Kaplan-Meier plot showing survival of *SNCG*$^{-/-}$ Thy1mγSN$^{TG/TG}$ (red) and Thy1mγSN$^{TG/TG}$ mice (blue). No significant difference was detected by log rank test for equality of survival (p=0.1532) nor by generalized Wilcoxon test for equality of survival (p=0.2285). n-values; *SNCG*$^{-/-}$ Thy1mγSN$^{TG/TG}$ = 28, Thy1mγSN$^{TG/TG}$ = 17.

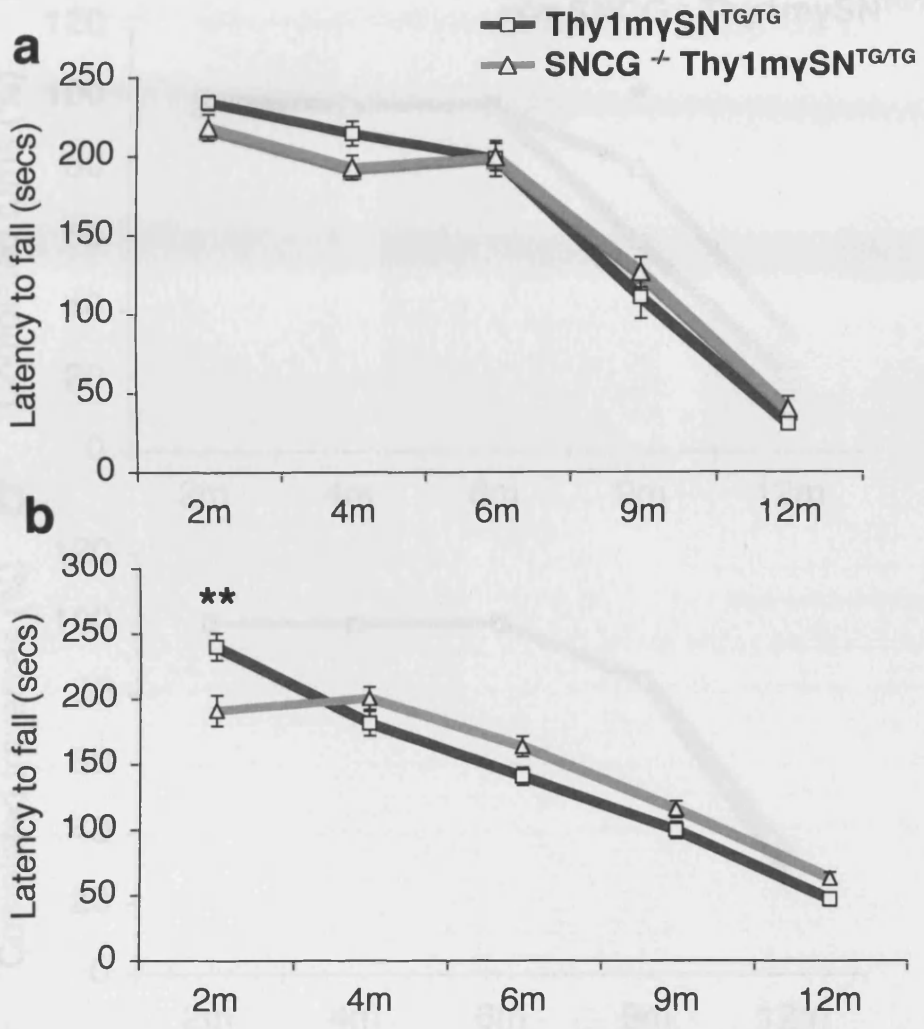

Fig. 41. Age related motor function decline in SNCG$^{-/-}$ Thy1mγSN$^{TG/TG}$ mice measured by rotarod. Mice were tested on both constant (a) and accelerating (b) rotarod modes. (mean±SEM ** = $p<0.01$ Mann-Whitney U-test). Thy1mγSN$^{TG/TG}$ n; 2m = 9; 4m = 11; 6m = 11; 9m = 12; 12m = 7. *SNCG$^{-/-}$* Thy1mγSN$^{TG/TG}$ n; 2m = 10; 4m = 20; 6m = 19; 9m = 21; 12m = 16.

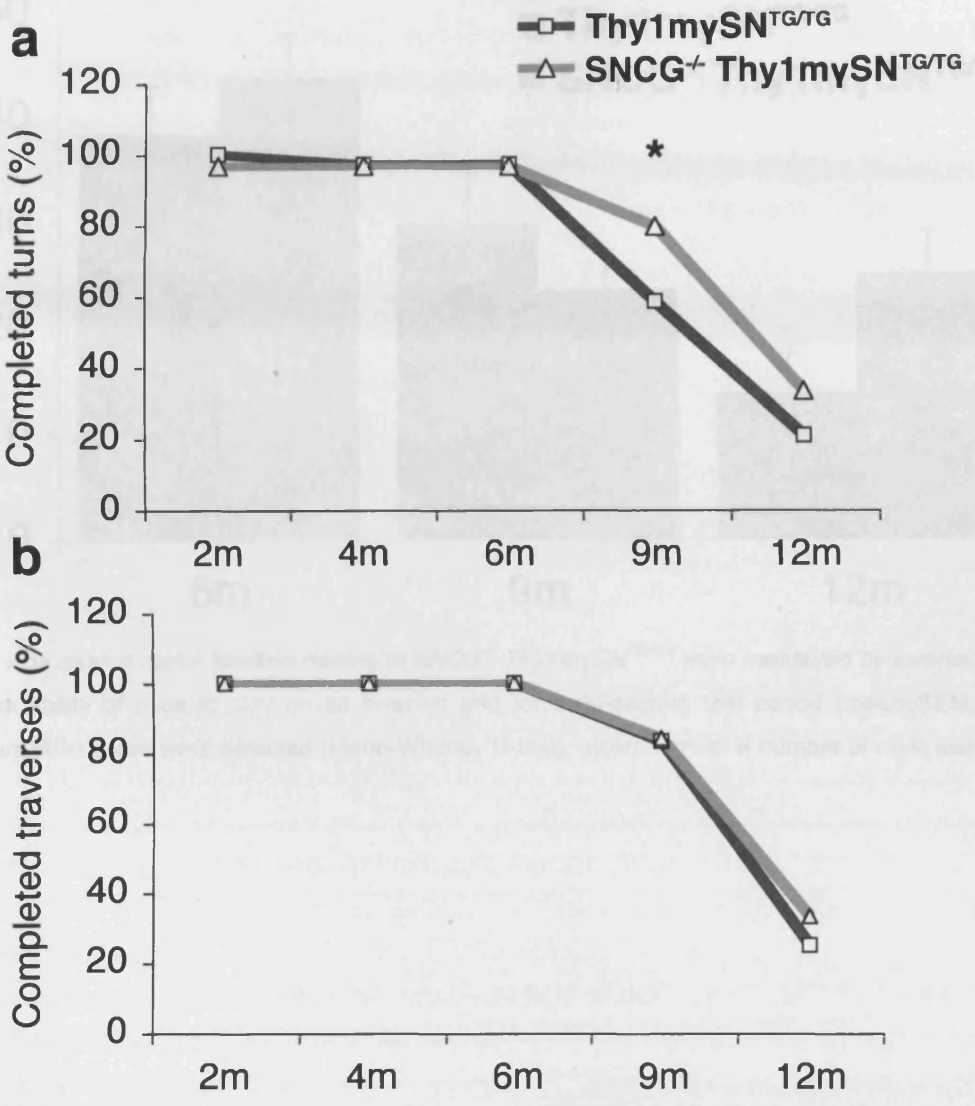

Fig. 42. Age related motor function decline in SNCG$^{-/-}$ Thy1mγSN$^{TG/TG}$ mice measured by beam test. The ability of mice to turn on (a) and traverse (b) a suspended beam were recorded over a one minute test period. The results are presented as the percentage of the cohort able to complete the test in the set period. * = χ^2 value greater than critical value at p=0.05. Thy1mγSN$^{TG/TG}$ n; 2m = 9; 4m = 11; 6m = 11; 9m = 12; 12m = 9. *SNCG$^{-/-}$* Thy1mγSN$^{TG/TG}$ n; 2m = 10; 4m = 20; 6m = 19; 9m = 21; 12m = 16.

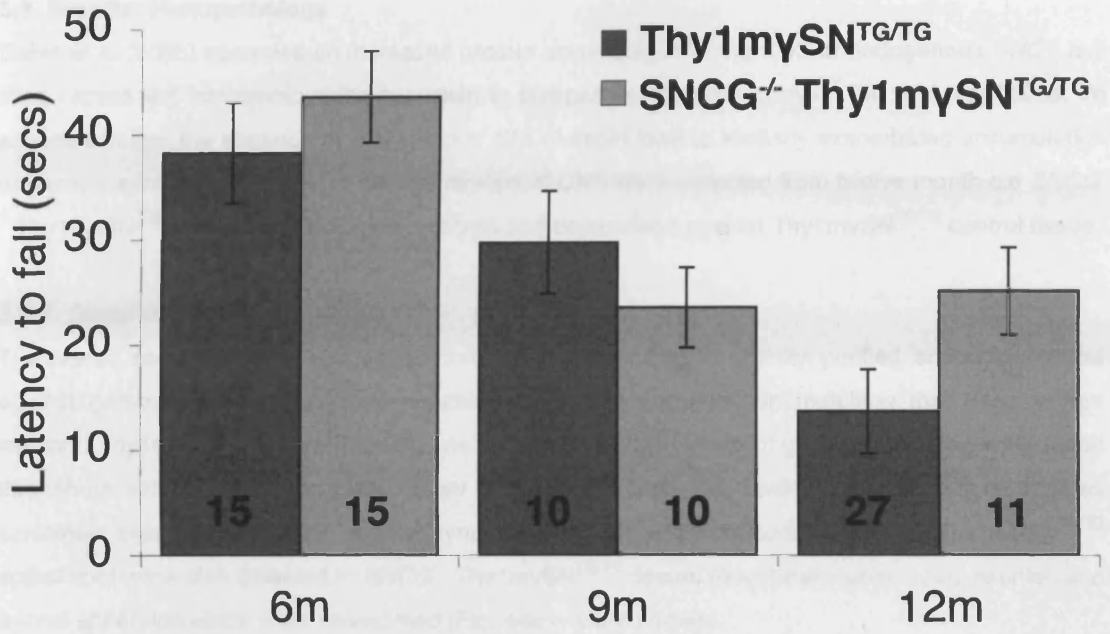

Fig. 43. *Age related motor function decline in SNCG$^{-/-}$ Thy1mγSN$^{TG/TG}$ mice measured by inverted grid test.* The ability of mice to stay on an inverted grid for a 60-second test period (mean±SEM). No significant differences were detected (Mann-Whitney U-test). Insert number = number of mice tested.

5.3. Results: Histopathology

Cabin et al (2005) observed an increased protein accumulation in the CNS of endogenous *SNCA* null mice expressing transgenic alpha-synuclein in comparison to those carrying the wild type locus. To assess whether the absence of endogenous *SNCG* might lead to similarly exacerbated accumulation of gamma-synuclein, samples of several regions of CNS were collected from twelve month old *SNCG*$^{-/-}$ Thy1mγSN$^{TG/TG}$ mice for histological analysis and comparison against Thy1mγSN$^{TG/TG}$ control tissue.

5.3.1. Spinal cord

Transverse sections of thoracic spinal cord immuno-stained with affinity purified antibodies raised against gamma-synuclein revealed a pattern of protein accumulation matching that seen in age matched Thy1mγSN$^{TG/TG}$ mice (Fig. 44, see section 3.3.). High levels of gamma-synuclein were found throughout both the grey and white matter of the spinal cord. Cell bodies, neurites and neuropil all contained intense staining for gamma-synuclein. Typical inclusion bodies seen in Thy1mγSN$^{TG/TG}$ spinal cord were also detected in *SNCG*$^{-/-}$ Thy1mγSN$^{TG/TG}$ tissue, most prominently Lewy neurites and axonal spheroids which were widespread (Fig. 44a – white arrows).

Concurrent with the clinical signs of neurodegeneration presented, immunostaining against GFAP revealed widespread infiltration of activated astrocytes in the spinal cord of twelve-month old *SNCG*$^{-/-}$ Thy1mγSN$^{TG/TG}$ mice at a level comparable with that observed in Thy1mγSN$^{TG/TG}$ control animals (Fig. 44b, see section 3.3). Furthermore staining with the biotinylated lectin RCA revealed infiltration of activated microglia occurring in parallel to astrogliosis (Fig. 44c).

5.3.2. Sciatic nerve

Overexpression of gamma-synuclein in the sciatic nerves of *SNCG*$^{-/-}$ Thy1mγSN$^{TG/TG}$ mice resulted in matching signs of pathology as seen in the Thy1mγSN$^{TG/TG}$ (Fig. 44d, also see section 4.2). In the sciatic nerves of twelve-month old *SNCG*$^{-/-}$ Thy1mγSN$^{TG/TG}$ mice gamma-synuclein was found to be distributed unevenly, suggesting the loss of unstained fibres. Furthermore typical signs of degeneration previously observed in the Thy1mγSN$^{TG/TG}$ nerves were also detected. Abnormal intra-axonal structures, including spheroid-like structures were detected, as were regions of neurite ballooning (Fig. 44d).

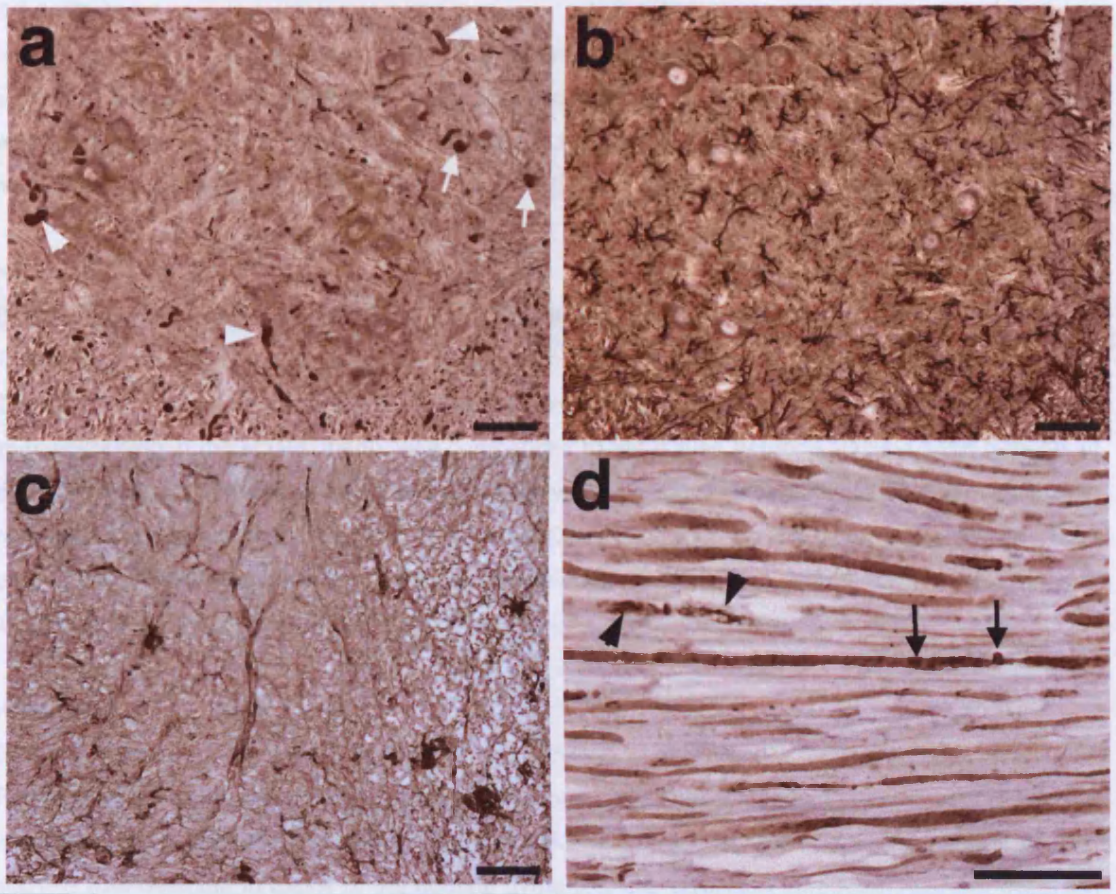

Fig. 44. Gamma-synuclein aggregation and gliosis in the central nervous system of SNCG$^{-/-}$ Thy1mγSN$^{TG/TG}$ mice. Representative transverse sections of thoracic spinal cord collected from twelve-month old *SNCG*$^{-/-}$ Thy1mγSN$^{TG/TG}$ immunostained with antibodies raised against gamma-synuclein (SK23, 1:100) (a), GFAP (1:400) (b) and biotinylated lectin RCA (1:100) (c). Representative longitudial section of *SNCG*$^{-/-}$ Thy1mγSN$^{TG/TG}$ sciatic nerve immuno-stained with antibodies raised against gamma-synuclein. White arrows = Lewy neurites, white arrowheads = axonal spheroids, black arrows = intra-axonal structures, black arrowheads = ballooned neurites. Scale bars = 50μm.

5.3.3. Brain

Immuno-staining of sagittal brain sections with affinity purified antibodies raised against gamma-synuclein revealed widespread expression and accumulation of the protein in the brains of twelve-month old *SNCG*$^{-/-}$ Thy1mγSN$^{TG/TG}$ (Fig. 45-47), consistent with the pattern seen in Thy1mγSN$^{TG/TG}$ mice (see section 3.4).

Nigra-striatal system

Dopaminergic regions were located using antibodies raised against tyrosine hydroxylase (Fig. 45a, c). TH immunostaining revealed no gross changes in the morphology of these structures in *SNCG*$^{-/-}$ Thy1mγSN$^{TG/TG}$ mice when compared to age matched wild type tissue (Fig. 45b, d). Gamma-synuclein immunostaining in the striatal matrix was comparable to the diffuse neuropil staining seen throughout the brain (Fig. 45b). Striatal white matter tracts were densely stained for gamma-synuclein with numerous dystrophic axons observed (Fig. 45b). Consistent with the low level expression of Thy1 promoter in dopaminergic neurons, little gamma-synuclein staining was detected in the cell bodies of the SNpc, though axonal spheroids were detected in the surrounding tissue (Fig. 45d).

Hippocampus

Gamma-synuclein was found throughout the *SNCG*$^{-/-}$ Thy1mγSN$^{TG/TG}$ hippocampus (Fig. 46). Perikaryal cytoplasm staining within pyramidal neurons and diffuse staining of the surrounding neuropil was detected in both the CA1 (Fig. 46b) and CA3 (Fig. 46c) regions. Gamma-synuclein positive staining was detected in axons of the dentate gyrus granular layer and infrequent neurons within the hilus (Fig. 46d). Abnormal intracellular inclusion bodies were not observed in neurons of the *SNCG*$^{-/-}$ Thy1mγSN$^{TG/TG}$ hippocampus.

Cerebellum

High levels of staining were detected within both the white matter region (Fig. 47b) and the granular layer (Fig. 47c) of the *SNCG*$^{-/-}$ Thy1mγSN$^{TG/TG}$ cerebellum. Substantial accumulation of gamma-synuclein within dystrophic neuritis was revealed, with spheroid inclusions frequently observed. Cytoplasmic staining of neurons within the Purkinje cell layer was also detected (Fig. 47c). As with Thy1mγSN mice, this was comparable to the endogenous levels seen in wild type mice (Fig. 14).

Cortex

Neuropil gamma-synuclein staining was observed throughout the cortex of *SNCG*$^{-/-}$ Thy1mγSN$^{TG/TG}$, with high levels detected in perikaryal and axonal cytoplasm in both the external (Fig. 47e) and internal (Fig. 47f) pyramidal cell layers. Granular layer staining was comparable to the widespread neuropil staining. Axonal spheroids and dystrophic axons were detected throughout the cortex, with a similar motor-sensory region gradient as described for the cortex of homozygous Thy1mγSN mice (see above).

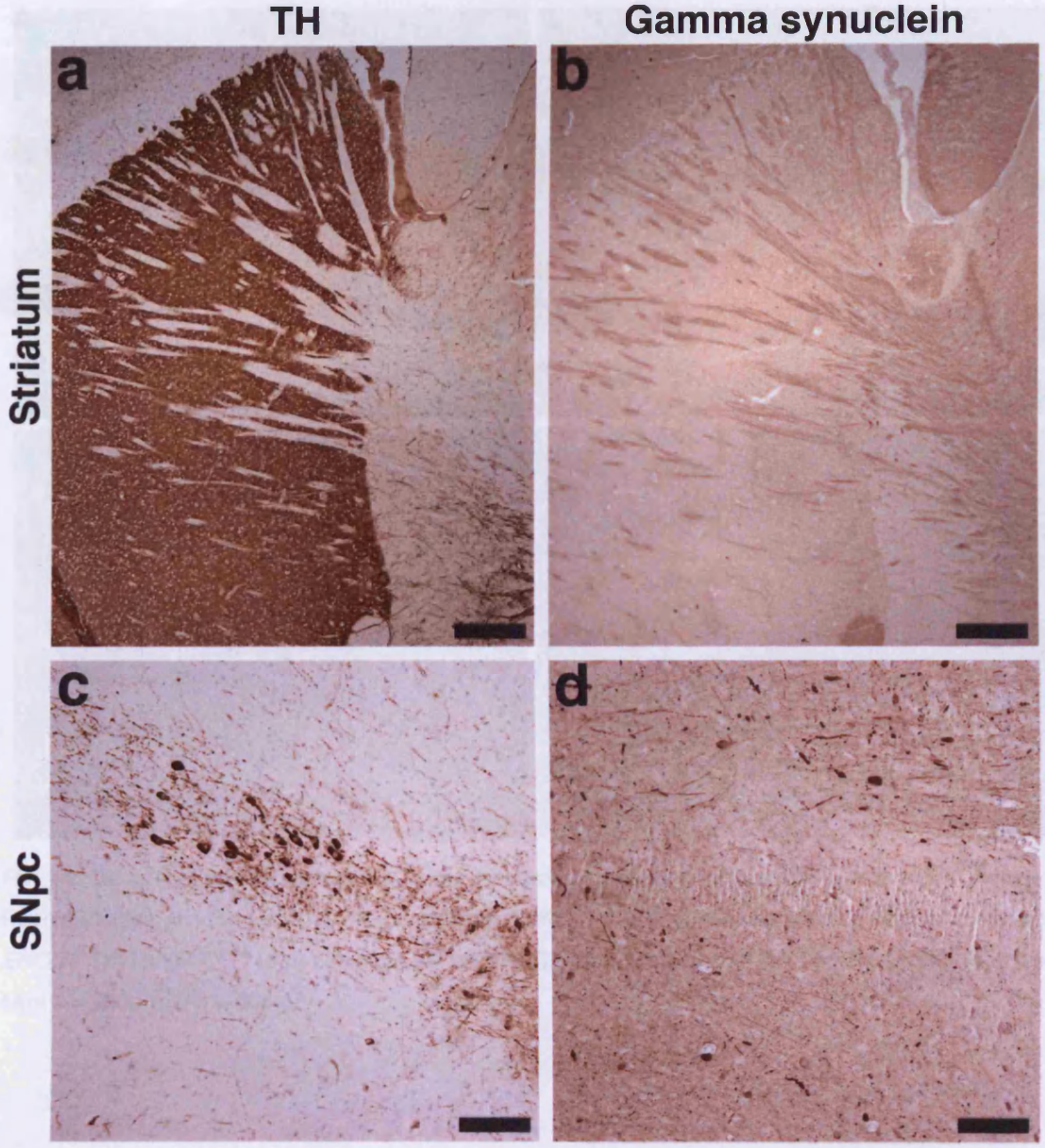

Fig. 45. Gamma-synuclein expression in the nigra-striatal system of SNCG$^{-/-}$ Thy1mγSN$^{TG/TG}$ mice. Representative tyrosine hydroxylase (1:1000) immunostained sagittal sections (lateral 1.44mm) of twelve-month old *SNCG$^{-/-}$* Thy1mγSN$^{TG/TG}$ (a) striatum and substantia nigra pars compacta (b). Corresponding sections immunostained with antibodies against gamma-synuclein (SK23, 1:100) show tracts of axons within the striatum of SNCG$^{-/-}$ Thy1mγSN$^{TG/TG}$ mice (b) and little staining in the SNpc (d). Scale bars a, b = 250μm; c, d = 100μm.

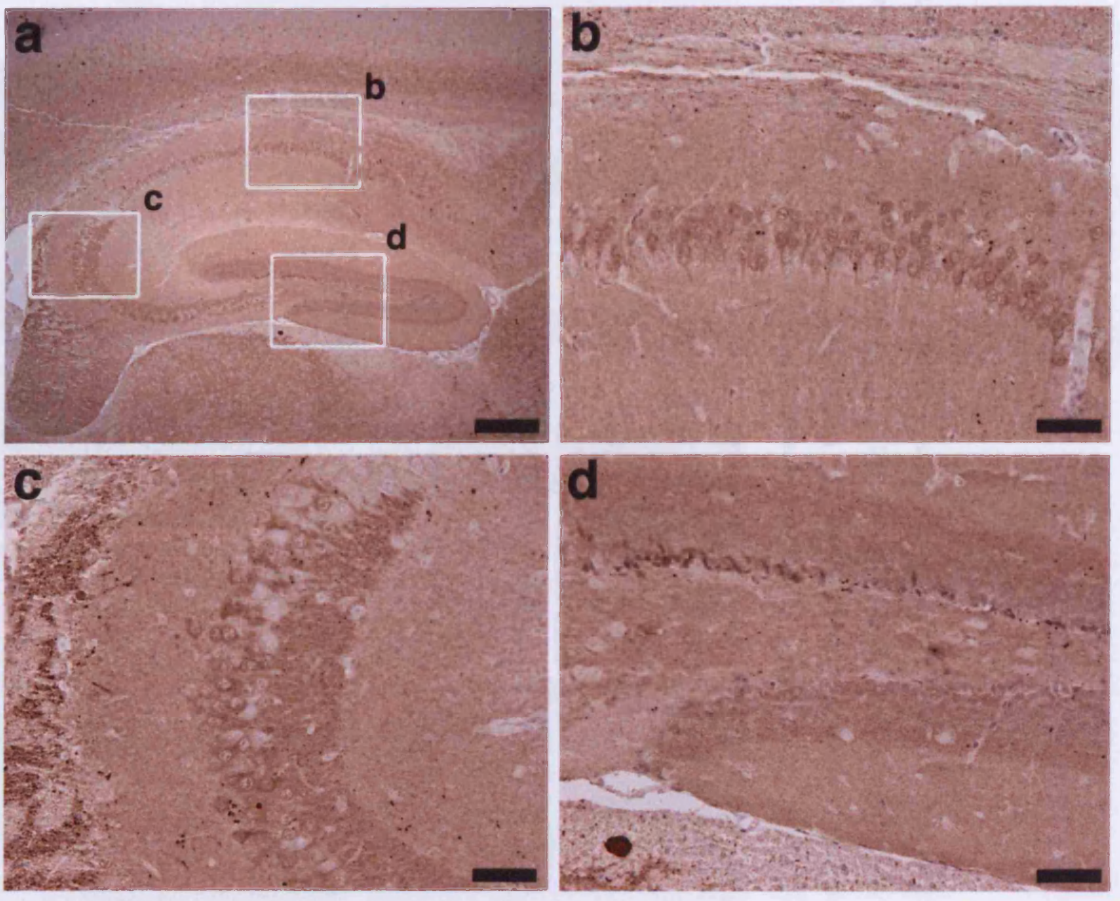

Fig. 46. Gamma-synuclein expression in the hippocampus system of SNCG$^{-/-}$ Thy1mγSN$^{TG/TG}$ mice. Representative gamma-synuclein immunostained (SK23, 1:100) sagittal sections of twelve-month old *SNCG$^{-/-}$* Thy1mγSN$^{TG/TG}$ (a-d) hippocampal regions CA1 (b), CA3 (c) and the dentate gyrus (d). Scale bars a = 250μm; b-d = 50μm.

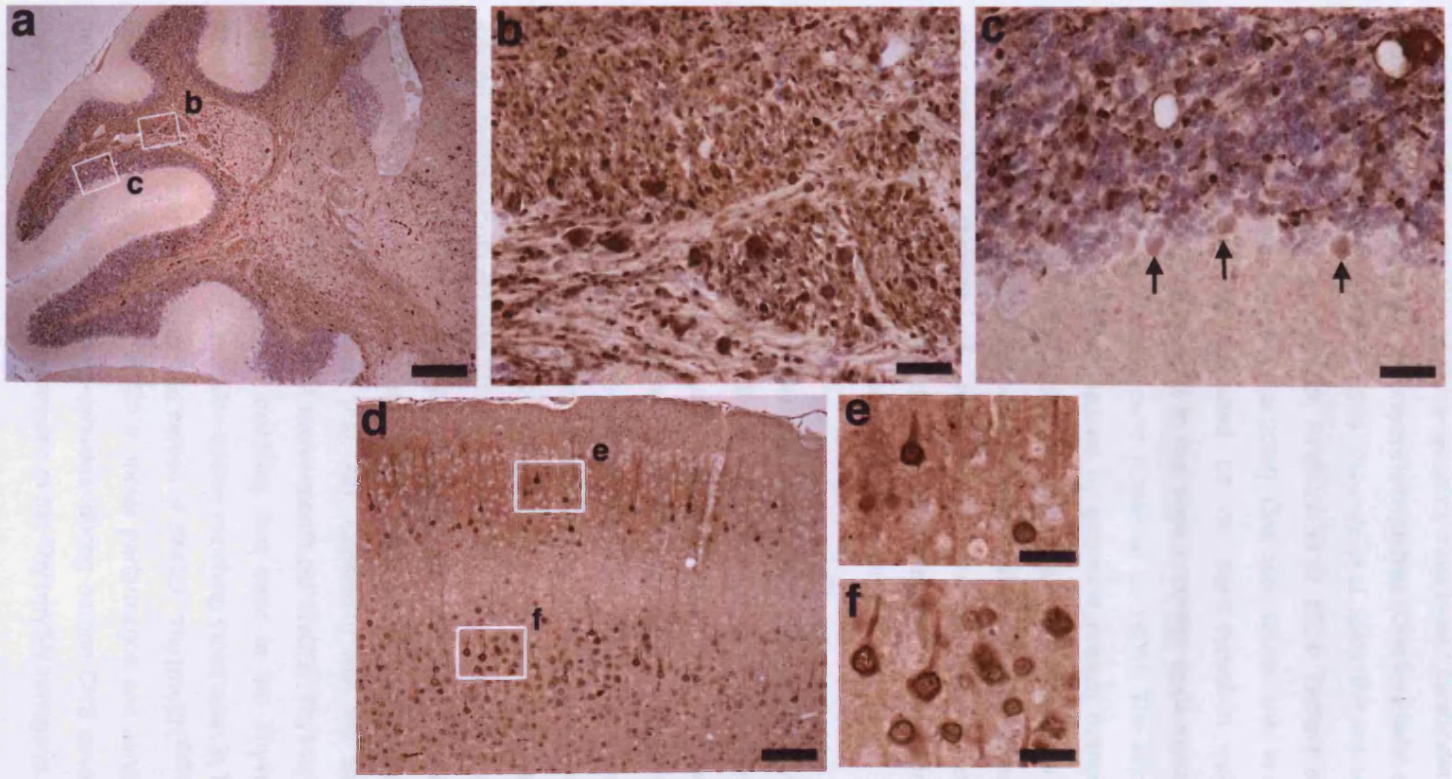

Fig. 47. Gamma-synuclein expression in the cerebellum and cortex of SNCG$^{-/-}$ Thy1mγSN$^{TG/TG}$ mice. Representative gamma-synuclein immunostained (SK23, 1:100) sagittal sections (lateral 1.44mm) of cerebellum (a-c) and cortex (d-f) from twelve-month old *SNCG*$^{-/-}$ Thy1mγSN$^{TG/TG}$ mice. Gamma-synuclein ia seen in the neurites of the white matter (b) and granular layer (c) of the 6th cerebellar lobule, and within cell bodies of the Purkinje cell layer (black arrows) (c). Gamma-synuclein positive cell bodies are seen in both the external (e) and internal (f) pyramidal cell layers of the S1 somatosensory region of cortex (d). Scale bars a = 250μm; d = 100μm; b, c, e, f, = 25μm.

5.4. Summary of results and discussion

Increases in the expression of alpha-synuclein have been robustly demonstrated to induce substantial neurodegeneration, both in human synucleinopathies (Chartier-Harlin et al. 2004; Edwards et al. 2010; Ibanez et al. 2004; Kruger et al. 1998; Pankratz et al. 2009; Polymeropoulos et al. 1997; Satake et al. 2009; Simon-Sanchez et al. 2009; Singleton et al. 2004; Zarranz et al. 2004) and animal models (reviewed in Buchman and Ninkina 2008). One such animal line, in which the mutant A53T form of alpha-synuclein was overexpressed on an alpha-synuclein null background, developed an exacerbated phenotype compared to that seen in control alpha-synuclein overexpressing mice on a wild type alpha-synuclein background (Cabin et al. 2005). The above chapters demonstrated the progressive neurodegeneration caused by gamma-synuclein overexpression in mice carrying the endogenous gamma-synuclein allele. To test whether endogenous gamma-synuclein confers any resistance to the pathology induced by overexpression of gamma-synuclein transgene, or conversely if developmental absence of endogenous gamma-synuclein causes an exacerbation of neurodegeneration, we developed a line of Thy1mγSN$^{TG/TG}$ mice on a pure C57Bl/6J and null for endogenous gamma-synuclein (SNCG$^{-/-}$ Thy1mγSN$^{TG/TG}$).

The animals developed a phenotype indistinguishable from that of the Thy1mγSN$^{TG/TG}$ line, characterised by identical motor abnormalities and an equally shortened lifespan (Fig. 40). Differences in motor behaviour were limited and inconsistent (Fig. 41-43). The most substantial difference was detected in the accelerating rotarod test, where significant impairment in *SNCG*$^{-/-}$ Thy1mγSN$^{TG/TG}$ performance was detected at two months (Fig. 41b). No further differences were seen at any other accelerating rotarod time-point and, furthermore, constant speed rotarod performance matched that of the Thy1mγSN$^{TG/TG}$ cohort (Fig. 41a). Converse to the early age deficit detected by the accelerating rotarod, twelve-month old *SNCG*$^{-/-}$ Thy1mγSN$^{TG/TG}$ mice outperformed control Thy1mγSN$^{TG/TG}$ on the inverted grid test (Fig. 43). A similar trend was also detected in the ability of the mice to turn on the beam test, with 9- and 12-month old *SNCG*$^{-/-}$ Thy1mγSN$^{TG/TG}$ mice completing the test more frequently than the Thy1mγSN$^{TG/TG}$ cohort (Fig. 42). Consistent with the similarity seen in motor activity, histological analysis of the CNS of twelve-month old *SNCG*$^{-/-}$ Thy1mγSN$^{TG/TG}$ mice revealed a pattern of gamma-synuclein expression matching that seen in the Thy1mγSN$^{TG/TG}$ cohort (Fig. 44-47). Abnormal gamma-synuclein inclusion bodies matching those seen in Thy1mγSN$^{TG/TG}$ mice were found in the brain, spinal cord and sciatic nerves of *SNCG*$^{-/-}$ Thy1mγSN$^{TG/TG}$ mice. It can thus be concluded from the lack of a consistent deficit in motor performance and similarity of CNS dystrophy that the presence of endogenous gamma-synuclein during murine CNS development has no influence upon the pathology induced by overexpression of the Thy1mγSN transgene.

Cabin et al. make several hypotheses for the exacerbated phenotype seen in the alpha-synuclein null mice expressing the mutant A53T human form of alpha-synuclein under a prion-promoter (-/-/A53T). The -/-/A53T mice were generated on a mixed FVB/129 background, whereas control mice expressing both endogenous alpha-synuclein and the A53T transgene (+/+/A53T) were a FVB/N stain. The

authors suggest that the introduction of unspecified FVB/129 alleles may sensitize the mice to alpha-synuclein overexpression. They suggest that interaction between the murine endogenous alpha-synuclein and the human transgene in +/+/A53T mice limits disease severity. However this possibility was dismissed, due to the mouse protein being more fibrillogenic than the human (Rochet et al. 2000). Though the autosomal dominant mutation of alanine to threonine at residue-53 is a known cause of PD in humans, threonine is the wild type residue-53 in mice. It is suggested that this, or one of the other six residual differences between mouse and human synuclein, confers some degree of developmental tolerence to the human synuclein protein. Furthermore, endogenous alpha-synuclein expression in the spinal cord is normally restricted to dorsal horn however the damage seen in +/+/A53T mice, where transgene expression is pan neuronal, occurs predominantly within motor neurons of the ventral horn (Cabin et al. 2005), again suggesting an innate protective role.

From the SNCG$^{-/-}$ Thy1mγSN$^{TG/TG}$ data it seems likely that the exacerbated phenotype seen by Cabin et al is most likely due to differences in either the genetic background of the animal lines used or that the endogenous murine *SNCA* confers protection against human *SNCA*. Our experimental design removed these two factors from the experiment. Both the gamma-synuclein null and Thy1mγSN$^{TG/TG}$ lines were produced on pure C57Bl/6J backgrounds, limiting the influence of any stain differences upon the experiment. Secondly both the endogenous and transgenic *SNCG* genes used in the Thy1mγSN$^{TG/TG}$ line are the murine form and thus neither differences in fibrillation propensity nor tolerance conferred by residual heterogeneity should be factors in pathogenesis. Thus as no substantial change in disease onset or severity was observed in the *SNCG*$^{-/-}$ Thy1mγSN$^{TG/TG}$ cohort, and it appears that the presence of endogenous gamma-synuclein plays no significant role in the neuropathy seen in Thy1mγSN$^{TG/TG}$ mice. In future it may be interesting to closer replicate the experiments of Cabin et al by using mice transgenic for the fibrillogenic human SNCG (Park and Lansbury 2003) and, if degeneration is induced, test whether the ablation of the murine endogenous *SNCG* would exacerbate the pathology.

It can thus be concluded that the presence of endogenous gamma-synuclein during development does not significantly protect mice against the toxicity induced by its postnatal overexpression. Furthermore, with regards to the findings of Cabin et al. 2005, the above suggests that the increased severity found in -/-/A53T mice is due to stain differences in the genetic background of the mice and/or the forms of SNCA expressed.

6. The impact of gamma-synuclein overexpression upon the CSPα-null phenotype

6.1. Overview

The deletion of cysteine string protein alpha (CSPα), a co-chaperone associated with SNARE complex assembly, induces a progressive neurodegenerative phenotype in mice (Chandra et al. 2005; Fernandez-Chacon et al. 2004). Degeneration is caused by the immature development of synaptic junctions, attributed to reductions in SNARE-complex assembly, specifically through a 30-50% reduction in levels of SNAP-25 (Burre et al. 2010; Chandra et al. 2005). Remarkably overexpression of both human and mouse wild type alpha-synuclein rescues CSPα-null mice from the neurodegenerative phenotype (Chandra et al. 2005). Conversely ablation of both alpha- and beta-synuclein induces a more pronounced phenotype (Chandra et al. 2005). Current data suggests that alpha-synuclein rescues the CSPα-null phenotype by promoting the assembly of SNARE complexes through direct interaction with synaptic phospholipid membranes and with the SNARE component synaptobrevin-2 (Burre et al. 2010).

To investigate whether the overexpression of gamma-synuclein is similarly able to rescue the phenotype seen in CSPα-null mice, we produced a line of C57Bl/6J mice null for CSPα and overexpressing high levels of the *Thy1*mγSN transgene.

6.2. Results

6.2.1. Phenotype of CSPα-null mice

We generated a line of CSPα$^{-/-}$ mice on a pure C57Bl/6J background. The survival of these animals was assessed to ensure a phenotype comparable to those previously reported was presented (Chandra et al. 2005; Fernandez-Chacon et al. 2004). CSPα$^{-/-}$ mice were indistinguishable from their wild type and CSPα$^{+/-}$ littermates during the first two weeks of their life. Similar to the previously reported observations of CSPα$^{-/-}$ mice on a mixed genetic background, the CSPα$^{-/-}$ mice on C57Bl/6J background stopped gaining weight after P14 and started to show signs of lethargy. From P22 emaciated pups began to die, with 50% of the cohort not surviving beyond P34 (Fig. 48b). No mice in the CSPα$^{-/-}$ cohort survived past P52 (Fig. 48b). No control wild-type littermates died during this period (data not shown).

6.2.2. Phenotype of CSPα$^{-/-}$ Thy1*mγSN mice*

To test the hypothesis that gamma-synuclein overexpression would rescue mice from the CSPα$^{-/-}$ phenotype we generated cohorts of CSPα$^{-/-}$ expressing the *Thy1*mγSN transgene either homo- or hemizygously. In neither case did the overexpression of the *Thy1*mγSN transgene increase either the survival of CSPα$^{-/-}$ mice or reduce the severity of their neurodegeneration. Thus for further analysis of lifespan, data for CSP-null hemi- and homozygous *Thy1*mγSN mice were combined (herein CSPα$^{-/-}$ *Thy1*mγSN). During the first two weeks CSPα$^{-/-}$ and CSPα$^{-/-}$ *Thy1*mγSN pups were indistinguishable. Beyond this point the growth of both groups was retarded (Fig. 48a). Lethargy was apparent, though mice were able to move when prompted. Similar to the CSPα$^{-/-}$ line, the majority of the CSPα$^{-/-}$

*Thy1*mγSN cohort had died at approximately P34. An insignificant fraction of the CSPα$^{-/-}$ *Thy1*mγSN cohort survived past P60. No significant difference was detected between the survival of CSPα$^{-/-}$ and CSPα$^{-/-}$ *Thy1*mγSN mice by either log rank (p=0.5284) or generalised Wilcoxon's tests for equality of survival (p=0.4109) (Fig. 48b).

* * *

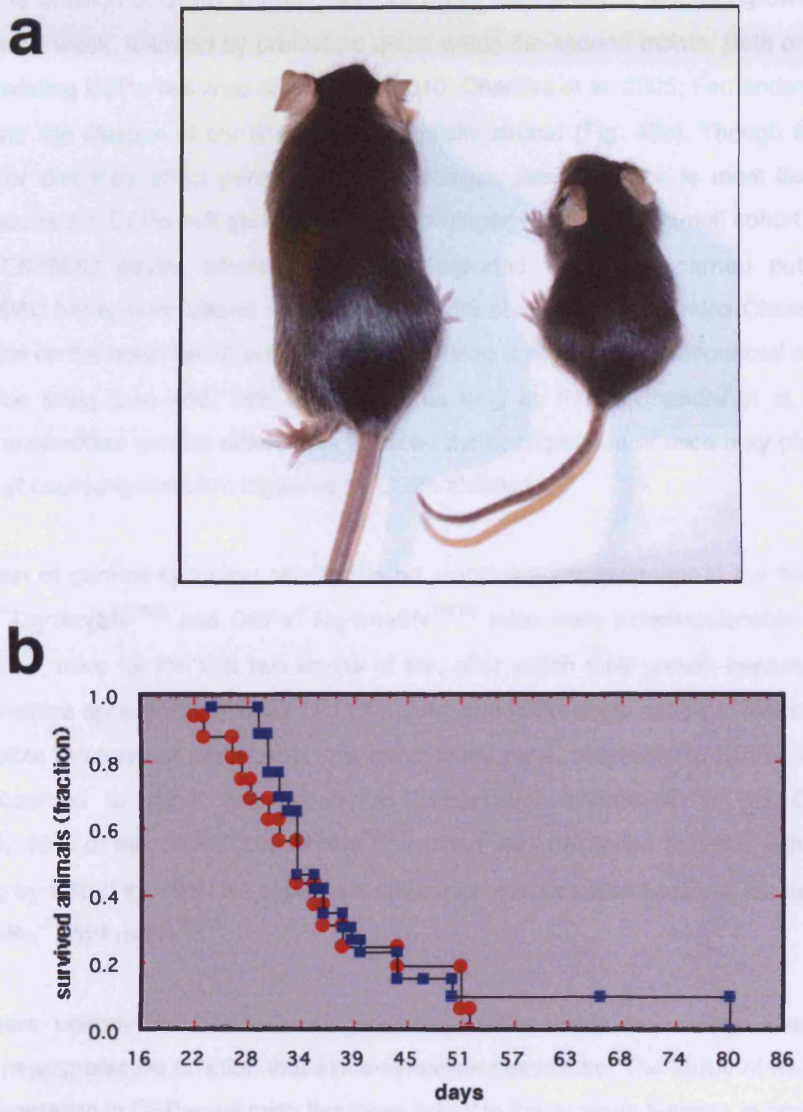

Fig. 48. Gamma-synuclein overexpression does not rescue the CSPα null phenotype. (a) Four-week old CSPα$^{+/+}$*Thy1*mγSN (left) are indistinguishable from wild type mice, where as CSPα$^{-/-}$*Thy1*mγSN (right) are visibly smaller and indistinguishable from CSPα-null mice. Log rank and generalized Wilcoxon tests for equality of survival (b) found no significant difference (p=0.5284 and 0.4109 respectively) between CSPα$^{-/-}$*Thy1*mγSN$^{-/-}$ mice (red) and either CSPα$^{-/-}$*Thy1*mγSN cohorts (blue). n-values: CSPα$^{-/-}$*Thy1*mγSN$^{-/-}$ =16; CSPα$^{-/-}$ *Thy1*mγSN = 26.

6.3. Summary of results and discussion

To assess whether gamma-synuclein is able to functionally replace alpha-synuclein in its capacity to rescue neurons from neurodegeneration induced by the ablation of CSPα, we produced a line of CSPα-null mice overexpressing the *Thy1*mγSN transgene on a pure C57Bl/6J background, with a control group of CSPα-null mice also generated on a matching background. Prior to assessment of the experimental cohort, we confirmed control animals developed a phenotype similar to that previously reported for the ablation of CSPα in mice. Our CSPα-null mice showed retarded growth following the second postnatal week, followed by premature death within the second month. Both of the above are observed in existing CSPα-null lines (Burre et al. 2010; Chandra et al. 2005; Fernandez-Chacon et al. 2004), however the lifespan of our line was substantially shorter (Fig. 48b). Though factors such as environment or diet may affect penetrance of phenotype, the difference is most likely due to the background stains the CSPα-null genotypes were developed on. Our CSPα-null cohort was produced on a pure C57Bl/6J strain, whereas previously reported work was carried out on a mixed Ola129xC57Bl/6J background (Burre et al. 2010; Chandra et al. 2005; Fernandez-Chacon et al. 2004). CSPα-null mice on the latter background appear to develop a slightly less pronounced phenotype, with numerous mice living past P60, with some living as long as P100 (Chandra et al. 2005). It thus appears that unspecified genetic differences between the backgrounds of mice may play a role in the development of neurodegeneration triggered by CSPα ablation.

Overexpression of gamma-synuclein resulted in no significant improvement in the health of $CSP\alpha^{-/-}$ mice. $CSP\alpha^{-/-}$*Thy1*m$\gamma SN^{TG/tg}$ and $CSP\alpha^{-/-}$*Thy1*m$\gamma SN^{TG/TG}$ mice were indistinguishable from both wild type and $CSP\alpha^{-/-}$ mice for the first two weeks of life, after which their growth became retarded and motor abnormalities apparent (Fig. 48a). Unfortunately, due to the rapid nature of neurodegeneration it was not possible to carry out any quantitative behavioural tests, however the $CSP\alpha^{-/-}$*Thy1*m$\gamma SN^{TG/TG}$ were not observed to show any substantial behavioural differences to the $CSP\alpha^{-/-}$ cohort. Approximately 90% of the $CSP\alpha^{-/-}$*Thy1*m$\gamma SN^{TG/TG}$ cohort was deceased by P50, with the remaining fraction dying by P80 (Fig. 48b). No significant difference was detected between the survival of either $CSP\alpha^{-/-}$ or $CSP\alpha^{-/-}$*Thy1*m$\gamma SN^{TG/TG}$.

It thus appears unlikely that the role of gamma-synuclein within the neuron overlaps with the downstream neuroprotective function that alpha-synuclein possesses. The ability of the latter to inhibit synaptic degeneration in CSPα-null mice has been linked to the proteins function in promoting SNARE complex formation in pre-synaptic terminals (Burre et al. 2010). Though the mechanism by which this is facilitated is unclear, alpha-synuclein directly interacts with vesicle phospholipid membranes through its N-terminal lipid-binding domain and with synaptobrevin-2 through its C-terminus (Burre et al. 2010; Perrin et al. 2000). There are data to suggest that crucial structural differences between alpha- and gamma-synuclein account for this functional disparity. The A30P mutant form of alpha-synuclein, the lipid-binding domain of which is disrupted by the polymorphism (Perrin et al. 2000), is unable to

facilitate the rescue of CSPα-null mice (Chandra et al. 2005). As gamma-synuclein has a lower propensity to bind phospholipid membranes, due to it having a less alpha-helical structure than alpha-synuclein (Sung and Eliezer 2007), it is feasible that it is less able or entirely unable to carry out the function of alpha-synuclein. The interaction between the C-terminus of alpha-synuclein and synaptobrevin-2 also appears essential for SNARE complex assembly. Defective SNARE complex assembly seen in triple synuclein null neurons is rescued by the expression of wild type alpha-synuclein, but not when a C-terminus truncated form of alpha-synuclein was expressed (Burre et al. 2010). The C-terminus of gamma-synuclein is significantly diverse compared to that of alpha- and beta-synuclein, being shorter and less ordered (Sung and Eliezer 2007). As with lipid-binding variability it is feasible that such variations in C-terminus sequence determine functional interaction between synuclein proteins and synaptobrevin-2.

Further investigation of the synaptic role of gamma-synuclein through replication of experiments carried out by Burre et al may allow some insight into its function. Alpha-synuclein was found to co-immunoprecipitate with SNAP-25, synapsin 1 and synaptobrevin in brain homogenate of wild type mice. Secondly, viral mediated overexpression of alpha-synuclein is able to rescue SNARE complex assembly deficits in cultured hippocampal neurons of triple synuclein null mice. Similar co-immunoprecipitation experiments would determine if the protein is capable of direct interaction with the synaptic vesicle fusion components. Absence of interaction may explain the inability of gamma-synuclein to rescue the CSPα-null phenotype. If gamma-synuclein were able to interact with such proteins, transfection of triple synuclein null hippocampal neurons with viral expressed gamma-synuclein would determine whether the protein is able to increase SNARE complex assembly. Ineffective promotion of such complexes may again explain the inability of gamma-synuclein to rescue mice from the effects of CSPα ablation.

7. Gamma-synuclein in human amyotrophic lateral sclerosis and frontotemporal lobar degeneration

7.1. Introduction

The previous chapters of this thesis have demonstrated that gamma-synuclein is capable of inducing widespread neurodegeneration when overexpressed in the murine nervous system. A pattern of damage is induced that recapitulates several features of human ALS, most notable the disproportionate vulnerability of motor neurons to degeneration. There is currently no evidence to suggest gamma-synuclein might be involved in human cases of the disorder, though research in the field is limited. A small study of 92 cases of familial and sporadic cases of ALS failed to detect any polymorphisms associated with increased risk of the disease (Flowers et al. 1999). The involvement of gamma-synuclein in neurodegeneration is not however unfeasible. The protein has been identified as a component of rare, atypical inclusion bodies in several human neurodegenerative disorders, including PD, Lewy body dementia (Galvin et al. 1999), Hallervorden-Spatz syndrome (Galvin et al. 2000) as well as glaucoma (Surgucheva et al. 2002). Furthermore the degeneration seen in animal models of both glaucoma and gracile axonal dystrophy has been associated with accumulation of gamma-synuclein (Nguyen et al. 2011; Wang et al. 2004).

In collaboration with Dr Tibor Hortobagyi and the MRC London Brain Bank for Neurodegenerative Diseases, King's College, London, we have studied expression and distribution of gamma-synuclein in the human spinal cord and frontal lobe using a set of histological samples from neurologically healthy individuals and patients with several types of neurological disorders. This allowed us to begin characterising the normal distribution of gamma-synuclein in the human CNS, and gave an invaluable opportunity to look for evidence of gamma-synucleinopathy in human disease. We were given access to tissues collected from patients with sporadic ALS, FUS/TLS or SOD1 associated familial ALS, frontotemporal lobar degeneration with motor neuron disease and TDP43-proteinopathy associated frontotemporal lobar degeneration.

7.2. Results: Healthy and ALS spinal cord samples

Transverse sections of cervical or thoracic spinal cord were assessed from samples group including healthy control individuals, patients with sporadic ALS (sALS) and familial SOD1 or FUS associated ALS (fALS) (appendix 10). Age of death varied from 35 to 79 years of age, with post-mortem dissection (PDM) of tissues generally carried out within 72 hours of death. Staining was carried out with two sets of antibodies raised against gamma-synuclein. Affinity purified rabbit anti-human gamma-synuclein polyclonal antibodies (SK109) were produced by ourselves (Ninkina et al. 1998) and following optimization were used at a working concentration of 1:250. For confirmation of results staining was then repeated using a commercially available goat anti-human gamma-synuclein polyclonal antibody (E20) produced by Santa Cruz Biotechnology Inc, used at a concentration of 1:100. No notable differences were detected between the patterns of staining produced by both antibodies. As such the findings obtained from each round of staining are discussed in unison.

7.2.1. Healthy control tissue samples

Immunostaining of healthy control tissue revealed a pattern of gamma-synuclein distribution comparable with that seen in wild type mice. The perikaryal cytoplasm of ventral horn motor neurons stained positive for the protein (Fig. 49a, b). No evidence of abnormally high levels or uneven distribution of gamma-synuclein within motor neuron cell bodies was detected. The surrounding neuropil was also weakly stained for the protein, with widespread punctate staining. The staining was observed in axons in both the grey and white matter (Fig. 49a-d). Transversely cut axons appeared as a small intensely stained central structure (~5μm) surrounded by a gamma-synuclein negative myelin sheath (Fig. 49c, d). Longitudinally cut axons were stained for gamma-synuclein in an even manner, with no evidence of ballooned neurites or axonal spheroids (Fig. 49c). A similar pattern of gamma-synuclein distribution was also detected within the axons of the dorsal and ventral spinal nerve roots (Fig. 49e, f). Levels of gamma-synuclein appeared comparable between the motor and sensory axon populations.

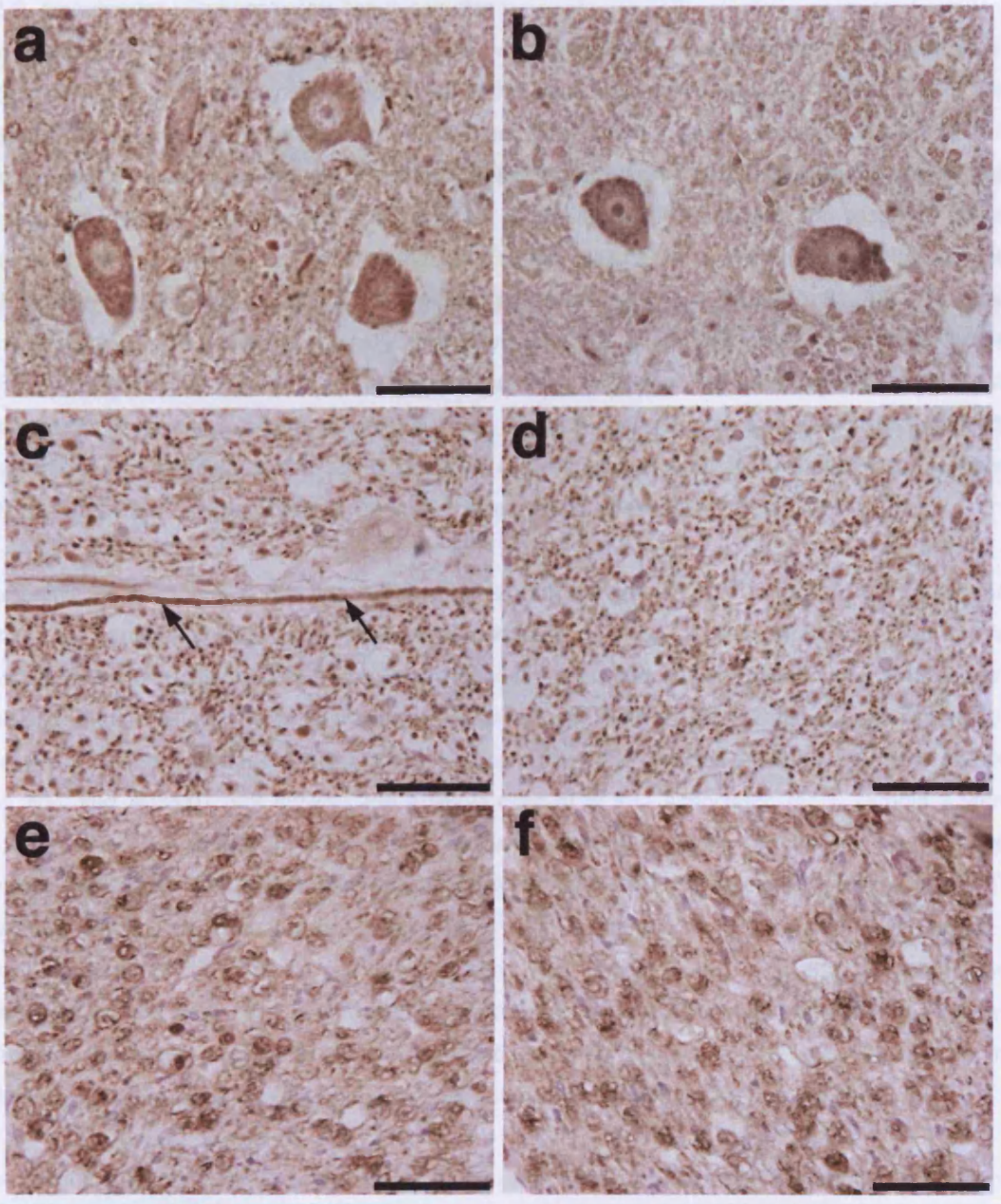

Fig. 49. Healthy spinal cord immunostained with antibodies against gamma-synuclein. Ventral horn motor neurons of healthy control tissue A049/03 immunostained with SK109 (a) and E20 (b) polyclonal antibodies. White matter region axons were not found to contain inclusion bodies following staining with SK109 antibodies, with gamma-synuclein distributed evenly (c). No abnormal structures were detected in the corticospinal tracts of either control case (d). Dorsal (e) and ventral (f) spinal nerve roots of healthy control tissue A130/09 immunostained with SK109 polyclonal antibody. Scale bars = 50μm.

7.2.2. Amyotrophic lateral sclerosis tissue samples

Immunostaining of tissues donated by patients with sporadic or familial forms of ALS revealed a pattern of staining that initially appeared similar to that seen in healthy control tissue, however detailed examination revealed the presence of abnormal gamma-synuclein positive structures in several of the tissue samples. A large portion of ventral horn motor neurons were clearly lost from the sporadic and familial ALS patients' spinal cords. Analysis of all remaining motor neurons in the tissue revealed a pattern of gamma-synuclein distribution that consistently matched that seen in the control samples, with an even distribution of protein throughout the perikaryal cytoplasm (Figs. 50, 51, 53). The typical intracellular inclusion structures normally associated with ALS, such as Bunina and skein-like bodies, were not detected by gamma-synuclein immunostaining in any of the samples studied (Fig. 53). Furthermore abnormal axonal structures, such as the ballooned neurites and axonal spheroids that were frequently detected in the spinal cords of gamma-synuclein overexpressing mice, were not detected in the grey matter of any of the human tissue samples assessed (Figs. 50, 51, 53).

Unexpectedly, assessment of white matter of several tissue samples did reveal structures intensely stained for gamma-synuclein that were not seen in control tissues. These appeared to fall into two classes, one prominent within the lateral corticospinal tracts, and a less defined class of structure in the peripheral dorsal and dorsolateral tissue. The lateral corticospinal tract structures were detected in four sets of sample tissue, being three cases of sporadic ALS, samples A251/09 (Fig. 50), A098/09 (Fig. 53), and A038/01 (not shown) and a single case of SOD-1 associated fALS, sample A348/08 (Fig. 51). The morphology of these structures was consistent across the tissues and samples, generally spherical, with a diameter of approximately 10-20μm, and granular in composition. The presence of these structures does not appear to be a prerequisite to ALS, as they were absent or highly infrequent in the corticospinal tracts of other ALS sample tissues (Fig. 52). Similar ubiquitin positive structures were not detected within the corticospinal tracts of tissue containing the gamma-synuclein structures, suggesting the accumulated gamma-synuclein is not ubiquitinated and that ubiquitin and other ubiquitinated proteins are not components of these structures (Fig. 53).

The second class of structure was detected in the peripheral regions of dorsal and dorsolateral white matter in sALS cases A190/06 and A038/01, in SOD1-fALS case A348/08 and in FUS-fALS case A018/93 (representative images shown in Fig. 54). The structures appear to be distinct from those seen in the corticospinal tract. Gamma-synuclein immunostaining of these was notably weaker than those of the corticospinal tract, though variation in tissue processing cannot be ruled out as a cause of this difference. Though of comparable size to the corticospinal tract structures (10-20μm width), the morphology of these structures was less regular and the shape was generally more angular. The occasional presence of nuclei within these structures suggests that they are most likely glial or a small class of neuronal cells (Fig. 54c, f).

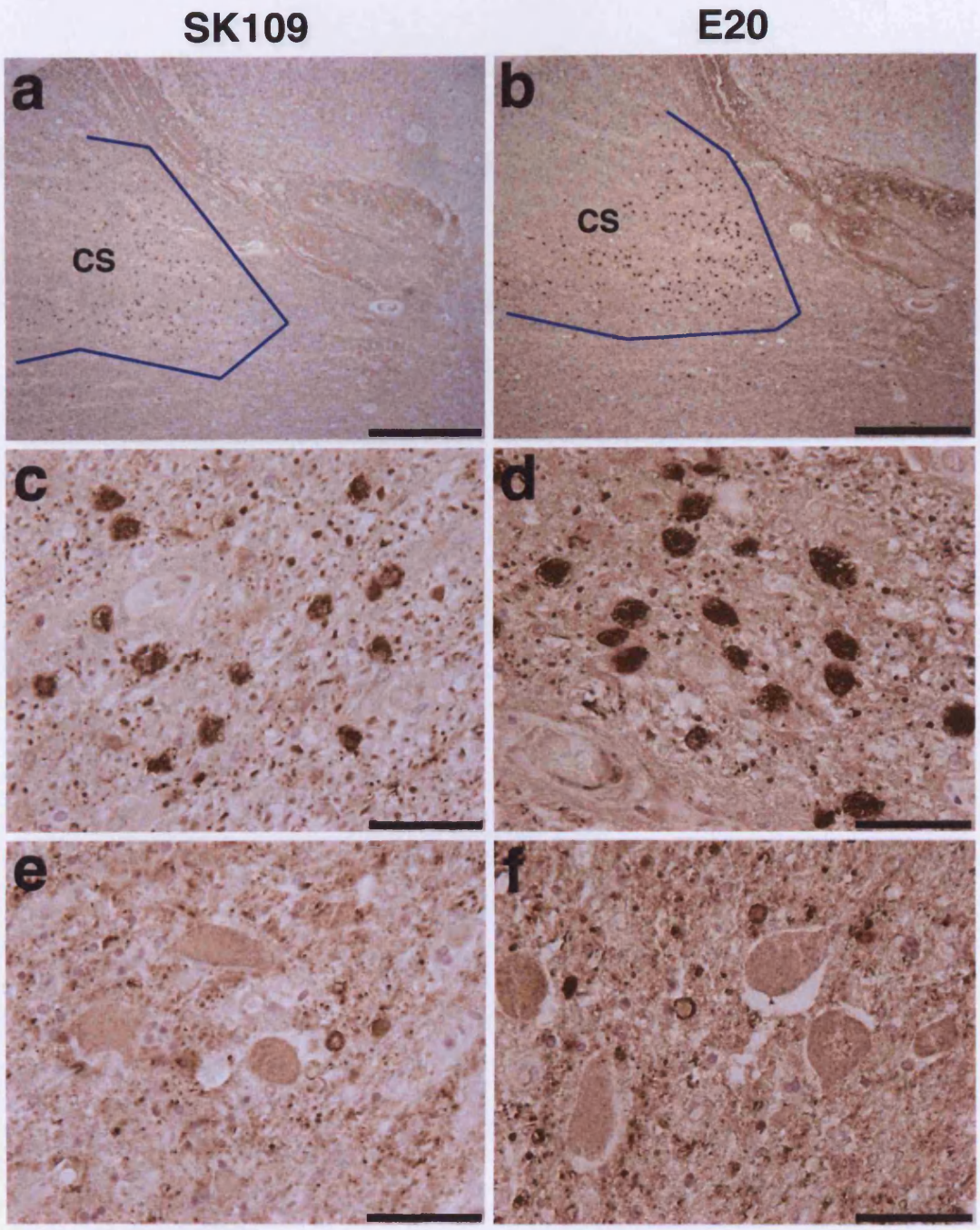

Fig. 50. Gamma-synuclein immunostained spinal cord tissue from sALS sample A251/09. Low magnification images of the lateral region of cervical spinal cord stained using antibodies SK109 (a, c, e) and E20 (b, d, f). The blue line denotes the corticospinal tract region (CS) containing unidentified structures intensely stained for gamma-synuclein. Of all tissues assessed these structures were most prominently detected in the lateral corticospinal tract of sample A251/09, and were generally spherical and of granular composition (c, d). Neither set of antibodies detected inclusion bodies within ventral horn motor neurons (e, f). Scale bars: a, b = 500μm, c-f = 50μm.

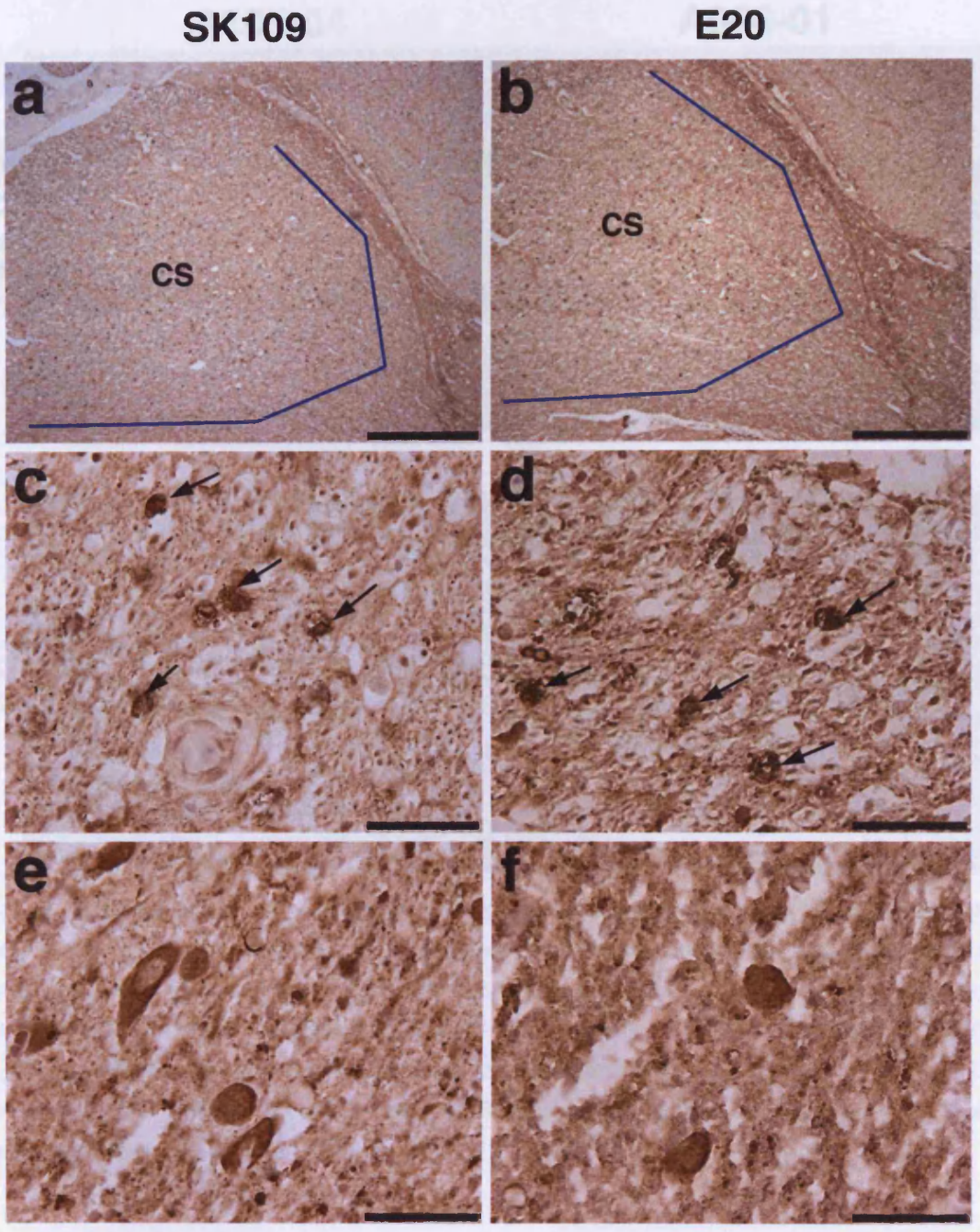

Fig. 51. Gamma-synuclein immunostained spinal cord tissue from SOD1-fALS sample A348/08. Low magnification images of the lateral corticospinal tract region (CS) of thoracic spinal cord stained using polyclonal antibodies SK109 (a, c, e) and E20 (b, d, f). Both sets of antibodies detected abnormal structures positive for gamma-synuclein (arrows) within this region (c, d). Gamma-synuclein positive inclusion bodies were not detected within the cytoplasm of ventral horn motor neurons (e, f). Scale bars: a, b = 500μm, c-f = 50μm.

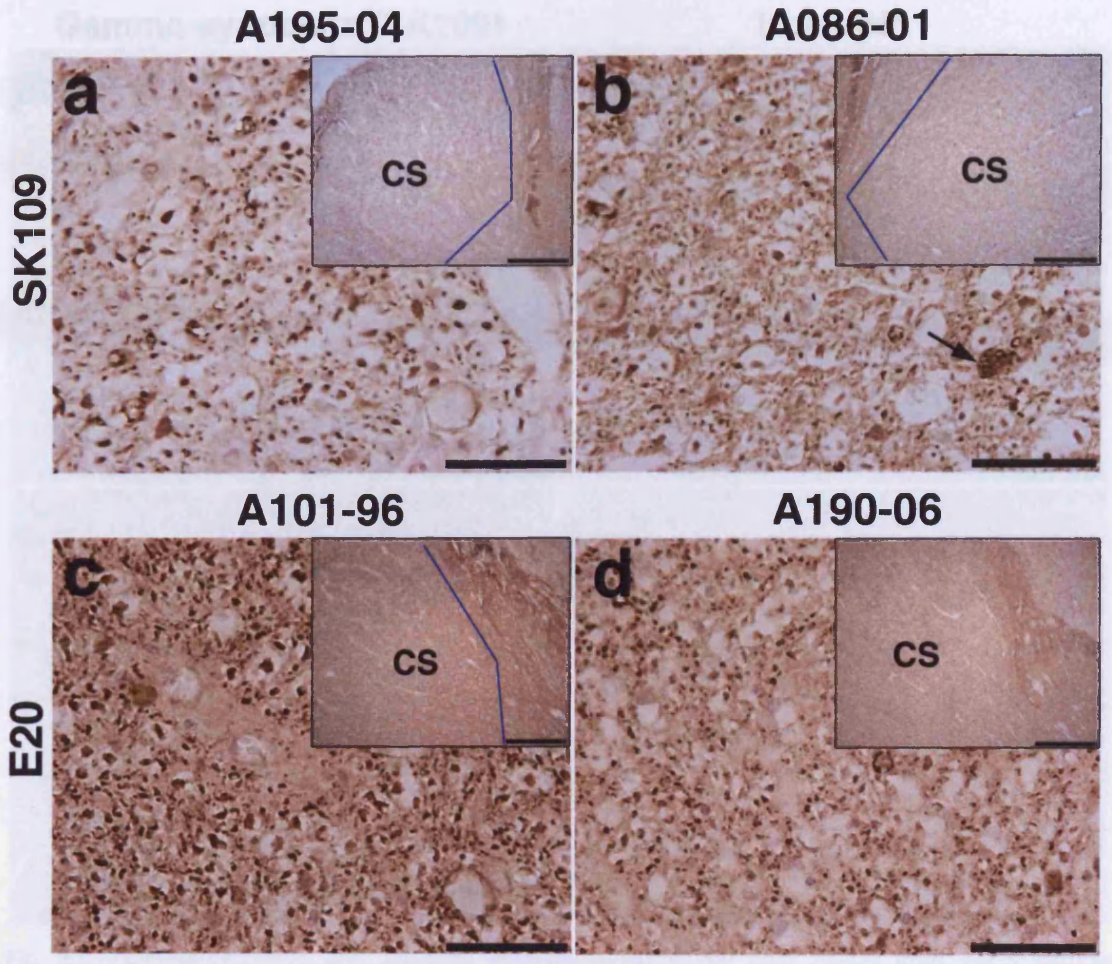

Fig. 52. Abnormal gamma-synuclein positive structures were not common to all ALS tissues. Low magnification images of gamma-synuclein immunostained lateral corticospinal tract (CS) region of spinal cord tissue samples from patients with sporadic ALS (A190/06 & A195/04), FUS associated fALS (A086/02) and SOD1 associated fALS (A101/96). Tissues were stained with antibodies SK109 (a, b) and E20 (c, d). Detailed assessment found abnormal gamma-synuclein positive structures to be absent (a, c, d) or highly infrequent (b) from the CS tracts of many of the ALS cases assessed. Scale bars: main panel = 50μm, insert = 50μm.

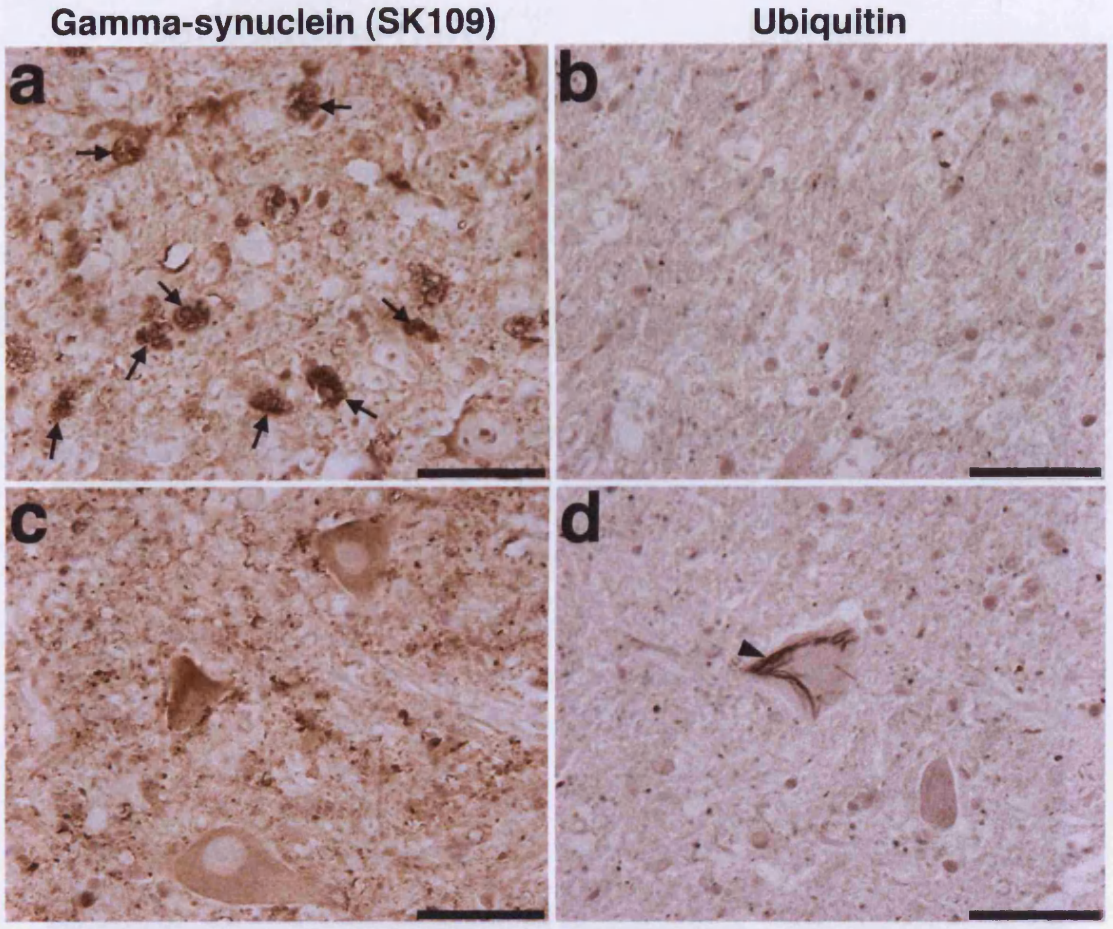

Fig. 53. Gamma-synuclein and ubiquitin immunostained spinal cord tissue from sALS sample A098/09. Lateral corticospinal tract region (a, b) and ventral horn motor neurons (c, d) of thoracic spinal cord stained using antibodies raised against gamma-synuclein (SK109, a, c) and ubiquitin (b, d). Abnormal structures in the corticospinal tract intensively stained for gamma-synuclein (a - arrows) were not detected with anti-ubiquitin antibody (b). In contrast intracellular, ubiquitin-positive, skein-like bodies (arrowhead, d) were not found to contain gamma-synuclein (c). Scale bars = 50μm.

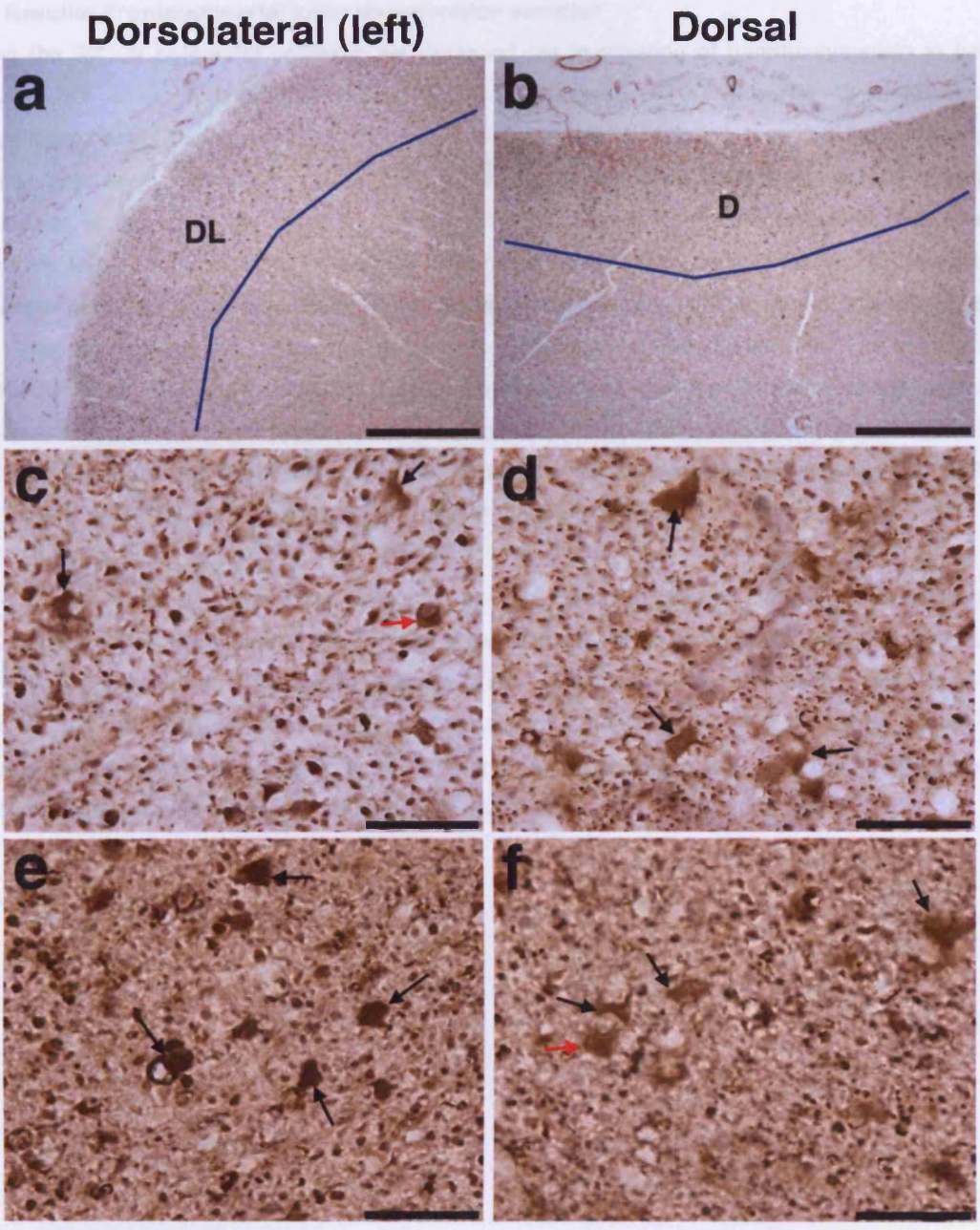

Fig. 54. Gamma-synuclein immunostained spinal cord tissue from FUS-fALS sample A018/93. Gamma-synuclein positive structures were detected in the peripheral dorsolateral (DL) (a, c, e) and dorsal (D) (b, d, f) spinal cord tissue of several samples. These structures (black arrows) stained positive for gamma-synuclein following incubation both with SK109 (c, e) and E20 (d, f) polyclonal antibodies. Red arrows indicate apparent nuclei seen in several of the structures. Scale bars: a, b = 500μm, c-f = 50μm.

7.3. Results: Frontotemportal lobar degeneration samples

Using the SK109 polyclonal antibody, we assessed the localization of gamma-synuclein in frontal lobes of five cases of sporadic FTLD-MND and two cases of FTLD with TDP-43 proteinopathy. Regrettably control tissue was unavailable for analysis. Immunostaining revealed the presence of gamma-synuclein in axons and neuron cell bodies of all frontal lobes analysed. A portion of neuron cell bodies in the inner and outer pyramidal cell layers stained for gamma-synuclein (Fig. 55a-d). Generally these neurons appeared healthy, with no obvious sign of degenerations. No intracellular inclusion bodies were detected in any of the tissue samples analysed. Widespread punctate staining was seen throughout the neuropil, signifying the presence of gamma-synuclein in transversely sectioned axons. Uniform distribution of gamma-synuclein was observed in longitudinally sectioned neurons, with no evidence of axonal spheroids (Fig. 55e). Axonal inclusions were not detected in any of the tissues assessed, but ballooned neurites containing gamma-synuclein were detected in TDP43-FTLD sample A409/08, though it should be noted these structures were rare (Fig. 55f, g).

Abnormal structures stained positive for gamma-synuclein were detected in the frontal lobe neuropil of FTLD-U/MND case A029/09 (Fig. 56). Several of the structures were detected on the periphery of cells null for gamma-synuclein (Fig. 56a-c). The structures were most likely not cellular; nuclei were not detected and the structures often had a width greater than 40μm, too large for neurons or glia. It is feasible that the structures might be the remnants of degenerating neurons. Dystrophic neurites containing gamma-synuclein were also detected (Fig. 56d).

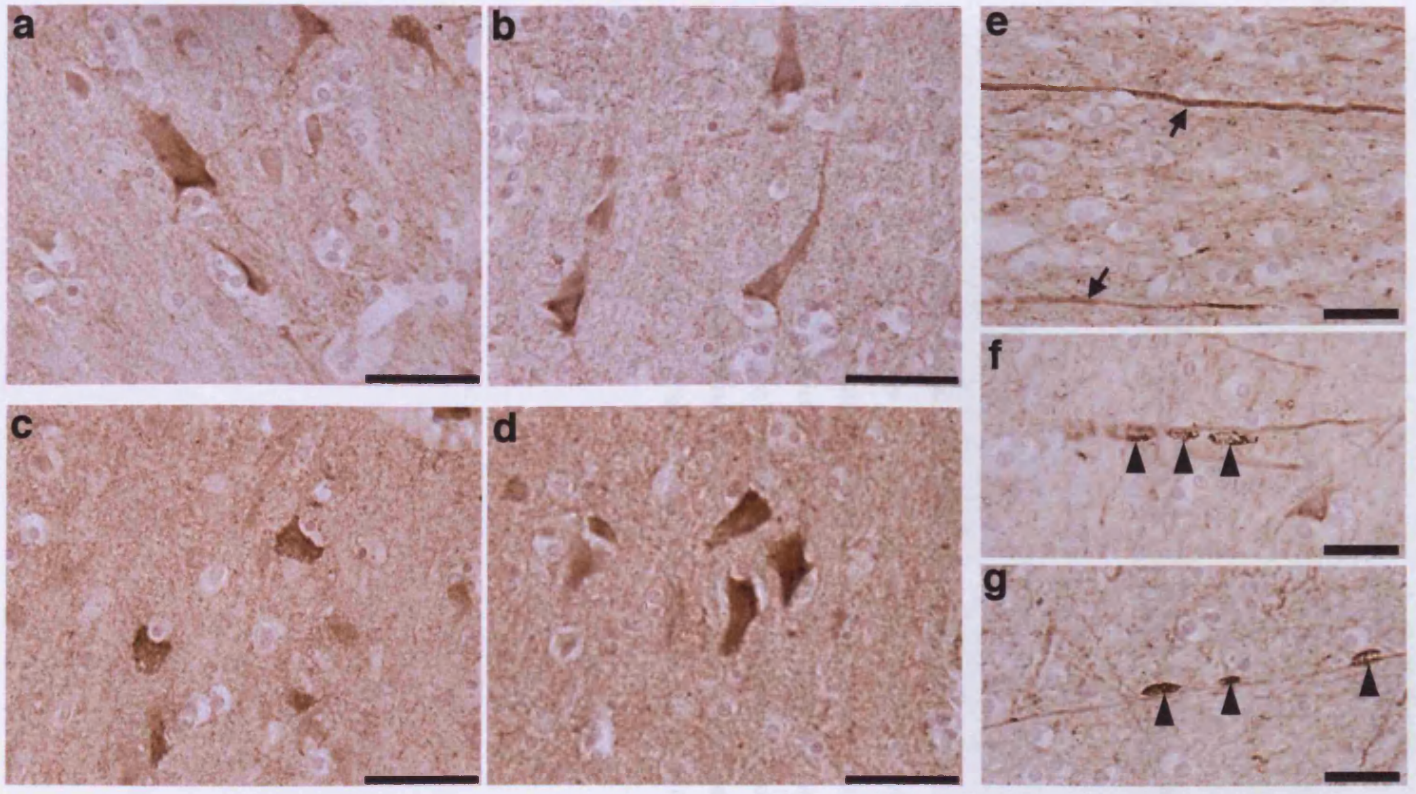

Fig. 55. Gamma-synuclein immunostaining in the frontal lobe of FTLD samples. Representative gamma-synuclein positive neurons in the frontal lobe stained SK109 polyclonal antibodies. Gamma-synuclein positive axons from TDP43-FTLD sample A409/08 (arrows) accompanied by punctate neuropil staining were detected in all FTLD tissues analysed (e-g). Occasional ballooned neurites (arrowheads) containing gamma-synuclein were detected (f, g). Scale bars a-d = 50μm, e-g = 25μm.

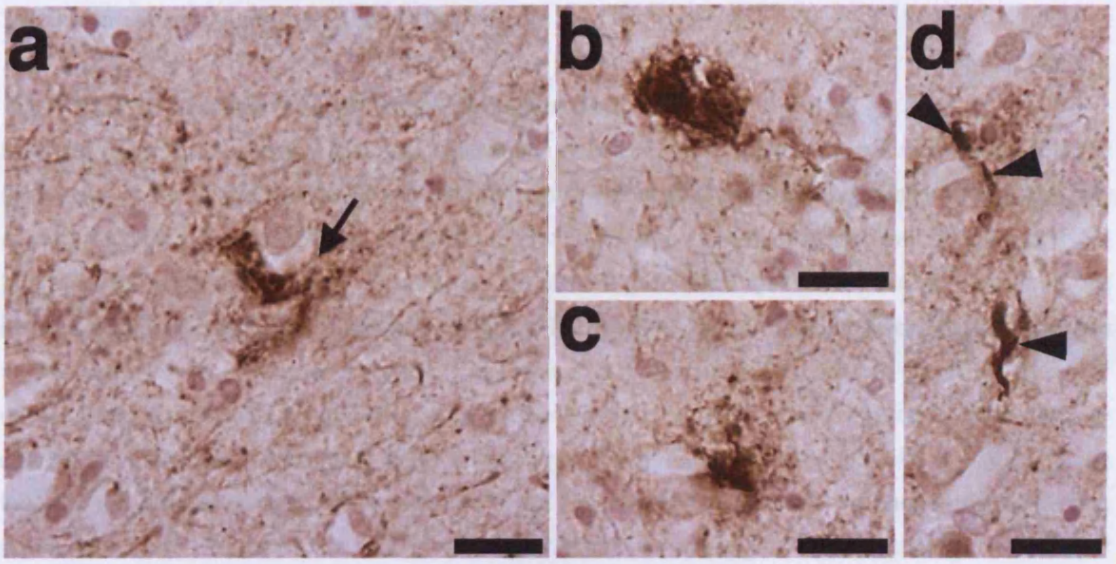

Fig. 56. Abnormal accumulation of gamma-synuclein in FTLD-U/MND case A029/09. Rare, extracellular, gamma-synuclein positive structures were detected in the frontal lobe neuropil of FTLD-U/MND sample A029/09 (a). Several of these structures appear to be remnants of degenerate cell bodies (a-c). Structures resembling dystrophic axons were also detected (d). Arrow = border between gamma-synuclein negative cell and gamma-synuclein positive extracellular structure; arrowheads = dystrophic neurite-like structure positive for gamma-synuclein. Scale bars = 20μm.

7.4. Summary of results and discussion

7.4.1. Gamma-synuclein in amyotrophic lateral sclerosis

Here we report the first evidence of an association between aberrant gamma-synuclein accumulation and cases of human ALS. Though gamma-synuclein was not found in the inclusions bodies typically present in motor neurons of ALS patients i.e. Bunina bodies or skein-like bodies, we detected 10-20μm spherical structures containing what appears to be granules of gamma-synuclein in three cases of sALS and one case of SOD1 associated fALS (Figs. 50, 51). These structures were tightly restricted to the lateral corticospinal tracts, areas of the spinal cord consisting of descending axons of motor neurons localised in cortical motor regions. Immunostaining against ubiquitin failed to detect similar structures within the corticospinal tract. Interestingly the gamma-synuclein positive structures were found in a subset of studied ALS cases, and were not detected in 10 of the 14 cases assessed (Fig. 52, appendix 11). Retrospective analysis of the clinical histopathological notes provided by the MRC London Brain Bank revealed that these four cases shared two common features that were absent in cases lacking the structures. Firstly, loss of Betz cells from the motor cortex was more pronounced in these cases than the loss seen in patients without the gamma-synuclein positive structures. A similar pattern was seen Secondly, the spinal cord of patients with gamma-synuclein positive structures displayed marked demyelination in the corticospinal tract, characterised by substantial myelin pallor not seen in the spinal cord of other patients. These findings suggest the accumulation of gamma-synuclein within the corticospinal tract might represent a causative factor, or marker of, a subtype of ALS with substantial upper motor neuron involvement. It the future would be intriguing to assess the condition of lower motor neuron axons in similar patients to this subgroup, as similar axonal pathologcial structures might be present Unfortunately this is currently unfeasible, as peripheral nerves such as the sciatic nerve are not frequently collected from late stage ALS patients, and those that are often in highly degenerate condition.

7.4.2. Gamma-synuclein in frontotemporal lobar degeneration

In addition to analysis of spinal cord tissue, we also assessed the presence of gamma-synuclein in seven cases of FTLD, a form of dementia that is often accompanied by the onset of ALS. In five of these cases abnormal gamma-synuclein positive structures were absent. However ballooned neurites containing gamma-synuclein were observed in one case of TDP43 associated FTLD and possible remnants of degenerate neuron cell bodies in a case of FTLD-U/MND. In both cases these structures were very rare and few conclusions can be drawn from the data. Further assessment of histological samples will be required to determine whether these structures are a frequent feature of FTLD.

7.4.3. Identity of corticospinal tract gamma-synuclein structures

The identity of the gamma-synuclein positive structures in the spinal cord was unclear, their size and morphology suggesting several possibilities. The diameter of the structures is comparable with that of axonal spheroids, a common form of inclusion seen in neurodegeneration consisting of densely

accumulated fibrillar, oligomeric protein (Galvin et al. 2000; Galvin et al. 1999; Wang et al. 2004). The likelihood of the structures being axonal inclusions is given further weight by the previous identification of gamma-synuclein as a component of axonal spheroids in several human neurodegenerative disorders. These include glaucoma (Surgucheva et al. 2002), PD, dementia with Lewy bodies and Hallervorden-Spatz syndrome (Galvin et al. 2000; Galvin et al. 1999). Similar structures have also been identified in mouse models of neurodegeneration. Gamma-synuclein positive axonal spheroids of a similar size are a feature of the progressive degeneration affecting sensory axons of the gracile tract of UCH-L1 deficient 'gad' mice (Wang et al. 2004). Furthermore comparable axonal inclusion structures, including spheroids and Lewy neurites, were frequently observed throughout the CNS of *Thy1*mγSN transgenic mice, particularly prominent in the grey and white matter of the spinal cord.

It should be noted however that the gamma-synuclein structures identified in the sALS and SOD1-fALS patients are more granular in appearance than typical axonal spheroids. This suggests a second, equally feasible possibility – that the structures represent the intraperikaryal accumulation of gamma-synuclein. The absence of neuronal cell bodies within the corticospinal tracts makes the likelihood of the structures being intraneuronal unlikely. They may however represent the accumulation of gamma-synuclein within glial or phagocytic cells. This possibility should be treated with caution however, as the structures lack a typical features of glial morphology, such as process. The suggestion is not however implausible, as gamma-synuclein was detected in cells resembling glia in peripheral dorsal/dorsolateral regions of the spinal cords of several cases (Fig. 54). Furthermore the accumulation of gamma-synuclein within astrocytes has previously been reported in human cases of glaucoma (Surgucheva et al. 2002) and in animal models of the disease (Nguyen et al. 2011). There is no robust evidence to suggest that gamma-synuclein is expressed by glia, and the protein most likely enters the cell via endocytosis. Thus, if the gamma-synuclein positive structures seen in the corticospinal tracts are indeed non-neuronal, the protein contained within the cell may represent that phagocytosed by cells clearing debris from degenerating axons. A further, more speculative, scenario is also feasible. Nguyen et al. demonstrated that following the onset of glaucoma in mice, the transfer of gamma-synuclein from axons to a subset of astrocytes within the myelination transition zone of the optic nerve induces phagocytic activity not normally associated with the glia (Nguyen et al. 2011). It is feasible that a similar mechanism might occur in ALS, for example gamma-synuclein released by degenerating axons in the corticospinal tract might accumulate within glial cells and activate further phagocytosis of damaged axons.

The apparent involvement of gamma-synuclein in both ALS and glaucoma links it to another ALS-associated protein, optineurin. Autosomal dominant and recessive mutations have been identified in OPTN in fALS (Maruyama et al. 2010), with dominant negative mutations in the gene accounting for 16.7% of cases of primary open angle glaucoma, the most common form of the disease (Rezaie et al. 2002). Furthermore the protein has been identified in several different forms of inclusion body in sALS and fALS (Maruyama et al. 2010). Though the normal function of both proteins are unclear, it is

tempting to speculate that optineurin and gamma-synuclein both induce degeneration through a similar mechanism, possibly through the formation of aberrant inclusions structures. Alternatively the proteins might disrupt an essential cellular function, for example protein degradation or cytoskeletal stability, such that a vulnerable class of neuron are lost.

In summary, we show that there is evidence of the aberrant accumulation of gamma-synuclein within the corticospinal tract, a mechanism that might represent a subtype of ALS in which the degeneration of upper motor neuron is notably pronounced. This conclusion should currently be interpreted with some caution, as it has been made from a small number of cases, utilising only histological samples. Further histological and biochemical assessment of ALS donor tissue should now be carried out to elucidate the role of gamma-synuclein in human ALS and fully identify the origin and composition of the corticospinal tract structures.

8. Final discussion, perspectives and conclusions

Though not currently recognised as a major contributing factor in human neurodegenerative disease, a growing body of evidence is beginning to suggest that under certain pathogenic conditions gamma-synuclein can play a role in neuronal dysfunction and degeneration. In this thesis we report that gamma-synuclein is potentially a contributing factor in the development of the motor neuron disease amyotrophic lateral sclerosis. This hypothesis is supported by evidence collected from tissue donated by patients affected by sporadic and familial forms of ALS and through the investigation of a novel mouse model of neuronal gamma-synucleinopathy.

8.1. Amyotrophic lateral sclerosis

We have identified large aberrant gamma-synuclein-positive structures in the lateral corticospinal tracts of the spinal cord in three cases of sALS and one case of SOD1-fALS. The presence of the structures correlates with myelin pallor of the lateral corticospinal tract and substantial loss of Betz cells from motor regions of the cortex, suggesting gamma-synuclein is associated with a subtype of ALS characterised by pronounced upper motor neuron involvement. Intriguingly the gamma-synuclein-positive structures do not match typical axonal inclusions such as spheroids, with analysis of available literature failing to identify similar corticospinal tract structures in ALS case studies. We therefore propose that these structures represent a novel form of pathological axonal inclusion associated with the loss of upper motor neuron populations, or alternatively represent a novel histopathological maker specific to cases of ALS with pronounced upper motor neuron damage. Whilst the identity of these structures remains unclear, both of the above possibilities are feasible.

Investigation into the role of gamma-synuclein in ALS thus requires much further research. We plan to continue our collaboration with Dr Tibor Hortobagyi and the MRC London Brain Bank for Neurodegenerative Diseases in an attempt to resolve the identity of the structures and assess their composition. We shall continue histological analysis of more tissue samples and additionally dissect lateral corticospinal tract tissue samples from donated spinal cord tissue held by the MRC Brain Bank. With these samples we hope to carry out sequential protein extraction experiments to determine the solubility of the gamma-synuclein contained within the corticospinal tract structures. Furthermore we currently have only had access to spinal cord tissue samples. This has allowed us to assess the condition of upper motor neuron axons, those within the corticospinal tract, however we have not been able to assess the condition of spinal cord motor neuron axons within the peripheral nerves. In future studies we hope to investigate the distribution of gamma-synuclein within these motor axon populations.

8.2. Thy1mγSN mice

Data collected from the *Thy1*mγSN transgenic mouse line further supports the hypothesis that gamma-synuclein is involved in ALS. The phenotype developed is remarkably similar to that developed in established transgenic mouse models of motor neuron disease (Bruijn et al. 1998; Gurney et al. 1994; Shan et al. 2010; Wegorzewska et al. 2009; Wils et al. 2010). Homozygous

*Thy1*mγSN mice were found to develop substantial neurodegeneration throughout the CNS, accompanied by the deposition of gamma-synuclein in axonal and perikaryal inclusion structures, the activation of glia and the reduction in cytoskeletal components. Neurons of the motor system were most compromised, resulting in significant loss of motor function that worsened with age. Pools of upper and lower motor neurons were affected in a selective manner, with the largest class of motor axons being disproportionately sensitive to degeneration. The sensory system appears to be spared from degeneration, with no substantial deficits in tactile sensory function or change in the health of DRG or RGC populations detected.

These data collected from *Thy1*mγSN mice have several shortcomings that should be addressed, primarily with regard to the tolerance of the sensory system to degeneration. Variations in neuron survival might be in part due to fluxuations in the level of Thy1-driven transgene expression, with a correlation between greater expression and increased vulnerability. Thus comparable expression in both motor and sensory neuron populations needs to be more robustly confirmed. The samples of DRG collected for quantification contained an almost pure population of sensory neurons and transgene levels determined by qPCR are likely to be accurate. Though qPCR is a powerful technique for quantification of gene expression, the results collect for the spinal cord motor neurons are 'contaminated' by the presence of other neuronal populations, and consequentially might not reflect the true level. Several techniques might be used to address this problem. More accurate dissection of spinal cord motor neurons is possible through use of laser capture dissection of frozen spinal cord samples. Unfortunately due to the number of neurons that would need to be dissected to collect enough DNA for analysis, this technique would be highly time consuming and is not practical. A more feasible option is utilising quantitative fluorescent *in situ* hybridization, whereby the level of fluorescence is proportional to transgene expression. To confirm that sensory neuron populations are universally less sensitive than motor populations it may be necessary to quantify further populations, for example neurons of the trigeminal ganglion. Finally, further behaviour test should be used to prove all sensory function is unaffected. Currently we have only tested tactile sensitivity, the response to touch. Protocols testing the response of mice to other sensations, such as heat and pain, are available and should be carried out upon the *Thy1*mγSN mice. Ultimately we hope to collect electrophysiological data of the animal's response to differing sensory stimuli.

Further effort should also be made to track the progression of pathological changes in the CNS of *Thy1*mγSN mice, in particular investigating early changes in neuronal function. Significant deficits in the motor function of homozygous *Thy1*mγSN mice were detected by accelerating rotarod from two months of age (Fig. 4), with the acoustic startle test detecting a substantially reduced response from as early as three weeks (Fig. 6). With regard to the latter, the young mice did not appear to be deaf, responding to noise in their proximity similarly to wild type mice. As the Thy1 promoter only becomes active during p4-10 (Aigner et al. 1995), these data suggest that substantial functional changes are occurring early in the model of gamma-synucleinopathy. Furthermore the data suggest a dissociation

between the expression of gamma-synuclein and the deterioration of motor function, with both hemi- and homozygous animals showing a substantially diminished response, suggesting that the deficits are due to aberrant activity of gamma-synuclein in young animals, rather than the damage its overexpression induces at latter stages of pathology. Precisely how gamma-synuclein is affecting startle response is highly unclear. Alterations in startle response have previously been reported in animals with motor system dysfunction, for example Huntington's disease models R6/1 (Brooks et al. 2011) and R6/2 (Carter et al. 1999), however these changes are only substantial at older ages where other motor deficits are also pronounced. The reduction of spinal cord noradrenaline concentration and loss of locus coeruleus dopaminergic neurons have been attributed to limited startle response in parkin null mice (Von Coelln et al. 2004). The concentration of noradrenaline and other spinal cord neurotransmitters can be assessed using the same HPLC methods used to assess striatal dopamine concentrations. The locus coeruleus population can also be quantified through immunostaining against tyrosine hydroxylase. Ultimately the acoustic startle response potential presents a novel endophenotype of ALS, and work should be carried out to identify if this deficit is common to other preexisting rodent models of ALS, for example mutant TDP-43 or SOD1 mice. There is currently no literature detailing such experiments in these animals. Ultimately if these animals do have a limited acoustic startle response, the test might have much use in the early, preclinical diagnosis of ALS in families where there is a risk of developing the disease. A variation on the protocol we used to assess *Thy1*mγSN mice is already currently used clinically to assess prepulse inhibition, deficits in which are a well defined endophenotype of schizophrenia, and the technique could be easily adapted for testing of acoustic startle response in ALS patients in the clinic,

Further electron microscopy analysis of peripheral nerves in younger *Thy1*mγSN mice should also be carried out, to allow us to determine whether large fibres are the most vulnerable and lost early in pathogenesis. Confirmation of this would confirm that the pathology seen in *Thy1*mγSN mice recapitulates the phenotype of other ALS models and the clinical pattern of disease progression. We additionally hope to characterise the morphology of neuromuscular junctions innervated by the peripheral nerves. There is compelling evidence to suggest the denervation of these motor end plates is the earliest event in the pathology affecting $SOD1^{G93A}$ transgenic mice (reviewed in Kanning et al. 2010). We are currently attempting to optimize histological techniques to visualize these junctions, with initial data suggesting gamma-synuclein accumulates within the NMJs of eight-week old *Thy1*mγSN mice (see appendix 12).

8.3. Can the *Thy1*mγSN be considered a true model of ALS?

We have demonstrated that the gamma-synucleinopathy seen in *Thy1*mγSN mice closely parallels the pattern of damage seen in both human ALS and mouse models of the disease. A question does however remain; does the *Thy1*mγSN phenotype represent a clinically relevant form of ALS, or an experimental model in which the same neurons become damaged, but through a mechanism that has no precedent in nature?

Clearly, the most compelling argument in support of the models clinical relevance is the identification of gamma-synuclein positive structures in the corticospinal tracts of several case of ALS. The presence of such structures is correlated with significant degeneration of upper motor neurons in motor regions of the cortex. Whether these structures are a direct causative agent in the degeneration of these neurons, or a secondary correlative marker is not clear. It is interesting to note that, though the population of upper motor neurons was not quantified in *Thy1*mγSN motor cortex, damage to the region was clear, demonstrated by the presence of substantial numbers of activated glial cells and deposition of ionic-detergent insoluble, gamma-synuclein positive inclusion bodies in the region. The presence of inclusion bodies suggests a pattern of dystrophy comparable to the formation of Betz cell inclusions in ALS. With regards to physiological relevance, it is essential to note that gamma-synuclein is normally present in upper motor neurons, though to a lesser extent than in spinal cord populations. Previously published data from our group demonstrated that endogenous *SNCG* is expressed in all regions of the murine adult cerebral cortex, increasing with age (Buchman et al. 1998b). Furthermore our studies of human motor cortex in FTLD confirmed the presence of the protein in these cortical regions, with data from healthy control spinal cords confirming the presence of the endogenous protein in corticospinal tract axons. It is therefore feasible that aberrant activity of gamma-synuclein might influence the health of upper motor neurons and their processes within the corticospinal tract. Further support for the clinical relevance of the *Thy1*mγSN model is provided by the formation of axonal inclusion bodies throughout the grey and white matter the *Thy1*mγSN mouse spinal cords, including the corticospinal tract regions. Identifying whether any of these structures match those detected in the human cases is not currently possible as the precise identity and composition of the human structures is unclear. They do not appear to be ubiquitinated and thus some of the gamma-synuclein-positive/ubiquitin-negative structures detected in the mouse spinal cord might be comparable structures. This speculation cannot be resolved until more is understood about the human structures, in particular we must identify further protein components that are specific markers of the structures. This will then allow us to accurately investigate the presence of comparable structures in the nervous system of *Thy1*mγSN mice.

With regard to treating the *Thy1*mγSN mice as an experimental model, our study of the progression of the ALS-like phenotype in Thy1mγSN mice has provided data that might help elucidate the mechanisms by which ALS develops in humans, several of which warrant further investigation to determine whether they provide therapeutic targets in the treatment of the disease. Two of these mechanisms shall be discussed below: the formation of intraneuronal inclusion bodies and the disruption of the neuronal cytoskeleton.

a. Aggregation

A common characteristic of overexpressed gamma-synuclein and the ALS associated forms of SOD1, TPD-43 and FUS/TLS is their heightened propensity to aggregate and produce inclusion bodies

(Bruijn et al. 1998; Kwiatkowski et al. 2009; Neumann et al. 2009; Vance et al. 2009; Wegorzewska et al. 2009). The presence of inclusion bodies varied between regions of the Thy1mγSN CNS, in particular between motor and sensory cell bodies. Inclusion bodies were not detected in the sensory cell bodies of lumbar dorsal root ganglia, and detergent insoluble inclusions were present at a lower concentration in sensory regions of the cortex than in motor regions. The infrequency of inclusion structures suggests that some sensory neuron populations might possess innate protection against their formation, or conversely that some protective mechanisms are compromised in the vulnerable populations. The mechanism responsible for the regulation of protein folding and degradation are a candidate process. Interestingly levels of HSPB1, a molecular chaperones involved in the processing of misfolded proteins, were reduced in the cytoplasm of spinal cord motor neurons. The presence of ubiquitin-positive, gamma-synuclein-negative structures in the spinal cord further supports this hypothesis. These ubiquitinated structures may be a consequence of UPS saturation, whereby the system is overwhelmed with high levels of gamma-synuclein, resulting in the neglect of normal ubiquitinated protein degradation. It is feasible that further innate cellular mechanisms for removing abnormally folded or excessive proteins, might act more efficiently in the surviving neuron populations, for example through the up regulation of components to handle an abnormal load of toxic proteins. Higher efficiency would allow neurons to clear the high volume of transgenic gamma-synuclein prior to the onset of aggregation. This conjecture can be tested, by for example comparison of protein degradation systems in the spinal cord and DRGs. Up regulation or modification of UPS components can be assessed through qPCR and quantitative western blotting. Levels of autophagy may be assessed through measurement of levels of the autophagosome-associated protein LC3 (Klionsky et al. 2008). LC3 is found in two forms, as free cytosolic LC3-I or when bound to the autophagosomes, LC3-II conjugated to phosphatidylethanolamine. The ratio between these two forms may be measured through quantitative western blotting. Assessment of UPS function may also be carried out relatively simply, through commercially available kits produced by several manufacturers. Unfortunately results of these assays will have to be treated with caution, as they shall be affected by the heterogeneous composition of the spinal cord. All cell types possess protein degradation mechanisms, and thus in addition to motor neuron protein degradation activity, that of non-motor neuron cell types, including glia, will be included in the data.

b. Cytoskeleton disruption

Profound disruption of the neuronal cytoskeleton, caused by changes in distribution and decreased levels of components was observed in the CNS of symptomatic *Thy1*mγSN mice. Similar changes have also been demonstrated in ALS. Rare dominant mutations in the gene encoding NF-H have been detected in several cases of familial ALS (Al-Chalabi et al. 1999; Figlewicz et al. 1994; Tomkins et al. 1998). Accumulated neurofilaments are often detected within spinal cord motor neuron perikaryal inclusion bodies of ALS patients (Hirano et al. 1984; Ince et al. 1998; Rouleau et al. 1996). The question does remain as to whether this event represents a direct cause of neuronal dystrophy or an indirect correlate. Several lines of mice with altered expression of neuronal cytoskeleton components

have demonstrated a clear association between the expression, assembly and homeostasis of neuronal intermediate filament and the development of ALS-like pathology. Selective degeneration of motor neurons and their axons has been reported in transgenic mice expressing mutant forms of NF-L (Lee et al. 1994), or overexpressing wild type NF-L (McLean et al. 2005; Xu et al. 1993), NF-M (Wong et al. 1995a), NF-H (Cote et al. 1993) or peripherin (Millecamps et al. 2006). Disruption of normal neurofilament homeostasis in these mouse lines was also linked to a prominent feature observed in *Thy1*mγSN mice, the highly selective dystrophy and loss of the largest caliber motor axons in the peripheral nerves (Cote et al. 1993; Lee et al. 1994; McLean et al. 2005; Wong et al. 1995a; Xu et al. 1993). Selective degeneration of large caliber motor neurons also occurs in mice null for NF-L (McLean et al. 2005; Zhu et al. 1997), with severe motor dysfunction and selective large fibre loss also being reported in a the NF-L deficient "Quiver" line of Japanese quail (Sakaguchi et al. 1993). Loss of large caliber fibres is also feature of SOD1 and TDP43 transgenic mice (Frey et al. 2000; Pun et al. 2006; Shan et al. 2010) and ALS patients (Bradley et al. 1983; Kawamura et al. 1981; Theys et al. 1999). As the supply and volume of neurofilaments determines the caliber of axons (Hoffman et al. 1984), it may be speculated that disruption of normal neurofilament homeostasis by gamma-synuclein structurally destabilizes the largest caliber of axon, leaving them highly vulnerable to degradation. This may explain the apparent tolerance of sensory fibres, which are predominantly of the smaller fibre classes.

ALS-linked mutations in SOD1 have been found to directly influence the neuronal production of neurofilament components. The familial $SOD1^{G93A}$ and SOD^{G41S} mutations were found to result in a surprising gain-of-function in NSC34 cells (Ge et al. 2005). Both mutations conferred the ability to bind and destabilize NF-L mRNA through direct interaction with the 3'-UTR of the transcript (Ge et al. 2005). Furthermore, mice expressing $SOD1^{G93A}$ progressively develop a selective down-regulation of NF-L mRNA, leading to reduced levels of NF-L subunits (Menzies et al. 2002). This hypothesis is given further credence by recent investigation of the ALS-associated, DNA/RNA binding protein TDP-43 and the finding of remarkably complementary data. The binding and stabilization of NF-L RNA was identified as a normal function of TDP-43 (Strong et al. 2007; Volkening et al. 2009). Strong et al demonstrated that TDP-43 was able to selectively interact with the 3'-UTR of NF-L mRNA in HEK293 and Neuro2a cells. Truncated forms of TDP-43 with disrupted DNA/RNA binding motifs were unable carry out such stabilization (Volkening et al. 2009). This function appeared to have physiological relevance in humans, with both NF-L and NF-H mRNA co-immunoprecipitated with TDP-43 in homogenate prepared from human spinal cord (Strong et al. 2007). Even more surprisingly, TDP-43 and SOD1 were also found to co-immunoprecipitate, along with 14-3-3 protein, suggesting that stabilization of neurofilament mRNA transcripts might be facilitated by a complex of the proteins. Thus loss-of-function mutation in TDP-43, or toxic gain-of-function mutations in SOD1 might disrupt normal neurofilament homeostasis by depleting the pool of free subunits through limited production.

Data collected from *Thy1*mγSN mice in this study, and also *in vitro* work carried out prior to this thesis, strongly suggests that gamma-synuclein toxicity might also be mediated through disruption of normal neurofilament homeostasis. Levels of several cytoskeletal components were diminished in the sciatic nerves of these mice and the distribution of NF-H & NF-L were altered. Our laboratory has previously reported the ability of acute gamma-synuclein overexpression to increase the susceptibility of the neurofilament networks of cultured neurons to degradation by calcium-dependent proteases (Buchman et al. 1998a). It seems feasible that this latter function may also occur *in vivo* and potentially be the cause of the neurofilament disassembly seen in spine and nerves of *Thy1*mγSN mice. If this hypothesis were correct, the co-immunoprecipitation of gamma-synuclein with soluble NF-L subunits in the spinal cords of *Thy1*mγSN mice would suggest that gamma-synuclein acts directly in the process, possibly through recruitment of calpains to the neurofilament network. In a second, protease-free hypothesis, aberrant binding of gamma-synuclein to NF-L monomers may block their incorporation into the cytoskeleton, limiting the available functional pool of this essential subunit.

How disruption of neurofilament homeostasis results in the degeneration of neurons is currently unclear. A deeper understanding of this mechanism may explain why the selective nature of neuronal degeneration seen in Thy1mγSN mice recapitulates ALS pathology. Dysfunctional axonal transportation is emerging as a causative factor in neurodegeneration, in particular in ALS due to the extraordinary length of motor axons. Defective transport "strangulates" the synaptic machinery of vital components, resulting in a Wallerian-like dying back of the distal axon (Williamson and Cleveland 1999), and has also been associated with the accumulation of perikaryal neurofilaments often observed in ALS cases (Lee et al. 1994; Xu et al. 1993). Deficits in both fast and slow axonal transport have been reported in SOD1 mutant mice (Murakami et al. 2001; Williamson and Cleveland 1999; Zhang et al. 1997). Interestingly, ALS associated, autosomal dominant mutations have been identified in a component of the axonal transport system, the $p150^{Glued}$ subunits of dynactin, (Puls et al. 2003). Dynactin is a multi-subunit complex and an essential component of the axonal transport system, facilitating the binding of the transport motor unit dyenin with its cargo and the microtubule network upon which it translocates (Waterman-Storer et al. 1997). Rodent models have further confirmed the association between axonal transport disruption and motor neuron loss. Mice transgenic for a missense point mutation form of dynactin develop a similar phenotype, accompanied by the presence of SOD1 and neurofilament positive inclusion bodies (Hafezparast et al. 2003). Furthermore transgenic mice expressing high levels of the dynactin component dynamitin have significantly decreased retrograde transport caused by the dissociation of dynein and $p150^{Glued}$, and develop neurodegeneration selective for motor neurons (LaMonte et al. 2002). Deficits in axonal transport have also been linked to disruption of neuronal neurofilament-network. Transgenic mouse lines expressing high levels of peripherin or NF-H both develop significant decreases in the speed of slow axonal transport (Collard et al. 1995; Marszalek et al. 1996; Millecamps et al. 2006; Xu et al. 1993).

Considering these findings it seems feasible that the reduced levels of cytoskeletal components observed in the spinal cord and sciatic nerves of *Thy1*mγSN mice are likely to cause similar disruption to axonal transport. The high levels of gamma-synuclein might also disrupt axonal transport through alternative mechanisms. The volume of the overexpressed protein targeted for translocation to the axon and synapse might place additional burden upon the axonal transport system, saturating the transport machinery, resulting in a decrease in essential components being transported to the synapses. A final possible mechanism by which gamma-synuclein might disrupt axonal is through the physical impairment. Large protein inclusions, for example axonal spheroids, are like to take up a large portion of the axons internal space, distorting/disrupting the neurofilament network and impeding the movement of cargo by axonal transport machinery. In summary, efforts should be made to assess the axonal transport system in *Thy1*mγSN mice, as significant disruption of the system might underlie the motor neuron loss developed by the animals.

8.4. Concluding remarks

This thesis has demonstrated that gamma-synuclein overexpression is able to induce widespread, though selective, degeneration of the murine nervous systems that has a pronounced effect upon the motor system. This resulted in a phenotype that remarkably recapitulates many features seen in the motor neuron disease ALS and is similar to phenotype of certain other rodent models of this disease. These findings led us to investigate the relationship between the protein and the human disease, resulting in the identification of previously unseen aberrant structures in the corticospinal tract of the spinal cord of a subset of ALS patients. Retrospective comparison of the pathology reports for the donor patients suggested a correlation between the presence of the gamma-synuclein positive structures and the loss of cortical Betz cells and the demyelination of the spinal cord portion of their axons. We thus propose that these gamma-synuclein positive structures are a causative agent or marker of upper motor neuron damage characteristic for a subtype of ALS with substantial upper motor neuron involvement. As only spinal cord tissue samples were available for analysis, we are currently unable to ascertain whether the structures seen in the upper motor neuron derived corticospinal tract are also present in the axons of spinal motor neurons. Thus assessment of spinal motor neuron axons in the peripheral nerves is necessary to fully determine the extent of gamma-synuclein structure distribution. Concerted effort should now be made to clarify the identity of the gamma-synuclein positive structures and assess their frequency in cases of both sALS and fALS.

The *Thy1*mγSN mouse line may prove a useful tool in assessing the progression of ALS, in particular if an importance of gamma-synuclein pathology in the pathogenesis of certain subtypes of the disease is confirmed. Their accurate recapitulation of ALS suggests gamma-synuclein induces toxicity in a similar mechanism to SOD1, TDP43, FUS/TLS and other ALS associated proteins. The identity of this mechanism is unclear, however all the above proteins share characteristics, having all been shown to aggregate and influence the stability and production of neurofilament networks. The *Thy1*mγSN mouse line might have use as a tool for testing much needed new therapeutics in the treatment of ALS. Future analysis of the *Thy1*mγSN line might allow us to identify some of the initial changes in ALS pathogenesis, allowing for early intervention in the diseases progression.

Appendix

Appendix 1. Congo red positive inclusion body quantification. Mean±SEM, (number) denotes number of spinal cord sections assessed. Statistics: Kruskal Wallis, Fischer's a priori test.

	Wild type	Homozygous Thy1mγSN (mild)	Homozygous Thy1mγSN (severe)	Hemizygous Thy1mγSN
Cervical	0.5 ± 0.19 (30)	7.3 ± 1.59 (35)	33.8 ± 2.81 (32)	15.7 ± 1.25 (43)
Thoracic	0.1± 0.08 (55)	10.3 ± 0.89 (17)	23.2 ± 1.73 (37)	14.7 ± 0.63 (51)
Lumbar	0.7 ± 0.29 (19)	10.1 ± 2.48 (20)	26.0 ± 1.74 (24)	12.4 ± 0.78 (27)
Mean	0.3±0.1 (104)	8.8±1.1 (72) p<0.0001	27.6±1.3 (93) p<0.0001	14.5±0.6 (121) p<0.0001

Appendix 2. Spinal motor neuron quantification. Mean±SEM, (number) denotes number of spinal cord sections assessed. Statistics: Kruskal-Wallis, Fischer's a priori.

	Wild type	Homozygous Thy1mγSN (mild)	Homozygous Thy1mγSN (severe)	Hemizygous Thy1mγSN
Cervical	7.3 ± 0.47 (39)	3.5 ± 0.53 (29)	2.3 ± 0.22 (50)	4.5 ± 0.26 (100)
Thoracic	5.5 ± 0.28 (79)	1.7 ± 0.20 (60)	2.0 ± 0.17 (103)	3.4 ± 0.15 (112)
Lumbar	5.3 ± 0.37 (42)	3.8 ± 0.28 (60)	2.5 ± 0.25 (42)	3.4 ± 0.16 (73)
Mean	5.9±0.2 (160)	2.8±0.2 (149)	2.2±0.1 (195)	3.8±0.1 (285)
		p<0.0001	p<0.0001	p<0.0001

Appendix 3. Dopaminergic neuron population quantification in the SNpc and VTA of twelve-month old wild type and homozygous *Thy1*mγSN mice. Mean±SEM, (number) denotes number of SNpc/VTA assessed. Statistics: Mann-Whitney U-test.

	SNpc	VTA
Wild type (6)	2632.7±474.7	2591.1±596.0
Homozygous *Thy1*mγSN (6)	2244.5±502.5 p=0.2491	2202.9±403.8 p=0.4712

Appendix 4. Spinal cord HPLC data. Mean±SEM, (number) denotes number of animals assessed. Statistics: Mann-Whitney U-test.

	Wild type (5)	**Homozygous Thy1mγSN (7)**
DA (pmol/mg)	52.1±3.92	64.0±5.72 p=0.2556
DOPAC (pmol/mg)	6.4±0.72	6.8±0.4 p=0.4168
HVA (pmol/mg)	5.2±0.49	6.6±0.79 p=0.2556
5-HIAA (pmol/mg)	2.0±0.26	2.4±0.25 p=0.8710
NA (pmol/mg)	0.9±0.16	0.8±0.19 p=0.6261
DOPAC:DA	0.12±0.01	0.10±0.01 p=0.6261
HVA:DA	0.11±0.01	0.11±0.01 p=0.4168

Appendix 5. Motor neurons pools are selectively sensitive to gamma-synuclein toxicity whereas sensory neurons are resistant. For cranial nuclei, left and right nuclei were quantified separately in each animal. For dorsal root ganglia, left and right ganglia for both lumbar 4 and 5 were quantified separately. Mean±SEM, (number) denotes number of nuclei/ganglion assessed. Statistics: Mann-Whitney U-test.

	Wild type	**Homozygous *Thy1*mγSN**
Abducens nu.	265.0 ± 22.3 (8)	248.0 ± 20.7 (10) p=0.9645
Facial nu.	2180.0 ± 105.9 (8)	2102.0 ± 71.7 (10) p=0.824
Motor trigeminal nu.	1010.0 ± 38.7 (9)	668.0 ± 57.9 (10) p=0.0012
L4/L5 dorsal root ganglion	4456.3 ± 150.6 (32)	4308.2 ± 117.2 (32) p=0.441

Appendix 6. Cytoskeletal components are depleted in the sciatic nerves of the most symptomatic homozygous *Thy1*mγSN mice. Levels of neuronal cytoskeletal proteins in the sciatic nerves of twelve-month old wild type, mildly and severely affected *Thy1*mγSN mice. Mean±SEM, (number) denotes number of nerves assessed. Statistics: Mann-Whitney U-test.

Protein	Wild type	Homozygous *Thy1*mγSN (Mild)	Homozygous *Thy1*mγSN (Severe)
Neurofilament-H	1.00±0.112 (5)	0.79±0.742 (6)	0.34±0.054 (5)
Neurofilament-M	1.00±0.025 (3)	0.74±0.124 (2)	0.45±0.153 (3)
Neurofilament-L	1.00±0.103 (5)	0.72±0.963 (6)	0.36±0.061 (5)
Peripherin	1.00±0.238 (3)	0.87±0.224 (3)	0.76±0.176 (3)
Alpha-tubulin	1.00±0.117 (3)	0.89±0.617 (3)	0.41±0.145 (3)
Actin	1.00±0.190 (3)	0.94±0.330 (3)	1.05±0.505 (3)
Myelin Basic Protein (21kDa)	1.00±0.095 (3)	0.61±0.100 (3)	0.47±0.101 (3)
Myelin Basic Protein (18kDa)	1.00±0.091 (3)	0.33±0.146 (3)	0.18±0.006 (3)

Appendix 7. Nerve fibre counts for sciatic nerve.

Mean±SEM, (number) denotes number of nerves from individual animals assessed.

Statistics: Mann-Whitney U-test

Sciatic Nerve	Total A-fibres	Healthy A-fibres	Damaged A-fibres
Wild type (7)	269.4 ± 14.3	264.4 ± 13.9	5.1 ± 1.1
***Thy1*mγSN (mild) (3)**	275.7 ± 19.2 p=0.9156	266.4 ± 20.2 p=0.9789	9.2 ± 2.5 p=0.0493
***Thy1*mγSN (severe) (7)**	202.2 ± 10.3 p=0.0005	162.8 ± 10.5 p=0.0001	39.4 ± 3.9 p<0.0001

Sciatic Nerve	Total C-fibres	Encapsulated C-fibres	Atypical C-fibres
Wild type (3)	576.0 ± 90.6	570.1 ± 91.2	5.9 ± 5.9
***Thy1*mγSN (mild) (3)**	556.0 ± 138.8 p=0.6458	553.6 ± 139.2 p=0.6756	2.5 ± 2.4 p=0.5997
***Thy1*mγSN (severe) (3)**	529.7 ± 45.8 p=0.8605	308.0 ± 54.7 p=0.0318	221.8 ± 36.5 p<0.0001

Appendix 8. A-fibre quantification of dorsal and ventral nerve roots from twelve-month old control and homozygous *Thy1*mγSN mice. Mean±SEM, (number) denotes number of nerves from individual animals assessed. Statistics: Mann-Whitney U-test.

Dorsal Nerve Root	Total A-fibres (per 100μm^2)	Healthy A-fibres (per 100μm^2)	Damaged A-fibres (per 100μm^2)	Phagocyte nuclei (per 100μm^2)	Mean A-fibre area (μm^2)
Wild type (9)	262.5±10.0	258.8±9.8	3.7±0.6	0.4±0.2	25.4±1.02
Homozygous *Thy1*mγSN (10)	254.6±9.7	239.0±9.8	15.6±1.1	4.6±0.8	25.0±1.08
	p=0.8493	p=0.2716	p<0.0001	p=0.0002	p=0.600

Ventral Nerve Root	Total A-fibres (per 100μm^2)	Healthy A-fibres (per 100μm^2)	Damaged A-fibres (per 100μm^2)	Phagocyte nuclei (per 100μm^2)	Mean A-fibre area (μm^2)
Wild type (9)	95.8 ± 3.4	94.3 ± 3.3	1.5 ± 0.4	0.1 ± 0.1	73.4±3.05
Homozygous *Thy1*mγSN (10)	78.6 ± 3.9	62.5 ± 3.1	16.2 ± 1.9	8.4 ± 1.2	37.1±1.08
	p=0.0005	p<0.0001	p<0.0001	p<0.0001	p<0.0001

Appendix 9. A-fibre quantification for optic nerves of twelve-month old wild type and homozygous *Thy1*mγSN mice. Mean±SEM, (number) denotes number of nerves from individual animals assessed. Statistics: Total A-fibres, Mean A-fibre area: Mann-Whitney U-test; g-ratio: Two-sample t-test

Optic Nerve	Total A-fibres (per 100μm^2)	Mean A-fibre area (μm^2)	g-ratio
Wild type (6)	4307.2±138.4	1.86±0.07	0.51±0.01
Homozygous *Thy1*mγSN (6)	3975.3±143.5 p=0.0750	1.90±0.07 p=0.9398	0.50±0.00 p=0.262

Appendix 10: Summary of spinal cord tissue.

					Gamma-synuclein positive structures		
Sample	**Sex**	**Age**	**PMD**	**Diagnosis**	**Motor neuron Cytoplasm**	**Corticospinal tract**	**Dorsal/Dorsolateral white matter**
A049/03	M	79	24	Control: Mild aging changes	No	No	No
A139/09	M	54	31	Control: Normal brain	No	No	No
A147/08	M	61	44	Unspecified MND	No	No	No
A175/08	M	71	58	Unspecified MND	No	No	No
A194/04	M	55	54	sALS	No	No	No
A195/04	F	78	69	sALS	No	No	No
A190/06	F	57	48	sALS	No	No	Yes
A038/01	M	68	8	sALS	No	Yes	Yes
A251/09	M	78	2	sALS	No	Yes	No
A098/09	M	72	26	sALS	No	Yes	No
A101/96	F	46	5	SOD1 fALS	No	No	No
A348/08	F	69	64	SOD1 fALS	No	Yes	Yes
A034/06	M	46	14	SOD1 fALS	No	No	No
A063/08	F	35	20	FUS fALS	No	No	No
A086/01	F	35	24	FUS fALS	No	No	No
A018/93	M	33	71	FUS fALS	No	No	Yes

Appendix 11. Summary of frontal lobe tissues assessed as part of this study.

Sample	Sex	Age	PMD	Diagnosis
A029/09	M	69	42	FTLD with ubiquitin inclusions and probable MND
A244/07	M	68	46	FTLD with MND
A211/05	F	67	6	FTLD with MND
A030/06	M	71	44	FTLD with MND
A174/08	F	43	69	FTLD with MND with ubiquitin & TDP-43 positive inclusion
A013/10	M	69	6	TDP43-FTLD
A409/08	M	78	N/A	TDP43-FTLD

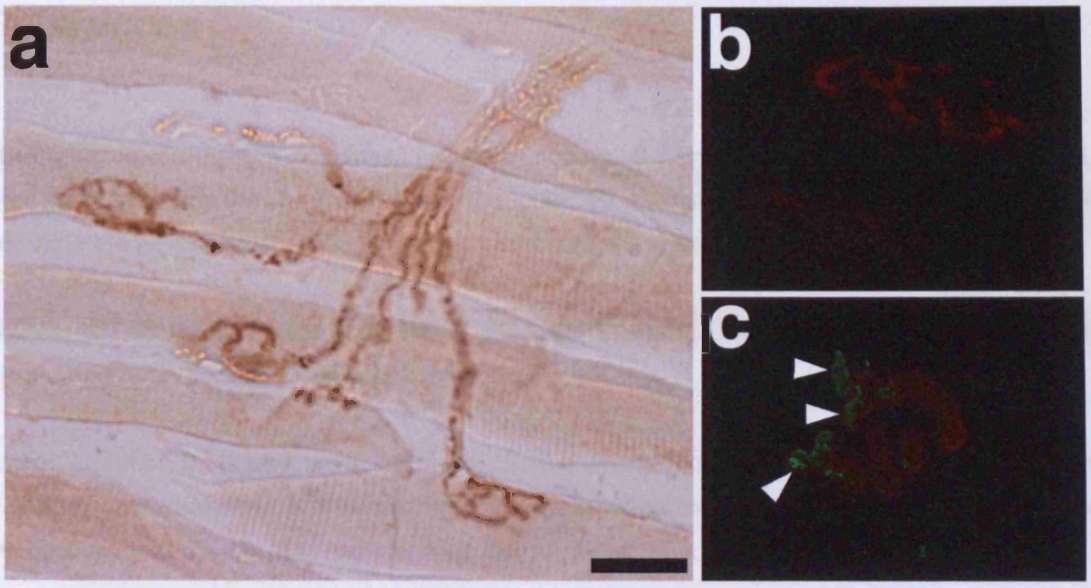

Appendix 12. Pilot data: Gamma-synuclein accumulation within the neuromuscular junctions of two-month old homozygous *Thy1*mγSN mice. Immunostaining against gamma-synuclein (SK23, 1:100) revealed high levels of the protein within the neuromuscular junctions of triceps surae muscles of two-month old *Thy1*mγSN mice (a). Similar immunostaining did not detect such structures in the muscles of wild type mice (not shown). To confirm the presence of accumulated gamma-synuclein in homozygous Thy1mγSN mouse NMJs, fluorescent immunostaining using acetylcholine receptor specific alexafluor-633 conjugated alpha-bungarotoxin (red) and antibodies against gamma-synuclein (green) was carried out on triceps surae muscles of two-month old wild type (b) and homozygous Thy1mγSN mice (c). Alpha-bungarotoxin consistently labeled NMJs of wild type mice, however endogenous gamma-synuclein levels were too low to detect by immunostaining (b). High levels of gamma-synuclein were frequently observed within the NMJs of homozygous Thy1mγSN muscles, though levels in the distal portion of motor axon were too low to detect (c). These finding suggest the abnormal accumlation of gamma-synuclein within the NMJs of homozygous Thy1mγSN mice is an early event in the gamma-synucleinopathy. White arrowheads = accumulation of gamma-synuclein, scale bar = 50μm.

References

Abeliovich, A., Schmitz, Y., Farinas, I., Choi-Lundberg, D., Ho, W.H., Castillo, P.E., Shinsky, N., Verdugo, J.M., Armanini, M., Ryan, A., et al. (2000). Mice lacking alpha-synuclein display functional deficits in the nigrostriatal dopamine system. Neuron 25, 239-252.

Ahmad, M., Attoub, S., Singh, M.N., Martin, F.L., and El-Agnaf, O.M. (2007). Gamma-synuclein and the progression of cancer. FASEB J 21, 3419-3430.

Aigner, L., Arber, S., Kapfhammer, J.P., Laux, T., Schneider, C., Botteri, F., Brenner, H.R., and Caroni, P. (1995). Overexpression of the neural growth-associated protein GAP-43 induces nerve sprouting in the adult nervous system of transgenic mice. Cell 83, 269-278.

Al-Chalabi, A., Andersen, P.M., Nilsson, P., Chioza, B., Andersson, J.L., Russ, C., Shaw, C.E., Powell, J.F., and Leigh, P.N. (1999). Deletions of the heavy neurofilament subunit tail in amyotrophic lateral sclerosis. Hum Mol Genet 8, 157-164.

Allen, B., Ingram, E., Takao, M., Smith, M.J., Jakes, R., Virdee, K., Yoshida, H., Holzer, M., Craxton, M., Emson, P.C., et al. (2002). Abundant tau filaments and nonapoptotic neurodegeneration in transgenic mice expressing human P301S tau protein. J Neurosci 22, 9340-9351.

Anand, V.S., Reichling, L.J., Lipinski, K., Stochaj, W., Duan, W., Kelleher, K., Pungaliya, P., Brown, E.L., Reinhart, P.H., Somberg, R., et al. (2009). Investigation of leucine-rich repeat kinase 2 : enzymological properties and novel assays. FEBS J 276, 466-478.

Andersen, P.M., Forsgren, L., Binzer, M., Nilsson, P., Ala-Hurula, V., Keranen, M.L., Bergmark, L., Saarinen, A., Haltia, T., Tarvainen, I., et al. (1996). Autosomal recessive adult-onset amyotrophic lateral sclerosis associated with homozygosity for Asp90Ala CuZn-superoxide dismutase mutation. A clinical and genealogical study of 36 patients. Brain 119 (Pt 4), 1153-1172.

Andres-Mateos, E., Mejias, R., Sasaki, M., Li, X., Lin, B.M., Biskup, S., Zhang, L., Banerjee, R., Thomas, B., Yang, L., et al. (2009). Unexpected lack of hypersensitivity in LRRK2 knock-out mice to MPTP (1-methyl-4-phenyl-1,2,3,6-tetrahydropyridine). J Neurosci 29, 15846-15850.

Arai, T., Hasegawa, M., Akiyama, H., Ikeda, K., Nonaka, T., Mori, H., Mann, D., Tsuchiya, K., Yoshida, M., Hashizume, Y., and Oda, T. (2006). TDP-43 is a component of ubiquitin-positive tau-negative

inclusions in frontotemporal lobar degeneration and amyotrophic lateral sclerosis. Biochem Biophys Res Commun 351, 602-611.

Bedford, L., Hay, D., Devoy, A., Paine, S., Powe, D.G., Seth, R., Gray, T., Topham, I., Fone, K., Rezvani, N., et al. (2008). Depletion of 26S proteasomes in mouse brain neurons causes neurodegeneration and Lewy-like inclusions resembling human pale bodies. J Neurosci 28, 8189-8198.

Belle, M.D., Pattison, E.F., Cheunsuang, O., Stewart, A., Kramer, I., Sigrist, M., Arber, S., and Morris, R. (2007). Characterization of a thy1.2 GFP transgenic mouse reveals a tissue-specific organization of the spinal dorsal horn. Genesis 45, 679-688.

Betarbet, R., Sherer, T.B., MacKenzie, G., Garcia-Osuna, M., Panov, A.V., and Greenamyre, J.T. (2000). Chronic systemic pesticide exposure reproduces features of Parkinson's disease. Nat Neurosci 3, 1301-1306.

Bonifati, V., Rizzu, P., Squitieri, F., Krieger, E., Vanacore, N., van Swieten, J.C., Brice, A., van Duijn, C.M., Oostra, B., Meco, G., and Heutink, P. (2003a). DJ-1(PARK7), a novel gene for autosomal recessive, early onset parkinsonism. Neurol Sci 24, 159-160.

Bonifati, V., Rizzu, P., van Baren, M.J., Schaap, O., Breedveld, G.J., Krieger, E., Dekker, M.C., Squitieri, F., Ibanez, P., Joosse, M., et al. (2003b). Mutations in the DJ-1 gene associated with autosomal recessive early-onset parkinsonism. Science 299, 256-259.

Bove, J., Zhou, C., Jackson-Lewis, V., Taylor, J., Chu, Y., Rideout, H.J., Wu, D.C., Kordower, J.H., Petrucelli, L., and Przedborski, S. (2006). Proteasome inhibition and Parkinson's disease modeling. Ann Neurol 60, 260-264.

Bradley, W.G., Good, P., Rasool, C.G., and Adelman, L.S. (1983). Morphometric and biochemical studies of peripheral nerves in amyotrophic lateral sclerosis. Ann Neurol 14, 267-277.

Brenner, M., Kisseberth, W.C., Su, Y., Besnard, F., and Messing, A. (1994). GFAP promoter directs astrocyte-specific expression in transgenic mice. J Neurosci 14, 1030-1037.

Brooks, A.I., Chadwick, C.A., Gelbard, H.A., Cory-Slechta, D.A., and Federoff, H.J. (1999). Paraquat elicited neurobehavioral syndrome caused by dopaminergic neuron loss. Brain Res 823, 1-10.

Brooks, S.P., Janghra, N., Workman, V.L., Bayram-Weston, Z., Jones, L., and Dunnett, S.B. Longitudinal analysis of the behavioural phenotype in R6/1 (C57BL/6J) Huntington's disease transgenic mice. Brain Res Bull.

Bruening, W., Giasson, B.I., Klein-Szanto, A.J., Lee, V.M., Trojanowski, J.Q., and Godwin, A.K. (2000). Synucleins are expressed in the majority of breast and ovarian carcinomas and in preneoplastic lesions of the ovary. Cancer 88, 2154-2163.

Bruijn, L.I., Houseweart, M.K., Kato, S., Anderson, K.L., Anderson, S.D., Ohama, E., Reaume, A.G., Scott, R.W., and Cleveland, D.W. (1998). Aggregation and motor neuron toxicity of an ALS-linked SOD1 mutant independent from wild-type SOD1. Science 281, 1851-1854.

Buchman, V.L., Adu, J., Pinon, L.G., Ninkina, N.N., and Davies, A.M. (1998a). Persyn, a member of the synuclein family, influences neurofilament network integrity. Nat Neurosci 1, 101-103.

Buchman, V.L., Hunter, H.J., Pinon, L.G., Thompson, J., Privalova, E.M., Ninkina, N.N., and Davies, A.M. (1998b). Persyn, a member of the synuclein family, has a distinct pattern of expression in the developing nervous system. J Neurosci 18, 9335-9341.

Buchman, V.L., and Ninkina, N. (2008). Modulation of alpha-synuclein expression in transgenic animals for modelling synucleinopathies--is the juice worth the squeeze? Neurotox Res 14, 329-341.

Buckingham, B.P., Inman, D.M., Lambert, W., Oglesby, E., Calkins, D.J., Steele, M.R., Vetter, M.L., Marsh-Armstrong, N., and Horner, P.J. (2008). Progressive ganglion cell degeneration precedes neuronal loss in a mouse model of glaucoma. J Neurosci 28, 2735-2744.

Burre, J., Sharma, M., Tsetsenis, T., Buchman, V., Etherton, M.R., and Sudhof, T.C. (2010). Alpha-synuclein promotes SNARE-complex assembly in vivo and in vitro. Science 329, 1663-1667.

Byrne, S., Walsh, C., Lynch, C., Bede, P., Elamin, M., Kenna, K., McLaughlin, R., and Hardiman, O. (2010). Rate of familial amyotrophic lateral sclerosis: a systematic review and meta-analysis. J Neurol Neurosurg Psychiatry.

Cabin, D.E., Gispert-Sanchez, S., Murphy, D., Auburger, G., Myers, R.R., and Nussbaum, R.L. (2005). Exacerbated synucleinopathy in mice expressing A53T SNCA on a Snca null background. Neurobiol Aging 26, 25-35.

Cabin, D.E., Shimazu, K., Murphy, D., Cole, N.B., Gottschalk, W., McIlwain, K.L., Orrison, B., Chen, A., Ellis, C.E., Paylor, R., et al. (2002). Synaptic vesicle depletion correlates with attenuated synaptic

responses to prolonged repetitive stimulation in mice lacking alpha-synuclein. J Neurosci 22, 8797-8807.

Carmine Belin, A., Westerlund, M., Bergman, O., Nissbrandt, H., Lind, C., Sydow, O., and Galter, D. (2007). S18Y in ubiquitin carboxy-terminal hydrolase L1 (UCH-L1) associated with decreased risk of Parkinson's disease in Sweden. Parkinsonism Relat Disord 13, 295-298.

Caroni, P. (1997). Overexpression of growth-associated proteins in the neurons of adult transgenic mice. J Neurosci Methods 71, 3-9.

Carter, R.J., Lione, L.A., Humby, T., Mangiarini, L., Mahal, A., Bates, G.P., Dunnett, S.B., and Morton, A.J. (1999). Characterization of progressive motor deficits in mice transgenic for the human Huntington's disease mutation. J Neurosci 19, 3248-3257.

Ceballos-Picot, I., Nicole, A., Briand, P., Grimber, G., Delacourte, A., Defossez, A., Javoy-Agid, F., Lafon, M., Blouin, J.L., and Sinet, P.M. (1991). Neuronal-specific expression of human copper-zinc superoxide dismutase gene in transgenic mice: animal model of gene dosage effects in Down's syndrome. Brain Res 552, 198-214.

Chandra, S., Fornai, F., Kwon, H.B., Yazdani, U., Atasoy, D., Liu, X., Hammer, R.E., Battaglia, G., German, D.C., Castillo, P.E., and Sudhof, T.C. (2004). Double-knockout mice for alpha- and beta-synucleins: effect on synaptic functions. Proc Natl Acad Sci U S A 101, 14966-14971.

Chandra, S., Gallardo, G., Fernandez-Chacon, R., Schluter, O.M., and Sudhof, T.C. (2005). Alpha-synuclein cooperates with CSPalpha in preventing neurodegeneration. Cell 123, 383-396.

Chartier-Harlin, M.C., Kachergus, J., Roumier, C., Mouroux, V., Douay, X., Lincoln, S., Levecque, C., Larvor, L., Andrieux, J., Hulihan, M., et al. (2004). Alpha-synuclein locus duplication as a cause of familial Parkinson's disease. Lancet 364, 1167-1169.

Chen, L., Ding, Y., Cagniard, B., Van Laar, A.D., Mortimer, A., Chi, W., Hastings, T.G., Kang, U.J., and Zhuang, X. (2008). Unregulated cytosolic dopamine causes neurodegeneration associated with oxidative stress in mice. J Neurosci 28, 425-433.

Chiba, K., Trevor, A., and Castagnoli, N., Jr. (1984). Metabolism of the neurotoxic tertiary amine, MPTP, by brain monoamine oxidase. Biochem Biophys Res Commun 120, 574-578.

Chiu, A.Y., Zhai, P., Dal Canto, M.C., Peters, T.M., Kwon, Y.W., Prattis, S.M., and Gurney, M.E. (1995). Age-dependent penetrance of disease in a transgenic mouse model of familial amyotrophic lateral sclerosis. Mol Cell Neurosci 6, 349-362.

Collard, J.F., Cote, F., and Julien, J.P. (1995). Defective axonal transport in a transgenic mouse model of amyotrophic lateral sclerosis. Nature 375, 61-64.

Conway, K.A., Harper, J.D., and Lansbury, P.T. (1998). Accelerated in vitro fibril formation by a mutant alpha-synuclein linked to early-onset Parkinson disease. Nat Med 4, 1318-1320.

Conway, K.A., Lee, S.J., Rochet, J.C., Ding, T.T., Williamson, R.E., and Lansbury, P.T., Jr. (2000). Acceleration of oligomerization, not fibrillization, is a shared property of both alpha-synuclein mutations linked to early-onset Parkinson's disease: implications for pathogenesis and therapy. Proc Natl Acad Sci U S A 97, 571-576.

Cote, F., Collard, J.F., and Julien, J.P. (1993). Progressive neuronopathy in transgenic mice expressing the human neurofilament heavy gene: a mouse model of amyotrophic lateral sclerosis. Cell 73, 35-46.

Cronin, S., Greenway, M.J., Ennis, S., Kieran, D., Green, A., Prehn, J.H., and Hardiman, O. (2006). Elevated serum angiogenin levels in ALS. Neurology 67, 1833-1836.

Dal Canto, M.C., and Gurney, M.E. (1995). Neuropathological changes in two lines of mice carrying a transgene for mutant human Cu,Zn SOD, and in mice overexpressing wild type human SOD: a model of familial amyotrophic lateral sclerosis (FALS). Brain Res 676, 25-40.

Dauer, W., Kholodilov, N., Vila, M., Trillat, A.C., Goodchild, R., Larsen, K.E., Staal, R., Tieu, K., Schmitz, Y., Yuan, C.A., et al. (2002). Resistance of alpha -synuclein null mice to the parkinsonian neurotoxin MPTP. Proc Natl Acad Sci U S A 99, 14524-14529.

Davis, G.C., Williams, A.C., Markey, S.P., Ebert, M.H., Caine, E.D., Reichert, C.M., and Kopin, I.J. (1979). Chronic Parkinsonism secondary to intravenous injection of meperidine analogues. Psychiatry Res 1, 249-254.

de Rijk, M.C., Tzourio, C., Breteler, M.M., Dartigues, J.F., Amaducci, L., Lopez-Pousa, S., Manubens-Bertran, J.M., Alperovitch, A., and Rocca, W.A. (1997). Prevalence of parkinsonism and Parkinson's disease in Europe: the EUROPARKINSON Collaborative Study. European Community Concerted Action on the Epidemiology of Parkinson's disease. J Neurol Neurosurg Psychiatry 62, 10-15.

DePaul, R., Abbs, J.H., Caligiuri, M., Gracco, V.L., and Brooks, B.R. (1988). Hypoglossal, trigeminal, and facial motoneuron involvement in amyotrophic lateral sclerosis. Neurology 38, 281-283.

Dev, K.K., Hofele, K., Barbieri, S., Buchman, V.L., and van der Putten, H. (2003). Part II: alpha-synuclein and its molecular pathophysiological role in neurodegenerative disease. Neuropharmacology 45, 14-44.

Di Giorgio, F.P., Carrasco, M.A., Siao, M.C., Maniatis, T., and Eggan, K. (2007). Non-cell autonomous effect of glia on motor neurons in an embryonic stem cell-based ALS model. Nat Neurosci 10, 608-614.

Di Monte, D.A., Royland, J.E., Irwin, I., and Langston, J.W. (1996). Astrocytes as the site for bioactivation of neurotoxins. Neurotoxicology 17, 697-703.

Dinis-Oliveira, R.J., Remiao, F., Carmo, H., Duarte, J.A., Navarro, A.S., Bastos, M.L., and Carvalho, F. (2006). Paraquat exposure as an etiological factor of Parkinson's disease. Neurotoxicology 27, 1110-1122.

Doi, H., Koyano, S., Suzuki, Y., Nukina, N., and Kuroiwa, Y. (2010). The RNA-binding protein FUS/TLS is a common aggregate-interacting protein in polyglutamine diseases. Neurosci Res 66, 131-133.

Doi, H., Okamura, K., Bauer, P.O., Furukawa, Y., Shimizu, H., Kurosawa, M., Machida, Y., Miyazaki, H., Mitsui, K., Kuroiwa, Y., and Nukina, N. (2008). RNA-binding protein TLS is a major nuclear aggregate-interacting protein in huntingtin exon 1 with expanded polyglutamine-expressing cells. J Biol Chem 283, 6489-6500.

Dyck, P.J., Stevens, J.C., Mulder, D.W., and Espinosa, R.E. (1975). Frequency of nerve fiber degeneration of peripheral motor and sensory neurons in amyotrophic lateral sclerosis. Morphometry of deep and superficial peroneal nerves. Neurology 25, 781-785.

Edwards, T.L., Scott, W.K., Almonte, C., Burt, A., Powell, E.H., Beecham, G.W., Wang, L., Zuchner, S., Konidari, I., Wang, G., et al. (2010). Genome-wide association study confirms SNPs in SNCA and the MAPT region as common risk factors for Parkinson disease. Ann Hum Genet 74, 97-109.

Ehringer, H., and Hornykiewicz, O. (1960). [Distribution of noradrenaline and dopamine (3-hydroxytyramine) in the human brain and their behavior in diseases of the extrapyramidal system]. Klin Wochenschr 38, 1236-1239.

El-Agnaf, O.M., Salem, S.A., Paleologou, K.E., Curran, M.D., Gibson, M.J., Court, J.A., Schlossmacher, M.G., and Allsop, D. (2006). Detection of oligomeric forms of alpha-synuclein protein in human plasma as a potential biomarker for Parkinson's disease. FASEB J 20, 419-425.

Eliezer, D., Kutluay, E., Bussell, R., Jr., and Browne, G. (2001). Conformational properties of alpha-synuclein in its free and lipid-associated states. J Mol Biol 307, 1061-1073.

Epstein, C.J., Avraham, K.B., Lovett, M., Smith, S., Elroy-Stein, O., Rotman, G., Bry, C., and Groner, Y. (1987). Transgenic mice with increased Cu/Zn-superoxide dismutase activity: animal model of dosage effects in Down syndrome. Proc Natl Acad Sci U S A 84, 8044-8048.

Facheris, M., Strain, K.J., Lesnick, T.G., de Andrade, M., Bower, J.H., Ahlskog, J.E., Cunningham, J.M., Lincoln, S., Farrer, M.J., Rocca, W.A., and Maraganore, D.M. (2005). UCHL1 is associated with Parkinson's disease: a case-unaffected sibling and case-unrelated control study. Neurosci Lett 381, 131-134.

Fan, Y., Limprasert, P., Murray, I.V., Smith, A.C., Lee, V.M., Trojanowski, J.Q., Sopher, B.L., and La Spada, A.R. (2006). Beta-synuclein modulates alpha-synuclein neurotoxicity by reducing alpha-synuclein protein expression. Hum Mol Genet 15, 3002-3011.

Farkas, R.H., Qian, J., Goldberg, J.L., Quigley, H.A., and Zack, D.J. (2004). Gene expression profiling of purified rat retinal ganglion cells. Invest Ophthalmol Vis Sci 45, 2503-2513.

Farrer, M., Chan, P., Chen, R., Tan, L., Lincoln, S., Hernandez, D., Forno, L., Gwinn-Hardy, K., Petrucelli, L., Hussey, J., et al. (2001). Lewy bodies and parkinsonism in families with parkin mutations. Ann Neurol 50, 293-300.

Fernandez-Chacon, R., Wolfel, M., Nishimune, H., Tabares, L., Schmitz, F., Castellano-Munoz, M., Rosenmund, C., Montesinos, M.L., Sanes, J.R., Schneggenburger, R., and Sudhof, T.C. (2004). The synaptic vesicle protein CSP alpha prevents presynaptic degeneration. Neuron 42, 237-251.

Ferrucci, M., Spalloni, A., Bartalucci, A., Cantafora, E., Fulceri, F., Nutini, M., Longone, P., Paparelli, A., and Fornai, F. (2010). A systematic study of brainstem motor nuclei in a mouse model of ALS, the effects of lithium. Neurobiol Dis 37, 370-383.

Figlewicz, D.A., Krizus, A., Martinoli, M.G., Meininger, V., Dib, M., Rouleau, G.A., and Julien, J.P. (1994). Variants of the heavy neurofilament subunit are associated with the development of amyotrophic lateral sclerosis. Hum Mol Genet 3, 1757-1761.

Fischer, L.R., Culver, D.G., Davis, A.A., Tennant, P., Wang, M., Coleman, M., Asress, S., Adalbert, R., Alexander, G.M., and Glass, J.D. (2005). The WldS gene modestly prolongs survival in the SOD1G93A fALS mouse. Neurobiol Dis 19, 293-300.

Fischer, L.R., Culver, D.G., Tennant, P., Davis, A.A., Wang, M., Castellano-Sanchez, A., Khan, J., Polak, M.A., and Glass, J.D. (2004). Amyotrophic lateral sclerosis is a distal axonopathy: evidence in mice and man. Exp Neurol 185, 232-240.

Fleming, S.M., Salcedo, J., Fernagut, P.O., Rockenstein, E., Masliah, E., Levine, M.S., and Chesselet, M.F. (2004). Early and progressive sensorimotor anomalies in mice overexpressing wild-type human alpha-synuclein. J Neurosci 24, 9434-9440.

Flowers, J.M., Leigh, P.N., Davies, A.M., Ninkina, N.N., Buchman, V.L., Vaughan, J., Wood, N.W., and Powell, J.F. (1999). Mutations in the gene encoding human persyn are not associated with amyotrophic lateral sclerosis or familial Parkinson's disease. Neurosci Lett 274, 21-24.

Forman, H.J., and Fridovich, I. (1973). On the stability of bovine superoxide dismutase. The effects of metals. J Biol Chem 248, 2645-2649.

Frey, D., Schneider, C., Xu, L., Borg, J., Spooren, W., and Caroni, P. (2000). Early and selective loss of neuromuscular synapse subtypes with low sprouting competence in motoneuron diseases. J Neurosci 20, 2534-2542.

Fujita, M., Sugama, S., Sekiyama, K., Sekigawa, A., Tsukui, T., Nakai, M., Waragai, M., Takenouchi, T., Takamatsu, Y., Wei, J., et al. (2010). A beta-synuclein mutation linked to dementia produces neurodegeneration when expressed in mouse brain. Nat Commun 1, 110.

Gai, W.P., Blumbergs, P.C., Geffen, L.B., and Blessing, W.W. (1992). Age-related loss of dorsal vagal neurons in Parkinson's disease. Neurology 42, 2106-2111.

Gai, W.P., Power, J.H., Blumbergs, P.C., and Blessing, W.W. (1998). Multiple-system atrophy: a new alpha-synuclein disease? Lancet 352, 547-548.

Galvin, J.E., Giasson, B., Hurtig, H.I., Lee, V.M., and Trojanowski, J.Q. (2000). Neurodegeneration with brain iron accumulation, type 1 is characterized by alpha-, beta-, and gamma-synuclein neuropathology. Am J Pathol 157, 361-368.

Galvin, J.E., Uryu, K., Lee, V.M., and Trojanowski, J.Q. (1999). Axon pathology in Parkinson's disease and Lewy body dementia hippocampus contains alpha-, beta-, and gamma-synuclein. Proc Natl Acad Sci U S A 96, 13450-13455.

Gan, W.B., Grutzendler, J., Wong, W.T., Wong, R.O., and Lichtman, J.W. (2000). Multicolor "DiOlistic" labeling of the nervous system using lipophilic dye combinations. Neuron 27, 219-225.

Ge, W.W., Wen, W., Strong, W., Leystra-Lantz, C., and Strong, M.J. (2005). Mutant copper-zinc superoxide dismutase binds to and destabilizes human low molecular weight neurofilament mRNA. J Biol Chem 280, 118-124.

George, J.M., Jin, H., Woods, W.S., and Clayton, D.F. (1995). Characterization of a novel protein regulated during the critical period for song learning in the zebra finch. Neuron 15, 361-372.

Giasson, B.I., Duda, J.E., Quinn, S.M., Zhang, B., Trojanowski, J.Q., and Lee, V.M. (2002). Neuronal alpha-synucleinopathy with severe movement disorder in mice expressing A53T human alpha-synuclein. Neuron 34, 521-533.

Giordana, M.T., Piccinini, M., Grifoni, S., De Marco, G., Vercellino, M., Magistrello, M., Pellerino, A., Buccinna, B., Lupino, E., and Rinaudo, M.T. (2010). TDP-43 redistribution is an early event in sporadic amyotrophic lateral sclerosis. Brain Pathol 20, 351-360.

Gispert, S., Del Turco, D., Garrett, L., Chen, A., Bernard, D.J., Hamm-Clement, J., Korf, H.W., Deller, T., Braak, H., Auburger, G., and Nussbaum, R.L. (2003). Transgenic mice expressing mutant A53T human alpha-synuclein show neuronal dysfunction in the absence of aggregate formation. Mol Cell Neurosci 24, 419-429.

Gitcho, M.A., Baloh, R.H., Chakraverty, S., Mayo, K., Norton, J.B., Levitch, D., Hatanpaa, K.J., White, C.L., 3rd, Bigio, E.H., Caselli, R., et al. (2008). TDP-43 A315T mutation in familial motor neuron disease. Ann Neurol 63, 535-538.

Gizzi, M., DiRocco, A., Sivak, M., and Cohen, B. (1992). Ocular motor function in motor neuron disease. Neurology 42, 1037-1046.

Gloeckner, C.J., Kinkl, N., Schumacher, A., Braun, R.J., O'Neill, E., Meitinger, T., Kolch, W., Prokisch, H., and Ueffing, M. (2006). The Parkinson disease causing LRRK2 mutation I2020T is associated with increased kinase activity. Hum Mol Genet 15, 223-232.

Goedert, M. (1997). Familial Parkinson's disease. The awakening of alpha-synuclein. Nature 388, 232-233.

Goldberg, M.S., Fleming, S.M., Palacino, J.J., Cepeda, C., Lam, H.A., Bhatnagar, A., Meloni, E.G., Wu, N., Ackerson, L.C., Klapstein, G.J., et al. (2003). Parkin-deficient mice exhibit nigrostriatal deficits but not loss of dopaminergic neurons. J Biol Chem 278, 43628-43635.

Goldberg, M.S., and Lansbury, P.T., Jr. (2000). Is there a cause-and-effect relationship between alpha-synuclein fibrillization and Parkinson's disease? Nat Cell Biol 2, E115-119.

Gomez-Isla, T., Irizarry, M.C., Mariash, A., Cheung, B., Soto, O., Schrump, S., Sondel, J., Kotilinek, L., Day, J., Schwarzschild, M.A., et al. (2003). Motor dysfunction and gliosis with preserved dopaminergic markers in human alpha-synuclein A30P transgenic mice. Neurobiol Aging 24, 245-258.

Gong, Y.H., Parsadanian, A.S., Andreeva, A., Snider, W.D., and Elliott, J.L. (2000). Restricted expression of G86R Cu/Zn superoxide dismutase in astrocytes results in astrocytosis but does not cause motoneuron degeneration. J Neurosci 20, 660-665.

Gordon, T., Tyreman, N., Li, S., Putman, C.T., and Hegedus, J. (2010). Functional over-load saves motor units in the SOD1-G93A transgenic mouse model of amyotrophic lateral sclerosis. Neurobiol Dis 37, 412-422.

Gorell, J.M., Johnson, C.C., Rybicki, B.A., Peterson, E.L., and Richardson, R.J. (1998). The risk of Parkinson's disease with exposure to pesticides, farming, well water, and rural living. Neurology 50, 1346-1350.

Gould, T.W., Buss, R.R., Vinsant, S., Prevette, D., Sun, W., Knudson, C.M., Milligan, C.E., and Oppenheim, R.W. (2006). Complete dissociation of motor neuron death from motor dysfunction by Bax deletion in a mouse model of ALS. J Neurosci 26, 8774-8786.

Greenfield, J.G., and Bosanquet, F.D. (1953). The brain-stem lesions in Parkinsonism. J Neurol Neurosurg Psychiatry 16, 213-226.

Greggio, E., Jain, S., Kingsbury, A., Bandopadhyay, R., Lewis, P., Kaganovich, A., van der Brug, M.P., Beilina, A., Blackinton, J., Thomas, K.J., et al. (2006). Kinase activity is required for the toxic effects of mutant LRRK2/dardarin. Neurobiol Dis 23, 329-341.

Greten-Harrison, B., Polydoro, M., Morimoto-Tomita, M., Diao, L., Williams, A.M., Nie, E.H., Makani, S., Tian, N., Castillo, P.E., Buchman, V.L., and Chandra, S.S. (2010). alphabetagamma-Synuclein

triple knockout mice reveal age-dependent neuronal dysfunction. Proc Natl Acad Sci U S A 107, 19573-19578.

Groll, M., Bajorek, M., Kohler, A., Moroder, L., Rubin, D.M., Huber, R., Glickman, M.H., and Finley, D. (2000). A gated channel into the proteasome core particle. Nat Struct Biol 7, 1062-1067.

Guo, Y.S., Wu, D.X., Wu, H.R., Wu, S.Y., Yang, C., Li, B., Bu, H., Zhang, Y.S., and Li, C.Y. (2009). Sensory involvement in the SOD1-G93A mouse model of amyotrophic lateral sclerosis. Exp Mol Med 41, 140-150.

Gurney, M.E., Pu, H., Chiu, A.Y., Dal Canto, M.C., Polchow, C.Y., Alexander, D.D., Caliendo, J., Hentati, A., Kwon, Y.W., Deng, H.X., and et al. (1994). Motor neuron degeneration in mice that express a human Cu,Zn superoxide dismutase mutation. Science 264, 1772-1775.

Guzman, J.N., Sanchez-Padilla, J., Wokosin, D., Kondapalli, J., Ilijic, E., Schumacker, P.T., and Surmeier, D.J. (2010). Oxidant stress evoked by pacemaking in dopaminergic neurons is attenuated by DJ-1. Nature 468, 696-700.

Haenggeli, C., and Kato, A.C. (2002). Differential vulnerability of cranial motoneurons in mouse models with motor neuron degeneration. Neurosci Lett 335, 39-43.

Hafezparast, M., Klocke, R., Ruhrberg, C., Marquardt, A., Ahmad-Annuar, A., Bowen, S., Lalli, G., Witherden, A.S., Hummerich, H., Nicholson, S., et al. (2003). Mutations in dynein link motor neuron degeneration to defects in retrograde transport. Science 300, 808-812.

Halliday, G.M., Blumbergs, P.C., Cotton, R.G., Blessing, W.W., and Geffen, L.B. (1990). Loss of brainstem serotonin- and substance P-containing neurons in Parkinson's disease. Brain Res 510, 104-107.

Hammad, M., Silva, A., Glass, J., Sladky, J.T., and Benatar, M. (2007). Clinical, electrophysiologic, and pathologic evidence for sensory abnormalities in ALS. Neurology 69, 2236-2242.

Hammer, R.P., Jr., Tomiyasu, U., and Scheibel, A.B. (1979). Degeneration of the human Betz cell due to amyotrophic lateral sclerosis. Exp Neurol 63, 336-346.

Han, H., Weinreb, P.H., and Lansbury, P.T., Jr. (1995). The core Alzheimer's peptide NAC forms amyloid fibrils which seed and are seeded by beta-amyloid: is NAC a common trigger or target in neurodegenerative disease? Chem Biol 2, 163-169.

Hardy, J. (2010). Genetic analysis of pathways to Parkinson disease. Neuron 68, 201-206.

Hashimoto, M., Rockenstein, E., Mante, M., Crews, L., Bar-On, P., Gage, F.H., Marr, R., and Masliah, E. (2004). An antiaggregation gene therapy strategy for Lewy body disease utilizing beta-synuclein lentivirus in a transgenic model. Gene Ther 11, 1713-1723.

Hashimoto, M., Rockenstein, E., Mante, M., Mallory, M., and Masliah, E. (2001). beta-Synuclein inhibits alpha-synuclein aggregation: a possible role as an anti-parkinsonian factor. Neuron 32, 213-223.

Haverkamp, L.J., Appel, V., and Appel, S.H. (1995). Natural history of amyotrophic lateral sclerosis in a database population. Validation of a scoring system and a model for survival prediction. Brain 118 (Pt 3), 707-719.

Hayatt, M. (1989). Principle and Techniques of Electron Microscopy, 3rd edn (MacMillan Press).

Heads, T., Pollock, M., Robertson, A., Sutherland, W.H., and Allpress, S. (1991). Sensory nerve pathology in amyotrophic lateral sclerosis. Acta Neuropathol 82, 316-320.

Hegedus, J., Putman, C.T., Tyreman, N., and Gordon, T. (2008). Preferential motor unit loss in the SOD1 G93A transgenic mouse model of amyotrophic lateral sclerosis. J Physiol 586, 3337-3351.

Heikkila, R.E., Manzino, L., Cabbat, F.S., and Duvoisin, R.C. (1984). Protection against the dopaminergic neurotoxicity of 1-methyl-4-phenyl-1,2,5,6-tetrahydropyridine by monoamine oxidase inhibitors. Nature 311, 467-469.

Hirano, A., Nakano, I., Kurland, L.T., Mulder, D.W., Holley, P.W., and Saccomanno, G. (1984). Fine structural study of neurofibrillary changes in a family with amyotrophic lateral sclerosis. J Neuropathol Exp Neurol 43, 471-480.

Hoffman, P.N., Griffin, J.W., and Price, D.L. (1984). Control of axonal caliber by neurofilament transport. J Cell Biol 99, 705-714.

Ibanez, P., Bonnet, A.M., Debarges, B., Lohmann, E., Tison, F., Pollak, P., Agid, Y., Durr, A., and Brice, A. (2004). Causal relation between alpha-synuclein gene duplication and familial Parkinson's disease. Lancet 364, 1169-1171.

Ikeda, K., Ikeda, S., Yoshimura, T., Kato, H., and Namba, M. (1978). Idiopathic Parkinsonism with Lewy-type inclusions in cerebral cortex. A case report. Acta Neuropathol 41, 165-168.

Ince, P.G., Tomkins, J., Slade, J.Y., Thatcher, N.M., and Shaw, P.J. (1998). Amyotrophic lateral sclerosis associated with genetic abnormalities in the gene encoding Cu/Zn superoxide dismutase: molecular pathology of five new cases, and comparison with previous reports and 73 sporadic cases of ALS. J Neuropathol Exp Neurol 57, 895-904.

Isaacs, J.D., Dean, A.F., Shaw, C.E., Al-Chalabi, A., Mills, K.R., and Leigh, P.N. (2007). Amyotrophic lateral sclerosis with sensory neuropathy: part of a multisystem disorder? J Neurol Neurosurg Psychiatry 78, 750-753.

Itier, J.M., Ibanez, P., Mena, M.A., Abbas, N., Cohen-Salmon, C., Bohme, G.A., Laville, M., Pratt, J., Corti, O., Pradier, L., et al. (2003). Parkin gene inactivation alters behaviour and dopamine neurotransmission in the mouse. Hum Mol Genet 12, 2277-2291.

Iwai, A., Masliah, E., Yoshimoto, M., Ge, N., Flanagan, L., de Silva, H.A., Kittel, A., and Saitoh, T. (1995). The precursor protein of non-A beta component of Alzheimer's disease amyloid is a presynaptic protein of the central nervous system. Neuron 14, 467-475.

J W Langston, J.P. (1995). The Case Of The Frozen Addicts, 1 edn (New York: Random House).

Jaarsma, D., Haasdijk, E.D., Grashorn, J.A., Hawkins, R., van Duijn, W., Verspaget, H.W., London, J., and Holstege, J.C. (2000). Human Cu/Zn superoxide dismutase (SOD1) overexpression in mice causes mitochondrial vacuolization, axonal degeneration, and premature motoneuron death and accelerates motoneuron disease in mice expressing a familial amyotrophic lateral sclerosis mutant SOD1. Neurobiol Dis 7, 623-643.

Jakes, R., Spillantini, M.G., and Goedert, M. (1994). Identification of two distinct synucleins from human brain. FEBS Lett 345, 27-32.

Javitch, J.A., D'Amato, R.J., Strittmatter, S.M., and Snyder, S.H. (1985). Parkinsonism-inducing neurotoxin, N-methyl-4-phenyl-1,2,3,6 -tetrahydropyridine: uptake of the metabolite N-methyl-4-phenylpyridine by dopamine neurons explains selective toxicity. Proc Natl Acad Sci U S A 82, 2173-2177.

Ji, H., Liu, Y.E., Jia, T., Wang, M., Liu, J., Xiao, G., Joseph, B.K., Rosen, C., and Shi, Y.E. (1997). Identification of a breast cancer-specific gene, BCSG1, by direct differential cDNA sequencing. Cancer Res 57, 759-764.

Kabashi, E., Valdmanis, P.N., Dion, P., Spiegelman, D., McConkey, B.J., Vande Velde, C., Bouchard, J.P., Lacomblez, L., Pochigaeva, K., Salachas, F., et al. (2008). TARDBP mutations in individuals with sporadic and familial amyotrophic lateral sclerosis. Nat Genet 40, 572-574.

Kachergus, J., Mata, I.F., Hulihan, M., Taylor, J.P., Lincoln, S., Aasly, J., Gibson, J.M., Ross, O.A., Lynch, T., Wiley, J., et al. (2005). Identification of a novel LRRK2 mutation linked to autosomal dominant parkinsonism: evidence of a common founder across European populations. Am J Hum Genet 76, 672-680.

Kandel, E. (2000). Principles of Neural Science, 4 edn (McGraw-Hill Medical).

Kanning, K.C., Kaplan, A., and Henderson, C.E. (2010). Motor neuron diversity in development and disease. Annu Rev Neurosci 33, 409-440.

Kawahara, M., and Kuroda, Y. (2000). Molecular mechanism of neurodegeneration induced by Alzheimer's beta-amyloid protein: channel formation and disruption of calcium homeostasis. Brain Res Bull 53, 389-397.

Kawai, S., Tsukuda, M., Mochimatsu, I., Enomoto, H., Kagesato, Y., Hirose, H., Kuroiwa, Y., and Suzuki, Y. (2003). A study of the early stage of Dysphagia in amyotrophic lateral sclerosis. Dysphagia 18, 1-8.

Kawamura, Y., Dyck, P.J., Shimono, M., Okazaki, H., Tateishi, J., and Doi, H. (1981). Morphometric comparison of the vulnerability of peripheral motor and sensory neurons in amyotrophic lateral sclerosis. J Neuropathol Exp Neurol 40, 667-675.

Kawata, A., Kato, S., Hayashi, H., and Hirai, S. (1997). Prominent sensory and autonomic disturbances in familial amyotrophic lateral sclerosis with a Gly93Ser mutation in the SOD1 gene. J Neurol Sci 153, 82-85.

Kiernan, J.A., and Hudson, A.J. (1991). Changes in sizes of cortical and lower motor neurons in amyotrophic lateral sclerosis. Brain 114 (Pt 2), 843-853.

Kisselev, A.F., and Goldberg, A.L. (2001). Proteasome inhibitors: from research tools to drug candidates. Chem Biol 8, 739-758.

Kitada, T., Asakawa, S., Hattori, N., Matsumine, H., Yamamura, Y., Minoshima, S., Yokochi, M., Mizuno, Y., and Shimizu, N. (1998). Mutations in the parkin gene cause autosomal recessive juvenile parkinsonism. Nature 392, 605-608.

Klionsky, D.J., Abeliovich, H., Agostinis, P., Agrawal, D.K., Aliev, G., Askew, D.S., Baba, M., Baehrecke, E.H., Bahr, B.A., Ballabio, A., et al. (2008). Guidelines for the use and interpretation of assays for monitoring autophagy in higher eukaryotes. Autophagy 4, 151-175.

Kong, J., and Xu, Z. (1998). Massive mitochondrial degeneration in motor neurons triggers the onset of amyotrophic lateral sclerosis in mice expressing a mutant SOD1. J Neurosci 18, 3241-3250.

Kopin, I.J., and Markey, S.P. (1988). MPTP toxicity: implications for research in Parkinson's disease. Annu Rev Neurosci 11, 81-96.

Kordower, J.H., Kanaan, N.M., Chu, Y., Suresh Babu, R., Stansell, J., 3rd, Terpstra, B.T., Sortwell, C.E., Steece-Collier, K., and Collier, T.J. (2006). Failure of proteasome inhibitor administration to provide a model of Parkinson's disease in rats and monkeys. Ann Neurol 60, 264-268.

Kruger, R., Kuhn, W., Muller, T., Woitalla, D., Graeber, M., Kosel, S., Przuntek, H., Epplen, J.T., Schols, L., and Riess, O. (1998). Ala30Pro mutation in the gene encoding alpha-synuclein in Parkinson's disease. Nat Genet 18, 106-108.

Kruger, R., Schols, L., Muller, T., Kuhn, W., Woitalla, D., Przuntek, H., Epplen, J.T., and Riess, O. (2001). Evaluation of the gamma-synuclein gene in German Parkinson's disease patients. Neurosci Lett 310, 191-193.

Kuhn, M., Haebig, K., Bonin, M., Ninkina, N., Buchman, V.L., Poths, S., and Riess, O. (2007). Whole genome expression analyses of single- and double-knock-out mice implicate partially overlapping functions of alpha- and gamma-synuclein. Neurogenetics 8, 71-81.

Kwiatkowski, T.J., Jr., Bosco, D.A., Leclerc, A.L., Tamrazian, E., Vanderburg, C.R., Russ, C., Davis, A., Gilchrist, J., Kasarskis, E.J., Munsat, T., et al. (2009). Mutations in the FUS/TLS gene on chromosome 16 cause familial amyotrophic lateral sclerosis. Science 323, 1205-1208.

Laemmli, U.K. (1970). Cleavage of structural proteins during the assembly of the head of bacteriophage T4. Nature 227, 680-685.

Lagier-Tourenne, C., Polymenidou, M., and Cleveland, D.W. (2010). TDP-43 and FUS/TLS: emerging roles in RNA processing and neurodegeneration. Hum Mol Genet 19, R46-64.

LaMonte, B.H., Wallace, K.E., Holloway, B.A., Shelly, S.S., Ascano, J., Tokito, M., Van Winkle, T., Howland, D.S., and Holzbaur, E.L. (2002). Disruption of dynein/dynactin inhibits axonal transport in motor neurons causing late-onset progressive degeneration. Neuron 34, 715-727.

Langston, J.W., Ballard, P., Tetrud, J.W., and Irwin, I. (1983). Chronic Parkinsonism in humans due to a product of meperidine-analog synthesis. Science 219, 979-980.

Lashuel, H.A., Petre, B.M., Wall, J., Simon, M., Nowak, R.J., Walz, T., and Lansbury, P.T., Jr. (2002). Alpha-synuclein, especially the Parkinson's disease-associated mutants, forms pore-like annular and tubular protofibrils. J Mol Biol 322, 1089-1102.

Lavedan, C. (1998). The synuclein family. Genome Res 8, 871-880.

Lavedan, C., Buchholtz, S., Auburger, G., Albin, R.L., Athanassiadou, A., Blancato, J., Burguera, J.A., Ferrell, R.E., Kostic, V., Leroy, E., et al. (1998a). Absence of mutation in the beta- and gamma-synuclein genes in familial autosomal dominant Parkinson's disease. DNA Res 5, 401-402.

Lavedan, C., Leroy, E., Dehejia, A., Buchholtz, S., Dutra, A., Nussbaum, R.L., and Polymeropoulos, M.H. (1998b). Identification, localization and characterization of the human gamma-synuclein gene. Hum Genet 103, 106-112.

Lavedan, C., Leroy, E., Torres, R., Dehejia, A., Dutra, A., Buchholtz, S., Nussbaum, R.L., and Polymeropoulos, M.H. (1998c). Genomic organization and expression of the human beta-synuclein gene (SNCB). Genomics 54, 173-175.

Lee, F.J., Liu, F., Pristupa, Z.B., and Niznik, H.B. (2001). Direct binding and functional coupling of alpha-synuclein to the dopamine transporters accelerate dopamine-induced apoptosis. FASEB J 15, 916-926.

Lee, M.K., Marszalek, J.R., and Cleveland, D.W. (1994). A mutant neurofilament subunit causes massive, selective motor neuron death: implications for the pathogenesis of human motor neuron disease. Neuron 13, 975-988.

Lee, M.K., Stirling, W., Xu, Y., Xu, X., Qui, D., Mandir, A.S., Dawson, T.M., Copeland, N.G., Jenkins, N.A., and Price, D.L. (2002). Human alpha-synuclein-harboring familial Parkinson's disease-linked Ala-53 --> Thr mutation causes neurodegenerative disease with alpha-synuclein aggregation in transgenic mice. Proc Natl Acad Sci U S A 99, 8968-8973.

Leigh, P.N., Anderton, B.H., Dodson, A., Gallo, J.M., Swash, M., and Power, D.M. (1988). Ubiquitin deposits in anterior horn cells in motor neurone disease. Neurosci Lett 93, 197-203.

Leroy, E., Boyer, R., Auburger, G., Leube, B., Ulm, G., Mezey, E., Harta, G., Brownstein, M.J., Jonnalagada, S., Chernova, T., et al. (1998). The ubiquitin pathway in Parkinson's disease. Nature 395, 451-452.

Lesage, S., and Brice, A. (2009). Parkinson's disease: from monogenic forms to genetic susceptibility factors. Hum Mol Genet 18, R48-59.

Li, J., Uversky, V.N., and Fink, A.L. (2001). Effect of familial Parkinson's disease point mutations A30P and A53T on the structural properties, aggregation, and fibrillation of human alpha-synuclein. Biochemistry 40, 11604-11613.

Li, J.Y., Henning Jensen, P., and Dahlstrom, A. (2002). Differential localization of alpha-, beta- and gamma-synucleins in the rat CNS. Neuroscience 113, 463-478.

Li, T.M., Alberman, E., and Swash, M. (1988). Comparison of sporadic and familial disease amongst 580 cases of motor neuron disease. J Neurol Neurosurg Psychiatry 51, 778-784.

Li, X., Patel, J.C., Wang, J., Avshalumov, M.V., Nicholson, C., Buxbaum, J.D., Elder, G.A., Rice, M.E., and Yue, Z. (2010). Enhanced striatal dopamine transmission and motor performance with LRRK2 overexpression in mice is eliminated by familial Parkinson's disease mutation G2019S. J Neurosci 30, 1788-1797.

Li, Y., Liu, W., Oo, T.F., Wang, L., Tang, Y., Jackson-Lewis, V., Zhou, C., Geghman, K., Bogdanov, M., Przedborski, S., et al. (2009). Mutant LRRK2(R1441G) BAC transgenic mice recapitulate cardinal features of Parkinson's disease. Nat Neurosci 12, 826-828.

Lincoln, S., Gwinn-Hardy, K., Goudreau, J., Chartier-Harlin, M.C., Baker, M., Mouroux, V., Richard, F., Destee, A., Becquet, E., Amouyel, P., et al. (1999). No pathogenic mutations in the persyn gene in Parkinson's disease. Neurosci Lett 259, 65-66.

Lino, M.M., Schneider, C., and Caroni, P. (2002). Accumulation of SOD1 mutants in postnatal motoneurons does not cause motoneuron pathology or motoneuron disease. J Neurosci 22, 4825-4832.

Lippa, C.F., Fujiwara, H., Mann, D.M., Giasson, B., Baba, M., Schmidt, M.L., Nee, L.E., O'Connell, B., Pollen, D.A., St George-Hyslop, P., et al. (1998). Lewy bodies contain altered alpha-synuclein in

brains of many familial Alzheimer's disease patients with mutations in presenilin and amyloid precursor protein genes. Am J Pathol 153, 1365-1370.

Lippa, C.F., Rosso, A.L., Stutzbach, L.D., Neumann, M., Lee, V.M., and Trojanowski, J.Q. (2009). Transactive response DNA-binding protein 43 burden in familial Alzheimer disease and Down syndrome. Arch Neurol 66, 1483-1488.

Liu, C., Dong, B., Lu, A., Qu, L., Xing, X., Meng, L., Wu, J., Eric Shi, Y., and Shou, C. (2010). Synuclein gamma predicts poor clinical outcome in colon cancer with normal levels of carcinoembryonic antigen. BMC Cancer 10, 359.

Liu, H., Liu, W., Wu, Y., Zhou, Y., Xue, R., Luo, C., Wang, L., Zhao, W., Jiang, J.D., and Liu, J. (2005). Loss of epigenetic control of synuclein-gamma gene as a molecular indicator of metastasis in a wide range of human cancers. Cancer Res 65, 7635-7643.

Liu, Y., Fallon, L., Lashuel, H.A., Liu, Z., and Lansbury, P.T., Jr. (2002). The UCH-L1 gene encodes two opposing enzymatic activities that affect alpha-synuclein degradation and Parkinson's disease susceptibility. Cell 111, 209-218.

Lockhart, P.J., O'Farrell, C.A., and Farrer, M.J. (2004). It's a double knock-out! The quaking mouse is a spontaneous deletion of parkin and parkin co-regulated gene (PACRG). Mov Disord 19, 101-104.

Lowe, J., McDermott, H., Landon, M., Mayer, R.J., and Wilkinson, K.D. (1990). Ubiquitin carboxyl-terminal hydrolase (PGP 9.5) is selectively present in ubiquitinated inclusion bodies characteristic of human neurodegenerative diseases. J Pathol 161, 153-160.

Majoor-Krakauer, D., Willems, P.J., and Hofman, A. (2003). Genetic epidemiology of amyotrophic lateral sclerosis. Clin Genet 63, 83-101.

Manning-Bog, A.B., Reaney, S.H., Chou, V.P., Johnston, L.C., McCormack, A.L., Johnston, J., Langston, J.W., and Di Monte, D.A. (2006). Lack of nigrostriatal pathology in a rat model of proteasome inhibition. Ann Neurol 60, 256-260.

Mannoji, H., Yeger, H., and Becker, L.E. (1986). A specific histochemical marker (lectin Ricinus communis agglutinin-1) for normal human microglia, and application to routine histopathology. Acta Neuropathol 71, 341-343.

Maraganore, D.M., Lesnick, T.G., Elbaz, A., Chartier-Harlin, M.C., Gasser, T., Kruger, R., Hattori, N., Mellick, G.D., Quattrone, A., Satoh, J., et al. (2004). UCHL1 is a Parkinson's disease susceptibility gene. Ann Neurol 55, 512-521.

Maroteaux, L., Campanelli, J.T., and Scheller, R.H. (1988). Synuclein: a neuron-specific protein localized to the nucleus and presynaptic nerve terminal. J Neurosci 8, 2804-2815.

Marszalek, J.R., Williamson, T.L., Lee, M.K., Xu, Z., Hoffman, P.N., Becher, M.W., Crawford, T.O., and Cleveland, D.W. (1996). Neurofilament subunit NF-H modulates axonal diameter by selectively slowing neurofilament transport. J Cell Biol 135, 711-724.

Maruyama, H., Morino, H., Ito, H., Izumi, Y., Kato, H., Watanabe, Y., Kinoshita, Y., Kamada, M., Nodera, H., Suzuki, H., et al. (2010). Mutations of optineurin in amyotrophic lateral sclerosis. Nature 465, 223-226.

Maskri, L., Zhu, X., Fritzen, S., Kuhn, K., Ullmer, C., Engels, P., Andriske, M., Stichel, C.C., and Lubbert, H. (2004). Influence of different promoters on the expression pattern of mutated human alpha-synuclein in transgenic mice. Neurodegener Dis 1, 255-265.

Masliah, E., and Hashimoto, M. (2002). Development of new treatments for Parkinson's disease in transgenic animal models: a role for beta-synuclein. Neurotoxicology 23, 461-468.

Masliah, E., Rockenstein, E., Veinbergs, I., Mallory, M., Hashimoto, M., Takeda, A., Sagara, Y., Sisk, A., and Mucke, L. (2000). Dopaminergic loss and inclusion body formation in alpha-synuclein mice: implications for neurodegenerative disorders. Science 287, 1265-1269.

Matsuoka, Y., Vila, M., Lincoln, S., McCormack, A., Picciano, M., LaFrancois, J., Yu, X., Dickson, D., Langston, W.J., McGowan, E., et al. (2001). Lack of nigral pathology in transgenic mice expressing human alpha-synuclein driven by the tyrosine hydroxylase promoter. Neurobiol Dis 8, 535-539.

McLean, J.R., Sanelli, T.R., Leystra-Lantz, C., He, B.P., and Strong, M.J. (2005). Temporal profiles of neuronal degeneration, glial proliferation, and cell death in hNFL(+/+) and NFL(-/-) mice. Glia 52, 59-69.

McNaught, K.S., and Olanow, C.W. (2006). Proteasome inhibitor-induced model of Parkinson's disease. Ann Neurol 60, 243-247.

McNaught, K.S., Olanow, C.W., Halliwell, B., Isacson, O., and Jenner, P. (2001). Failure of the ubiquitin-proteasome system in Parkinson's disease. Nat Rev Neurosci 2, 589-594.

McNaught, K.S., Perl, D.P., Brownell, A.L., and Olanow, C.W. (2004). Systemic exposure to proteasome inhibitors causes a progressive model of Parkinson's disease. Ann Neurol 56, 149-162.

Menegon, A., Board, P.G., Blackburn, A.C., Mellick, G.D., and Le Couteur, D.G. (1998). Parkinson's disease, pesticides, and glutathione transferase polymorphisms. Lancet 352, 1344-1346.

Menzies, F.M., Grierson, A.J., Cookson, M.R., Heath, P.R., Tomkins, J., Figlewicz, D.A., Ince, P.G., and Shaw, P.J. (2002). Selective loss of neurofilament expression in Cu/Zn superoxide dismutase (SOD1) linked amyotrophic lateral sclerosis. J Neurochem 82, 1118-1128.

Millecamps, S., Robertson, J., Lariviere, R., Mallet, J., and Julien, J.P. (2006). Defective axonal transport of neurofilament proteins in neurons overexpressing peripherin. J Neurochem 98, 926-938.

Mizuno, Y., Amari, M., Takatama, M., Aizawa, H., Mihara, B., and Okamoto, K. (2006). Transferrin localizes in Bunina bodies in amyotrophic lateral sclerosis. Acta Neuropathol 112, 597-603.

Mori, H., Kondo, T., Yokochi, M., Matsumine, H., Nakagawa-Hattori, Y., Miyake, T., Suda, K., and Mizuno, Y. (1998). Pathologic and biochemical studies of juvenile parkinsonism linked to chromosome 6q. Neurology 51, 890-892.

Mourelatos, Z., Gonatas, N.K., Stieber, A., Gurney, M.E., and Dal Canto, M.C. (1996). The Golgi apparatus of spinal cord motor neurons in transgenic mice expressing mutant Cu,Zn superoxide dismutase becomes fragmented in early, preclinical stages of the disease. Proc Natl Acad Sci U S A 93, 5472-5477.

Mu, X., Beremand, P.D., Zhao, S., Pershad, R., Sun, H., Scarpa, A., Liang, S., Thomas, T.L., and Klein, W.H. (2004). Discrete gene sets depend on POU domain transcription factor Brn3b/Brn-3.2/POU4f2 for their expression in the mouse embryonic retina. Development 131, 1197-1210.

Murakami, T., Nagano, I., Hayashi, T., Manabe, Y., Shoji, M., Setoguchi, Y., and Abe, K. (2001). Impaired retrograde axonal transport of adenovirus-mediated E. coli LacZ gene in the mice carrying mutant SOD1 gene. Neurosci Lett 308, 149-152.

Nagai, M., Re, D.B., Nagata, T., Chalazonitis, A., Jessell, T.M., Wichterle, H., and Przedborski, S. (2007). Astrocytes expressing ALS-linked mutated SOD1 release factors selectively toxic to motor neurons. Nat Neurosci 10, 615-622.

Nakajo, S., Tsukada, K., Omata, K., Nakamura, Y., and Nakaya, K. (1993). A new brain-specific 14-kDa protein is a phosphoprotein. Its complete amino acid sequence and evidence for phosphorylation. Eur J Biochem 217, 1057-1063.

Nakashima-Yasuda, H., Uryu, K., Robinson, J., Xie, S.X., Hurtig, H., Duda, J.E., Arnold, S.E., Siderowf, A., Grossman, M., Leverenz, J.B., et al. (2007). Co-morbidity of TDP-43 proteinopathy in Lewy body related diseases. Acta Neuropathol 114, 221-229.

Narhi, L., Wood, S.J., Steavenson, S., Jiang, Y., Wu, G.M., Anafi, D., Kaufman, S.A., Martin, F., Sitney, K., Denis, P., et al. (1999). Both familial Parkinson's disease mutations accelerate alpha-synuclein aggregation. J Biol Chem 274, 9843-9846.

Neumann, M., Rademakers, R., Roeber, S., Baker, M., Kretzschmar, H.A., and Mackenzie, I.R. (2009). A new subtype of frontotemporal lobar degeneration with FUS pathology. Brain 132, 2922-2931.

Neumann, M., Sampathu, D.M., Kwong, L.K., Truax, A.C., Micsenyi, M.C., Chou, T.T., Bruce, J., Schuck, T., Grossman, M., Clark, C.M., et al. (2006). Ubiquitinated TDP-43 in frontotemporal lobar degeneration and amyotrophic lateral sclerosis. Science 314, 130-133.

Nguyen, J.V., Soto, I., Kim, K.Y., Bushong, E.A., Oglesby, E., Valiente-Soriano, F.J., Yang, Z., Davis, C.H., Bedont, J.L., Son, J.L., et al. (2011). Myelination transition zone astrocytes are constitutively phagocytic and have synuclein dependent reactivity in glaucoma. Proc Natl Acad Sci U S A 108, 1176-1181.

Nimchinsky, E.A., Young, W.G., Yeung, G., Shah, R.A., Gordon, J.W., Bloom, F.E., Morrison, J.H., and Hof, P.R. (2000). Differential vulnerability of oculomotor, facial, and hypoglossal nuclei in G86R superoxide dismutase transgenic mice. J Comp Neurol 416, 112-125.

Ninkina, N., Papachroni, K., Robertson, D.C., Schmidt, O., Delaney, L., O'Neill, F., Court, F., Rosenthal, A., Fleetwood-Walker, S.M., Davies, A.M., and Buchman, V.L. (2003). Neurons expressing the highest levels of gamma-synuclein are unaffected by targeted inactivation of the gene. Mol Cell Biol 23, 8233-8245.

Ninkina, N., Peters, O., Millership, S., Salem, H., van der Putten, H., and Buchman, V.L. (2009). Gamma-synucleinopathy: neurodegeneration associated with overexpression of the mouse protein. Hum Mol Genet 18, 1779-1794.

Ninkina, N.N., Alimova-Kost, M.V., Paterson, J.W., Delaney, L., Cohen, B.B., Imreh, S., Gnuchev, N.V., Davies, A.M., and Buchman, V.L. (1998). Organization, expression and polymorphism of the human persyn gene. Hum Mol Genet 7, 1417-1424.

Ninkina, N.N., Privalova, E.M., Pinon, L.G., Davies, A.M., and Buchman, V.L. (1999). Developmentally regulated expression of persyn, a member of the synuclein family, in skin. Exp Cell Res 246, 308-311.

Nishimura, A.L., Mitne-Neto, M., Silva, H.C., Richieri-Costa, A., Middleton, S., Cascio, D., Kok, F., Oliveira, J.R., Gillingwater, T., Webb, J., et al. (2004). A mutation in the vesicle-trafficking protein VAPB causes late-onset spinal muscular atrophy and amyotrophic lateral sclerosis. Am J Hum Genet 75, 822-831.

Nishioka, K., Wider, C., Vilarino-Guell, C., Soto-Ortolaza, A.I., Lincoln, S.J., Kachergus, J.M., Jasinska-Myga, B., Ross, O.A., Rajput, A., Robinson, C.A., et al. (2010). Association of alpha-, beta-, and gamma-Synuclein with diffuse lewy body disease. Arch Neurol 67, 970-975.

Ohtake, H., Limprasert, P., Fan, Y., Onodera, O., Kakita, A., Takahashi, H., Bonner, L.T., Tsuang, D.W., Murray, I.V., Lee, V.M., et al. (2004). Beta-synuclein gene alterations in dementia with Lewy bodies. Neurology 63, 805-811.

Okamoto, K., Hirai, S., Amari, M., Iizuka, T., Watanabe, M., Murakami, N., and Takatama, M. (1993a). Oculomotor nuclear pathology in amyotrophic lateral sclerosis. Acta Neuropathol 85, 458-462.

Okamoto, K., Hirai, S., Amari, M., Watanabe, M., and Sakurai, A. (1993b). Bunina bodies in amyotrophic lateral sclerosis immunostained with rabbit anti-cystatin C serum. Neurosci Lett 162, 125-128.

Okamoto, K., Mizuno, Y., and Fujita, Y. (2008). Bunina bodies in amyotrophic lateral sclerosis. Neuropathology 28, 109-115.

Oort, P.J., Knotts, T.A., Grino, M., Naour, N., Bastard, J.P., Clement, K., Ninkina, N., Buchman, V.L., Permana, P.A., Luo, X., et al. (2008). Gamma-synuclein is an adipocyte-neuron gene coordinately expressed with leptin and increased in human obesity. J Nutr 138, 841-848.

Orrell, R.W., Habgood, J.J., Malaspina, A., Mitchell, J., Greenwood, J., Lane, R.J., and deBelleroche, J.S. (1999). Clinical characteristics of SOD1 gene mutations in UK families with ALS. J Neurol Sci 169, 56-60.

Osaka, H., Wang, Y.L., Takada, K., Takizawa, S., Setsuie, R., Li, H., Sato, Y., Nishikawa, K., Sun, Y.J., Sakurai, M., et al. (2003). Ubiquitin carboxy-terminal hydrolase L1 binds to and stabilizes monoubiquitin in neuron. Hum Mol Genet 12, 1945-1958.

Ou, S.H., Wu, F., Harrich, D., Garcia-Martinez, L.F., and Gaynor, R.B. (1995). Cloning and characterization of a novel cellular protein, TDP-43, that binds to human immunodeficiency virus type 1 TAR DNA sequence motifs. J Virol 69, 3584-3596.

Paisan-Ruiz, C., Jain, S., Evans, E.W., Gilks, W.P., Simon, J., van der Brug, M., Lopez de Munain, A., Aparicio, S., Gil, A.M., Khan, N., et al. (2004). Cloning of the gene containing mutations that cause PARK8-linked Parkinson's disease. Neuron 44, 595-600.

Pals, P., Lincoln, S., Manning, J., Heckman, M., Skipper, L., Hulihan, M., Van den Broeck, M., De Pooter, T., Cras, P., Crook, J., et al. (2004). alpha-Synuclein promoter confers susceptibility to Parkinson's disease. Ann Neurol 56, 591-595.

Pankratz, N., Nichols, W.C., Elsaesser, V.E., Pauciulo, M.W., Marek, D.K., Halter, C.A., Wojcieszek, J., Rudolph, A., Pfeiffer, R.F., and Foroud, T. (2009). Alpha-synuclein and familial Parkinson's disease. Mov Disord 24, 1125-1131.

Papachroni, K., Ninkina, N., Wanless, J., Kalofoutis, A.T., Gnuchev, N.V., and Buchman, V.L. (2005). Peripheral sensory neurons survive in the absence of alpha- and gamma-synucleins. J Mol Neurosci 25, 157-164.

Park, J.Y., and Lansbury, P.T., Jr. (2003). Beta-synuclein inhibits formation of alpha-synuclein protofibrils: a possible therapeutic strategy against Parkinson's disease. Biochemistry 42, 3696-3700.

Pearson, J.P., Williams, N.M., Majounie, E., Waite, A., Stott, J., Newsway, V., Murray, A., Hernandez, D., Guerreiro, R., Singleton, A.B., et al. (2010). Familial frontotemporal dementia with amyotrophic lateral sclerosis and a shared haplotype on chromosome 9p. J Neurol.

Perez, R.G., Waymire, J.C., Lin, E., Liu, J.J., Guo, F., and Zigmond, M.J. (2002). A role for alpha-synuclein in the regulation of dopamine biosynthesis. J Neurosci 22, 3090-3099.

Perrin, R.J., Woods, W.S., Clayton, D.F., and George, J.M. (2000). Interaction of human alpha-Synuclein and Parkinson's disease variants with phospholipids. Structural analysis using site-directed mutagenesis. J Biol Chem 275, 34393-34398.

Pickart, C.M. (2000). Ubiquitin in chains. Trends Biochem Sci 25, 544-548.

Polymeropoulos, M.H., Lavedan, C., Leroy, E., Ide, S.E., Dehejia, A., Dutra, A., Pike, B., Root, H., Rubenstein, J., Boyer, R., et al. (1997). Mutation in the alpha-synuclein gene identified in families with Parkinson's disease. Science 276, 2045-2047.

Pramatarova, A., Laganiere, J., Roussel, J., Brisebois, K., and Rouleau, G.A. (2001). Neuron-specific expression of mutant superoxide dismutase 1 in transgenic mice does not lead to motor impairment. J Neurosci 21, 3369-3374.

Pramstaller, P.P., Schlossmacher, M.G., Jacques, T.S., Scaravilli, F., Eskelson, C., Pepivani, I., Hedrich, K., Adel, S., Gonzales-McNeal, M., Hilker, R., et al. (2005). Lewy body Parkinson's disease in a large pedigree with 77 Parkin mutation carriers. Ann Neurol 58, 411-422.

Pugdahl, K., Fuglsang-Frederiksen, A., de Carvalho, M., Johnsen, B., Fawcett, P.R., Labarre-Vila, A., Liguori, R., Nix, W.A., and Schofield, I.S. (2007). Generalised sensory system abnormalities in amyotrophic lateral sclerosis: a European multicentre study. J Neurol Neurosurg Psychiatry 78, 746-749.

Puls, I., Jonnakuty, C., LaMonte, B.H., Holzbaur, E.L., Tokito, M., Mann, E., Floeter, M.K., Bidus, K., Drayna, D., Oh, S.J., et al. (2003). Mutant dynactin in motor neuron disease. Nat Genet 33, 455-456.

Pun, S., Santos, A.F., Saxena, S., Xu, L., and Caroni, P. (2006). Selective vulnerability and pruning of phasic motoneuron axons in motoneuron disease alleviated by CNTF. Nat Neurosci 9, 408-419.

Quigley, H.A., and Broman, A.T. (2006). The number of people with glaucoma worldwide in 2010 and 2020. Br J Ophthalmol 90, 262-267.

Rabbitts, T.H., Forster, A., Larson, R., and Nathan, P. (1993). Fusion of the dominant negative transcription regulator CHOP with a novel gene FUS by translocation t(12;16) in malignant liposarcoma. Nat Genet 4, 175-180.

Rathke-Hartlieb, S., Kahle, P.J., Neumann, M., Ozmen, L., Haid, S., Okochi, M., Haass, C., and Schulz, J.B. (2001). Sensitivity to MPTP is not increased in Parkinson's disease-associated mutant alpha-synuclein transgenic mice. J Neurochem 77, 1181-1184.

Ray, S.S., Nowak, R.J., Strokovich, K., Brown, R.H., Jr., Walz, T., and Lansbury, P.T., Jr. (2004). An intersubunit disulfide bond prevents in vitro aggregation of a superoxide dismutase-1 mutant linked to familial amytrophic lateral sclerosis. Biochemistry 43, 4899-4905.

Reaume, A.G., Elliott, J.L., Hoffman, E.K., Kowall, N.W., Ferrante, R.J., Siwek, D.F., Wilcox, H.M., Flood, D.G., Beal, M.F., Brown, R.H., Jr., et al. (1996). Motor neurons in Cu/Zn superoxide dismutase-deficient mice develop normally but exhibit enhanced cell death after axonal injury. Nat Genet 13, 43-47.

Reed, C.H.M. (1998). Unbiased Stereology: Three-Dimensional Measurement in Microscopy (Advanced Methods) (Bios Scientific Publishers Ltd).

Reynolds, E.S. (1963). The use of lead citrate at high pH as an electron-opaque stain in electron microscopy. J Cell Biol 17, 208-212.

Rezaie, T., Child, A., Hitchings, R., Brice, G., Miller, L., Coca-Prados, M., Heon, E., Krupin, T., Ritch, R., Kreutzer, D., et al. (2002). Adult-onset primary open-angle glaucoma caused by mutations in optineurin. Science 295, 1077-1079.

Richfield, E.K., Thiruchelvam, M.J., Cory-Slechta, D.A., Wuertzer, C., Gainetdinov, R.R., Caron, M.G., Di Monte, D.A., and Federoff, H.J. (2002). Behavioral and neurochemical effects of wild-type and mutated human alpha-synuclein in transgenic mice. Exp Neurol 175, 35-48.

Robertson, D.C., Schmidt, O., Ninkina, N., Jones, P.A., Sharkey, J., and Buchman, V.L. (2004). Developmental loss and resistance to MPTP toxicity of dopaminergic neurones in substantia nigra pars compacta of gamma-synuclein, alpha-synuclein and double alpha/gamma-synuclein null mutant mice. J Neurochem 89, 1126-1136.

Rochet, J.C., Conway, K.A., and Lansbury, P.T., Jr. (2000). Inhibition of fibrillization and accumulation of prefibrillar oligomers in mixtures of human and mouse alpha-synuclein. Biochemistry 39, 10619-10626.

Rockenstein, E., Mallory, M., Hashimoto, M., Song, D., Shults, C.W., Lang, I., and Masliah, E. (2002). Differential neuropathological alterations in transgenic mice expressing alpha-synuclein from the platelet-derived growth factor and Thy-1 promoters. J Neurosci Res 68, 568-578.

Rodriguez, J.A., Valentine, J.S., Eggers, D.K., Roe, J.A., Tiwari, A., Brown, R.H., Jr., and Hayward, L.J. (2002). Familial amyotrophic lateral sclerosis-associated mutations decrease the thermal stability of distinctly metallated species of human copper/zinc superoxide dismutase. J Biol Chem 277, 15932-15937.

Rosen, D.R., Siddique, T., Patterson, D., Figlewicz, D.A., Sapp, P., Hentati, A., Donaldson, D., Goto, J., O'Regan, J.P., Deng, H.X., and et al. (1993). Mutations in Cu/Zn superoxide dismutase gene are associated with familial amyotrophic lateral sclerosis. Nature 362, 59-62.

Ross, C.A., and Poirier, M.A. (2005). Opinion: What is the role of protein aggregation in neurodegeneration? Nat Rev Mol Cell Biol 6, 891-898.

Rouleau, G.A., Clark, A.W., Rooke, K., Pramatarova, A., Krizus, A., Suchowersky, O., Julien, J.P., and Figlewicz, D. (1996). SOD1 mutation is associated with accumulation of neurofilaments in amyotrophic lateral sclerosis. Ann Neurol 39, 128-131.

Sahlender, D.A., Roberts, R.C., Arden, S.D., Spudich, G., Taylor, M.J., Luzio, J.P., Kendrick-Jones, J., and Buss, F. (2005). Optineurin links myosin VI to the Golgi complex and is involved in Golgi organization and exocytosis. J Cell Biol 169, 285-295.

Saigoh, K., Wang, Y.L., Suh, J.G., Yamanishi, T., Sakai, Y., Kiyosawa, H., Harada, T., Ichihara, N., Wakana, S., Kikuchi, T., and Wada, K. (1999). Intragenic deletion in the gene encoding ubiquitin carboxy-terminal hydrolase in gad mice. Nat Genet 23, 47-51.

Sakaguchi, T., Okada, M., Kitamura, T., and Kawasaki, K. (1993). Reduced diameter and conduction velocity of myelinated fibers in the sciatic nerve of a neurofilament-deficient mutant quail. Neurosci Lett 153, 65-68.

Sasaki, S., Horie, Y., and Iwata, M. (2007). Mitochondrial alterations in dorsal root ganglion cells in sporadic amyotrophic lateral sclerosis. Acta Neuropathol 114, 633-639.

Satake, W., Nakabayashi, Y., Mizuta, I., Hirota, Y., Ito, C., Kubo, M., Kawaguchi, T., Tsunoda, T., Watanabe, M., Takeda, A., et al. (2009). Genome-wide association study identifies common variants at four loci as genetic risk factors for Parkinson's disease. Nat Genet 41, 1303-1307.

Saxena, S., Cabuy, E., and Caroni, P. (2009). A role for motoneuron subtype-selective ER stress in disease manifestations of FALS mice. Nat Neurosci 12, 627-636.

Schapira, A.H., Cleeter, M.W., Muddle, J.R., Workman, J.M., Cooper, J.M., and King, R.H. (2006). Proteasomal inhibition causes loss of nigral tyrosine hydroxylase neurons. Ann Neurol 60, 253-255.

Schluter, O.M., Fornai, F., Alessandri, M.G., Takamori, S., Geppert, M., Jahn, R., and Sudhof, T.C. (2003). Role of alpha-synuclein in 1-methyl-4-phenyl-1,2,3,6-tetrahydropyridine-induced parkinsonism in mice. Neuroscience 118, 985-1002.

Schwab, C., Arai, T., Hasegawa, M., Yu, S., and McGeer, P.L. (2008). Colocalization of transactivation-responsive DNA-binding protein 43 and huntingtin in inclusions of Huntington disease. J Neuropathol Exp Neurol 67, 1159-1165.

Seaton, T.A., Cooper, J.M., and Schapira, A.H. (1997). Free radical scavengers protect dopaminergic cell lines from apoptosis induced by complex I inhibitors. Brain Res 777, 110-118.

Setsuie, R., and Wada, K. (2007). The functions of UCH-L1 and its relation to neurodegenerative diseases. Neurochem Int 51, 105-111.

Shan, X., Chiang, P.M., Price, D.L., and Wong, P.C. (2010). Altered distributions of Gemini of coiled bodies and mitochondria in motor neurons of TDP-43 transgenic mice. Proc Natl Acad Sci U S A 107, 16325-16330.

Shaw, B.F., and Valentine, J.S. (2007). How do ALS-associated mutations in superoxide dismutase 1 promote aggregation of the protein? Trends Biochem Sci 32, 78-85.

Sherer, T.B., Kim, J.H., Betarbet, R., and Greenamyre, J.T. (2003). Subcutaneous rotenone exposure causes highly selective dopaminergic degeneration and alpha-synuclein aggregation. Exp Neurol 179, 9-16.

Shibata, N., Hirano, A., Kobayashi, M., Siddique, T., Deng, H.X., Hung, W.Y., Kato, T., and Asayama, K. (1996). Intense superoxide dismutase-1 immunoreactivity in intracytoplasmic hyaline inclusions of familial amyotrophic lateral sclerosis with posterior column involvement. J Neuropathol Exp Neurol 55, 481-490.

Shimura, H., Hattori, N., Kubo, S., Mizuno, Y., Asakawa, S., Minoshima, S., Shimizu, N., Iwai, K., Chiba, T., Tanaka, K., and Suzuki, T. (2000). Familial Parkinson disease gene product, parkin, is a ubiquitin-protein ligase. Nat Genet 25, 302-305.

Shimura, H., Hattori, N., Kubo, S., Yoshikawa, M., Kitada, T., Matsumine, H., Asakawa, S., Minoshima, S., Yamamura, Y., Shimizu, N., and Mizuno, Y. (1999). Immunohistochemical and subcellular localization of Parkin protein: absence of protein in autosomal recessive juvenile parkinsonism patients. Ann Neurol 45, 668-672.

Simon-Sanchez, J., Schulte, C., Bras, J.M., Sharma, M., Gibbs, J.R., Berg, D., Paisan-Ruiz, C., Lichtner, P., Scholz, S.W., Hernandez, D.G., et al. (2009). Genome-wide association study reveals genetic risk underlying Parkinson's disease. Nat Genet 41, 1308-1312.

Singleton, A., Gwinn-Hardy, K., Sharabi, Y., Li, S.T., Holmes, C., Dendi, R., Hardy, J., Crawley, A., and Goldstein, D.S. (2004). Association between cardiac denervation and parkinsonism caused by alpha-synuclein gene triplication. Brain 127, 768-772.

Smith, W.W., Pei, Z., Jiang, H., Dawson, V.L., Dawson, T.M., and Ross, C.A. (2006). Kinase activity of mutant LRRK2 mediates neuronal toxicity. Nat Neurosci 9, 1231-1233.

Smith, W.W., Pei, Z., Jiang, H., Moore, D.J., Liang, Y., West, A.B., Dawson, V.L., Dawson, T.M., and Ross, C.A. (2005). Leucine-rich repeat kinase 2 (LRRK2) interacts with parkin, and mutant LRRK2 induces neuronal degeneration. Proc Natl Acad Sci U S A 102, 18676-18681.

Soto, I., Oglesby, E., Buckingham, B.P., Son, J.L., Roberson, E.D., Steele, M.R., Inman, D.M., Vetter, M.L., Horner, P.J., and Marsh-Armstrong, N. (2008). Retinal ganglion cells downregulate gene expression and lose their axons within the optic nerve head in a mouse glaucoma model. J Neurosci 28, 548-561.

Specht, C.G., and Schoepfer, R. (2001). Deletion of the alpha-synuclein locus in a subpopulation of C57BL/6J inbred mice. BMC Neurosci 2, 11.

Spillantini, M.G., Crowther, R.A., Jakes, R., Cairns, N.J., Lantos, P.L., and Goedert, M. (1998a). Filamentous alpha-synuclein inclusions link multiple system atrophy with Parkinson's disease and dementia with Lewy bodies. Neurosci Lett 251, 205-208.

Spillantini, M.G., Crowther, R.A., Jakes, R., Hasegawa, M., and Goedert, M. (1998b). alpha-Synuclein in filamentous inclusions of Lewy bodies from Parkinson's disease and dementia with lewy bodies. Proc Natl Acad Sci U S A 95, 6469-6473.

Spillantini, M.G., Divane, A., and Goedert, M. (1995). Assignment of human alpha-synuclein (SNCA) and beta-synuclein (SNCB) genes to chromosomes 4q21 and 5q35. Genomics 27, 379-381.

Spillantini, M.G., Schmidt, M.L., Lee, V.M., Trojanowski, J.Q., Jakes, R., and Goedert, M. (1997). Alpha-synuclein in Lewy bodies. Nature 388, 839-840.

Sreedharan, J., Blair, I.P., Tripathi, V.B., Hu, X., Vance, C., Rogelj, B., Ackerley, S., Durnall, J.C., Williams, K.L., Buratti, E., et al. (2008). TDP-43 mutations in familial and sporadic amyotrophic lateral sclerosis. Science 319, 1668-1672.

Stewart, A.F., DO; William, J; Weiner, MD (2002). Parkinson's Disease: Diagnosis and Clinical Management (New York: Demos Medical Publishing).

Stichel, C.C., Zhu, X.R., Bader, V., Linnartz, B., Schmidt, S., and Lubbert, H. (2007). Mono- and double-mutant mouse models of Parkinson's disease display severe mitochondrial damage. Hum Mol Genet 16, 2377-2393.

Strong, M.J., Volkening, K., Hammond, R., Yang, W., Strong, W., Leystra-Lantz, C., and Shoesmith, C. (2007). TDP43 is a human low molecular weight neurofilament (hNFL) mRNA-binding protein. Mol Cell Neurosci 35, 320-327.

Sun, W., Funakoshi, H., and Nakamura, T. (2002). Overexpression of HGF retards disease progression and prolongs life span in a transgenic mouse model of ALS. J Neurosci 22, 6537-6548.

Sung, Y.H., and Eliezer, D. (2007). Residual structure, backbone dynamics, and interactions within the synuclein family. J Mol Biol 372, 689-707.

Surgucheva, I., McMahan, B., Ahmed, F., Tomarev, S., Wax, M.B., and Surguchov, A. (2002). Synucleins in glaucoma: implication of gamma-synuclein in glaucomatous alterations in the optic nerve. J Neurosci Res 68, 97-106.

Theys, P.A., Peeters, E., and Robberecht, W. (1999). Evolution of motor and sensory deficits in amyotrophic lateral sclerosis estimated by neurophysiological techniques. J Neurol 246, 438-442.

Thiruchelvam, M.J., Powers, J.M., Cory-Slechta, D.A., and Richfield, E.K. (2004). Risk factors for dopaminergic neuron loss in human alpha-synuclein transgenic mice. Eur J Neurosci 19, 845-854.

Thomas, K.J., McCoy, M.K., Blackinton, J., Beilina, A., van der Brug, M., Sandebring, A., Miller, D., Maric, D., Cedazo-Minguez, A., and Cookson, M.R. (2010). DJ-1 acts in parallel to the PINK1/parkin pathway to control mitochondrial function and autophagy. Hum Mol Genet 20, 40-50.

Tobaben, S., Thakur, P., Fernandez-Chacon, R., Sudhof, T.C., Rettig, J., and Stahl, B. (2001). A trimeric protein complex functions as a synaptic chaperone machine. Neuron 31, 987-999.

Tomkins, J., Usher, P., Slade, J.Y., Ince, P.G., Curtis, A., Bushby, K., and Shaw, P.J. (1998). Novel insertion in the KSP region of the neurofilament heavy gene in amyotrophic lateral sclerosis (ALS). Neuroreport 9, 3967-3970.

Tompkins, M.M., and Hill, W.D. (1997). Contribution of somal Lewy bodies to neuronal death. Brain Res 775, 24-29.

Tong, Y., Pisani, A., Martella, G., Karouani, M., Yamaguchi, H., Pothos, E.N., and Shen, J. (2009). R1441C mutation in LRRK2 impairs dopaminergic neurotransmission in mice. Proc Natl Acad Sci U S A 106, 14622-14627.

Tong, Y., Yamaguchi, H., Giaime, E., Boyle, S., Kopan, R., Kelleher, R.J., 3rd, and Shen, J. (2010). Loss of leucine-rich repeat kinase 2 causes impairment of protein degradation pathways, accumulation of alpha-synuclein, and apoptotic cell death in aged mice. Proc Natl Acad Sci U S A 107, 9879-9884.

Touchman, J.W., Dehejia, A., Chiba-Falek, O., Cabin, D.E., Schwartz, J.R., Orrison, B.M., Polymeropoulos, M.H., and Nussbaum, R.L. (2001). Human and mouse alpha-synuclein genes: comparative genomic sequence analysis and identification of a novel gene regulatory element. Genome Res 11, 78-86.

Trimarchi, J.M., Stadler, M.B., Roska, B., Billings, N., Sun, B., Bartch, B., and Cepko, C.L. (2007). Molecular heterogeneity of developing retinal ganglion and amacrine cells revealed through single cell gene expression profiling. J Comp Neurol 502, 1047-1065.

Tsigelny, I.F., Bar-On, P., Sharikov, Y., Crews, L., Hashimoto, M., Miller, M.A., Keller, S.H., Platoshyn, O., Yuan, J.X., and Masliah, E. (2007). Dynamics of alpha-synuclein aggregation and inhibition of pore-like oligomer development by beta-synuclein. FEBS J 274, 1862-1877.

Tu, P.H., Galvin, J.E., Baba, M., Giasson, B., Tomita, T., Leight, S., Nakajo, S., Iwatsubo, T., Trojanowski, J.Q., and Lee, V.M. (1998). Glial cytoplasmic inclusions in white matter oligodendrocytes of multiple system atrophy brains contain insoluble alpha-synuclein. Ann Neurol 44, 415-422.

Ueda, K., Fukushima, H., Masliah, E., Xia, Y., Iwai, A., Yoshimoto, M., Otero, D.A., Kondo, J., Ihara, Y., and Saitoh, T. (1993). Molecular cloning of cDNA encoding an unrecognized component of amyloid in Alzheimer disease. Proc Natl Acad Sci U S A 90, 11282-11286.

Uversky, V.N., Li, J., and Fink, A.L. (2001). Metal-triggered structural transformations, aggregation, and fibrillation of human alpha-synuclein. A possible molecular NK between Parkinson's disease and heavy metal exposure. J Biol Chem 276, 44284-44296.

Uversky, V.N., Li, J., Souillac, P., Millett, I.S., Doniach, S., Jakes, R., Goedert, M., and Fink, A.L. (2002). Biophysical properties of the synucleins and their propensities to fibrillate: inhibition of alpha-synuclein assembly by beta- and gamma-synucleins. J Biol Chem 277, 11970-11978.

Valente, E.M., Abou-Sleiman, P.M., Caputo, V., Muqit, M.M., Harvey, K., Gispert, S., Ali, Z., Del Turco, D., Bentivoglio, A.R., Healy, D.G., et al. (2004). Hereditary early-onset Parkinson's disease caused by mutations in PINK1. Science 304, 1158-1160.

Valentine, J.S., Doucette, P.A., and Zittin Potter, S. (2005). Copper-zinc superoxide dismutase and amyotrophic lateral sclerosis. Annu Rev Biochem 74, 563-593.

van der Putten, H., Wiederhold, K.H., Probst, A., Barbieri, S., Mistl, C., Danner, S., Kauffmann, S., Hofele, K., Spooren, W.P., Ruegg, M.A., et al. (2000). Neuropathology in mice expressing human alpha-synuclein. J Neurosci 20, 6021-6029.

van Dongen, P.A. (1981). The human locus coeruleus in neurology and psychiatry. (Parkinson's, Lewy body, Hallervorden-Spatz, Alzheimer's and Korsakoff's disease, (pre)senile dementia, schizophrenia, affective disorders, psychosis). Prog Neurobiol 17, 97-139.

van Es, M.A., Veldink, J.H., Saris, C.G., Blauw, H.M., van Vught, P.W., Birve, A., Lemmens, R., Schelhaas, H.J., Groen, E.J., Huisman, M.H., et al. (2009). Genome-wide association study identifies 19p13.3 (UNC13A) and 9p21.2 as susceptibility loci for sporadic amyotrophic lateral sclerosis. Nat Genet 41, 1083-1087.

Vance, C., Rogelj, B., Hortobagyi, T., De Vos, K.J., Nishimura, A.L., Sreedharan, J., Hu, X., Smith, B., Ruddy, D., Wright, P., et al. (2009). Mutations in FUS, an RNA processing protein, cause familial amyotrophic lateral sclerosis type 6. Science 323, 1208-1211.

Voges, D., Zwickl, P., and Baumeister, W. (1999). The 26S proteasome: a molecular machine designed for controlled proteolysis. Annu Rev Biochem 68, 1015-1068.

Volkening, K., Leystra-Lantz, C., Yang, W., Jaffee, H., and Strong, M.J. (2009). Tar DNA binding protein of 43 kDa (TDP-43), 14-3-3 proteins and copper/zinc superoxide dismutase (SOD1) interact to modulate NFL mRNA stability. Implications for altered RNA processing in amyotrophic lateral sclerosis (ALS). Brain Res 1305, 168-182.

Volles, M.J., Lee, S.J., Rochet, J.C., Shtilerman, M.D., Ding, T.T., Kessler, J.C., and Lansbury, P.T., Jr. (2001). Vesicle permeabilization by protofibrillar alpha-synuclein: implications for the pathogenesis and treatment of Parkinson's disease. Biochemistry 40, 7812-7819.

Von Coelln, R., Thomas, B., Savitt, J.M., Lim, K.L., Sasaki, M., Hess, E.J., Dawson, V.L., and Dawson, T.M. (2004). Loss of locus coeruleus neurons and reduced startle in parkin null mice. Proc Natl Acad Sci U S A 101, 10744-10749.

Vyas, I., Heikkila, R.E., and Nicklas, W.J. (1986). Studies on the neurotoxicity of 1-methyl-4-phenyl-1,2,3,6-tetrahydropyridine: inhibition of NAD-linked substrate oxidation by its metabolite, 1-methyl-4-phenylpyridinium. J Neurochem 46, 1501-1507.

Wakabayashi, K., Yoshimoto, M., Fukushima, T., Koide, R., Horikawa, Y., Morita, T., and Takahashi, H. (1999). Widespread occurrence of alpha-synuclein/NACP-immunoreactive neuronal inclusions in juvenile and adult-onset Hallervorden-Spatz disease with Lewy bodies. Neuropathol Appl Neurobiol 25, 363-368.

Wang, Y.L., Takeda, A., Osaka, H., Hara, Y., Furuta, A., Setsuie, R., Sun, Y.J., Kwon, J., Sato, Y., Sakurai, M., et al. (2004). Accumulation of beta- and gamma-synucleins in the ubiquitin carboxyl-terminal hydrolase L1-deficient gad mouse. Brain Res 1019, 1-9.

Waterman-Storer, C.M., Karki, S.B., Kuznetsov, S.A., Tabb, J.S., Weiss, D.G., Langford, G.M., and Holzbaur, E.L. (1997). The interaction between cytoplasmic dynein and dynactin is required for fast axonal transport. Proc Natl Acad Sci U S A 94, 12180-12185.

Wegorzewska, I., Bell, S., Cairns, N.J., Miller, T.M., and Baloh, R.H. (2009). TDP-43 mutant transgenic mice develop features of ALS and frontotemporal lobar degeneration. Proc Natl Acad Sci U S A 106, 18809-18814.

Wei, J., Fujita, M., Nakai, M., Waragai, M., Watabe, K., Akatsu, H., Rockenstein, E., Masliah, E., and Hashimoto, M. (2007). Enhanced lysosomal pathology caused by beta-synuclein mutants linked to dementia with Lewy bodies. J Biol Chem 282, 28904-28914.

Weinreb, P.H., Zhen, W., Poon, A.W., Conway, K.A., and Lansbury, P.T., Jr. (1996). NACP, a protein implicated in Alzheimer's disease and learning, is natively unfolded. Biochemistry 35, 13709-13715.
Weser, U., Miesel, R., and Hartmann, H.J. (1989). Mummified enzymes. Nature 341, 696.

West, A.B., Moore, D.J., Choi, C., Andrabi, S.A., Li, X., Dikeman, D., Biskup, S., Zhang, Z., Lim, K.L., Dawson, V.L., and Dawson, T.M. (2007). Parkinson's disease-associated mutations in LRRK2 link enhanced GTP-binding and kinase activities to neuronal toxicity. Hum Mol Genet 16, 223-232.

Wijesekera, L.C., and Leigh, P.N. (2009). Amyotrophic lateral sclerosis. Orphanet J Rare Dis 4, 3.

Wilkinson, K.D., Lee, K.M., Deshpande, S., Duerksen-Hughes, P., Boss, J.M., and Pohl, J. (1989). The neuron-specific protein PGP 9.5 is a ubiquitin carboxyl-terminal hydrolase. Science 246, 670-673.

Williamson, T.L., and Cleveland, D.W. (1999). Slowing of axonal transport is a very early event in the toxicity of ALS-linked SOD1 mutants to motor neurons. Nat Neurosci 2, 50-56.

Wils, H., Kleinberger, G., Janssens, J., Pereson, S., Joris, G., Cuijt, I., Smits, V., Ceuterick-de Groote, C., Van Broeckhoven, C., and Kumar-Singh, S. (2010). TDP-43 transgenic mice develop spastic paralysis and neuronal inclusions characteristic of ALS and frontotemporal lobar degeneration. Proc Natl Acad Sci U S A 107, 3858-3863.

Wilson, P.O., Barber, P.C., Hamid, Q.A., Power, B.F., Dhillon, A.P., Rode, J., Day, I.N., Thompson, R.J., and Polak, J.M. (1988). The immunolocalization of protein gene product 9.5 using rabbit polyclonal and mouse monoclonal antibodies. Br J Exp Pathol 69, 91-104.

Wintermeyer, P., Kruger, R., Kuhn, W., Muller, T., Woitalla, D., Berg, D., Becker, G., Leroy, E., Polymeropoulos, M., Berger, K., et al. (2000). Mutation analysis and association studies of the UCHL1 gene in German Parkinson's disease patients. Neuroreport 11, 2079-2082.

Wong, P.C., Marszalek, J., Crawford, T.O., Xu, Z., Hsieh, S.T., Griffin, J.W., and Cleveland, D.W. (1995a). Increasing neurofilament subunit NF-M expression reduces axonal NF-H, inhibits radial growth, and results in neurofilamentous accumulation in motor neurons. J Cell Biol 130, 1413-1422.

Wong, P.C., Pardo, C.A., Borchelt, D.R., Lee, M.K., Copeland, N.G., Jenkins, N.A., Sisodia, S.S., Cleveland, D.W., and Price, D.L. (1995b). An adverse property of a familial ALS-linked SOD1 mutation causes motor neuron disease characterized by vacuolar degeneration of mitochondria. Neuron 14, 1105-1116.

Worms, P.M. (2001). The epidemiology of motor neuron diseases: a review of recent studies. J Neurol Sci 191, 3-9.

Wu, J., Ichihara, N., Chui, D.H., Yamazaki, K., and Kikuchi, T. (1995). [Ubiquitin immunoreactivity in the central nervous system of gracile axonal dystrophy (GAD) mouse]. No To Shinkei 47, 881-885.

Xu, Z., Cork, L.C., Griffin, J.W., and Cleveland, D.W. (1993). Increased expression of neurofilament subunit NF-L produces morphological alterations that resemble the pathology of human motor neuron disease. Cell 73, 23-33.

Yamazaki, K., Wakasugi, N., Tomita, T., Kikuchi, T., Mukoyama, M., and Ando, K. (1988). Gracile axonal dystrophy (GAD), a new neurological mutant in the mouse. Proc Soc Exp Biol Med 187, 209-215.

Yang, Y., Hentati, A., Deng, H.X., Dabbagh, O., Sasaki, T., Hirano, M., Hung, W.Y., Ouahchi, K., Yan, J., Azim, A.C., et al. (2001). The gene encoding alsin, a protein with three guanine-nucleotide exchange factor domains, is mutated in a form of recessive amyotrophic lateral sclerosis. Nat Genet 29, 160-165.

Zang, D.W., Yang, Q., Wang, H.X., Egan, G., Lopes, E.C., and Cheema, S.S. (2004). Magnetic resonance imaging reveals neuronal degeneration in the brainstem of the superoxide dismutase 1 transgenic mouse model of amyotrophic lateral sclerosis. Eur J Neurosci 20, 1745-1751.

Zarranz, J.J., Alegre, J., Gomez-Esteban, J.C., Lezcano, E., Ros, R., Ampuero, I., Vidal, L., Hoenicka, J., Rodriguez, O., Atares, B., et al. (2004). The new mutation, E46K, of alpha-synuclein causes Parkinson and Lewy body dementia. Ann Neurol 55, 164-173.

Zeng, B.Y., Bukhatwa, S., Hikima, A., Rose, S., and Jenner, P. (2006). Reproducible nigral cell loss after systemic proteasomal inhibitor administration to rats. Ann Neurol 60, 248-252.

Zhang, B., Tu, P., Abtahian, F., Trojanowski, J.Q., and Lee, V.M. (1997). Neurofilaments and orthograde transport are reduced in ventral root axons of transgenic mice that express human SOD1 with a G93A mutation. J Cell Biol 139, 1307-1315.

Zhu, Q., Couillard-Despres, S., and Julien, J.P. (1997). Delayed maturation of regenerating myelinated axons in mice lacking neurofilaments. Exp Neurol 148, 299-316.

Zimprich, A., Biskup, S., Leitner, P., Lichtner, P., Farrer, M., Lincoln, S., Kachergus, J., Hulihan, M., Uitti, R.J., Calne, D.B., et al. (2004). Mutations in LRRK2 cause autosomal-dominant parkinsonism with pleomorphic pathology. Neuron 44, 601-607.

Human Molecular Genetics, 2009, Vol. 18, No. 10 **1779–1794**
doi:10.1093/hmg/ddp090
Advance Access published on February 26, 2009

γ-Synucleinopathy: neurodegeneration associated with overexpression of the mouse protein

Natalia Ninkina[1], Owen Peters[1], Steven Millership[1], Hatem Salem[1], Herman van der Putten[2] and Vladimir L. Buchman[1,*]

[1]School of Biosciences, Cardiff University, Museum Avenue, Cardiff CF10 3AX, UK and [2]Neuroscience, Novartis Institutes for Biomedical Research, Novartis AG CH-4002, Basel, Switzerland

Received January 8, 2009; Revised February 12, 2009; Accepted February 20, 2009

The role of α-synuclein in pathogenesis of familial and idiopathic forms of Parkinson's disease, and other human disorders known as α-synucleinopathies, is well established. In contrast, the involvement of two other members of the synuclein family, β-synuclein and γ-synuclein, in the development and progression of neurodegeneration is poorly studied. However, there is a growing body of evidence that α-synuclein and β-synuclein have opposite neuropathophysiological effects. Unlike α-synuclein, overexpressed β-synuclein does not cause pathological changes in the nervous system of transgenic mice and even ameliorates the pathology caused by overexpressed α-synuclein. To assess the consequences of excess expression of the third family member, γ-synuclein, on the nervous system we generated transgenic mice expressing high levels of mouse γ-synuclein under control of Thy-1 promoter. These animals develop severe age- and transgene dose-dependent neuropathology, motor deficits and die prematurely. Histopathological changes include aggregation of γ-synuclein, accumulation of various inclusions in neuronal cell bodies and processes, and astrogliosis. These changes are seen throughout the nervous system but are most prominent in the spinal cord where they lead to loss of spinal motor neurons. Our data suggest that down-regulation of small heat shock protein HSPB1 and disintegration of neurofilament network play a role in motor neurons dysfunction and death. These findings demonstrate that γ-synuclein can be involved in neuropathophysiological changes and the death of susceptible neurons suggesting the necessity of further investigations of the potential role of this synuclein in disease.

INTRODUCTION

The importance of α-synuclein in the development and progression of the human disorders known as synucleinopathies is beyond doubt although the exact mechanism of neurodegeneration induced by dysfunction of this protein is the subject of heated debate [for recent reviews see Ref. (1)]. On the other hand, β-synuclein is believed to be a neuroprotective factor—in several experimental *in vivo* systems, expression of this protein ameliorated neuronal pathology caused by overexpression of α-synuclein (2–7).

Despite limited information, certain known properties of γ-synuclein place it structurally and functionally in between the other two members of the synuclein family. For instance, γ-synuclein adopts a free-state residual secondary structure similar to α-synuclein whereas in an extended mode its structure resembles β-synuclein (8). These structural differences correlate with different propensities of the synucleins to aggregate. Aggregation of α-synuclein *in vivo* is believed to be a crucial event in pathogenesis of these diseases, with intermediates (i.e. soluble oligomers) and final products (i.e. larger, insoluble and immunohistochemically detectable aggregates) playing different but equally important roles (1,9,10). Conversely, a protective function of β-synuclein seems to correlate with its negligible propensity to aggregate and its ability to retard the aggregation of α-synuclein *in vitro* (2,11–13). γ-Synuclein is able, albeit less efficiently than α-synuclein, to aggregate and form fibrils *in vitro*. However, like

*To whom correspondence should be addressed at: Cardiff University, Museum Avenue, Cardiff, CF10 3AX, UK. Tel: +44 2920879068; Fax: +44 2920874116; Email: buchmanvl@cardiff.ac.uk

β-synuclein, it has also been shown to inhibit the aggregation of α-synuclein (11,12). In contrast to α-synuclein, acute overexpression of γ-synuclein does not induce death of cultured neurons but perturbs their neurofilament network by an unknown mechanism (14,15).

While α-synuclein is the major component of Lewy bodies and other histopathological hallmarks of synucleinopathies, neither β-synuclein nor γ-synuclein have been found in these structures. Nonetheless, changes in their expression or distribution (16–18) and accumulation of these proteins in unconventional histopathological lesions within neurons and axons (Refs 19–21 and our unpublished observations) have been observed in several human neurodegenerative disorders as well as certain transgenic or pharmacological animal models of neurodegeneration (16,22–26). Therefore, it is tempting to speculate that accumulation and aggregation of γ-synuclein might be a causative factor in the development of certain, yet to be identified, types of neurological disorders.

To test whether increased and/or ectopic expression of mouse γ-synuclein could trigger neurohistopathological changes and phenotypes typical for synucleinopathies, we produced transgenic mice with pan-neuronal overexpression of this protein. Animals expressing high levels of γ-synuclein develop severe and fatal neurological disease associated with aggregation of the overexpressed protein and its deposition in cytoplasmic and axonal lesions.

RESULTS

Production of transgenic animals and analysis of transgene expression

Transgenic mice expressing elevated levels of mouse wild-type γ-synuclein were generated using the Thy-1 neuron-specific expression cassette (Fig. 1A) that we and others have used previously for generating lines expressing high levels of either α-synuclein (27–30) or β-synuclein (5). Mice from one line, Thy1mγSN, expressed high levels of mouse γ-synuclein throughout the nervous system and developed an age-dependent neurological phenotype. Mice of a second line with lower levels of the transgene expression did not develop a noticeable phenotype and were excluded from this study.

Transgenic mice were produced on a pure genetic background and the colony was maintained by backcrossing hemizygous Thy1mγSN mice with C57Bl6 mice. These hemizygous animals were indistinguishable from their wild-type littermates during the first year of their life. Later most of these mice developed a clasping reflex, abnormal posture and gait, as well as other signs of motor dysfunction (see below). In an attempt to augment the pathology we bred Thy1mγSN mice to homozygosity. This resulted in an approximate doubling of the transgene expression levels, which in dorsal root ganglia (DRG) of 12-month-old mice reached the level that was approximately seven times higher than the level of endogenous γ-synuclein mRNA in these ganglia (Fig. 1B). Offspring from intercrosses of hemizygous parents showed a normal Mendelian distribution of genotypes. Homozygous animals appeared normal during the first few months of life despite a very high level of γ-synuclein mRNA expression throughout their nervous system. For instance, in the spinal cord of young adult homozygous transgenic animals, the level of this mRNA was approximately 16 times higher than in the trigeminal ganglion of wild-type mice that was used for reference due to the high endogenous level of γ-synuclein mRNA expression and homogeneity of cell population in this structure (Fig. 1B, top panel). In the spinal cord of wild-type animals, only motor neurons express γ-synuclein (31), but in Thy1mγSN mice, motorneurons and additional types of spinal neurons expressed γ-synuclein, which explains, in part, the robust increase of both γ-synuclein mRNA (Fig. 1B, bottom panel) and protein (Fig. 1C and D) levels. The same applied to other regions (Fig. 1D and data not shown) where endogeneous γ-synuclein expression is restricted to certain neuronal populations (32) but the transgene is expressed in the majority of neurons. Substantial accumulation of γ-synuclein did not affect the levels of expression of the other two members of synuclein family (Fig. 1D).

Overexpression of γ-synuclein is associated with a severe neurological phenotype and early lethality of transgenic mice

The health of homozygous animals started to deteriorate substantially from the age of 6–9 months. The first signs of pathology were similar to those observed in the older hemizygous mice, including clasping reflex, hunchback posture and abnormal gait (Fig. 2A–C and Supplementary Material movie). In contrast to hemizygous animals, clinical signs of pathology in homozygous animals progressed rapidly with all animals developing pareses of their limbs by the age of 9–16 months followed by paralyses and loss of the righting reflex (Fig. 2D). At this stage, the animals were sacrificed to prevent further suffering. Typically, the paraparesis of the forelimbs became obvious earlier than that of the hindlimbs. Lifespan of homozygous transgenic mice was also limited; not a single mouse survived beyond the age of 16 months in two independent cohorts (total 74 mice) housed in two animal facilities (Fig. 2E).

The onset and progression of motor dysfunction was quantified using several different tests. Balance and coordination were already significantly impeded in homozygous Thy1mγSN mice younger than 6 months before they displayed obvious clinical signs of pathology (Fig. 3 and Supplementary Material Tables S1 and S2). Their ability to turn on an 11 mm diameter beam and their performance on a constant speed rotarod were both compromised by the age of 4 months (Fig. 3A and Supplementary Material Table S1). Using the accelerating rotarod test, it was possible to demonstrate motor impairments as early as at 2 months of age. At this time point the homozygous Thy1mγSN mice were indistinguishable from wild-type mice by any other criteria examined (Fig. 3B). Hemizygous Thy1mγSN mice developed a similar motor dysfunction but with a much greater latency and slower progression. This is exemplified by their performance on the rotarod that only declined significantly after the age of 18 months (Fig. 3). In the footprint test, the length of stride of hemizygous 18-month-old animals was significantly shorter than that of their wild-type littermates, while

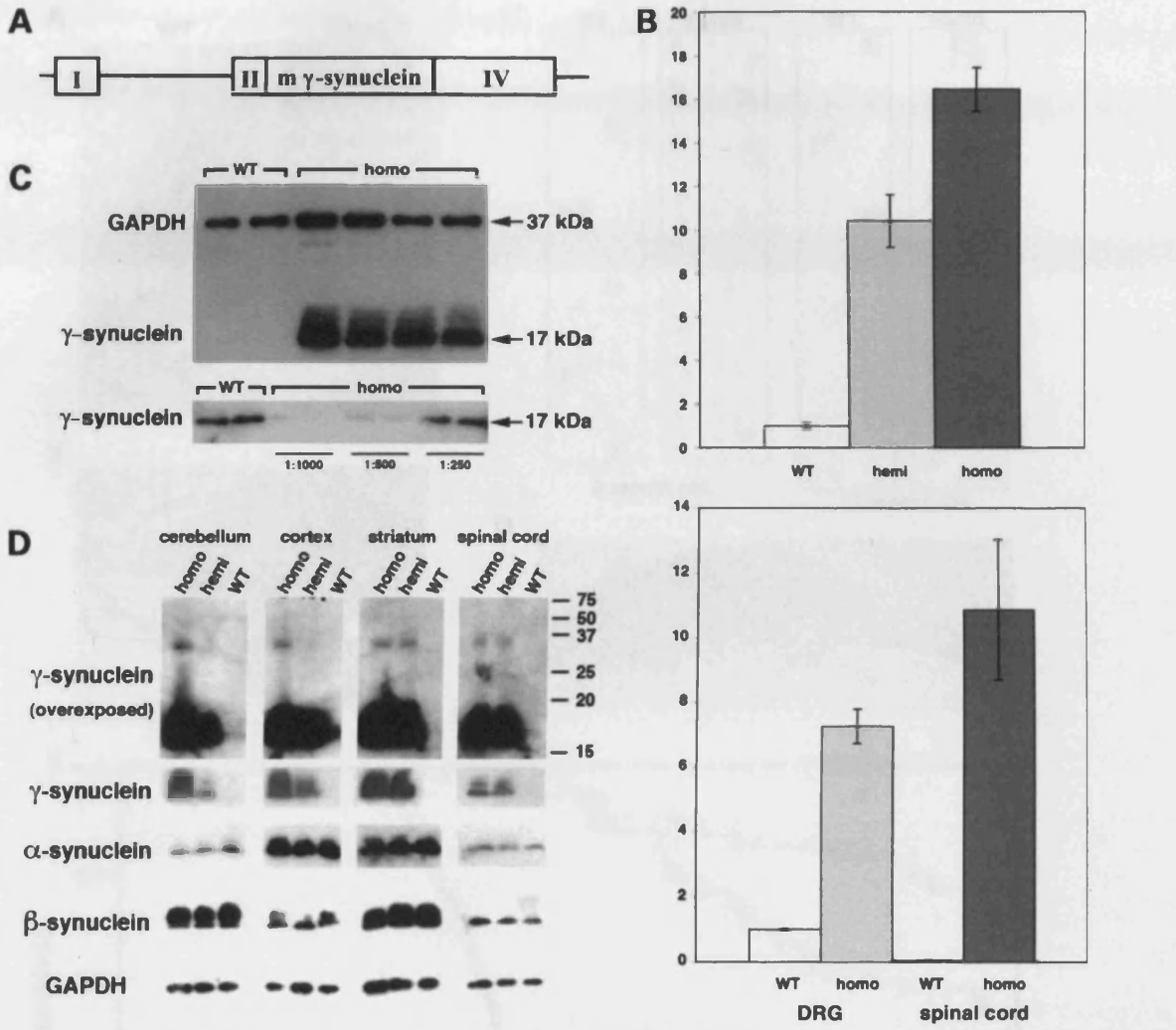

Figure 1. Expression of γ-synuclein in wild-type and transgenic mice. (**A**) A map of DNA fragment used for producing transgenic animals. A mouse γ-synuclein cDNA fragment was inserted between exons II and IV of the mouse Thy-1 gene. (**B**) Expression of γ-synuclein mRNA in neuronal tissues of wild-type and transgenic animals measured by quantitative real-time RT–PCR. Bar charts show the fold γ-synuclein mRNA level increase (mean ± SEM) in the spinal cord of homozygous and heterozygous 8-week-old Thy1mγSN mice compared with the level in the trigeminal ganglion of newborn wild-type mice (top chart) and in the DRG and spinal cord of homozygous 12-month-old Thy1mγSN mice compared with the level in the DRG of 12-month-old wild-type mice (bottom chart). (**C**) Western blot analysis of γ-synuclein in the spinal cord of 1-year-old wild-type and homozygous Thy1mγSN animals. The top panel shows a normalization western blot simultaneously probed with antibodies against GAPDH and γ-synuclein. The same undiluted wild-type samples and 1:1000, 1:500 or 1:250 diluted transgenic samples were analysed on a western blot shown in the bottom panel. (**D**) Western blot analysis of three synucleins in the spinal cord and brain regions of 1-year-old wild-type and Thy1mγSN transgenic (hemi- and homozygous) animals. More γ-synuclein accumulates in neuronal tissues of homozygous than hemizygous mice but a ladder of multimeric γ-synuclein-positive bands is not observed even on overexposed western blots (top panels).

homozygous mice already showed this impairment at the age of 6 months (Supplementary Material Fig. S1 and data not shown). The horizontal beam test was most sensitive for detecting early signs of motor deficit in hemizigous Thy1mγSN animals; their ability to perform both parts of the task was already obviously compromised at the age of 12 months (Supplementary Material Tables 1 and 2).

In summary, pan-neuronal overexpression of mouse γ-synuclein in transgenic mice was associated with a progressive age- and gene dose-dependent motor phenotype that recapitulates phenotypes described earlier for several lines expressing human α-synuclein under control of the same Thy-1 promoter or other pan-neuronal promoters (27,30,33–39).

Aggregation and fibrillation of γ-synuclein in the nervous system of transgenic mice

It was feasible to suggest that pathological changes in the nervous system of Thy1mγSN transgenic mice would also be similar to the changes observed in the nervous system of

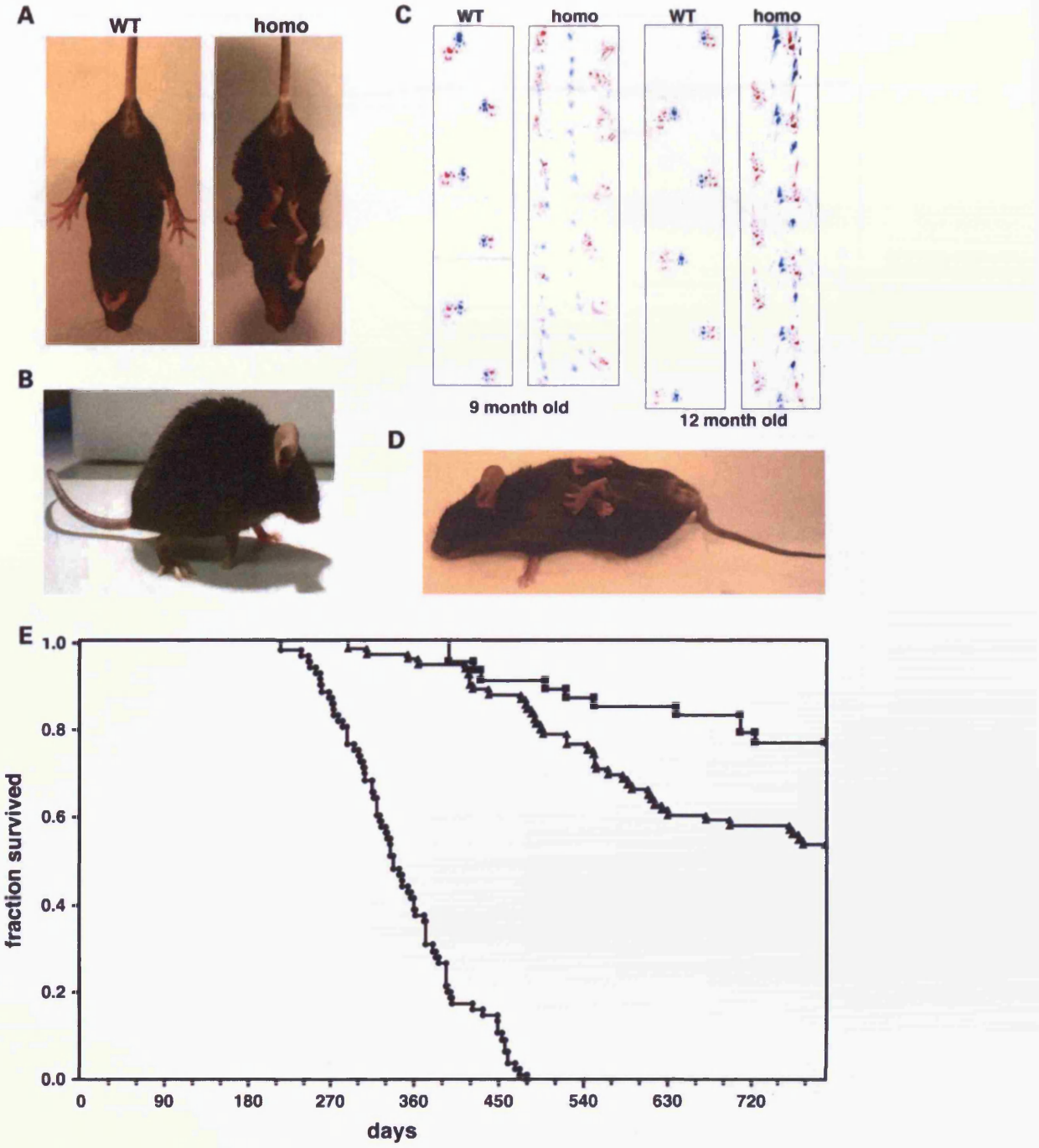

Figure 2. Transgenic animals develop pathology that leads to premature death. Typical appearance of Thy1mγSN transgenic mice at the initial stage of pathology development with clasping of all limbs when hanging by the tail (**A**) and a hunchback posture (**B**). Examples of severe gait abnormality in 9- and 12-month-old homozygous γ-synuclein transgenic mice detected by the footprint test. Forefeet prints are blue and hindfeet prints are red (**C**). At the advanced stage of pathology, the righting reflex is substantially impaired (**D**). Kaplan–Meier plot of wild-type (squares, $n = 49$), hemizygous Thy1mγSN (triangles, $n = 87$) and homozygous Thy1mγSN (circles, $n = 74$) mice survival over the 26 months period (**E**).

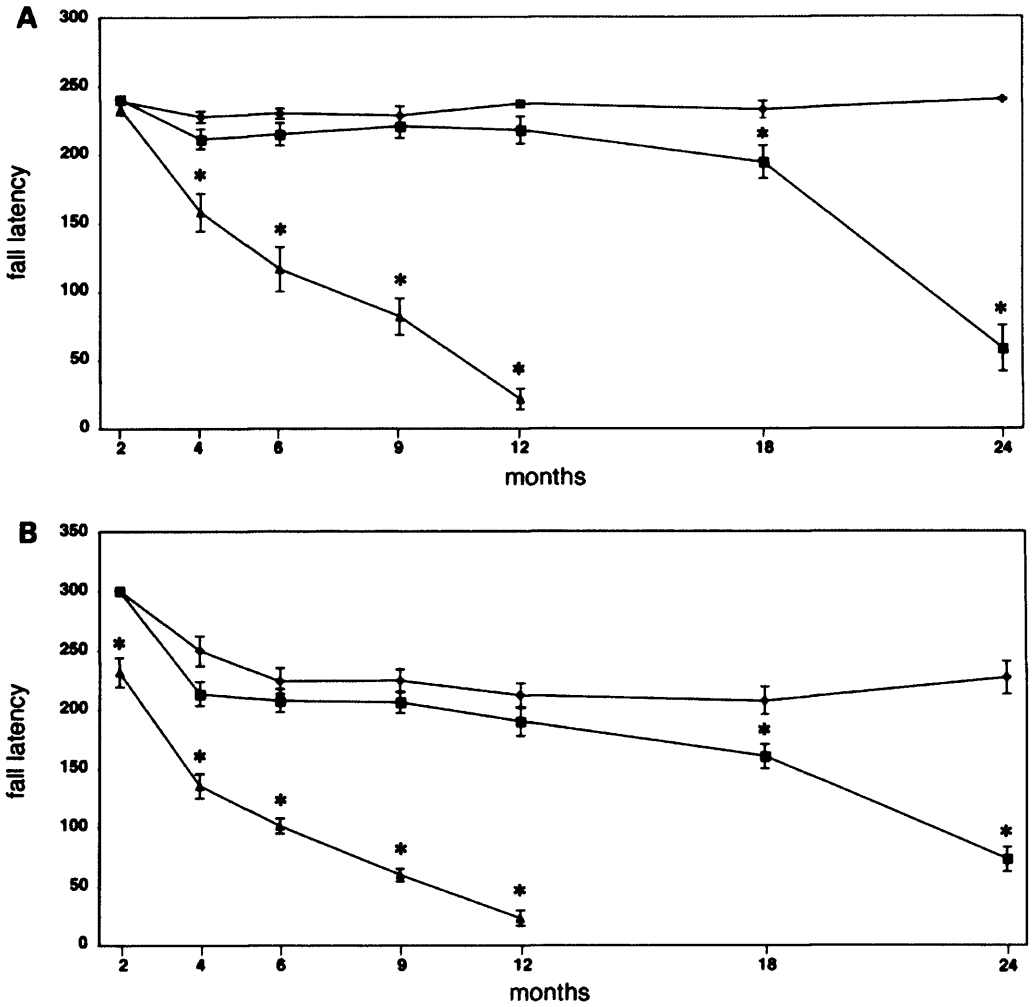

Figure 3. Rotarod performance of γ-synuclein transgenic mice. Groups of mice of different ages and genotypes were tested on Ugo Basile rotarod using constant speed (**A**) or accelerating (**B**) modes as described in Material and methods. Line graphs show mean ± SEM of latency to fall for wild-type (diamonds), hemizygous Thy1mγSN (squares) and homozygous (triangles) Thy1mγSN mice at different age. Statistically significant difference ($P < 0.01$, Student's *t*-test) in performance between transgenic and wild type groups at particular age is denoted by asterisks.

α-synuclein transgenic animals and might be accompanied by aggregation of γ-synuclein in neurons and their processes. Therefore, we looked for signs of γ-synuclein aggregation throughout the nervous system of homozygous Thy1mγSN mice that developed obvious pathology.

Immunohistochemical analysis of Thy1mγSN brain and spinal cord sections stained with highly specific SK23 antibody (31) revealed increased production of γ-synuclein in many neurons expressing endogenous γ-synuclein as well as ectopic production in other neurons normally devoid of this protein. In contrast to the predominantly neuritic localization of endogenous γ-synuclein in the brain of adult wild-type mice (32), overproduced protein also accumulated in the neuronal cell bodies (Supplementary Material Fig. S2). Although immunostaining in the majority of transgenic mouse brain neurons was diffusely distributed throughout the cytoplasm, in subsets of neurons, we detected γ-synuclein-positive cytoplasmic inclusions which, in some cases, were clearly eosinophilic and also showed some remarkable resemblance to the α-synuclein-positive structures seen in Lewy body diseases (Fig. 4A and Supplementary Material Fig. S2D and E). However, much more typical was the presence of γ-synuclein-positive spheroids and dystrophic neurites (Fig. 4A and Supplementary Material Fig. 2D and E) that were not seen in the nervous system of wild-type littermates (Fig. 4A and data not shown).

These abnormal structures were observed throughout the nervous system but were most abundant in the spinal cord (Fig. 4A), which is consistent with the observed clinical pattern of pathology. Therefore, the spinal cord was used to determine whether aggregated and fibrillated forms of γ-synuclein were present in neuronal tissues of animals overexpressing this protein. Sequential fractionation of the spinal cord tissues demonstrated that, in contrast to endogenous

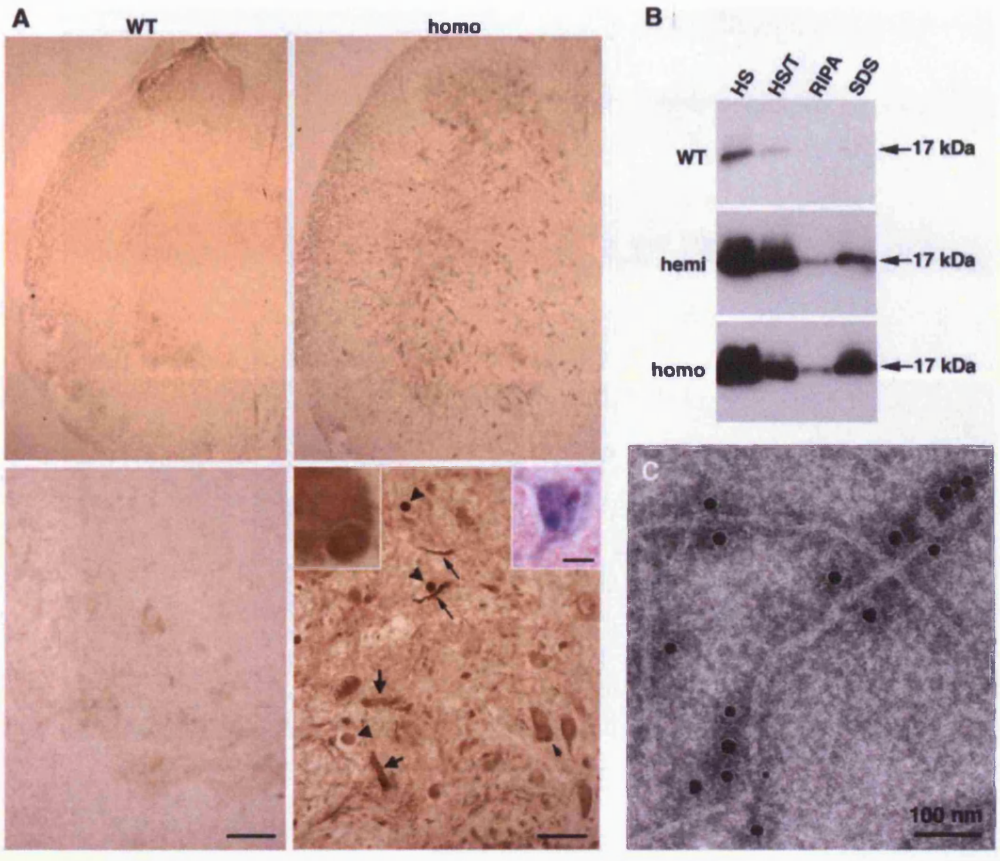

Figure 4. γ-Synuclein-positive aggregates and fibrils in the spinal cord of 12-month-old transgenic mice detected by anti-mouse γ-synuclein SK23 antibody. (**A**) Immunostained transverse sections through the spinal cord of wild-type and homozygous γ-synuclein transgenic mice. Higher magnification images of the ventral horn region are shown on lower panels, scale bars = 50 μm. A γ-synuclein-positive cytoplasmic inclusion (further magnified in the left inset) is indicated by the small arrowheads, spheroids by large arrowheads, dystrophic and ballooned neurites by small and large arrows, correspondingly. The right insert shows a hematoxylin and eosin-stained spinal cord motor neuron with an eosinophilic cytoplasmic inclusion, scale bar = 20 μm. (**B**) Western blot analysis of γ-synuclein in high salt (HS), HS/Triton X-100 (HS/T), RIPA- and SDS-soluble fractions of the spinal cord of wild-type, hemizygous and homozygous mice. (**C**) Immuno-electron microscopy detection of γ-synuclein fibrils in a sarcosyl-insoluble fraction of the homozygous Thy1mγSN mouse spinal cord.

γ-synuclein, which was completely soluble in salt/non-ionic detergent buffers, a substantial fraction of γ-synuclein in the spinal cord of Thy1mγSN mice remained insoluble after extraction with these solutions but could be partially solubilized in the ionic detergent-containing buffers (Fig. 4B) or in formic acid (data not shown). Immuno-electron microscopy of sarcosyl-insoluble material revealed the presence of filaments decorated with antibody against γ-synuclein (Fig. 4C). These results demonstrate that increased expression of γ-synuclein in mouse neurons can cause aggregation and fibrillation of this protein followed by formation of large intracellular inclusions.

Histopathology in the spinal cord of transgenic mice

Amyloid-like inclusions were detected by Congo Red (Fig. 5B–D) or thioflavine S (data not shown) staining of spinal cord or brain tissue of hemi- and homozygous mice, even at a stage when clinical signs of pathology were mild (only clasping reflex). The number of the Congo Red-positive inclusions substantially increased as disease progressed (Fig. 5E).

Neuronal degeneration is commonly associated with the activation of microglia and astroglia in affected regions of the nervous system. A large number of GFAP-positive cells with morphology typical for activated astrocytes were found in the spinal cord gray matter of severely affected homozygous Thy1mγSN mice (Fig. 6A). The level of GFAP was also substantially increased in the spinal cord tissue of homozygous and, to a lesser extent, age-matched hemizygous animals without obvious signs of pathology (Fig. 6B) but not in the spinal cord of young homozygous mice. However, using antibodies against two different markers, Iba1 and CD11b, we failed to detect clear signs of microglia activation (data not shown).

Another common feature of synucleinopathies is the presence of ubiquitin-positive inclusions in affected regions of the nervous system. In the spinal cord of γ-synuclein

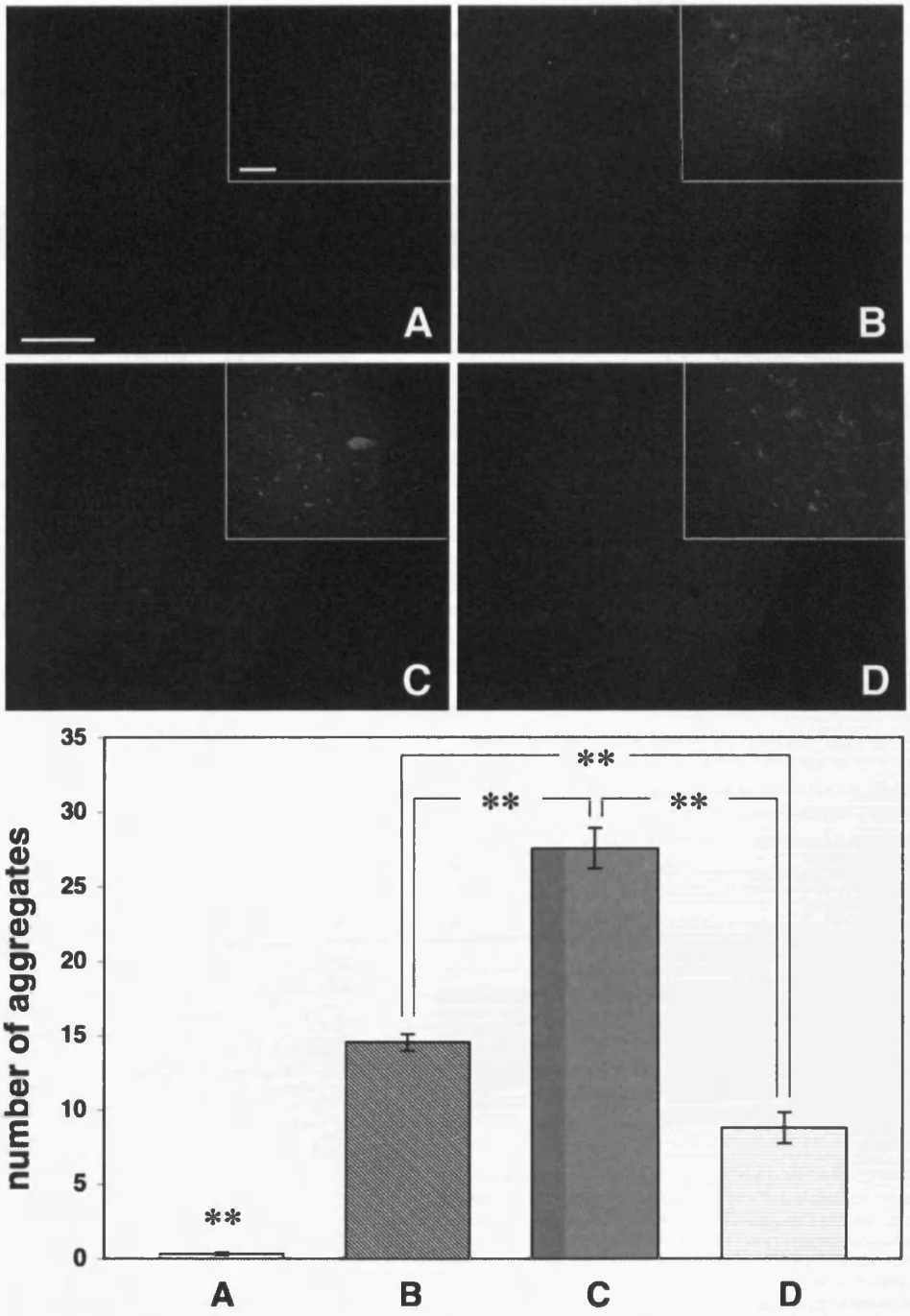

Figure 5. Amyloid deposits in the spinal cord of γ-synuclein transgenic mice. Representative images of Congo Red-stained spinal cord sections of 12-month-old wild-type mouse (**A**), hemizygous Thy1mγSN mouse (**B**), homozygous Thy1mγSN mouse at the advance stage of pathology (**C**) and homozygous Thy1mγSN mouse with mild signs of pathology (**D**) are shown. Scale bar = 200 μm for all main panels and 25 μm for all insets. The bar chart shows mean ± SEM. of the number of deposits per randomly selected 0.1 mm^2 area of the spinal cord gray matter. Sections for counting [104 for (A), 121 for (B), 93 for (C) and 72 for (D)] were randomly selected throughout the length of cervical, thoracic and lumbar parts of the spinal cord of at least four animals per group. One-way ANOVA with *post hoc* Fisher's protected *t*-test demonstrated significant ($^{**}P < 0.01$) difference between all four experimental groups.

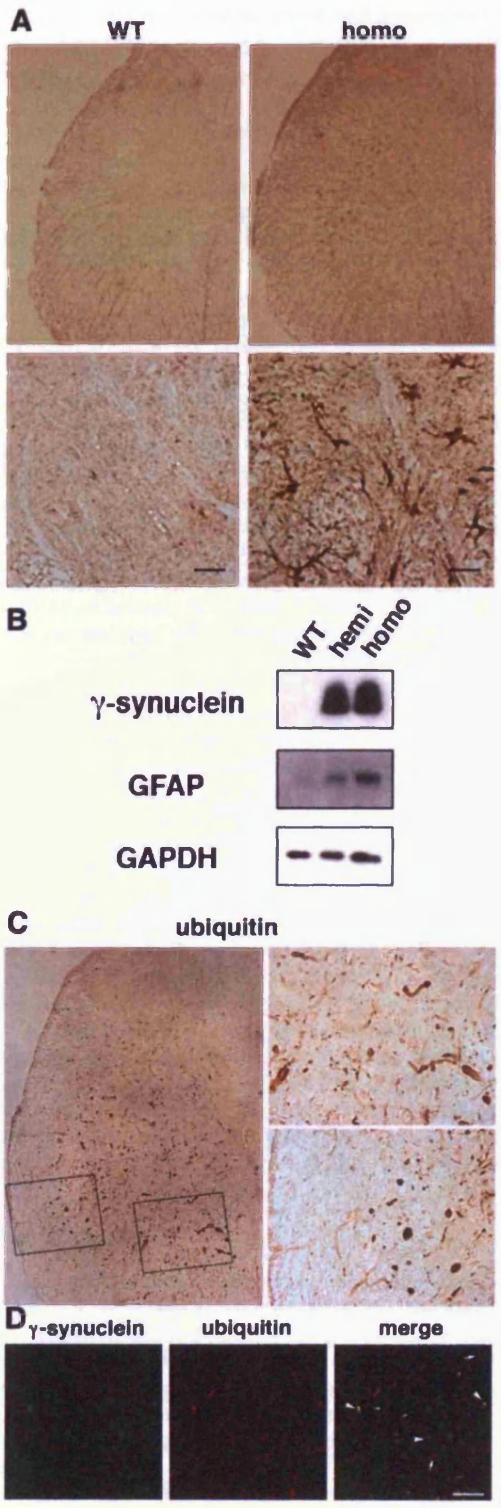

transgenic animals, we detected multiple abnormal ubiquitin-positive structures (Fig. 6C). However, double immunofluorescence revealed only partial overlap between γ-synuclein-positive and ubiquitin-positive profiles (Fig. 6D). Furthermore, western blot analysis did not reveal γ-synuclein-laddered staining patterns reminiscent of different degrees of ubiquitination (for example, see Fig. 1D). Therefore, most of the aggregated γ-synuclein in the spinal cord of Thy1mγSN mice are probably not ubiquitinated, but ubiquitin and/or some ubiquitinated proteins are present in the inclusions that appear in the nervous system of these mice.

Loss of motor neurons in the spinal cord of transgenic mice

The emergence of pathological inclusions and astrogliosis in Thy1mγSN mice coincides with the loss of motor neurons in the spinal cord (Fig. 7). Twelve-month-old homozygous animals with severe motor impairments possessed less than 40% of their wild-type littermates spinal motor neuron complement (Fig. 7E). Age-matched hemizygous and homozygous mice that developed milder motor impairment (clasping reflex and pareses of one limb but normal righting, for example see Supplementary Material movie) also displayed motor neuron loss but to a far lesser extent (Fig. 7E). Similar results were obtained in cervical, thoracic and lumbar parts of the spinal cord (data not shown).

Neurodegeneration in the spinal cord of motor neuron disease patients is often associated with dysfunction of intracellular systems that are responsible for correct folding of protein molecules. Survival of spinal motor neurons seems to rely on molecular chaperons including small heat shock proteins (40–44). Therefore, we used western blot analysis to examine the levels of large (HSP70) and small (HSPB1 also known as HSP27 or, in mouse, HSP25) heat shock proteins in the spinal cords of Thy1mγSN mice. While the levels of HSP70 were similar in age-matched transgenic and wild-type animals, the levels of HSPB1 were dramatically increased in all ageing transgenic animals and particularly in those that displayed severe motor impairment (Supplementary Material Fig. S3). However, this increase was due to high levels of HSPB1 in activated astrocytes (Fig. 7F and Supplementary Material Fig. S4), whereas in spinal motor neurons of transgenic animals the level of this protein was substantially lower than in spinal motor neurons of wild-type mice (Fig. 7F).

Figure 6. Astrogliosis and ubiquitin-positive inclusions in the spinal cord of γ-synuclein transgenic mice. (**A**) Transverse sections through the spinal cord of wild-type and severely affected homozygous Thy1mγSN mice immunostained for GFAP. Higher magnification images are shown on lower panels, scale bars = 20 μm. (**B**) Western blot of total protein extracts from 12-month-old wild-type, hemizygous and homozygous transgenic mice probed with antibodies against γ-synuclein, GFAP and GAPDH as a loading control. (**C**) Transverse sections through the spinal cord of severely affected homozygous Thy1mγSN mouse immunostained for ubiquitin. Boxed areas of gray and white matter are shown at higher magnification on the right top and right bottom panels, correspondingly. (**D**) Double immunofluorescent staining of severely affected Thy1mγSN mouse spinal cord section with antibodies against ubiquitin (green) and γ-synuclein (red). Examples of dystrophic neuritis and spheroids positive only for γ-synuclein are marked with large arrows, positive only for ubiquitin—with small arrows and positive for both proteins—with arrowheads. Scale bar = 50 μm.

Neurofilaments in the spinal cord and peripheral nerves of transgenic mice

HSPB1 is thought to be involved in regulation of the neurofilament network assembly in normal motor neurons and its mutant variants affect neurofilament-L (NF-L) aggregation in certain forms of Charcot–Marie–Tooth disease (45–47). An acute overexpression of γ-synuclein in cultured neurons also perturbs their neurofilament network integrity (15). Therefore, we analysed neurofilaments in the spinal motor neurons of transgenic mice chronically overexpressing γ-synuclein. Western blot analysis of the non-ionic detergent soluble fraction of Thy1mγSN mouse spinal cord revealed not only monomeric full-length 67 kDa NF-L but also distinct lower molecular weight NF-L species (Fig. 8A), possibly products of specific and restricted breakdown that were not seen in similar fractions of wild-type mouse spinal cord tissue. Decrease of these truncated species in the spinal cord of severely affected animals probably reflects loss of neurons that produced them. Overexpressed γ-synuclein co-immunoprecipitated with soluble NF-L, although substantially less amount of this protein was pulled-down from spinal cord lysates of animals at the advance stages of pathology than from similar lysates of less-affected animals (Fig. 8B).

Immunostaining of histological sections with antibody against NF-L did not reveal accumulation of this protein in γ-synuclein-positive or any other pathological profiles in the spinal cord of transgenic animals (Fig. 8C). However, substantial reduction in staining intensity in the spinal cord of Thy1mγSN mice when compared with wild-type tissue was observed (Fig. 8C). This reduction was mainly confined to neuronal processes and not the motor neuron cell bodies (Fig. 8D, upper panels). It was even more obvious in longitudinal sections through peripheral nerves of Thy1mγSN mice where only thin and wavy neurofilament-positive strings were found (Fig. 8D, lower panels). In addition, severe axonal pathology in the form of multiple nerve fibre swellings was revealed in the sciatic nerve of ageing homozygous Thy1mγSN mice (Fig. 8D, lower panels). Similar changes were also observed in tissue sections stained with antibodies against two other neurofilament proteins (data not shown). These results suggest that overexpression of γ-synuclein in transgenic mouse neurons seriously compromises the organization of neurofilaments in neuronal processes and, consequently, the architecture and function of axons.

DISCUSSION

Previous studies of transgenic mice overexpressing members of the synuclein family have revealed the contrasting effects of α-synuclein and β-synuclein on the development of pathological changes in the nervous system of these animals. High levels of α-synuclein in neurons cause a prominent neurological phenotype although the manifestations are variable and dependent on the α-synuclein isoform and type of promoter used for production of that particular transgenic line (reviewed in Refs. 48–50). In contrast, overexpression of β-synuclein does not have a harmful effect on animal health and even counteracts α-synuclein neurotoxicity (5–7). These results echo differences in aggregation propensity, cytotoxicity and certain structural features of these two proteins. As discussed in the Introduction, γ-synuclein has molecular features shared with both α- and β-synuclein. Therefore, it was not possible to predict the consequences of γ-synuclein overexpression in the nervous system of transgenic animals. Revealing the effects of aberrant expression of γ-synuclein *in vivo* is important not only for better understanding of relationships between structure and function within synuclein family. This information would also be valuable for development of new therapeutic approaches to combat synucleinopathies.

No disease-associated mutations of γ-synuclein gene or obvious cases of idiopathic human γ-synucleinopathies have been reported so far and the amino acid similarity between human and mouse proteins is high. Taking these facts into consideration, we decided to create a simple homologous model in which mouse γ-synuclein was overexpressed in the majority of neurons of the mouse nervous system. To achieve this we produced Thy1mγSN transgenic mice, expressing high levels of mouse γ-synuclein under control of the Thy-1 promoter cassette that has previously been used for producing several α-synuclein (27–30) and a β-synuclein (5) transgenic animal lines. In relatively homogeneous populations of neurons that normally express γ-synuclein, for example the DRG, there was approximately a 7-fold increase of γ-synuclein mRNA expression in homozygous Thy1mγSN transgenic mice compared with wild-type mice.

In homozygous transgenic mice, γ-synuclein aggregates and accumulates in abnormal structures within neuronal cell bodies and neurites. These γ-synuclein-positive structures resemble pathological hallmarks of synucleinopathies, namely dystrophic, beaded and ballooned neurites, spheroids, and even, occasionally, Lewy bodies. Like aggregated α-synuclein, aggregated γ-synuclein could not be extracted from transgenic mouse neural tissues using non-ionic detergents, but is partially soluble in sarcosyl-containing buffers. At least a fraction of aggregated γ-synuclein forms linear fibrils that are structurally similar, although not identical to products of α-synuclein fibrillation *in vivo* or *in vitro*.

Multimeric forms of α-synuclein are commonly detected on western blots of SDS-soluble proteins extracted from neural tissues of patients suffered from synucleinopathies or α-synuclein transgenic mice (35,37,38,51–55). These higher molecular weight bands represent either SDS-resistant α-synuclein oligomers or ubiquinated forms of the protein. We did not observe similar concatomeric γ-synuclein species in extracts of γ-synuclein transgenic mouse brain or spinal cord. This might suggest that the oligomeric intermediates of γ-synuclein aggregates are either not accumulating to a significant level in neurons of transgenic mice or that they are readily solubilized to monomeric γ-synuclein in SDS-containing buffers. It also suggests that even aggregated γ-synuclein is rarely ubiquitinated, which is consistent with our observation that γ-synuclein-positive inclusions in the spinal cord of transgenic mice often do not co-localize with ubiquitin-positive structures. The most probable explanation of our results is that ubiqutination is neither required for nor accompanies γ-synuclein aggregation but ubiquitin or certain ubiquitinated proteins may accumulate in pathological inclusions. Moreover, pathological changes in the nervous system of transgenic mice may trigger secondary events,

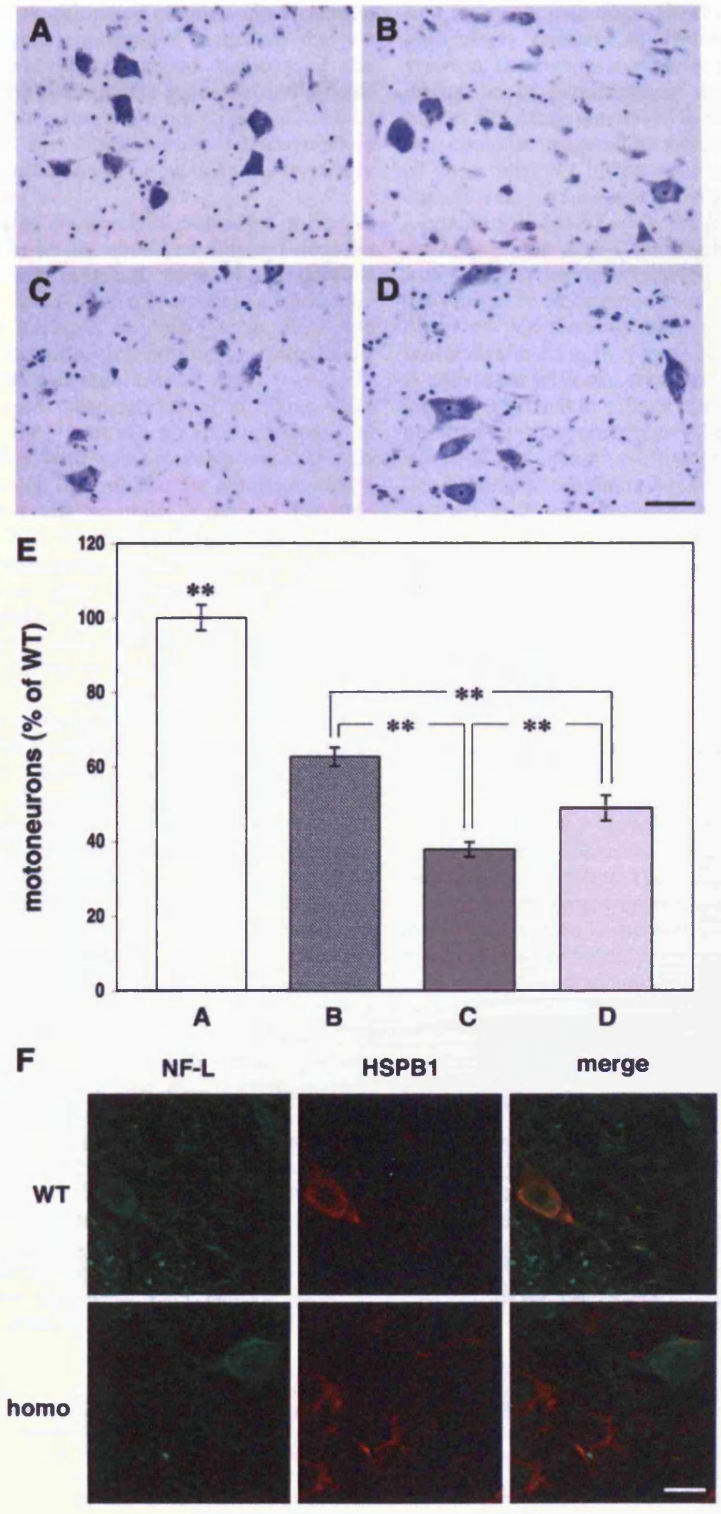
A
B
C
D
E
motoneurons (% of WT)
120
100
80
60
40
20
0
**
**
**
**
A
B
C
D
F
NF-L
HSPB1
merge
WT
homo

including aggregation of ubiquitinated proteins and formation of ubiquitin-positive/γ-synuclein-negative inclusions that we have observed on double-immunostained sections of the spinal cord. Similar partial overlap of α-synuclein and ubiquitin staining patterns has been found previously in the nervous systems of patients with synucleinopathies and α-synuclein transgenic mice, though ubiquinated α-synuclein is relatively abundant in these tissues (56).

The common features of α-synuclein pathology in human patients and transgenic mice are abundant amyloid deposits and activated glial cells in affected areas of the nervous system. In the brain and spinal cord of γ-synuclein transgenic mice, we also observed multiple amyloid (Congo Red- and Thioflavin S-positive) deposits and prominent astrogliosis, but no activated microglia was detected.

Although all pathological changes described above were observed throughout the central nervous system of Thy1mγSN mice, the spinal cord was noticeably more affected than any other region, which is similar to the reports on transgenic mice expressing α-synuclein under control of the same Thy-1 promoter (Refs 27,29,57 and our unpublished observations). This probably reflects the higher sensitivity of spinal cord neurons, particularly motor neurons, to high levels of both members of the synuclein family.

The ultimate consequence of γ-synuclein overexpression in transgenic mice is death of motor neurons. Correspondingly, these mice display clinical signs typical for motor neuron disease, namely a gradual development of motor deficit followed by pareses and paralyses, which are most obvious in limb muscles. At this terminal stage of the disease, γ-synuclein transgenic animals lose more than 60% of ventral horn motor neurons.

The development of neurological phenotype and histopathological findings in our mice suggests that pan-neuronal overexpression of γ-synuclein in mice could trigger pathological changes typical for synucleinopathies and most apparent in the spinal cord. The burden of pathology increases with age, which leads to a gradual loss of spinal motor neurons and the development of motor dysfunction. The onset, penetrance and degree of neuropathology directly correlate with the level of transgene expression because the hemizygous animals, which express 50% less transgenic γ-synuclein than the homozygous animals, develop clinical signs later in their life and show less pronounced histopathological changes in their nervous system.

One intriguing question is which molecular and cellular processes previously linked to the development of neurodegeneration become compromised in the nervous system of γ-synuclein transgenic mice? Recent studies on the mechanisms of neurodegeneration in humans and in various model organisms demonstrate that simultaneous dysfunction of several systems safeguarding cell homeostasis is required for the development of a full-scale pathology. However, some types of neurons are particularly sensitive to dysfunction in certain intracellular systems. Pathogenesis of motor neuron diseases often involves disruption of neurofilament networks in motor neuron cell bodies and axons (reviewed in Refs 58–61). While this disruption could be triggered by various mechanisms, in the majority of cases changes in the structure or metabolism of NF-L, a subunit required for assembly of neurofilaments *in vivo*, play a crucial role (45,62–67). We have demonstrated that chronic overexpression of γ-synuclein in mouse motor neurons leads to substantial depletion of neurofilaments in neuronal processes. This might be an essential event in pathogenesis of axonal pathology in peripheral nerves and consequent development of motor dysfunction in γ-synuclein transgenic mice. This result is consistent with our previous findings that acute overexpression of γ-synuclein affects neurofilament network integrity in cultured neurons, particularly their axons (15). The exact mechanism of the disruptive effect of overexpressed γ-synuclein on neurofilaments remains to be elucidated but its ability to interact with soluble NF-L and accumulation of abnormal NF-L-reactive soluble polypeptides in the spinal cord of Thy1mγSN mice suggest that normal homeostasis, including transport of NF-L to axons, might be at least partially prevented by trapping this protein in complexes with γ-synuclein and/or abnormal degradation. Disruption of axonal neurofilaments follows the reduction of NF-L axonal traffic. Moreover, truncated NF-L species could also affect neurofilament assembly and/or stability.

Some histopathological changes observed in Thy1mγSN mice, including astrocytosis and loss of motor neurons and their axons, are similar to those observed in aged NF-L null mutant mice (67). However in γ-synuclein transgenic mice, the pathological phenotype develops much earlier and is substantially more severe. This suggests that, in addition to the disrupted neurofilament network, other intracellular systems are also compromised in the motor neurons of these animals. Molecular chaperons belonging to the family of heat shock proteins play an important protective role in motor neurons. These cells seem to be particularly vulnerable to dysfunction of the small heat shock protein HSPB1 (40–44) and mutations of the HSPB1 gene cause certain types of motor neuron diseases (45–47). In motor neurons of γ-synuclein transgenic mice, the level of HSP25, a mouse ortholog of HSPB1, is substantially reduced, potentially compromising the survival of these cells.

Although some α-synuclein transgenic mice develop similar clinical signs of the spinal cord pathology to γ-synuclein transgenic mice, neither down-regulation of HSPB1 nor changes of the neurofilament network in their motor neurons has been reported. Taken together with other data, this suggests that diverse but partially overlapping mechanisms underlie development of pathology in these two mouse models.

Figure 7. Loss of motor neurons and changes of HSPB1 expression in the spinal cord of γ-synuclein transgenic mice. Representative images of cresyl fast violet-stained spinal cord sections of 12-month-old wild-type mouse (**A**), hemizygous Thy1mγSN mouse (**B**), homozygous Thy1mγSN mouse at the advance stage of pathology (**C**) and homozygous Thy1mγSN mouse with mild pathology (**D**) are shown. (**E**) The bar chart shows mean ± SEM. of the number of motor neurons per section expressed as percent of the average number of motor neurons per section of the wild-type mouse spinal cord. Sections for counting [160 for (A), 332 for (B), 215 for (C) and 139 for (D)] were randomly selected throughout the length of cervical, thoracic and lumbar parts of the spinal cord of at least four animals per group. One-way ANOVA with *post hoc* Fisher's protected *t*-test demonstrated significant (**$P<0.01$) difference between all four experimental groups. (**F**) Double immunofluorescent staining of spinal cord sections from a wild-type mouse and severely affected homozygous Thy1mγSN mouse with antibodies against neurofilament-L (green) and HSPB1 (red). Scale bar = 20 μm.

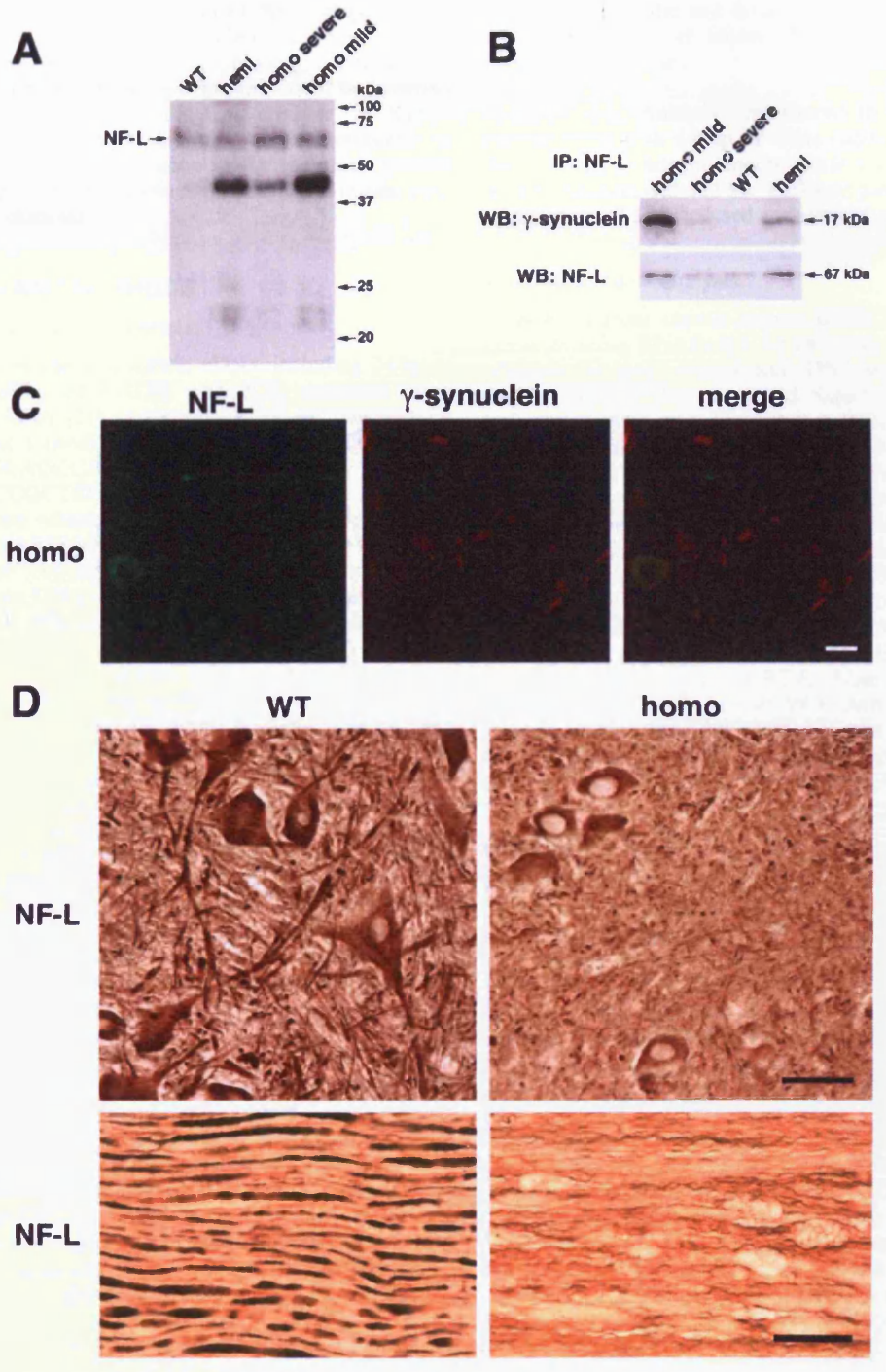

Figure 8. Neurofilaments in the spinal cord and peripheral nerve of γ-synuclein transgenic animals. (**A**) Western blot analysis of soluble neurofilament-L in the cytosolic (10 000*g* supernatant) fraction of the spinal cord of 12-month-old wild-type mice, hemizygous Thy1mγSN mice, homozygous Thy1mγSN mice with mild clinical signs of pathology and homozygous Thy1mγSN mice at the advance stage of pathology. (**B**) Co-immunoprecipitation of γ-synuclein and soluble neurofilament-L from the same cytosolic fractions. (**C**) Double immunofluorescent staining of severely affected Thy1mγSN mouse spinal cord section with antibodies against neurofilament-L (green) and γ-synuclein (red) shows the absence of NF-L accumulation in γ-synuclein-positive pathological profiles. (**D**) Substantial reduction of neurofilament-L staining in the ventral horns of the spinal cord (upper panels) and sciatic nerve (lower panels) of 12-month-old homozygous Thy1mγSN mice at the advance stage of pathology compared with their wild-type littermates. Scale bars = 20 μm for (C) and 50 μm for (D).

In conclusion, we have demonstrated that transgenic mice expressing high levels of γ-synuclein in their neurons develop a severe neurodegenerative pathology. It is feasible that, under certain conditions, γ-synuclein could be involved in the development of pathological changes in human neurons. Further studies on the role of this synuclein in normal and degenerating neurons might therefore provide additional insight into the mechanisms leading to human neurodegenerative diseases.

MATERIALS AND METHODS

Generation of transgenic animals

A fragment of mouse γ-synuclein cDNA including 34 bp of 5′-UTR and 64 bp of 3′-UTR was PCR amplified using pD53 plasmid DNA (31) as a template and oligonucleotides with *Xho*I linkers (mγSN *Xho*I-F: 5′-CTACTGTCCGCTCG AGCTTGCAGCAGCCAGGTTC-3′ and mγSN *Xho*I-R: 5′-CTACTGTCCGCTCGAGGCCTTCTAGTCTTCTCCA-C-3′) to facilitate subsequent cloning into *Xho*I site of Thy-1 promoter plasmid 323-pTSC21k (27). The fragment for microinjecting mouse oocytes was isolated by digestion of the resulting plasmid DNA with *Not*I. Transgenic founders were produced on C57Bl6 genetic background. Animals positive for transgene expression were crossed with C57Bl6 wild-type mice. Transgenic and wild-type animals were identified by PCR analysis of DNA from ear biopsies. The presence of a 1 kb product in the amplification reaction with primers HP45 *Thy*I f2 (5′-ACACCCCTAAAGCATACAGTCAGAC C-3′) and HP84 m γSN (5′-GGCCTTCTAGTCTTCTCCA CTCTTG-3′) indicated the presence of transgene in the mouse genome. Experimental cohorts were formed from litters produced by intercrossing hemizygous animals. Hemi- and homozygous animals were discriminated by quantitative real-time PCR analysis of DNA from ear biopsies and verified by analytical backcrossing followed by offspring genotyping. All animal work was carried in accordance with the United Kingdom Animals (Scientific Procedures) Act (1986).

Motor performance tests

Rotarod tests. Animals were tested on Ugo Basile 7650 rotarod at 2, 4, 6, 9, 12, 18 and 24 months of age. A constant (24 rpm) speed test was carried out for 4 min and accelerating (4–40 rpm) speed test for 5 min as described previously (68). Each mouse was tested three times in each mode with at least 30 min rest between trials. The mean of latency to fall for these three trials was included in final statistics. Eleven wild type, 12 hemizygous and 13 homozygous mice were tested at 2 months: 28, 27 and 21, at 4 months; 35, 40 and 23, at 6 months; 34, 36 and 23, at 9 months; 25, 26 and 14, at 12 months of age. No homozygous animals survived beyond 16 months therefore at this age and at 24 months only wild-type (12 and 15, respectively) and hemizygous (21 and 15, respectively) animals were tested.

Horizontal beam test. Animal coordination was tested on an 11 mm diameter and 50 cm long horizontal wooden rod at 4, 6, 9 and 12 months of age. A mouse was placed at the free hanging end of the rod facing its end. The ability to turn 180° and to reach an escape black box at the other end of the rod was recorded.

Footprint test. Animals were trained to run along a narrow passage lined with a strip of white paper before carrying out the test run. For this run, mouse forefeet were coated with blue ink and hindfeet with red ink. Different parameters of the stride were measured and analysed as described previously (69).

RNA expression analysis

Total RNA from various regions of the nervous system was extracted using RNAEasy+ kit as recommended by the manufacturer (Qiagen). First-strand cDNA was synthesized using random primers (Promega) and SuperScriptIII reverse transcriptase (Invitrogen). Quantitative PCR was performed on StepOne Real-Time PCR System (Applied Biosystems) with DyNAmo HS SYBR Green supermix (Finnzymes) and ROX as a passive reference dye. Reactions were carried out in one-piece thin-wall 48-well PCR plates (Bioplastics). GAPDH mRNA was used as a normalization standard. Primers 5′-CCATGGACGTCTTCAAGAAAGG-3′ and 5′-CGTTCTC CTTGGTTTTGGTG-3′ were used for amplification of γ-synuclein cDNA, and primers 5′-CACTGAGCATCTCC CTCACA-3′ and 5′-GTGGGTGCAGCGAACTTTAT-3′ for amplification of GAPDH mRNA. After hot start (10 min at 95°C), 40 cycles of 15 s at 95°C and 60 s at 60°C were carried out followed by melting curve determination with 0.3°C steps. Fold change was determined by $2^{-\Delta\Delta CT}$ method as described previously (70) using StepOne v2.0 software.

Protein extraction

Total tissue proteins were extracted by homogenization of tissues directly in SDS–PAGE loading buffer followed by incubation for 10 min at 100°C. For analysis of cytosolic proteins, tissues were homogenized in 50 mM Tris–HCl, pH 7.5; 150 mM NaCl; 1% Triton X-100 buffer with protease inhibitors (Complete Mini from Roche) and cytosolic fraction was obtained by centrifugation for 10 min at 10 000*g*.

Sequential protein extraction

A previously described protocol (37) was used with minor modifications. Briefly, neuronal tissues were homogenized in 5 volumes of high salt (HS) buffer (50 mM Tris–HCl, pH 7.5; 750 mM NaCl; 5 mM EDTA) with protease inhibitors (Complete Mini from Roche) and centrifuged at 100 000*g* for 20 min at 4°C. Pellets were washed in the same buffer and then re-extracted in HS buffer containing 1% Triton X-100 (HS/T-soluble fraction). Subsequent centrifugations and re-extractions produced RIPA-soluble and SDS-soluble fractions. The presence of γ-synuclein in these fractions was analysed by SDS–PAGE/western blotting.

Isolation and visualization of γ-synuclein filaments

Sarcosyl-insoluble filaments were extracted from mouse spinal cords as described previously for human neuronal tissues (71).

Final 100 000*g* pellets were resuspended in 50 mM Tris–HCl (pH 7.5) buffer and aliquots were applied onto glow-discharged carbon-coated 400-mesh copper grids. After blocking in 1% BSA/PBS, grids were incubated in 1:50 diluted affinity purified rabbit anti-mouse γ-synuclein SK23 antibody (31) for 60 min at room temperature followed by goat anti-rabbit immunoglobulin secondary antibody (Amersham) conjugated to 10 nm gold particles. Fibrils were negatively stained with 1% dodeca-tungstophosphoric acid neutralized with KOH to pH 6.2 as described previously (72) and observed at ×40 000 or ×50 000 magnification under a Philips TEM 208 transmission electron microscope.

Western blotting and antibodies

Proteins separated by SDS–PAGE were transferred to PVDF membrane using iBlot technology according to manufacturer (Invitrogen) instructions. Membrane blocking, incubation with antibodies, washing and chemiluminescent detection using ECL or ECL$^+$ techniques were carried out as described previously (31,68). Intensities of bands obtained using AlphaImager 2200 were analysed using AlphaEase 2200 Analysis Software (AlphaInnotech Corporation). Primary antibodies against GAPDH (mouse monoclonal, clone 6C5, Santa Cruz Biotechnology), α-synuclein (mouse monoclonal, clone 42, BD Transduction Laboratories), β-synuclein (mouse monoclonal, clone 8, BD Transduction Laboratories), γ-synuclein (rabbit polyclonal SK23, affinity purified), GFAP (rabbit polyclonal, Sigma), Iba1 (mouse monoclonal, clone 1022-5, Santa Cruz), CD11b (rat monoclonal, clone M1/70.15, Serotec), NF-L (rabbit monoclonal, clone C28E10, and mouse monoclonal, clone DA2, both Cell Signalling), neurofilament H (rabbit polyclonal, Sigma), heat shock protein B1 (rabbit monoclonal, Cell Signalling) and heat shock protein 70 (rabbit monoclonal, Cell Signalling) were used.

Immunoprecipitation

Freshly dissected spinal cords from individual animals were homogenized in 0.5 ml of IP buffer (50 mM Tris–HCl, pH 7.5, 300 mM NaCl, 1.5 mM $MgCl_2$, 1% Triton X-100) with protease inhibitors (Complete Mini from Roche) and Triton-soluble fraction was obtained by ×10 000*g* centrifugation for 10 min at 4°C. After presorption on Protein G Sepharose (Amersham) for 30 min at 4°C and removal of beads by centrifugation for 1 min at 1000*g*, 5 μl of antibody against NF-L (mouse monoclonal, clone DA2, Cell Signalling) or 20 μl of antibody against γ-synuclein (rabbit polyclonal SK23) were added, followed by 50 μl of fresh Protein G Sepharose. The suspension was rotated at 4°C for 2 h Sepharose beads were collected by centrifugation for 1 min at 1000*g* and washed four times with IP buffer. Bound proteins were eluted by boiling beads in 50 μl of SDS–PAGE loading buffer for 10 min.

Histological techniques

Dissected tissues were post-fixed in 4% paraformaldehyde/PBS or Carnoy's fixative and embedded in paraffin wax. Eight micrometre thick sections were cut and immunostained as described previously (32) using Elite plus kits (Vector laboratories) and 3,3′-diaminobenzidine as a substrate. For double immunofluorescence, secondary Alexa Fluor-conjugated antibody (Invitrogen) were used. Images were prepared using laser scanning confocal microscope Leica TCS SP2 (Leica Microsystems) and LEICA CONFOCAL 2.00 software. For detection and counting of amyloid aggregates, spinal cord sections (four to five animals per age/genotype/condition group) were stained in 0.5% Congo red solution in 50% ethanol for 7 min followed by a brief differentiation in potassium hydroxide (0.2% in 80% ethanol) and, after several washes in dH_2O, were mounted using Immu-mount (Thermo Electron Corporation). Fluorescent microscopy was used to analyse the number of aggregates within a randomly selected 0.1 mm^2 area of the spinal cord gray matter. For assessing number of spinal motor neurons, transverse spinal cord sections were stained in 0.5% cresyl fast violet (CFV) solution in dH_2O and dissociated in acidified ethanol (0.25% acetic acid in ethanol). The number of motor neurons (identified by a large cell body containing Nissl granules, with a clear nuclear envelope containing a strongly stained nucleolus) within the ventral horn was counted. Results were expressed as per cent of the average number of motor neurons per ventral horn section in the wild-type animals.

SUPPLEMENTARY MATERIAL

Supplementary Material is available at *HMG* online.

ACKNOWLEDGEMENTS

We are grateful to K.H. Wiederhold, Simone Danner, Sabine Kauffmann, Chiara Mencarelly, Abdelmojib Al-Wandi and Robert Durkin for preliminary analysis done at an early stage of this project; Matthias Mueller and Bernd Kinzel for help in generating the transgenic lines; Anthony Hann and Simon Brooks for valuable advices and Rosalind John for critical reading of the manuscript.

Conflict of Interest statement. None declared.

FUNDING

This work was supported by The Wellcome Trust [grant number 075615]. Funding to pay the Open Access publication charges for this article was provided by The Wellcome Trust.

REFERENCES

1. Cookson, M.R. and van der Brug, M. (2008) Cell systems and the toxic mechanism(s) of alpha-synuclein. *Exp. Neurol.*, **209**, 5–11.
2. Park, J.Y. and Lansbury, P.T. Jr (2003) Beta-synuclein inhibits formation of alpha-synuclein protofibrils: a possible therapeutic strategy against Parkinson's disease. *Biochemistry*, **42**, 3696–3700.
3. da Costa, C.A., Masliah, E. and Checler, F. (2003) Beta-synuclein displays an antiapoptotic p53-dependent phenotype and protects neurons from 6-hydroxydopamine-induced caspase 3 activation: cross-talk with alpha-synuclein and implication for Parkinson's disease. *J. Biol. Chem.*, **278**, 37330–37335.
4. Windisch, M., Hutter-Paier, B., Rockenstein, E., Hashimoto, M., Mallory, M. and Masliah, E. (2002) Development of a new treatment for

Alzheimer's disease and Parkinson's disease using anti-aggregatory beta-synuclein-derived peptides. *J. Mol. Neurosci.*, **19**, 63–69.
5. Hashimoto, M., Rockenstein, E., Mante, M., Mallory, M. and Masliah, E. (2001) β-Synuclein inhibits alpha-synuclein aggregation: a possible role as an anti-parkinsonian factor. *Neuron*, **32**, 213–223.
6. Fan, Y., Limprasert, P., Murray, I.V., Smith, A.C., Lee, V.M., Trojanowski, J.Q., Sopher, B.L. and La Spada, A.R. (2006) Beta-synuclein modulates alpha-synuclein neurotoxicity by reducing alpha-synuclein protein expression. *Hum. Mol. Genet.*, **15**, 3002–3011.
7. Hashimoto, M., Rockenstein, E., Mante, M., Crews, L., Bar-On, P., Gage, F.H., Marr, R. and Masliah, E. (2004) An antiaggregation gene therapy strategy for Lewy body disease utilizing beta-synuclein lentivirus in a transgenic model. *Gene Ther.*, **11**, 1713–1723.
8. Sung, Y.H. and Eliezer, D. (2007) Residual structure, backbone dynamics, and interactions within the synuclein family. *J. Mol. Biol.*, **372**, 689–707.
9. Volles, M.J. and Lansbury, P.T. Jr (2003) Zeroing in on the pathogenic form of alpha-synuclein and its mechanism of neurotoxicity in Parkinson's disease. *Biochemistry*, **42**, 7871–7878.
10. Dev, K.K., Hofele, K., Barbieri, S., Buchman, V.L. and van der Putten, H. (2003) Part II: alpha-synuclein and its molecular pathophysiological role in neurodegenerative disease. *Neuropharmacology*, **45**, 14–44.
11. Biere, A.L., Wood, S.J., Wypych, J., Steavenson, S., Jiang, Y., Anafi, D., Jacobsen, F.W., Jarosinski, M.A., Wu, G.M., Louis, J.C. *et al.* (2000) Parkinson's disease-associated alpha-synuclein is more fibrillogenic than beta- and gamma-synuclein and cannot cross-seed its homologs. *J. Biol. Chem.*, **275**, 34574–34579.
12. Uversky, V.N., Li, J., Souillac, P., Millett, I.S., Doniach, S., Jakes, R., Goedert, M. and Fink, A.L. (2002) Biophysical properties of the synucleins and their propensities to fibrillate: inhibition of alpha-synuclein assembly by beta- and gamma-synucleins. *J. Biol. Chem.*, **277**, 11970–11978.
13. Zibaee, S., Jakes, R., Fraser, G., Serpell, L.C., Crowther, R.A. and Goedert, M. (2007) Sequence determinants for amyloid fibrillogenesis of human alpha-synuclein. *J. Mol. Biol.*, **374**, 454–464.
14. Saha, A.R., Ninkina, N.N., Hanger, D.P., Anderton, B.H., Davies, A.M. and Buchman, V.L. (2000) Induction of neuronal death by alpha-synuclein. *Eur. J. Neurosci.*, **12**, 3073–3077.
15. Buchman, V.L., Adu, J., Pinon, L.G., Ninkina, N.N. and Davies, A.M. (1998) Persyn, a member of the synuclein family, influences neurofilament network integrity. *Nat. Neurosci.*, **1**, 101–103.
16. Surgucheva, I., McMahan, B., Ahmed, F., Tomarev, S., Wax, M.B. and Surguchov, A. (2002) Synucleins in glaucoma: implication of gamma-synuclein in glaucomatous alterations in the optic nerve. *J. Neurosci. Res.*, **68**, 97–106.
17. Rockenstein, E., Hansen, L.A., Mallory, M., Trojanowski, J.Q., Galasko, D. and Masliah, E. (2001) Altered expression of the synuclein family mRNA in Lewy body and Alzheimer's disease. *Brain Res.*, **914**, 48–56.
18. Mukaetova-Ladinska, E.B., Milne, J., Andras, A., Abdel-All, Z., Cerejeira, J., Greally, E., Robson, J., Jaros, E., Perry, R., McKeith, I.G. *et al.* (2008) Alpha- and gamma-synuclein proteins are present in cerebrospinal fluid and are increased in aged subjects with neurodegenerative and vascular changes. *Dement. Geriatr. Cogn. Disord.*, **26**, 32–42.
19. Mori, F., Hayashi, S., Yamagishi, S., Yoshimoto, M., Yagihashi, S., Takahashi, H. and Wakabayashi, K. (2002) Pick's disease: alpha- and beta-synuclein-immunoreactive Pick bodies in the dentate gyrus. *Acta Neuropathol. (Berl.)*, **104**, 455–461.
20. Galvin, J.E., Giasson, B., Hurtig, H.I., Lee, V.M. and Trojanowski, J.Q. (2000) Neurodegeneration with brain iron accumulation, type 1 is characterized by alpha-, beta-, and gamma-synuclein neuropathology. *Am. J. Pathol.*, **157**, 361–368.
21. Galvin, J.E., Uryu, K., Lee, V.M. and Trojanowski, J.Q. (1999) Axon pathology in Parkinson's disease and Lewy body dementia hippocampus contains alpha-, beta-, and gamma-synuclein. *Proc. Natl Acad. Sci. USA*, **96**, 13450–13455.
22. Mu, X., Beremand, P.D., Zhao, S., Pershad, R., Sun, H., Scarpa, A., Liang, S., Thomas, T.L. and Klein, W.H. (2004) Discrete gene sets depend on POU domain transcription factor Brn3b/Brn-3.2/POU4f2 for their expression in the mouse embryonic retina. *Development*, **131**, 1197–1210.
23. Brenz Verca, M.S., Bahi, A., Boyer, F., Wagner, G.C. and Dreyer, J.L. (2003) Distribution of alpha- and gamma-synucleins in the adult rat brain and their modification by high-dose cocaine treatment. *Eur. J. Neurosci.*, **18**, 1923–1938.
24. Soto, I., Oglesby, E., Buckingham, B.P., Son, J.L., Roberson, E.D., Steele, M.R., Inman, D.M., Vetter, M.L., Horner, P.J. and Marsh-Armstrong, N. (2008) Retinal ganglion cells downregulate gene expression and lose their axons within the optic nerve head in a mouse glaucoma model. *J. Neurosci.*, **28**, 548–561.
25. Buckingham, B.P., Inman, D.M., Lambert, W., Oglesby, E., Calkins, D.J., Steele, M.R., Vetter, M.L., Marsh-Armstrong, N. and Horner, P.J. (2008) Progressive ganglion cell degeneration precedes neuronal loss in a mouse model of glaucoma. *J. Neurosci.*, **28**, 2735–2744.
26. Wang, Y.L., Takeda, A., Osaka, H., Hara, Y., Furuta, A., Setsuie, R., Sun, Y.J., Kwon, J., Sato, Y., Sakurai, M. *et al.* (2004) Accumulation of beta- and gamma-synucleins in the ubiquitin carboxyl-terminal hydrolase L1-deficient gad mouse. *Brain Res.*, **1019**, 1–9.
27. van der Putten, H., Wiederhold, K.H., Probst, A., Barbieri, S., Mistl, C., Danner, S., Kauffmann, S., Hofele, K., Spooren, W.P., Ruegg, M.A. *et al.* (2000) Neuropathology in mice expressing human alpha-synuclein. *J. Neurosci.*, **20**, 6021–6029.
28. Rockenstein, E., Mallory, M., Hashimoto, M., Song, D., Shults, C.W., Lang, I. and Masliah, E. (2002) Differential neuropathological alterations in transgenic mice expressing alpha-synuclein from the platelet-derived growth factor and Thy-1 promoters. *J. Neurosci. Res.*, **68**, 568–578.
29. Chandra, S., Gallardo, G., Fernandez-Chacon, R., Schluter, O.M. and Sudhof, T.C. (2005) Alpha-synuclein cooperates with CSPalpha in preventing neurodegeneration. *Cell*, **123**, 383–396.
30. Zhou, W., Schutzman, J. and Freed, C.R. (2008) Transgenic mice overexpressing tyrosine-to-cysteine mutant human alpha-synuclein: a progressive neurodegenerative model of diffuse Lewy body disease. *J. Biol. Chem.*, **283**, 9863–9870.
31. Buchman, V.L., Hunter, H.J., Pinon, L.G., Thompson, J., Privalova, E.M., Ninkina, N.N. and Davies, A.M. (1998) Persyn, a member of the synuclein family, has a distinct pattern of expression in the developing nervous system. *J. Neurosci.*, **18**, 9335–9341.
32. Ninkina, N., Papachroni, K., Robertson, D.C., Schmidt, O., Delaney, L., O'Neill, F., Court, F., Rosenthal, A., Fleetwood-Walker, S.M., Davies, A.M. *et al.* (2003) Neurons expressing the highest levels of gamma-synuclein are unaffected by targeted inactivation of the gene. *Mol. Cell. Biol.*, **23**, 8233–8245.
33. Yavich, L., Oksman, M., Tanila, H., Kerokoski, P., Hiltunen, M., van Groen, T., Puolivali, J., Mannisto, P.T., Garcia-Horsman, A., MacDonald, E. *et al.* (2005) Locomotor activity and evoked dopamine release are reduced in mice overexpressing A30P-mutated human alpha-synuclein. *Neurobiol. Dis.*, **20**, 303–313.
34. Masliah, E., Rockenstein, E., Veinbergs, I., Mallory, M., Hashimoto, M., Takeda, A., Sagara, Y., Sisk, A. and Mucke, L. (2000) Dopaminergic loss and inclusion body formation in alpha-synuclein mice: implications for neurodegenerative disorders. *Science*, **287**, 1265–1269.
35. Lee, M.K., Stirling, W., Xu, Y., Xu, X., Qui, D., Mandir, A.S., Dawson, T.M., Copeland, N.G., Jenkins, N.A. and Price, D.L. (2002) Human alpha-synuclein-harboring familial Parkinson's disease-linked Ala-53 –> Thr mutation causes neurodegenerative disease with alpha-synuclein aggregation in transgenic mice. *Proc. Natl Acad. Sci. USA*, **99**, 8968–8973.
36. Gispert, S., Del Turco, D., Garrett, L., Chen, A., Bernard, D.J., Hamm-Clement, J., Korf, H.W., Deller, T., Braak, H., Auburger, G. *et al.* (2003) Transgenic mice expressing mutant A53T human alpha-synuclein show neuronal dysfunction in the absence of aggregate formation. *Mol. Cell. Neurosci.*, **24**, 419–429.
37. Giasson, B.I., Duda, J.E., Quinn, S.M., Zhang, B., Trojanowski, J.Q. and Lee, V.M. (2002) Neuronal alpha-synucleinopathy with severe movement disorder in mice expressing A53T human alpha-synuclein. *Neuron*, **34**, 521–533.
38. Freichel, C., Neumann, M., Ballard, T., Muller, V., Woolley, M., Ozmen, L., Borroni, E., Kretzschmar, H.A., Haass, C., Spooren, W. *et al.* (2007) Age-dependent cognitive decline and amygdala pathology in alpha-synuclein transgenic mice. *Neurobiol. Aging*, **28**, 1421–1435.
39. Fleming, S.M., Salcedo, J., Fernagut, P.O., Rockenstein, E., Masliah, E., Levine, M.S. and Chesselet, M.F. (2004) Early and progressive sensorimotor anomalies in mice overexpressing wild-type human alpha-synuclein. *J. Neurosci.*, **24**, 9434–9440.
40. Sharp, P.S., Akbar, M.T., Bouri, S., Senda, A., Joshi, K., Chen, H.J., Latchman, D.S., Wells, D.J. and de Belleroche, J. (2008) Protective

effects of heat shock protein 27 in a model of ALS occur in the early stages of disease progression. *Neurobiol. Dis.*, **30**, 42–55.
41. Maatkamp, A., Vlug, A., Haasdijk, E., Troost, D., French, P.J. and Jaarsma, D. (2004) Decrease of Hsp25 protein expression precedes degeneration of motoneurons in ALS-SOD1 mice. *Eur. J. Neurosci.*, **20**, 14–28.
42. Bruening, W., Roy, J., Giasson, B., Figlewicz, D.A., Mushynski, W.E. and Durham, H.D. (1999) Up-regulation of protein chaperones preserves viability of cells expressing toxic Cu/Zn-superoxide dismutase mutants associated with amyotrophic lateral sclerosis. *J. Neurochem.*, **72**, 693–699.
43. Adachi, H., Waza, M., Tokui, K., Katsuno, M., Minamiyama, M., Tanaka, F., Doyu, M. and Sobue, G. (2007) CHIP overexpression reduces mutant androgen receptor protein and ameliorates phenotypes of the spinal and bulbar muscular atrophy transgenic mouse model. *J. Neurosci.*, **27**, 5115–5126.
44. Adachi, H., Katsuno, M., Minamiyama, M., Sang, C., Pagoulatos, G., Angelidis, C., Kusakabe, M., Yoshiki, A., Kobayashi, Y., Doyu, M. *et al.* (2003) Heat shock protein 70 chaperone overexpression ameliorates phenotypes of the spinal and bulbar muscular atrophy transgenic mouse model by reducing nuclear-localized mutant androgen receptor protein. *J. Neurosci.*, **23**, 2203–2211.
45. Zhai, J., Lin, H., Julien, J.P. and Schlaepfer, W.W. (2007) Disruption of neurofilament network with aggregation of light neurofilament protein: a common pathway leading to motor neuron degeneration due to Charcot–Marie–Tooth disease-linked mutations in NFL and HSPB1. *Hum. Mol. Genet.*, **16**, 3103–3116.
46. Evgrafov, O.V., Mersiyanova, I., Irobi, J., Van Den Bosch, L., Dierick, I., Leung, C.L., Schagina, O., Verpoorten, N., Van Impe, K., Fedotov, V. *et al.* (2004) Mutant small heat-shock protein 27 causes axonal Charcot–Marie–Tooth disease and distal hereditary motor neuropathy. *Nat. Genet.*, **36**, 602–606.
47. Ackerley, S., James, P.A., Kalli, A., French, S., Davies, K.E. and Talbot, K. (2006) A mutation in the small heat-shock protein HSPB1 leading to distal hereditary motor neuronopathy disrupts neurofilament assembly and the axonal transport of specific cellular cargoes. *Hum. Mol. Genet.*, **15**, 347–354.
48. Springer, W. and Kahle, P.J. (2006) Mechanisms and models of alpha-synuclein-related neurodegeneration. *Curr. Neurol. Neurosci. Rep.*, **6**, 432–436.
49. Chesselet, M.F. (2008) In vivo alpha-synuclein overexpression in rodents: a useful model of Parkinson's disease? *Exp. Neurol.*, **209**, 22–27.
50. Buchman, V.L. and Ninkina, N. (2008) Modulation of alpha-synuclein expression in transgenic animals for modelling synucleinopathies—is the juice worth the squeeze? *Neurotox. Res.*, **14**, 329–341.
51. Yazawa, I., Giasson, B.I., Sasaki, R., Zhang, B., Joyce, S., Uryu, K., Trojanowski, J.Q. and Lee, V.M. (2005) Mouse model of multiple system atrophy alpha-synuclein expression in oligodendrocytes causes glial and neuronal degeneration. *Neuron*, **45**, 847–859.
52. Masliah, E., Rockenstein, E., Veinbergs, I., Sagara, Y., Mallory, M., Hashimoto, M. and Mucke, L. (2001) Beta-amyloid peptides enhance alpha-synuclein accumulation and neuronal deficits in a transgenic mouse model linking Alzheimer's disease and Parkinson's disease. *Proc. Natl Acad. Sci. USA*, **98**, 12245–12250.
53. Klucken, J., Shin, Y., Masliah, E., Hyman, B.T. and McLean, P.J. (2004) Hsp70 reduces alpha-synuclein aggregation and toxicity. *J. Biol. Chem.*, **279**, 25497–25502.
54. Kahle, P.J., Neumann, M., Ozmen, L., Muller, V., Odoy, S., Okamoto, N., Jacobsen, H., Iwatsubo, T., Trojanowski, J.Q., Takahashi, H. *et al.* (2001) Selective insolubility of alpha-synuclein in human Lewy body diseases is recapitulated in a transgenic mouse model. *Am. J. Pathol.*, **159**, 2215–2225.
55. Gomez-Isla, T., Irizarry, M.C., Mariash, A., Cheung, B., Soto, O., Schrump, S., Sondel, J., Kotilinek, L., Day, J., Schwarzschild, M.A. *et al.* (2003) Motor dysfunction and gliosis with preserved dopaminergic markers in human alpha-synuclein A30P transgenic mice. *Neurobiol. Aging*, **24**, 245–258.
56. Sampathu, D.M., Giasson, B.I., Pawlyk, A.C., Trojanowski, J.Q. and Lee, V.M. (2003) Ubiquitination of alpha-synuclein is not required for formation of pathological inclusions in alpha-synucleinopathies. *Am. J. Pathol.*, **163**, 91–100.
57. Neumann, M., Kahle, P.J., Giasson, B.I., Ozmen, L., Borroni, E., Spooren, W., Muller, V., Odoy, S., Fujiwara, H., Hasegawa, M. *et al.* (2002) Misfolded proteinase K-resistant hyperphosphorylated alpha-synuclein in aged transgenic mice with locomotor deterioration and in human alpha-synucleinopathies. *J. Clin. Invest.*, **110**, 1429–1439.
58. Xiao, S., McLean, J. and Robertson, J. (2006) Neuronal intermediate filaments and ALS: a new look at an old question. *Biochim. Biophys. Acta*, **1762**, 1001–1012.
59. Lariviere, R.C. and Julien, J.P. (2004) Functions of intermediate filaments in neuronal development and disease. *J. Neurobiol.*, **58**, 131–148.
60. Julien, J.P. and Kriz, J. (2006) Transgenic mouse models of amyotrophic lateral sclerosis. *Biochim. Biophys. Acta*, **1762**, 1013–1024.
61. Bruijn, L.I., Miller, T.M. and Cleveland, D.W. (2004) Unraveling the mechanisms involved in motor neuron degeneration in ALS. *Annu. Rev. Neurosci.*, **27**, 723–749.
62. Perez-Olle, R., Leung, C.L. and Liem, R.K. (2002) Effects of Charcot–Marie–Tooth-linked mutations of the neurofilament light subunit on intermediate filament formation. *J. Cell Sci.*, **115**, 4937–4946.
63. Perez-Olle, R., Jones, S.T. and Liem, R.K. (2004) Phenotypic analysis of neurofilament light gene mutations linked to Charcot–Marie–Tooth disease in cell culture models. *Hum. Mol. Genet.*, **13**, 2207–2220.
64. Mersiyanova, I.V., Perepelov, A.V., Polyakov, A.V., Sitnikov, V.F., Dadali, E.L., Oparin, R.B., Petrin, A.N. and Evgrafov, O.V. (2000) A new variant of Charcot–Marie–Tooth disease type 2 is probably the result of a mutation in the neurofilament-light gene. *Am. J. Hum. Genet.*, **67**, 37–46.
65. De Jonghe, P., Mersivanova, I., Nelis, E., Del Favero, J., Martin, J.J., Van Broeckhoven, C., Evgrafov, O. and Timmerman, V. (2001) Further evidence that neurofilament light chain gene mutations can cause Charcot–Marie–Tooth disease type 2E. *Ann. Neurol.*, **49**, 245–249.
66. Beaulieu, J.M., Jacomy, H. and Julien, J.P. (2000) Formation of intermediate filament protein aggregates with disparate effects in two transgenic mouse models lacking the neurofilament light subunit. *J. Neurosci.*, **20**, 5321–5328.
67. McLean, J.R., Sanelli, T.R., Leystra-Lantz, C., He, B.P. and Strong, M.J. (2005) Temporal profiles of neuronal degeneration, glial proliferation, and cell death in hNFL(+/+) and NFL(−/−) mice. *Glia*, **52**, 59–69.
68. Robertson, D.C., Schmidt, O., Ninkina, N., Jones, P.A., Sharkey, J. and Buchman, V.L. (2004) Developmental loss and resistance to MPTP toxicity of dopaminergic neurones in substantia nigra pars compacta of gamma-synuclein, alpha-synuclein and double alpha/gamma-synuclein null mutant mice. *J. Neurochem.*, **89**, 1126–1136.
69. Carter, R.J., Lione, L.A., Humby, T., Mangiarini, L., Mahal, A., Bates, G.P., Dunnett, S.B. and Morton, A.J. (1999) Characterization of progressive motor deficits in mice transgenic for the human Huntington's disease mutation. *J. Neurosci.*, **19**, 3248–3257.
70. Livak, K.J. and Schmittgen, T.D. (2001) Analysis of relative gene expression data using real-time quantitative PCR and the 2(-Delta Delta C(T)) method. *Methods*, **25**, 402–408.
71. Spillantini, M.G., Crowther, R.A., Jakes, R., Hasegawa, M. and Goedert, M. (1998) Alpha-synuclein in filamentous inclusions of Lewy bodies from Parkinson's disease and dementia with Lewy bodies. *Proc. Natl Acad. Sci. USA*, **95**, 6469–6473.
72. Serpell, L.C., Berriman, J., Jakes, R., Goedert, M. and Crowther, R.A. (2000) Fiber diffraction of synthetic alpha-synuclein filaments shows amyloid-like cross-beta conformation. *Proc. Natl Acad. Sci. USA*, **97**, 4897–4902.